

北京航空航天大学四年级博士生和五年级直博生 学校奖学金申报表

(请按填表说明填写, 本表填写的内容必须为非涉密可公开!)

| | | | | | | |
|----------------------------------------|---------------------------------------------------------------------------------------------------------------------|----------|-----------|---------------------------------|-----------|--|
| 姓 名 | 王雪彤 | 学 号 | BY1510117 | 指导教师 | 李淑宇 | |
| 类 别 | <input checked="" type="checkbox"/> 三年级博士生 <input type="checkbox"/> 四年级直博生 | | 学科/专业 | 生物与医学工程 | | |
| 承担 科研 任务 情况 | 项目名称 | 课题来源 | 课题负责人 | 本人承担的具体工作 | | |
| | 基于音乐训练的老年人脑可塑造功能区多模态影像研究 | 国家自然科学基金 | 李淑宇 | 影像数据采集、筛查 | | |
| | 海马亚区的结构与功能连接方法的研究及在轻度认知障碍疾病中的应用 | 国家自然科学基金 | 李淑宇 | 海马亚区在 aMCI、svMCI 应用 | | |
| | 计算神经解剖 | 国家自然科学基金 | 李淑宇 | 大脑网络构建方法研究 | | |
| 已取得 研究成 果(论 文、专 利、获 奖等) | 论文题目 | 本人排名 | 发表年月 | 期刊(会议)名称 | 被检索 类型 | |
| | Altered whole-brain structural covariance of the hippocampal subfields in svMCI and aMCI patients | 1 | 2018 | Frontiers in Neurology | SCI 源 | |
| | Individual Morphological Brain Network Construction Based on Multivariate Euclidean Distances Between Brain Regions | 2 | 2018 | Frontiers in Human Neuroscience | SCI 源 | |
| | Musical training induces functional and structural auditory - motor network plasticity in young adults. | 2 | 2018 | Human brain mapping | SCI 源 | |
| | Differential age-related changes in structural covariance networks of human anterior and posterior hippocampus | 3 | 2018 | Frontiers in Physiology | SCI 源 | |

| | | | | | |
|--------------|---------------------------------------------------------------------------------------------------------------------------------------|------|------|-------------------|-------|
| | Topological properties of large-scale cortical networks based on multiple morphological features in amnesic mild cognitive impairment | 3 | 2016 | Neural Plasticity | SCI 源 |
| | 专利名称 | 本人排名 | 发布年月 | 专利号 | 专利类型 |
| | | | | | |
| | | | | | |
| | 获科技成果奖励名称 | 本人排名 | 获奖年月 | 证书编号 | 奖励级别 |
| | | | | | |
| | | | | | |
| 本人承诺 | 本人所填写的以上内容均为真实情况。 本人签字：_____ 年 月 日 | | | | |
| 导师意见 | 同意 / 不同意 该同学申报学校奖学金。 导师签字：_____ 年 月 日 | | | | |
| 学院学位评定分委员会意见 | 同意 / 不同意 该同学获得学校奖学金。 签字：_____ (学院代盖) 年 月 日 | | | | |



Altered Whole-Brain Structural Covariance of the Hippocampal Subfields in Subcortical Vascular Mild Cognitive Impairment and Amnestic Mild Cognitive Impairment Patients

OPEN ACCESS

Xuetong Wang^{1,2†}, Yang Yu^{3,4†}, Weina Zhao^{3,4,5†}, Qionglin Li^{1,2}, Xinwei Li^{1,2}, Shuyu Li^{1,2*}, Changhao Yin^{5*} and Ying Han^{3,4*}

Edited by:

HuaLin Cai,
Central South University,
China

Reviewed by:

Ricardo Insausti,
Universidad de Castilla-
La Mancha, Spain
Julie A. Dumas,
University of Vermont,
United States

*Correspondence:

Shuyu Li
shuyuli@buaa.edu.cn;
Changhao Yin
yinchanghao7916@sina.com;
Ying Han
hanying@xwh.ccmu.edu.cn

[†]These authors have contributed
equally to this work.

Specialty section:

This article was submitted
to Neuropharmacology,
a section of the journal
Frontiers in Neurology

Received: 11 December 2017

Accepted: 30 April 2018

Published: 22 May 2018

Citation:

Wang X, Yu Y, Zhao W, Li Q, Li X,
Li S, Yin C and Han Y (2018) Altered
Whole-Brain Structural Covariance of
the Hippocampal Subfields in
Subcortical Vascular Mild Cognitive
Impairment and Amnestic Mild
Cognitive Impairment Patients.
Front. Neurol. 9:342.
doi: 10.3389/fneur.2018.00342

¹School of Biological Science and Medical Engineering, Beihang University, Beijing, China, ²Beijing Advanced Innovation Centre for Biomedical Engineering, Beihang University, Beijing, China, ³Center of Alzheimer's Disease, Beijing Institute for Brain Disorders, Beijing, China, ⁴Department of Neurology, XuanWu Hospital, Capital Medical University, Beijing, China, ⁵Department of Neurology, Hongqi Hospital, Mudanjiang Medical University, Mudanjiang, China

The hippocampus plays important roles in memory processing. However, the hippocampus is not a homogeneous structure, which consists of several subfields. The hippocampal subfields are differently affected by many neurodegenerative diseases, especially mild cognitive impairment (MCI). Amnestic mild cognitive impairment (aMCI) and subcortical vascular mild cognitive impairment (svMCI) are the two subtypes of MCI. aMCI is characterized by episodic memory loss, and svMCI is characterized by extensive white matter hyperintensities and multiple lacunar infarctions on magnetic resonance imaging. The primary cognitive impairment in svMCI is executive function, attention, and semantic memory. Some variations or disconnections within specific large-scale brain networks have been observed in aMCI and svMCI patients. The aim of this study was to investigate abnormalities in structural covariance networks (SCNs) between hippocampal subfields and the whole cerebral cortex in aMCI and svMCI patients, and whether these abnormalities are different between the two groups. Automated segmentation of hippocampal subfields was performed with FreeSurfer 5.3, and we selected five hippocampal subfields as the seeds of SCN analysis: CA1, CA2/3, CA4/dentate gyrus (DG), subiculum, and presubiculum. SCNs were constructed based on these hippocampal subfield seeds for each group. Significant correlations between hippocampal subfields, fusiform gyrus (FFG), and entorhinal cortex (ERC) in gray matter volume were found in each group. We also compared the differences in the strength of structural covariance between any two groups. In the aMCI group, compared to the normal controls (NC) group, we observed an increased association between the left CA1/CA4/DG/subiculum and the left temporal pole. Additionally, the hippocampal subfields (bilateral CA1, left CA2/3) significantly covaried with the orbitofrontal cortex in the svMCI group compared to the NC group. In the aMCI group compared to the svMCI group, we observed decreased association between hippocampal subfields and the right FFG, while we also

observed an increased association between the bilateral subiculum/presubiculum and bilateral ERC. These findings provide new evidence that there is altered whole-brain structural covariance of the hippocampal subfields in svMCI and aMCI patients and provide insights to the pathological mechanisms of different MCI subtypes.

Keywords: hippocampal subfields, amnesic mild cognitive impairment, subcortical vascular mild cognitive impairment, structural covariance networks, MRI

INTRODUCTION

The hippocampus is part of the limbic system. It plays important roles in memory processing, especially spatial memory (1). Studies have shown that the hippocampus can be affected by a variety of neurological diseases such as epilepsy and schizophrenia (2, 3). Importantly, hippocampal disruption is an early sign of Alzheimer's disease (AD) and other forms of dementia (4).

However, the hippocampus is not a homogeneous structure, which consists of several subfields, specifically the cornu ammonis (CA) areas 1–4, the dentate gyrus (DG), the subiculum, and the presubiculum (5). The hippocampus subfields have distinct anatomy and functions (6). Notably, evidence supports the distinct connectivity between hippocampal subfields and other brain regions. The major input to the hippocampus is the perforant path, coming from the entorhinal cortex (ERC) that connects with the DG and CA3 pyramidal neurons. In addition, the efferent fibers, which may originate from CA or subiculum, terminate in many brain regions (e.g., entorhinal area, posterior cingulate, medial frontal cortex, and gyrus rectus) (7). Previous studies reported that the hippocampal subfields were differently affected by many neurodegenerative diseases, especially mild cognitive impairment (MCI) (8, 9).

Mild cognitive impairment is a diagnosis given to older adults who have cognitive impairments but that does not interfere significantly with their daily activities (10). It is regarded as the transitional stage between normal aging and dementia. Amnesic mild cognitive impairment (aMCI) and subcortical vascular mild cognitive impairment (svMCI) are two subtypes of MCI, both associated with deficits in multiple cognitive domains, with the same chief complaints in memory deficits, but the pathogenesis of aMCI and svMCI are different (11, 12). The aMCI is characterized by episodic memory loss (13) and represents the prodromal stage of AD (14, 15). The svMCI is regarded as a prodromal stage of subcortical vascular dementia, showing extensive white matter hyperintensities and multiple lacunar infarctions on magnetic resonance imaging (16). The cognitive impairment of svMCI is mainly manifested in executive function, attention, and semantic memory (17–19). Importantly, some variations or disconnections within specific large-scale brain networks were observed in aMCI and svMCI patients (20–24). For example, patients with aMCI showed a pattern of brain disconnection between the posterior cingulate cortex (PCC), the medial prefrontal cortex (PFC), and the rest of the brain (21). A few studies have reported that aMCI patients were characterized by aberrance in resting-state functional connectivity of specific hippocampal subregions (such as DG and subiculum) (25, 26).

Additionally, svMCI patients presented extensive decreased functional connectivity density and functional amplitude of spontaneous low-frequency oscillations in the medial PFC (22). However, it is unknown whether aMCI and svMCI patients have abnormalities in structural connections between hippocampal subfields and the cerebral cortex and whether these abnormalities are different between aMCI and svMCI.

Structural covariance networks (SCNs), based on voxel-based morphometry (VBM), generate a map of correlation between the gray matter (GM) volume of a region of interest and the other regions (27, 28). SCNs are regarded as the potential tool to reflect developmental coordination or synchronized maturation between regions of the brain (29). In addition, SCN analysis has been successfully applied to obtain the abnormality in brain connectivity in some neuropsychiatric disorders (30–32). In this study, SCNs were employed to characterize the structural connections between hippocampal subfields and the cerebral cortex. We selected five hippocampal subfields using an automated segmentation method as seeds to build the SCNs in aMCI patients, svMCI patients, and normal controls (NC). Finally, we compared the differences in strength of structural covariance between groups.

MATERIALS AND METHODS

Participants

Patients with svMCI and aMCI were recruited through the memory clinic of the neurology department of Xuanwu Hospital, Capital Medical University, Beijing, China. Two experienced neurologists diagnosed all patients using the Petersen criteria (33). Healthy controls were recruited from the local community through advertisements. Subjects were excluded if they had the following clinical characteristics: (i) depressive symptoms with a Hamilton Depression Rating Scale score > 24; (ii) non-MCI disease that cause cognitive impairments, such as psychiatric disease, systemic disease, or alcohol or drug abuse; (iii) factors that would make neuropsychological testing infeasible, such as visual abnormalities, severe aphasia, or motor disorders. Written informed consent was obtained from all participants. According to the diagnostic criteria and exclusion criteria, there were 29 svMCI patients, 33 aMCI patients, and 36 NC subjects included in this study. All participants received a standardized clinical evaluation protocol including a global cognitive functioning test [i.e., Mini Mental Status Examination (MMSE)] and other cognitive assessments (i.e., AVLT). **Table 1** shows the detailed demographic characteristics of the participants. This study was

TABLE 1 | Demographics of participants [mean \pm SD (range)].

| | NC (n = 36) | svMCI (n = 29) | aMCI (n = 33) |
|-----------------------|--------------------------|---------------------------|-------------------------|
| Gender (M/F) | 16/20 | 11/18 | 13/20 |
| Age (years) | 62.5 \pm 6.6 (46–76) | 63 \pm 8.7 (46–77) | 66 \pm 8.4 (51–80) |
| Years of education | 9.9 \pm 4.6 (0–17) | 8.6 \pm 3.7 (0–17) | 10.8 \pm 4.1 (0–18) |
| AVLT-immediate recall | 8.8 \pm 1.9 (5.3–13.7) | 6.9 \pm 1.9 (3.3–10.3)* | 6.0 \pm 1.5 (3.3–9)* |
| AVLT-delayed recall | 9.39 \pm 3.26 (0–15) | 6.2 \pm 3.0 (0–13)* | 3.5 \pm 3.0 (0–12)* |
| AVLT-recognition | 11.17 \pm 2.68 (3–15) | 10.07 \pm 2.4 (3–14) | 7.1 \pm 4.2 (3–14) |
| MMSE | 27.3 \pm 2.3 (21–30) | 25.6 \pm 3.4 (16–30) | 24.9 \pm 3.1 (17–30)* |
| MoCa | 26.0 \pm 3.5 (15–30) | 19.9 \pm 3.9 (13–26)* | 19.7 \pm 4.1 (11–26)* |

ANOVA was performed, followed by Bonferroni post hoc analysis.

* $P < 0.05$ between NC and svMCI or aMCI.

NC, normal controls; svMCI, vascular mild cognitive impairment; aMCI, amnesic mild cognitive impairment; AVLT, auditory verbal learning test; MMSE, Mini Mental Status Examination; MoCa, Montreal Cognitive Assessment.

approved by the medical research ethics committee and the institutional review board of Xuanwu Hospital, Capital Medical University, Beijing, China.

Image Acquisition

Structural MR images were acquired using sagittal magnetization-prepared rapid gradient echo (MP-RAGE) three-dimensional T1-weighted imaging sequence on a 3.0 T Siemens scanner at Xuanwu Hospital, Capital Medical University. The image parameters included repetition time (TR) = 1,900 ms; echo time (TE) = 2.2 ms; inversion time = 900 ms; flip angle = 9°; field of view = 224 mm \times 256 mm; matrix size = 448 \times 512; 176 slices; and slice thickness = 1.0 mm.

Segmentation of Hippocampal Subfields

Automated segmentation of the hippocampal subfields was performed with the hippo-subfields module in FreeSurfer version 5.3,¹ which uses the Bayesian statistical model built from manual segmentation of the right hippocampus in 0.38 mm \times 0.38 mm \times 0.8 mm *in vivo* MRI scans in 10 subjects (34). The results consisted of a collection of images that indicated each voxel's posterior probability of belonging to different subregions in native space. By maximizing the posterior probability of the different subregions, the hippocampus of each subject was segmented to seven subfields: CA1, CA2/3, CA4/DG, presubiculum, subiculum, fimbria, and the hippocampal fissure. Previous research has reported that the fimbria and the hippocampal fissure showed relatively lower segmentation accuracies than other subfields (35, 36). Importantly, because the fimbria (white matter) and hippocampal fissure (cerebrospinal fluid) did not belong to GM, they were discarded in the subsequent SCN analysis. There is an illustration for the right hippocampal subfield segmentations for one NC subject in **Figure 1**.

Image Processing

First, non-uniformity intensity correction of the structural magnetic resonance imaging data was performed with FreeSurfer.

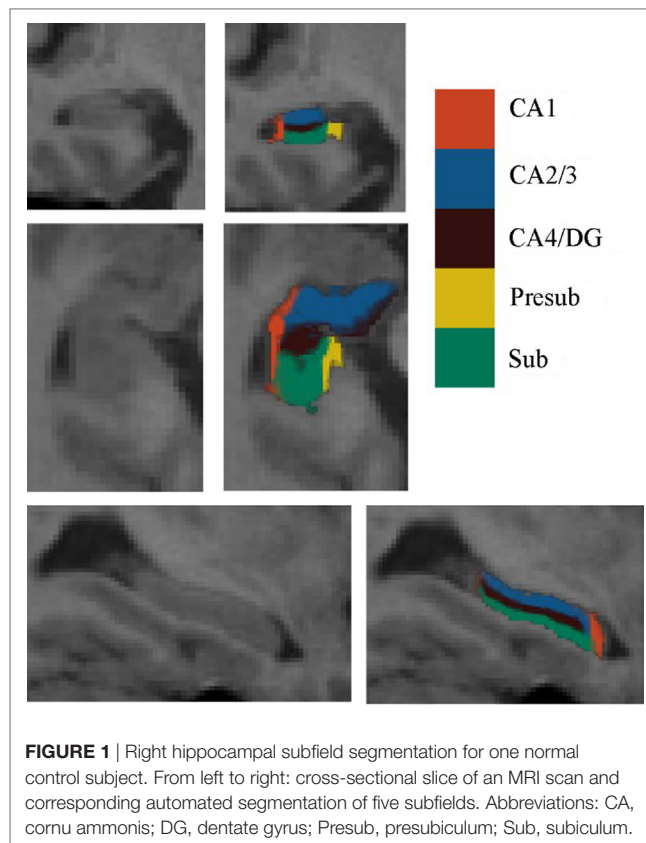


FIGURE 1 | Right hippocampal subfield segmentation for one normal control subject. From left to right: cross-sectional slice of an MRI scan and corresponding automated segmentation of five subfields. Abbreviations: CA, cornu ammonis; DG, dentate gyrus; Presub, presubiculum; Sub, subiculum.

Then, the results after NU intensity correction were analyzed using Statistical Parametric Mapping software package in MATLAB (SPM12²). Following the inspection of image quality, we used VBM (VBM8 toolbox³) to extract the GM volume map of each subject (37). Additionally, we employed a spatially adaptive non-local denoising filter (38) and a hidden Markov random field model (39) to reduce the impact of noise in the GM volume map. Then, the images were transformed into the DARTEL template (40) from the Montreal Neurological Institute (MNI) space through the high-dimensional diffeomorphic anatomical registration using the exponentiated lie algebra (DARTEL) approach, which is a non-linear spatial normalization method. Subsequently, the voxel values were modulated to preserve regional volume information using the Jacobian determinants (41). Finally, we smoothed the modulated images using Gaussian Kernel specified in 12 mm full width at half maximum.

Definition of Seed Regions

For each subject, the deformation field derived from the NU intensity corrected image to normalized image was applied to the hippocampal subfields' label image in native space. To reduce the possible impact of segmentation inaccuracy on subsequent analysis, the transformed hippocampal subfield labels were combined for all subjects and the 100% overlapped regions were

¹<http://freesurfer.net>.

²<http://www.fil.ion.ucl.ac.uk/spm>.

³<http://www.neuro.uni-jena.de/vbm/>.

selected. Then, these regions on each side were masked using the hippocampal label from the Harvard-Oxford subcortical structural atlas. Additionally, if there existed overlap for any two hippocampal subfields, the overlapped regions were removed. After that, the seed region for each hippocampal subfield was defined in MNI space. All the seed regions (in black color) were overlaid to the probabilistic atlas (in Heat color) of hippocampal subfields (34), as shown in **Figure 2**. The seeds almost located within the atlas.

Construction of Structural Covariance Networks

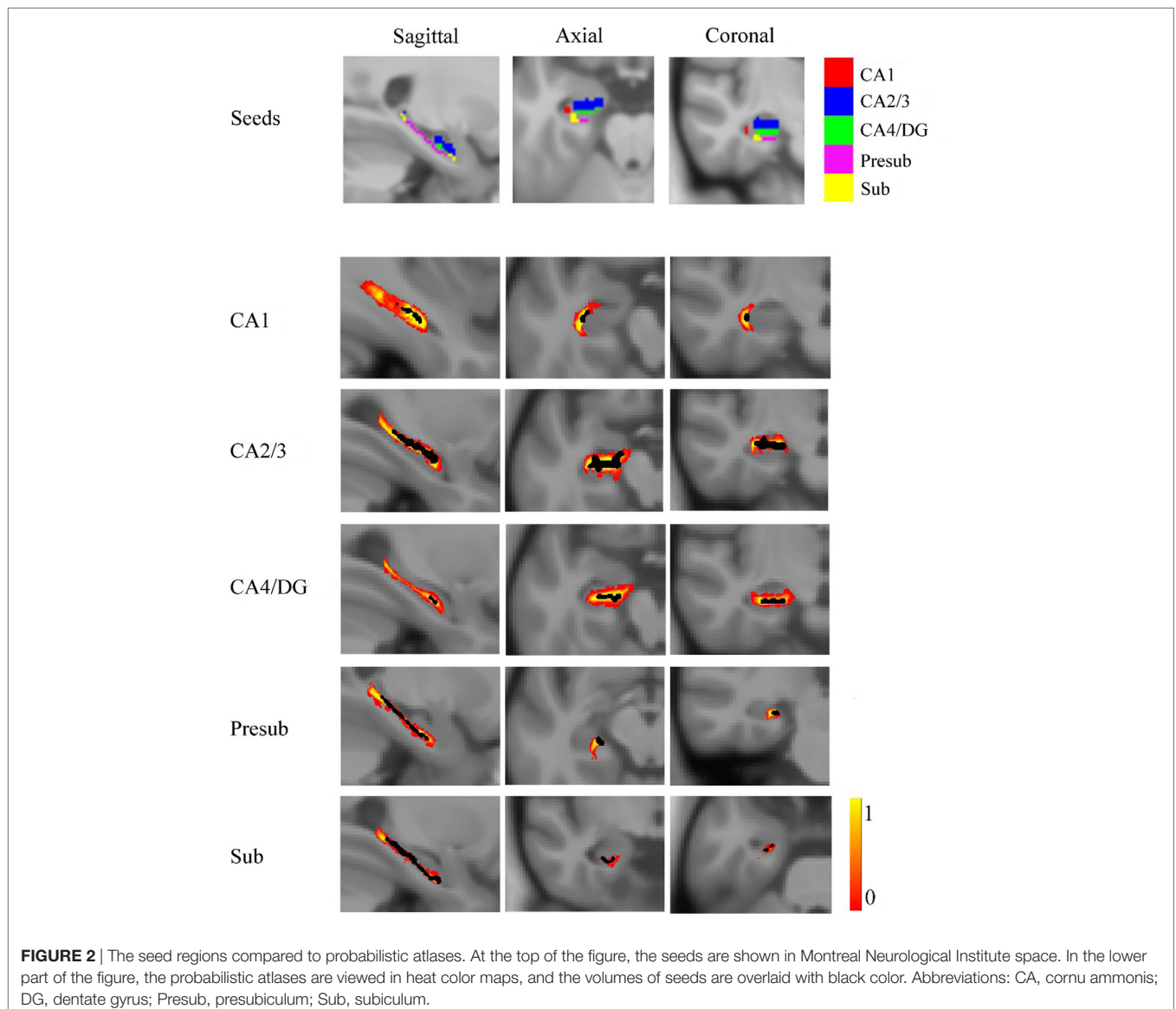
For each group, the strength of structural covariance between each subfield seed and all other regions across the whole brain were obtained by applying multiple regression models in SPM12 to perform a voxel-based statistical analysis on the smoothed and modulated GM image. We imported the extracted mean

GM volume from each seed as a covariate. As the age and gender would influence the GM volumes, we removed the effects of gender and age on the structural covariance networks by entering them as confounding covariates. The resulting covariance patterns were employed with thresholds at $P < 0.05$ with the false discovery rate (FDR) correction and reserved positive covariance. Finally, the results were displayed on the MNI template in the BrainNet Viewer software⁴ (42).

Between-Group Differences in the Structural Association

Many studies have indicated that the different slopes for any pair of voxels may represent the difference in their structural association (43, 44). To evaluate the difference in strength of structural covariance between groups, we performed a between-group

⁴<http://www.nitrc.org/projects/bnv/>.



analysis of slopes. The analysis used a multiple classic interaction linear model:

$$y = \beta_0 + \beta_1 X + \beta_2 G + \beta_3 (G \times X) + \beta_4 \text{Age} + \beta_5 \text{Gender} + \varepsilon$$

G was used as a grouping variable, and two groups were put into the same model, where $G = 1$ for the one group, and $G = 0$ for another group. The gender and age may affect the association of two voxels, so they were considered as independent variables in a linear model, where X represented the averaged GM volume in each seed, and y represented the GM volumes of each voxel in whole brain. Then, the linear regression model between y and X was adjusted by adding a gender term *Gender*, an age term *Age*, a group term G , and an interaction term $G \times X$. Specific t -value contrasts were established to map the significant different voxels in slopes between any two groups. The significant differences between groups were obtained based on the two-tailed Gaussian random field (GRF) correction, with a voxel level of $P < 0.01$ and a cluster level of $P < 0.05$.

RESULTS

Demographics

Table 1 shows demographics of the healthy controls, svMCI patients, and aMCI patients. There were no significant differences in sex, age, and years of education between groups. However, significant differences between groups were found in the AVLT-immediate recall ($F = 12.059$, $P < 0.001$), AVLT-delayed recall ($F = 11.501$, $P < 0.001$), AVLT-recognition recall ($F = 2.804$, $P = 0.066$), MMSE ($F = 3.3765$, $P = 0.27$), and Montreal Cognitive Assessment ($F = 27.276$, $P < 0.001$) through one-way analysis of variance. The following *post hoc* test revealed that AVLT-immediate recall, AVLT-delayed recall, and MoCa in patients of aMCI and svMCI were significantly lower than scores in controls. In addition, the score of MMSE was significantly lower in the aMCI group than in the control group, but there was no significant difference in score of MMSE between the svMCI and NC groups.

Structural Covariance Networks Within Groups

The SCN patterns of the left and right hippocampal subfields in the three groups are shown in **Figures 3** and **4**, respectively. Each of the hippocampal subfield seed regions covaried with the ERC and fusiform gyrus (FFG) among the three groups. The regions showing significant correlations with hippocampal subfields were relatively larger in the aMCI group than the svMCI group and NC group.

Structural Covariance Networks in the aMCI Group

Left

In the aMCI group, in addition to the ERC and FFG, the left CA1 covaried with the left temporal pole (TP), right angular gyrus, subcallosal cortex, and thalamus. For the left CA2/3 network, the structural maps involved the ERC and FFG, subcallosal cortex, thalamus, and angular gyrus. The left CA4/DG correlated regions were similar to the regions in the left CA2/3 network in

the aMCI group, but it additionally included the right superior frontal gyrus. For the aMCI group, the left subiculum and left presubiculum covariance maps involved the left TP, subcallosal cortex, thalamus, superior and middle frontal gyrus, right middle occipital gyrus, and bilateral angular gyrus.

Right

In the aMCI group, the right CA1 covaried with the ERC and FFG, right TP, PCC, and angular gyrus. CA2/3 showed significant correlation with entorhinal areas, thalamus, bilateral TP, middle frontal gyrus, PCC, and angular gyrus. The CA4/DG correlated regions were similar to the regions covaried with the right CA2/3 subfield in the aMCI group. For the right presubiculum networks, the covariance maps of the right presubiculum involved entorhinal areas, thalamus, bilateral TP, PCC, and angular gyrus. The subiculum showed significant covariance with the ERC, FFG, and right angular gyrus.

Structural Covariance Networks in the svMCI Group

Left

The left CA1 showed significant correlations with the ERC, FFG, superior occipital gyrus, orbitofrontal cortex (OFC), and right TP in the svMCI group. The covariance maps of the left CA2/3 involved the FFG, right TP, OFC, occipital pole, and entorhinal areas in the svMCI group. The left CA4/DG covariance maps were similar to the covariance maps of the left CA2/3 in the svMCI group. In the svMCI group, the maps of the left presubiculum and left subiculum were virtually identical, and the covaried regions included the FFG, ERC, fusiform, and right TP.

Right

The right CA1 covaried with the ERC, FFG, superior occipital gyrus, right TP, and OFC in the svMCI group. The right CA2/3 covaried with entorhinal areas, right TP, and superior occipital gyrus. The right CA4/DG covaried with entorhinal areas, fusiform, right TP, superior occipital gyrus, and subcallosal cortex. The regions covaried with the right presubiculum were similar to those regions connected with the right CA4/DG subfield in the svMCI group. In addition, the covariance maps of the right subiculum hippocampal subfields involved entorhinal areas, fusiform, right TP, and superior occipital gyrus.

Structural Covariance Networks in the NC Group

Left

The left CA1 covaried with the bilateral ERC and FFG in the NC group. In addition to the ERC and FFG, the covariance regions with the left CA2/3 also included the left precuneus cortex. The left CA4/DG covariance maps were extremely similar to the maps of the left CA1 subfield in the NC group. For the left subiculum and left presubiculum networks, both covariance maps involved the left precentral gyrus, FFG, and ERC in NC subjects.

Right

The right CA1 covaried with the ERC and FFG in the NC group. In addition to the ERC and FFG, the covariance regions with the right CA2/3 also involved the right OFC. The right CA4/DG

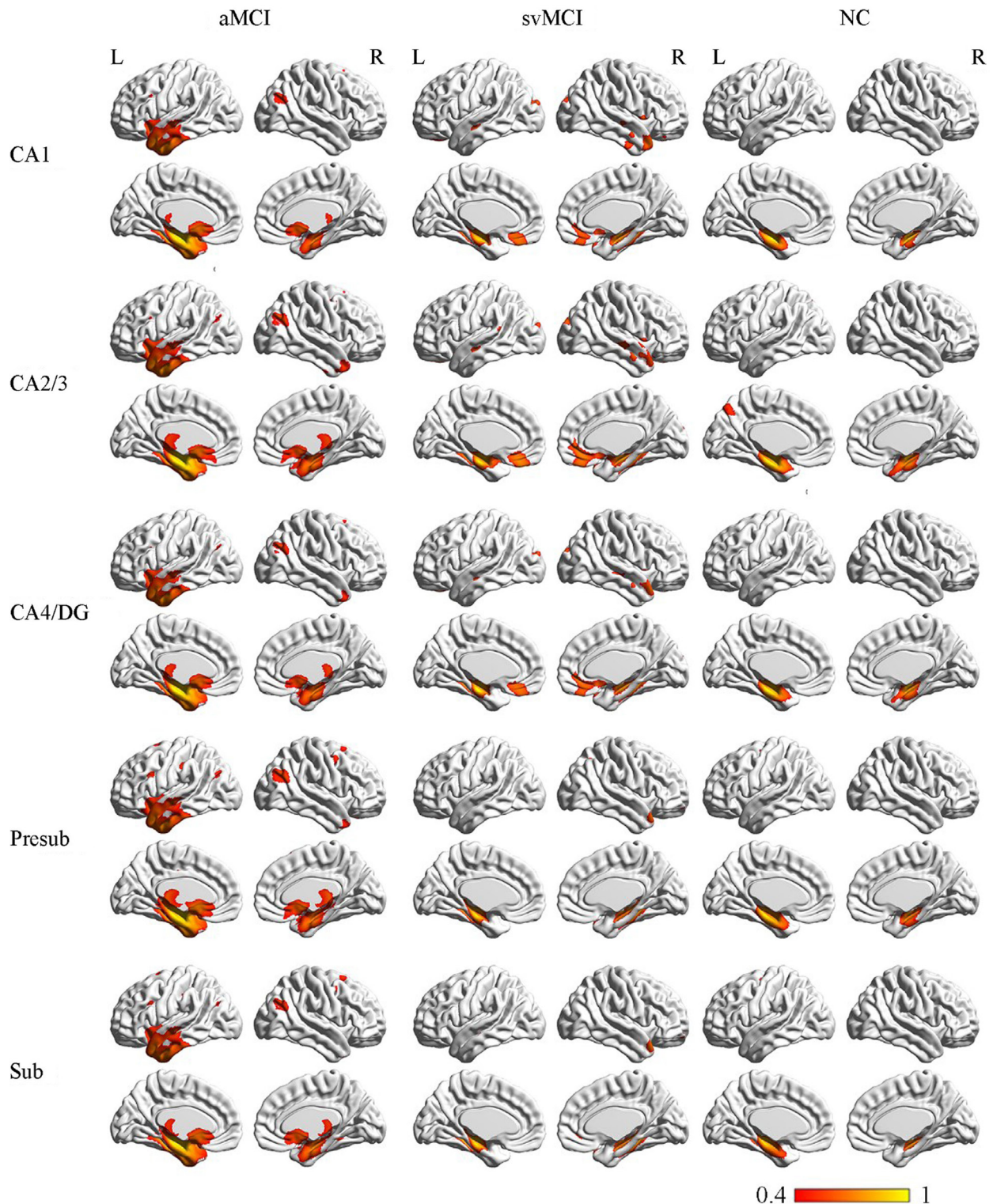


FIGURE 3 | Structural covariance networks of left hippocampal subfields in the three groups. Statistical maps of regions significantly correlated with the seed region in each group. The results are presented as CC values ($P < 0.05$, false discovery rate corrected). Abbreviations: L, left; R, right; CC, correlation coefficient; NC, normal controls; svMCI, vascular mild cognitive impairment; aMCI, amnesic mild cognitive impairment; CA, cornu ammonis; DG, dentate gyrus; Presub, presubiculum; Sub, subiculum.

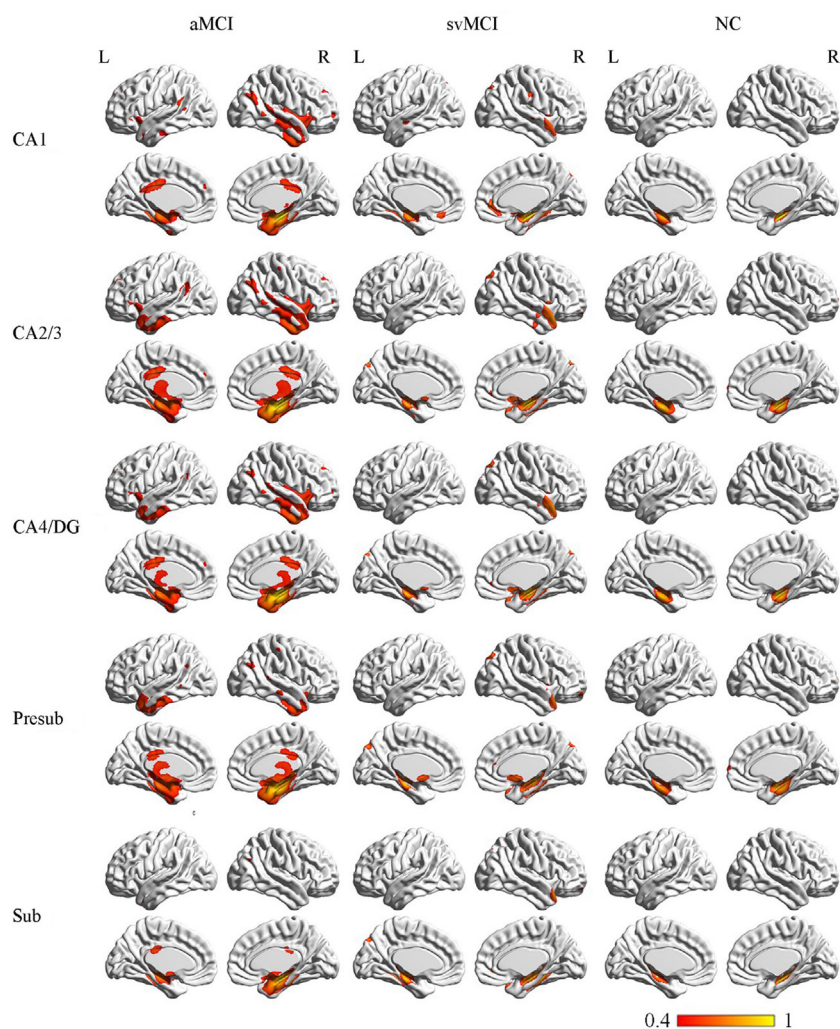


FIGURE 4 | Structural covariance networks of right hippocampal subfields in the three groups. Statistical maps of regions significantly correlated with the seed region in each group. The results are presented as CC values ($P < 0.05$, false discovery rate corrected). Abbreviations: L, left; R, right; CC, correlation coefficient; NC, normal controls; svMCI, subcortical vascular mild cognitive impairment; aMCI, amnesic mild cognitive impairment; CA, cornu ammonis; DG, dentate gyrus; Presub, presubiculum; Sub, subiculum.

correlated regions included the ERC and FFG in the NC group. The right presubiculum showed significant correlations with the right OFC, FFG, and ERC in NC subjects. The right subiculum covaried with the ERC and FFG.

Significant Difference in the Structural Associations Between Groups

aMCI Group vs. NC Group

There were some significant differences observed between the aMCI group and NC group when the strength of the structural correlations was considered (Table 2; Figure 5). There was a significant increased association between the hippocampal subfields and other brain regions that was found in the aMCI group compared to the NC group. The left CA1, left CA4/DG, left presubiculum, and left subiculum showed increased covariance with the left pole in the aMCI group compared to NC.

In addition, increased significant covariance was found between the left CA1/left subiculum and left postcentral gyrus (POG), right CA2/3 and right middle/inferior temporal gyrus (ITG), and right CA1 and left angular gyrus in the aMCI group compared to the NC group.

svMCI Group vs. NC Group

The significant differences of the association slope between the svMCI group and the NC group are shown in Table 2 and Figure 6. There were significant increased associations between the bilateral CA1/left CA2/3 and OFC in the svMCI group compared to the NC group. Then, the left presubiculum showed increased covariance with the right FFG in the aMCI group relative to the svMCI group. The right CA1 showed increased covariance with the right prefrontal gyrus in the svMCI group compared to the NC group.

TABLE 2 | Significant between-group differences in structural association between selected regions of interest and other cortical areas.

| Contrast | Seed | BA | Region | MNI coordinates | | | Peak intensity | Cluster size (voxels) |
|-----------------------|----------------|----------|-----------|-----------------|-----|-----|----------------|-----------------------|
| | | | | X | Y | Z | | |
| aMCI vs. NC | | | | | | | | |
| aMCI > NC | L_CA1 | 21/20 | L TP | -60 | 6 | -23 | 3.58 | 3,132 |
| | L_CA1 | 3/4/6 | L POG/PRG | -47 | -23 | 63 | 3.75 | 1,472 |
| | L_CA4/DG | 21/20 | L TP | -59 | 6 | -23 | 3.49 | 2,047 |
| | L_presubiculum | 21/20 | L TP | -57 | 9 | -26 | 3.44 | 5,562 |
| | L subiculum | 3/4/6 | L POG/PRG | -50 | -23 | 60 | 3.93 | 1,796 |
| | L subiculum | 21/20 | L TP | -57 | 8 | -23 | 3.63 | 3,135 |
| | R_CA1 | 40/39 | L ANG/SMG | -51 | -51 | 15 | 3.76 | 1,594 |
| | R_CA2/3 | 21/20 | R MTG/ITG | 53 | -33 | -17 | 3.71 | 1,386 |
| svMCI vs. NC | | | | | | | | |
| svMCI > NC | L_CA1 | 11/10 | OFC | -8 | 39 | -23 | 4.23 | 2,359 |
| | R_CA1 | 11/10 | OFC | -8 | 39 | -17 | 3.91 | 2,432 |
| | R_CA1 | 10 | R PFC | 36 | 62 | 11 | 3.99 | 1,657 |
| | L_CA2/3 | 11 | OFC | -5 | 41 | -24 | 3.91 | 1,564 |
| | L_presubiculum | 36/37 | R FFG | 35 | -33 | -14 | 4.05 | 2,261 |
| aMCI vs. svMCI | | | | | | | | |
| aMCI > svMCI | L_presubiculum | 34/28/35 | L ERC/PRC | -11 | -6 | -21 | 4.58 | 1,653 |
| | L_subiculum | 34/28/35 | L ERC/PRC | -11 | -5 | -21 | 4.17 | 1,811 |
| | R_presubiculum | 34/28/35 | R ERC/PRC | 15 | -9 | -21 | 4.37 | 1,188 |
| | R_subiculum | 34/28/35 | R ERC/PRC | 15 | -9 | -26 | 3.79 | 1,214 |
| svMCI > aMCI | L_CA4/DG | 36/37 | R FFG | 35 | -33 | -17 | 4.36 | 1,403 |
| | L_presubiculum | 36/37 | R FFG | 27 | -33 | -14 | 4.32 | 1,987 |
| | L_subiculum | 36/37 | R FFG | 38 | -38 | -11 | 4.59 | 2,208 |

The regions listed showed significant between-group differences (Gaussian random field-corrected at voxel level: $P < 0.01$ and cluster level: $P < 0.05$), and peak coordinates are reported in standard MNI space.

BA, Brodmann area; L, left; R, right; NC, normal controls; svMCI, vascular mild cognitive impairment; aMCI, amnesic mild cognitive impairment; CA, cornu ammonis; DG, dentate gyrus; ERC, entorhinal cortex; FFG, fusiform gyrus; TP, temporal pole; MTG, middle temporal gyrus; ITG, inferior temporal gyrus; POG, postcentral gyrus; PRG, precentral gyrus; PRC, perirhinal cortex; OFC, orbitofrontal cortex; PFC, prefrontal cortex; SMG, supramarginal gyrus; ANG, angular gyrus.

aMCI Group vs. svMCI Group

As shown in **Table 2** and **Figure 7**, there were significant increased associations between several hippocampal subfields (bilateral presubiculum, bilateral subiculum) and the bilateral ERC in the aMCI group compared to the svMCI group. Then, left hippocampal subfields mostly showed decreased covariance with the right FFG in the aMCI group relative to the svMCI group.

DISCUSSION

In this study, we selected hippocampal subfields as seeds to build SCNs among three groups. Specifically, hippocampal subfields correlated with the TP, thalamus, subcallosal cortex, and posterior cingula cortex in the aMCI group, while hippocampal subfields significantly covaried with the OFC in the svMCI group. Finally, we compared the differences in strength of structural covariance between groups. The results demonstrated that there were abnormal structural associations between hippocampal subfields and the cerebral cortex in aMCI and svMCI patients, and these abnormalities were different between them.

Structural Covariance Networks Within Groups

In our study, positive correlations between hippocampal subfields and FFG, and ERC in GM volume were found in each group.

To some extent, these positive correlations suggested synchronous GM changes in these regions (29, 32). The ERC and FFG are anatomically adjacent to the hippocampus. Importantly, there were many intrinsic connections between the hippocampus, ERC, and FFG (7).

All the hippocampal subfields showed significantly positive structural covariance with the thalamus in the aMCI group. A previous study reported atrophy of the thalamus in aMCI patients (45). The positive structural covariance could be explained by the synchronous atrophy between the thalamus and hippocampus in the aMCI group. The subiculum and entorhinal cortices were found to project to the thalamus (1). There were many disruptions in the thalamus functional connectivity in aMCI including thalamo-hippocampus, thalamo-temporal, thalamo-visual, and thalamo-default network (46). Some cognitive impairments in aMCI, such as visual-spatial perception syndrome and visual hallucinations, may be due to thalamus atrophy and abnormalities in thalamus-related networks.

We also observed positive structural associations between the left hippocampal subfields and subcallosal cortex in the aMCI group. This suggested right subcallosal cortex atrophy in aMCI patients (47). In addition, significant correlations between cognitive scores on the episodic memory task and increased functional connectivity between the subcallosal cortex and hippocampus were found in aMCI patients (48). This indicated

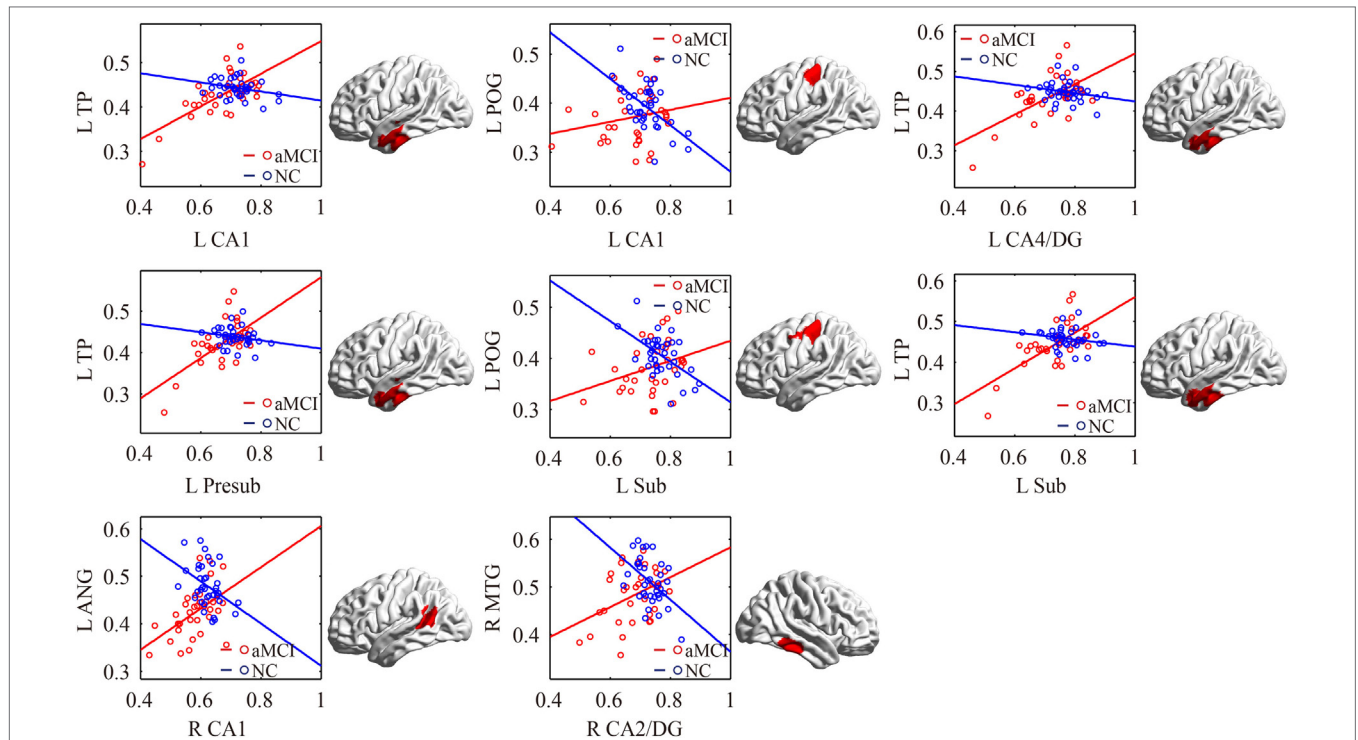


FIGURE 5 | Significant between-group differences in structural association for aMCI and NC. A cluster showing significant structural difference (Gaussian random field-corrected at voxel level: $P < 0.01$ and cluster level: $P < 0.05$) between aMCI and NC is presented on the right, and a plot of slope differences between the seed region and cluster region is presented on the left. Abbreviations: L, left; R, right; NC, normal controls; aMCI, amnesic mild cognitive impairment; CA, cornu ammonis; DG, dentate gyrus; Presub, presubiculum; Sub, subiculum; TP, temporal pole; POG, postcentral gyrus; ANG, angular gyrus.

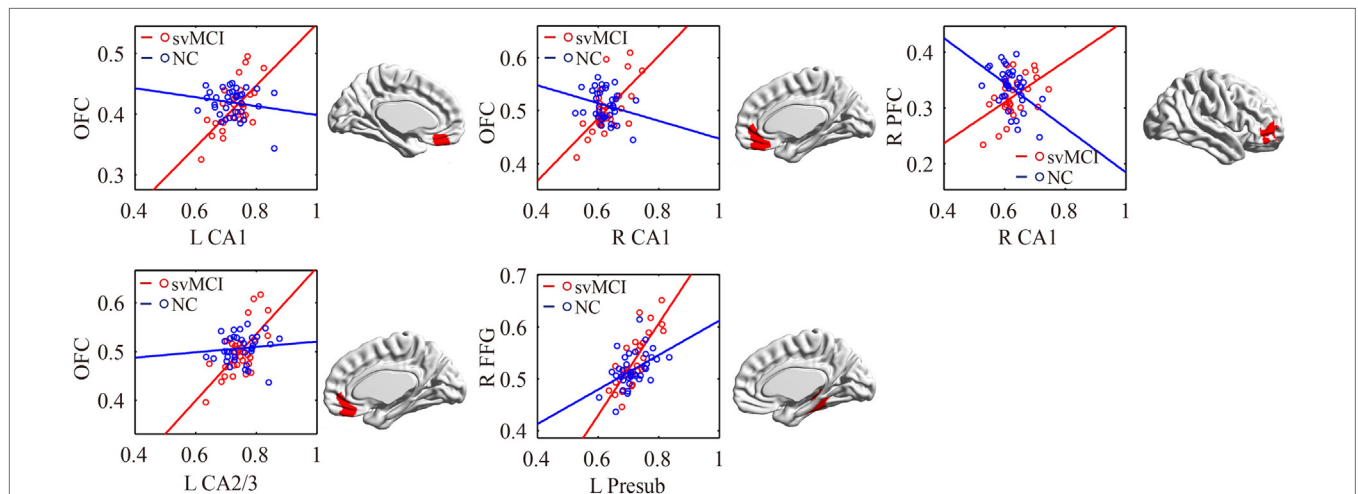
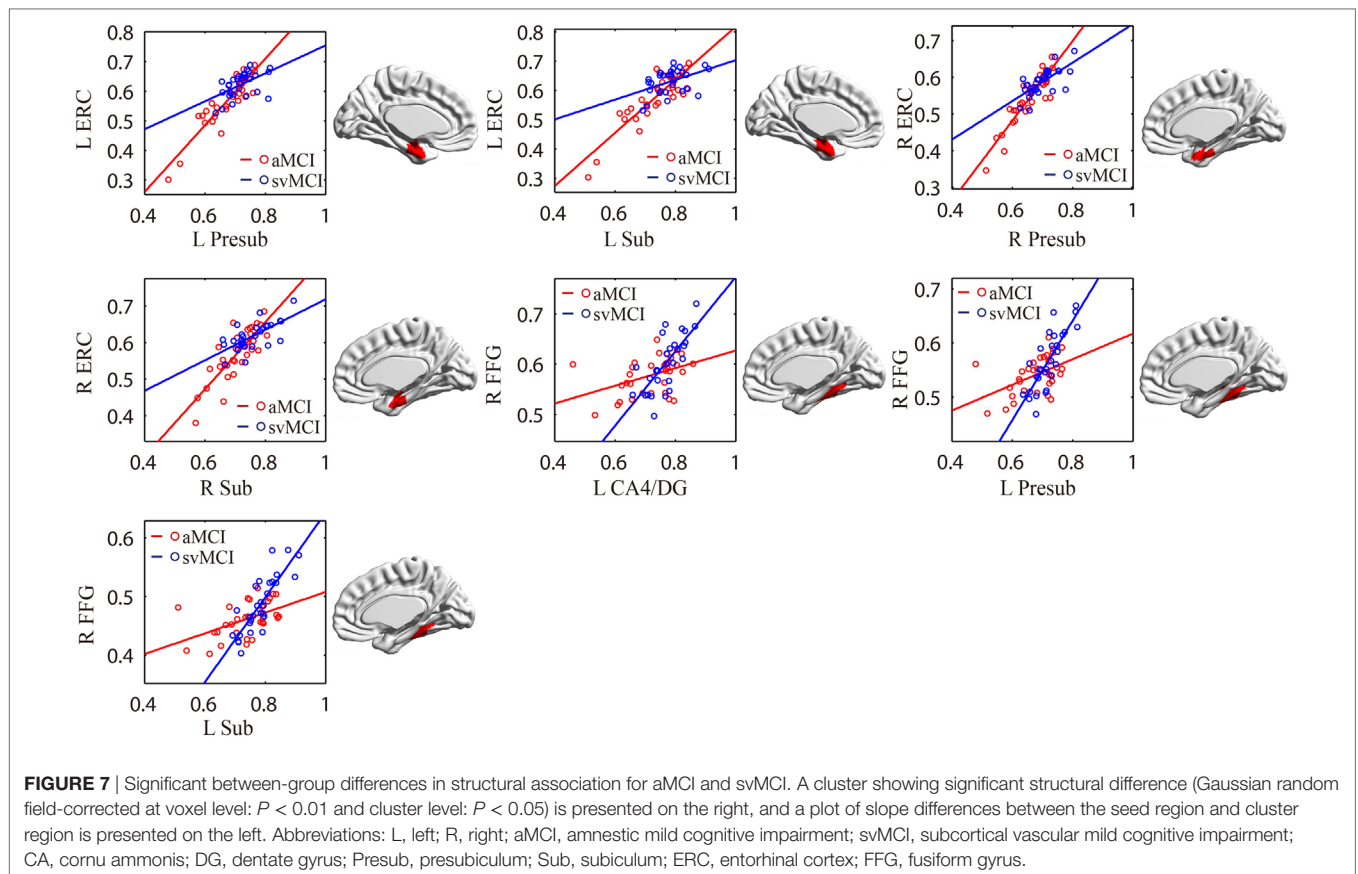


FIGURE 6 | Significant between-group differences in structural association for svMCI and NC. A cluster showing significant structural difference (Gaussian random field-corrected at voxel level: $P < 0.01$ and cluster level: $P < 0.05$) between svMCI and NC is presented on the right, and a plot of slope differences between the seed region and cluster region is presented on the left. Abbreviations: L, left; R, right; NC, normal controls; svMCI, subcortical vascular mild cognitive impairment; CA, cornu ammonis; DG, dentate gyrus; Presub, presubiculum; Sub, subiculum; OFC, orbitofrontal cortex; PFC, prefrontal cortex; FFG, fusiform gyrus.

that the abnormal structural correlations in the subcallosal cortex could be related to the observed memory deficits in aMCI patients.

We found significantly positive structural associations between the right hippocampal subfields and PCC in the aMCI

group. Many histopathological (49), structural (50), and functional imaging (51, 52) studies consistently reported that the PCC was an important structure in the pathophysiology of AD and aMCI. Importantly, the functional disconnection of hippocampal subregions and PCC may be a main factor of impaired episodic



memory in aMCI (20). Because the developmental trajectory of the structural network may associate with its functional specialization (53), the abnormality between PCC and hippocampal subfields may underpin the episodic memory deficits observed in aMCI.

Significant Differences in SCNs Between Groups

We observed that the increased connections between the right FFG and left presubiculum were stronger in svMCI than in the aMCI and NC groups. Previous studies have shown FFG atrophy in svMCI patients (24, 54). The FFG is related to semantic processing (55). Thus, the abnormal structural correlations between hippocampal subfields and the FFG could have an effect on the reduced capacity for semantic memory. Our results indicated that abnormality between the hippocampal subfields and FFG was distinct in svMCI, which was characterized by the main deficit of semantic memory compared to aMCI.

In the aMCI group, compared to the svMCI group, we observed an increased association between the bilateral presubiculum/subiculum and the ERC. The pathway from CA1 to the subiculum and projections to the ERC form the principal output from the hippocampus. The connections between CA1, subiculum, and ERC were associated with episodic memory processing (26). Therefore, the synchronous atrophy in the ERC and hippocampal subregions may suggest the disruption of episodic memory distinctly in aMCI patients.

The left CA1/CA4/DG/subiculum showed significantly increased structural association with the left TP in aMCI patients compared to NC. The stronger structural covariance potentially indicates synchronous GM changes in these regions affected by the disease (29). Thus, we speculate that the increased structural covariance between hippocampal subfields and the temporal gyrus suggests synchronous atrophy in the aMCI group. Several studies have shown atrophy in the temporal gyrus, especially in the medial and ITG, which supports our results (8, 56). The TP is associated with both social and emotional processes, which mainly involves face recognition and theory of mind (57). Chen et al. also indicated decreased connectivity between the middle hippocampus and middle temporal gyrus (MTG) in functional connectivity (26). We assumed that the synchronous atrophy between the hippocampus and MTG could explain the disrupted functional connectivity between them.

We also observed increased structural associations between the left CA1/subiculum and left POG in aMCI compared to NC. Left POG atrophy was reported in aMCI patients (58). Additionally, NC subjects had greater activations than aMCI patients during “Binds,” which probe object memory in the left POG, and our findings on the abnormal structural correlation with the left POG could be related to early signs of object memory deficits in aMCI patients (53).

In addition, bilateral CA1 and left CA2/3 showed significantly positive associations with the OFC in the svMCI group compared

to the NC group. In addition, we found increased covariance between the right CA1 and right PFC in svMCI compared to NC. For PET imaging, the patients with svMCI showed hypometabolism in the inferior and medial frontal cortices adjacent to the cingulate gyrus (59). Importantly, the prefrontal gyrus is associated with executive function, which has a deficit in svMCI patients (60). Additionally, frontal-subcortical circuits, including hippocampus and OFC, mediate many aspects of human behavior, especially executive function (61). We assume that abnormal structural covariance between hippocampal subfields and the OFC indicates deficit of executive function in svMCI patients.

This study still has several limitations. First, we did not study the structural connectivity based on diffusion-weighted imaging (DWI) of the white matter pathway between hippocampal subfields and the whole brain cortex. There was a lack of systematic comparisons of structural covariance networks and DWI-based networks. Our findings of SCNs among the three groups should be cautiously extended to other structural networks. Second, in this study, due to the limited segmentation accuracies of hippocampal subfields in regular T1 images, we focused on the SCN analysis of each subfield instead of volumetric analysis of subfields. In the future, the volumetric analysis of hippocampal subfields would be helpful to understand the hippocampal

abnormalities in the two MCI subtypes with the improvement of segmentation accuracies of hippocampal subfields in regular T1 images.

ETHICS STATEMENT

This study was approved by the medical research ethics committee and the institutional review board of Xuanwu Hospital, Capital Medical University, Beijing, China.

AUTHOR CONTRIBUTIONS

Conceived and designed the experiments: SL and XL. Analyzed the data: XW. Contributed reagents/materials/analysis tools: YY, YH, CY, and WZ. Wrote the paper: XW, SL, XL, QL, and YY.

FUNDING

This work was supported by National Natural Science Foundation of China (Grant No. 81622025, 81471731, 31371007, 81430037, 81771795 and 61633018), the Fundamental Research Funds for the Central Universities (No. YWF-17-BJ-J-11), and National Key Research and Development Program of China (No. 2016YFC1306300).

REFERENCES

- Amaral D, Lavenex P. Hippocampal neuroanatomy. In: Andersen P, Morris R, Amaral D, Bliss T, O'Keefe J, editors. *The Hippocampus Book*. New York: Oxford University Press (2007). p. 37–144.
- Harrison PJ. The hippocampus in schizophrenia: a review of the neuropathological evidence and its pathophysiological implications. *Psychopharmacology* (2004) 174(1):151–62. doi:10.1007/s00213-003-1761-y
- Kuruba R, Hattiangady B, Shetty AK. Hippocampal neurogenesis and neural stem cells in temporal lobe epilepsy. *Epilepsy Behav* (2009) 14(1):65–73. doi:10.1016/j.yebeh.2008.08.020
- Hampel H, Bürger K, Teipel SJ, Bokde AL, Zetterberg H, Blennow K. Core candidate neurochemical and imaging biomarkers of Alzheimer's disease. *Alzheimer Dement* (2008) 4(1):38–48. doi:10.1016/j.jalz.2007.08.006
- Duvernoy HM. *The Human Hippocampus: Functional Anatomy, Vascularization and Serial Sections with MRI*. Springer Science & Business Media (2005).
- Fanselow MS, Dong H-W. Are the dorsal and ventral hippocampus functionally distinct structures? *Neuron* (2010) 65(1):7–19. doi:10.1016/j.neuron.2009.11.031
- Rajmohan V, Mohandas E. The limbic system. *Indian J Psychiatry* (2007) 49(2):132. doi:10.4103/0019-5545.33264
- Whitwell JL, Shiung MM, Przybelski S, Weigand SD, Knopman DS, Boeve BF, et al. MRI patterns of atrophy associated with progression to AD in amnesic mild cognitive impairment. *Neurology* (2008) 70(7):512–20. doi:10.1212/01.wnl.0000280575.77437.a2
- Li X, Li D, Li Q, Li Y, Li K, Li S, et al. Hippocampal subfield volumetry in patients with subcortical vascular mild cognitive impairment. *Sci Rep* (2016) 6. doi:10.1038/srep20873
- Petersen RC, Smith GE, Waring SC, Ivnik RJ, Tangalos EG, Kokmen E. Mild cognitive impairment: clinical characterization and outcome. *Arch Neurol* (1999) 56(3):303–8. doi:10.1001/archneur.56.3.303
- Petersen RC, Aisen P, Boeve BF, Geda YE, Ivnik RJ, Knopman DS, et al. Mild cognitive impairment due to Alzheimer disease in the community. *Ann Neurol* (2013) 74(2):199–208. doi:10.1002/ana.23931
- Sachdev P, Kalaria R, O'Brien J, Skoog I, Alladi S, Black SE, et al. Diagnostic criteria for vascular cognitive disorders: a VASCOG statement. *Alzheimer Dis Assoc Disord* (2014) 28(3):206. doi:10.1097/WAD.0000000000000034
- Murphy KJ, Troyer AK, Levine B, Moscovitch M. Episodic, but not semantic, autobiographical memory is reduced in amnesic mild cognitive impairment. *Neuropsychologia* (2008) 46(13):3116–23. doi:10.1016/j.neuropsychologia.2008.07.004
- Petersen RC. Mild cognitive impairment clinical trials. *Nat Rev Drug Discov* (2003) 2(8):646. doi:10.1038/nrd1155
- Visser PJ, Kester A, Jolles J, Verhey F. Ten-year risk of dementia in subjects with mild cognitive impairment. *Neurology* (2006) 67(7):1201–7. doi:10.1212/01.wnl.0000238517.59286.c5
- Mendonca A, Ribeiro F, Guerreiro M, Palma T, Garcia C. Clinical significance of subcortical vascular disease in patients with mild cognitive impairment. *Eur J Neurol* (2005) 12(2):125–30. doi:10.1111/j.1468-1331.2004.00892.x
- Erkinjuntti T. Subcortical ischemic vascular disease and dementia. *Int Psychogeriatr* (2003) 15(S1):23–6. doi:10.1017/S1041610203008925
- Kim SH, Kang HS, Kim HJ, Moon Y, Ryu HJ, Kim MY, et al. The effect of ischemic cholinergic damage on cognition in patients with subcortical vascular cognitive impairment. *J Geriatr Psychiatry Neurol* (2012) 25(2):122–7. doi:10.1177/0891988712445089
- Kwon OD. Cognitive features of vascular dementia. In: Heinbockel T, editor. *Neuroscience*. Rijeka, Croatia: InTech (2012). p 127–38.
- Bai F, Liao W, Watson DR, Shi Y, Wang Y, Yue C, et al. Abnormal whole-brain functional connection in amnesic mild cognitive impairment patients. *Behav Brain Res* (2011) 216(2):666–72. doi:10.1016/j.bbr.2010.09.010
- Gili T, Cercignani M, Serra L, Perri R, Giove F, Maraviglia B, et al. Regional brain atrophy and functional disconnection across Alzheimer's disease evolution. *J Neurol Neurosurg Psychiatry* (2011) 82(1):58–66. doi:10.1136/jnnp.2009.199935
- Yi L, Wang J, Jia L, Zhao Z, Lu J, Li K, et al. Structural and functional changes in subcortical vascular mild cognitive impairment: a combined voxel-based morphometry and resting-state fMRI study. *PLoS One* (2012) 7(9):e44758. doi:10.1371/journal.pone.0044758
- Nowrangi MA, Lyketsos CG, Leoutsakos J-MS, Oishi K, Albert M, Mori S, et al. Longitudinal, region-specific course of diffusion tensor imaging measures in mild cognitive impairment and Alzheimer's disease. *Alzheimer Dement* (2013) 9(5):519–28. doi:10.1016/j.jalz.2012.05.2186
- Zhou X, Hu X, Zhang C, Wang H, Zhu X, Xu L, et al. Aberrant functional connectivity and structural atrophy in subcortical vascular cognitive

- impairment: relationship with cognitive impairments. *Front Aging Neurosci* (2016) 8:14. doi:10.3389/fnagi.2016.00014
25. Bai F, Xie C, Watson DR, Shi Y, Yuan Y, Wang Y, et al. Aberrant hippocampal subregion networks associated with the classifications of aMCI subjects: a longitudinal resting-state study. *PLoS One* (2011) 6(12):e29288. doi:10.1371/journal.pone.0029288
 26. Chen J, Duan X, Shu H, Wang Z, Long Z, Liu D, et al. Differential contributions of subregions of medial temporal lobe to memory system in amnesic mild cognitive impairment: insights from fMRI study. *Sci Rep* (2016) 6:sre26148. doi:10.1038/srep26148
 27. Mechelli A, Friston KJ, Frackowiak RS, Price CJ. Structural covariance in the human cortex. *J Neurosci* (2005) 25(36):8303–10. doi:10.1523/JNEUROSCI.0357-05.2005
 28. Zielinski BA, Gennatas ED, Zhou J, Seeley WW. Network-level structural covariance in the developing brain. *Proc Natl Acad Sci U S A* (2010) 107(42):18191–6. doi:10.1073/pnas.1003109107
 29. Alexanderbloch A, Giedd JN, Bullmore E. Imaging structural co-variance between human brain regions. *Nat Rev Neurosci* (2013) 14(5):322–36. doi:10.1038/nrn3465
 30. McAlonan GM, Cheung V, Cheung C, Suckling J, Lam GY, Tai K, et al. Mapping the brain in autism. A voxel-based MRI study of volumetric differences and intercorrelations in autism. *Brain* (2004) 128(2):268–76. doi:10.1093/brain/awh332
 31. Cardoner N, Soriano-Mas C, Pujol J, Alonso P, Harrison BJ, Deus J, et al. Brain structural correlates of depressive comorbidity in obsessive-compulsive disorder. *Neuroimage* (2007) 38(3):413–21. doi:10.1016/j.neuroimage.2007.07.039
 32. Li X, Cao Q, Pu F, Li D, Fan Y, An L, et al. Abnormalities of structural covariance networks in drug-naïve boys with attention deficit hyperactivity disorder. *Psychiatry Res* (2015) 231(3):273–8. doi:10.1016/j.psychres.2015.01.006
 33. Petersen RC. Mild cognitive impairment as a diagnostic entity. *J Intern Med* (2004) 256(3):183–94. doi:10.1111/j.1365-2796.2004.01388.x
 34. Van Leemput K, Bakker K, Benner T, Wiggins G, Wald LL, Augustinack J, et al. Automated segmentation of hippocampal subfields from ultra-high resolution in vivo MRI. *Hippocampus* (2009) 19(6):549–57. doi:10.1002/hipo.20615
 35. Kühn S, Musso F, Mobascher A, Warbrick T, Winterer G, Gallinat J. Hippocampal subfields predict positive symptoms in schizophrenia: first evidence from brain morphometry. *Transl Psychiatry* (2012) 2(6):e127. doi:10.1038/tp.2012.51
 36. Koch K, Reess TJ, Rus OG, Zimmer C. Extensive learning is associated with gray matter changes in the right hippocampus. *Neuroimage* (2016) 125:627–32. doi:10.1016/j.neuroimage.2015.10.056
 37. Tohka J, Zijdenbos A, Evans A. Fast and robust parameter estimation for statistical partial volume models in brain MRI. *Neuroimage* (2004) 23(1):84–97. doi:10.1016/j.neuroimage.2004.05.007
 38. Manjón JV, Coupé P, Martí-Bonmati L, Collins DL, Robles M. Adaptive non-local means denoising of MR images with spatially varying noise levels. *J Magn Reson Imaging* (2010) 31(1):192–203. doi:10.1002/jmri.22003
 39. Rajapakse JC, Giedd JN, Rapoport JL. Statistical approach to segmentation of single-channel cerebral MR images. *IEEE Trans Med Imaging* (1997) 16(2):176–86. doi:10.1109/42.563663
 40. Ashburner J. A fast diffeomorphic image registration algorithm. *Neuroimage* (2007) 38(1):95–113. doi:10.1016/j.neuroimage.2007.07.007
 41. Good CD, Johnsrude IS, Ashburner J, Henson RNA, Friston KJ, Frackowiak RSJ. A voxel-based morphometric study of ageing in 465 normal adult human brains. *Neuroimage* (2001) 14(1):21–36. doi:10.1006/nimg.2001.0786
 42. Xia M, Wang J, He Y. BrainNet Viewer: a network visualization tool for human brain connectomics. *PLoS One* (2013) 8(7):e68910. doi:10.1371/journal.pone.0068910
 43. Lerch JP, Worsley K, Shaw WP, Greenstein DK, Lenroot RK, Giedd J, et al. Mapping anatomical correlations across cerebral cortex (MACACC) using cortical thickness from MRI. *Neuroimage* (2006) 31(3):993–1003. doi:10.1016/j.neuroimage.2006.01.042
 44. Li X, Pu F, Fan Y, Niu H, Li S, Li D. Age-related changes in brain structural covariance networks. *Front Hum Neurosci* (2013) 7(1):265–9. doi:10.3389/fnhum.2013.00098
 45. Balthazar M, Yasuda C, Pereira F, Pedro T, Damasceno B, Cendes F. Differences in grey and white matter atrophy in amnesic mild cognitive impairment and mild Alzheimer's disease. *Eur J Neurol* (2009) 16(4):468–74. doi:10.1111/j.1468-1331.2008.02408.x
 46. Cai S, Huang L, Zou J, Jing L, Zhai B, Ji G, et al. Changes in thalamic connectivity in the early and late stages of amnesic mild cognitive impairment: a resting-state functional magnetic resonance study from ADNI. *PLoS One* (2015) 10(2):e0115573. doi:10.1371/journal.pone.0115573
 47. Shiino A, Watanabe T, Maeda K, Kotani E, Akiguchi I, Matsuda M. Four subgroups of Alzheimer's disease based on patterns of atrophy using VBM and a unique pattern for early onset disease. *Neuroimage* (2006) 33(1):17–26. doi:10.1016/j.neuroimage.2006.06.010
 48. Bai F, Zhang Z, Watson DR, Yu H, Shi Y, Yuan Y, et al. Abnormal functional connectivity of hippocampus during episodic memory retrieval processing network in amnesic mild cognitive impairment. *Biol Psychiatry* (2009) 65(11):951–8. doi:10.1016/j.biopsych.2008.10.017
 49. Rowe CC, Ng S, Ackermann U, Gong SJ, Pike K, Savage G, et al. Imaging-amyloid burden in aging and dementia. *Neurology* (2007) 68(20):1718. doi:10.1212/01.wnl.0000261919.22630.ea
 50. Pengas G, Hodges JR, Watson P, Nestor PJ. Focal posterior cingulate atrophy in incipient Alzheimer's disease. *Neurobiol Aging* (2010) 31(1):25. doi:10.1016/j.neurobiolaging.2008.03.014
 51. Liang WS, Reiman EM, Valla J, Dunckley T, Beach TG, Grover A, et al. Alzheimer's disease is associated with reduced expression of energy metabolism genes in posterior cingulate neurons. *Proc Natl Acad Sci U S A* (2008) 105(11):4441. doi:10.1073/pnas.0709259105
 52. Sole AD, Clerici F, Chiti A, Lecchi M, Mariani C, Maggiore L, et al. Individual cerebral metabolic deficits in Alzheimer's disease and amnesic mild cognitive impairment: an FDG PET study. *Eur J Nucl Med Mol Imaging* (2008) 35(7):1357–66. doi:10.1007/s00259-008-0773-6
 53. Chiang HS, Mudar R, Rackley A, Venza E, Pudhivadath A, Van JJ, et al. An early fMRI marker of semantic memory deficits in people with amnesic mild cognitive impairment. *Alzheimers Dement* (2013) 9(4):580–580. doi:10.1016/j.jalz.2013.05.1151
 54. Li M, Meng Y, Wang M, Yang S, Wu H, Zhao B, et al. Cerebral gray matter volume reduction in subcortical vascular mild cognitive impairment patients and subcortical vascular dementia patients, and its relation with cognitive deficits. *Brain Behav* (2017) 7(8):e00745. doi:10.1002/brb3.745
 55. Wagner AD, Schacter DL, Rotte M, Koutstaal W, Maril A, Dale AM, et al. Building memories: remembering and forgetting of verbal experiences as predicted by brain activity. *Science* (1998) 281(5380):1188–91. doi:10.1126/science.281.5380.1188
 56. Duara R, Loewenstein D, Potter E, Appel J, Greig M, Urs R, et al. Medial temporal lobe atrophy on MRI scans and the diagnosis of Alzheimer disease. *Neurology* (2008) 71(24):1986–92. doi:10.1212/01.wnl.0000336925.79704.9f
 57. Olson IR, Plotzker A, Ezzyat Y. The enigmatic temporal pole: a review of findings on social and emotional processing. *Brain* (2007) 130(7):1718–31. doi:10.1093/brain/awm052
 58. Zhang H, Sachdev PS, Wen W, Kochan NA, Crawford JD, Brodaty H, et al. Gray matter atrophy patterns of mild cognitive impairment subtypes. *J Neurol Sci* (2012) 315(1–2):26–32. doi:10.1016/j.jns.2011.12.011
 59. Seo SW, Cho SS, Park A, Chin J, Na DL. Subcortical vascular versus amnesic mild cognitive impairment: comparison of cerebral glucose metabolism. *J Neuroimaging* (2009) 19(3):213–9. doi:10.1111/j.1552-6569.2008.00292.x
 60. Koehlin E, Summerfield C. An information theoretical approach to prefrontal executive function. *Trends Cogn Sci* (2007) 11(6):229–35. doi:10.1016/j.tics.2007.04.005
 61. Bonelli RM, Cummings JL. Frontal-subcortical circuitry and behavior. *Dialogues Clin Neurosci* (2007) 9(2):141–51.

Conflict of Interest Statement: The authors declare that the research was conducted in the absence of any commercial or financial relationships that could be construed as a potential conflict of interest.

Copyright © 2018 Wang, Yu, Zhao, Li, Li, Yin and Han. This is an open-access article distributed under the terms of the Creative Commons Attribution License (CC BY). The use, distribution or reproduction in other forums is permitted, provided the original author(s) and the copyright owner are credited and that the original publication in this journal is cited, in accordance with accepted academic practice. No use, distribution or reproduction is permitted which does not comply with these terms.



Differential Age-Related Changes in Structural Covariance Networks of Human Anterior and Posterior Hippocampus

Xinwei Li^{1,2}, Qionglin Li^{1,2}, Xuotong Wang^{1,2}, Deyu Li^{1,2*} and Shuyu Li^{1,2*}

¹ School of Biological Science and Medical Engineering, Beihang University, Beijing, China, ² Beijing Advanced Innovation Centre for Biomedical Engineering, Beihang University, Beijing, China

OPEN ACCESS

Edited by:

Chunhua Bian,
Nanjing University, China

Reviewed by:

Ronny P. Bartsch,
Bar-Ilan University, Israel
Paul Bogdan,
University of Southern California,
United States

*Correspondence:

Deyu Li
deyuli@buaa.edu.cn
Shuyu Li
shuyuli@buaa.edu.cn

Specialty section:

This article was submitted to
Fractal Physiology,
a section of the journal
Frontiers in Physiology

Received: 23 October 2017

Accepted: 20 April 2018

Published: 09 May 2018

Citation:

Li X, Li Q, Wang X, Li D and Li S
(2018) Differential Age-Related
Changes in Structural Covariance
Networks of Human Anterior
and Posterior Hippocampus.
Front. Physiol. 9:518.
doi: 10.3389/fphys.2018.00518

The hippocampus plays an important role in memory function relying on information interaction between distributed brain areas. The hippocampus can be divided into the anterior and posterior sections with different structure and function along its long axis. The aim of this study is to investigate the effects of normal aging on the structural covariance of the anterior hippocampus (aHPC) and the posterior hippocampus (pHPC). In this study, 240 healthy subjects aged 18–89 years were selected and subdivided into young (18–23 years), middle-aged (30–58 years), and older (61–89 years) groups. The aHPC and pHPC was divided based on the location of uncus apex in the MNI space. Then, the structural covariance networks were constructed by examining their covariance in gray matter volumes with other brain regions. Finally, the influence of age on the structural covariance of these hippocampal sections was explored. We found that the aHPC and pHPC had different structural covariance patterns, but both of them were associated with the medial temporal lobe and insula. Moreover, both increased and decreased covariances were found with the aHPC but only increased covariance was found with the pHPC with age ($p < 0.05$, family-wise error corrected). These decreased connections occurred within the default mode network, while the increased connectivity mainly occurred in other memory systems that differ from the hippocampus. This study reveals different age-related influence on the structural networks of the aHPC and pHPC, providing an essential insight into the mechanisms of the hippocampus in normal aging.

Keywords: network, structural covariance, normal aging, anterior hippocampus, posterior hippocampus, MRI

INTRODUCTION

With the population aging, understanding normal brain changes are as important as understanding demented diseases. Memory decline is a typical characteristic of normal aging. The hippocampus is considered critical in human memory and spatial navigation (Scoville and Milner, 1957; Buzsáki and Moser, 2013). Evidence suggests that hippocampal volume changes throughout the lifespan, which stays relatively stable until the age of 60 shows a sharp decline (Raz et al., 2010; Schuff et al., 2012; Fjell et al., 2013). Functional imaging studies have revealed and hypometabolism (de Leon et al., 2001; Wu et al., 2008) of the hippocampus in aging. Moreover, a reduced fractal dimension of hippocampal dynamics with age was reported (Goldberger et al., 2002; Wink et al., 2006).

The hippocampus differs in structure and function along its longitudinal axis (Poppenk et al., 2013). The anterior hippocampus (aHPC) and posterior hippocampus (pHPC) vary in pyramidal cell density (Babb et al., 1984; King et al., 2008) and have different developmental trajectories (DeMaster et al., 2014). Compared with young adults, both the aHPC and the pHPC showed volumetric atrophy in old adults (Pruessner et al., 2001; Chen et al., 2010; Rajah et al., 2010), and their rates of atrophy were different (Malykhin et al., 2008; Chen et al., 2010). Besides, an fMRI study reported the functional connectivity of the aHPC and pHPC were differentially affected in aging (Damoiseaux et al., 2016).

For structural connectivity, the structural covariance network (SCN) approach provides an effective way to characterize inter-regional structural covariance pattern of gray matter (GM) morphological properties (Mechelli et al., 2005; Modinos et al., 2009; Seeley et al., 2009; Zielinski et al., 2010; Montembeault et al., 2012; Li et al., 2013; DuPre and Spreng, 2017). The GM morphological covariance may result from direct white matter connection or neuronal co-activation (Alexander-Bloch et al., 2013). Studies have revealed a consistency among SCNs, anatomical connectivity networks, and functional connectivity networks, which provides strong support for using SCN mapping approach to assess network integrity. Age-related alteration of structural covariance in sensorimotor and cognitive networks has been found (Montembeault et al., 2012; Li et al., 2013). However, the effects of aging on the structural covariance of the aHPC and pHPC remain to be studied, which may provide insights into the hippocampal-related mechanism of aging and demented diseases.

In this study, we utilized a seed-based SCN approach to investigate the anterior and posterior hippocampal structural networks in 240 healthy subjects that were subdivided into young, middle-aged, and elderly groups. We first defined aHPC and pHPC based on the location of uncus apex in the MNI space. Then, we identified the SCNs seeding from aHPC and pHPC and compared the structural covariance differences between age groups. We expected the SCNs of the aHPC and pHPC have different patterns and were differently affected by age.

MATERIALS AND METHODS

Participants

The MRI data were obtained from the publicly available Open Access Series of Imaging Studies (OASIS) database (Marcus et al., 2007). The OASIS database consists of 416 subjects aged 18–96, including 100 mild dementia and 316 healthy subjects. Based on the age distribution of the OASIS database, we selected 240 participants from the healthy subcohort and grouped them into young (18–23 years), middle-aged (30–58 years), and elderly (61–89 years) groups, with 80 participants in each group (see **Table 1**). All the subjects are right-handed and cognitively normal, with the Mini-Mental State Examination scores (Folstein et al., 1975) above 29 and the Clinical Dementia Rating scores (Folstein et al., 1975) equal zero. The same group of subjects was used in our previous study (Li et al., 2013).

Data Acquisition

All MRI scans were performed on 1.5 Tesla Siemens scanners. For each individual, three to four T1-weighted images were acquired using a magnetization-prepared rapid gradient echo (MPRAGE) sequence with the following parameters: repetition time = 9.7 ms; echo time = 4 ms; inversion time = 20 ms; delay time = 200 ms; flip angle = 10°; matrix = 256 × 256; field of view = 256 mm; slices = 128; slice thickness = 1.25 mm. After motion corrected, the images of each subject were averaged to improve the contrast-to-noise ratio.

Image Preprocessing

We used the VBM8 toolbox¹ runs within SPM8 to implement voxel-based morphometry analysis (Ashburner and Friston, 2000) of the structural images. The acquired anatomical images were tissue classified into GM, white matter and cerebrospinal fluid images using tissue priors. Then, the segmented images were bias corrected and registered to a standard space using an affine transformation and a high-dimensional non-linear registration approach (Ashburner and Friston, 2005). Next, modulation of the segmented images was performed to correct for different individual brain size by using the non-linear registration parameters. Finally, the modulated GM segments were smoothed using an isotropic 12 mm full-width at half maximum Gaussian kernel for the structural covariance analysis.

Definition of the Hippocampal Seeds

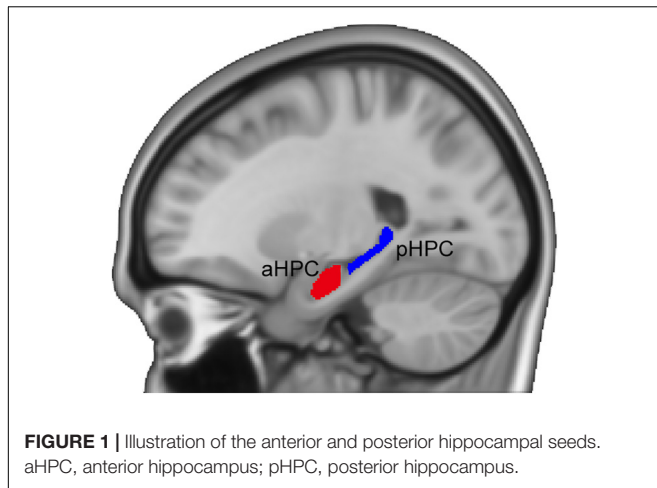
Following previous studies (Poppenk et al., 2013; Persson et al., 2014), we adopted a MNI-coordinate-based segmentation method to partition the hippocampus. The hippocampus was identified using the Harvard-Oxford subcortical structural atlas (Desikan et al., 2006) from the FSL Software Library (Smith et al., 2004). Next, the left and right hippocampi were divided into the anterior and posterior sections separately based on the location of uncus apex in the MNI space (i.e., $Y = -21$ mm) (Poppenk et al., 2013). To avoid contamination effects between the aHPC and the pHPC, we removed a 2-mm coronal slice from each of the two adjacent ends (see **Figure 1**). For each subject, we measured the mean volumes of the hippocampal subfields from the modulated GM images using the MarsBar ROI toolbox². Then a quadratic regression model was used to investigate age effects on the mean volumes of the anterior and posterior hippocampal segments. We also assessed the age-related hippocampal volumetric dispersion. To do so, for age = t , we calculated the variance of hippocampal volumes of subjects with age $\in [t-2, t+2]$ and examined its quadratic relationship with age.

¹<http://www.neuro.uni-jena.de/vbm/>

²<http://marsbar.sourceforge.net/>

TABLE 1 | Participant characteristics by age group.

| Group | Sample size (Females) | Age in years (mean ± SD) |
|-------------|-----------------------|--------------------------|
| Young | 80 (50) | 18–23 (20.66 ± 1.47) |
| Middle-aged | 80 (50) | 30–58 (47.43 ± 8.23) |
| Old | 80 (55) | 61–89 (73.75 ± 7.12) |



Structural Covariance Analysis

Four separate regression analyses were executed on the modulated GM images data to map SCNs of the bilateral aHPC and pHPC in the young group. The model fitted the target voxel GM volume Y as:

$$Y \sim \beta_0 + \beta_1(\text{Seed}) + \beta_2(\text{Gender})$$

where β_0 is the intercept term, β_1 model the relationship between the target voxel volume and the seed volume, and the Gender term was included as a nuisance variable. Total intracranial volume was not included because the modulation step already considered the brain size differences. These statistical analyses enable us to determine voxels that expressed a significant positive correlation with each seed. The criterion for significance was set at height and extent thresholds of $p < 0.05$, family-wise error (FWE) corrected for multiple comparisons. The resulting correlation maps were displayed on a standard brain template using the BrainNet Viewer (Xia et al., 2013) to allow qualitative comparisons the structural covariance patterns of hippocampal seeds.

We further assessed the influence of age on the regional structural covariance between the hippocampus and the rest brain regions by using a classic linear interaction model (Lerch et al., 2006). For any two age groups, the target voxel volume Y was modeled as follows:

$$Y \sim \beta_0 + \beta_1(\text{Seed}) + \beta_2(\text{Group}) + \beta_3(\text{Gender}) + \beta_4(\text{Group} \times \text{Seed})$$

where β_0 is the intercept term, $\beta_1 \sim \beta_4$ models the relationship between the target voxel volume and the seed volume, group term, gender term, and interaction term (group by seed), respectively. To obtain between-group differences, specific t contrasts were established to test the statistical significance of the interaction term. Clusters with height and extent thresholds set at $p < 0.05$ (FWE corrected) were considered significant.

RESULTS

Hippocampal Volume Analyses

Results for the regression analysis of anterior and posterior hippocampal mean GM volumes versus age are presented in **Figure 2**. Similar nonlinear relationship between the bilateral hippocampal volumes and age were found: the volumes slightly increased before the age of 50 and then decreased sharply (left aHPC: $R^2 = 0.187$, $p < 0.001$; right aHPC: $R^2 = 0.136$, $p < 0.001$; left pHPC: $R^2 = 0.089$, $p < 0.001$; right pHPC: $R^2 = 0.106$, $p < 0.001$). Moreover, the results suggested that the mean volume of the aHPC was larger than the pHPC, and the left hippocampal volume was slightly greater than the right side. In addition, we found the variance of the bilateral anterior hippocampal volumes has an age-related U-shaped relationship (left aHPC: $R^2 = 0.489$, $p < 0.001$; right aHPC: $R^2 = 0.666$, $p < 0.001$). Specifically, the anterior hippocampal volumes of the young and old subjects were more dispersed than the middle age. However, the variance of the posterior hippocampal volumes did not significantly relate to age (left pHPC: $R^2 = 0.015$, $p = 0.646$; right pHPC: $R^2 = 0.051$, $p = 0.215$).

Structural Covariance Networks of the Anterior and Posterior Hippocampus

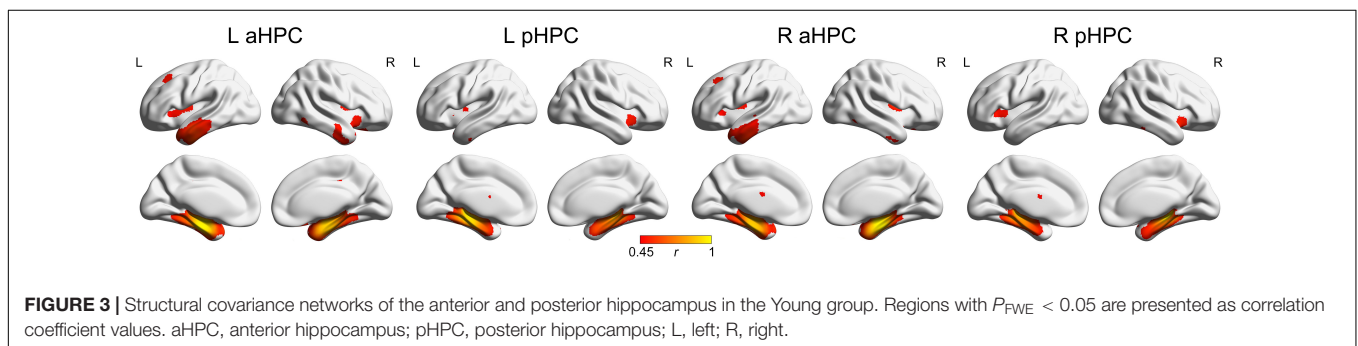
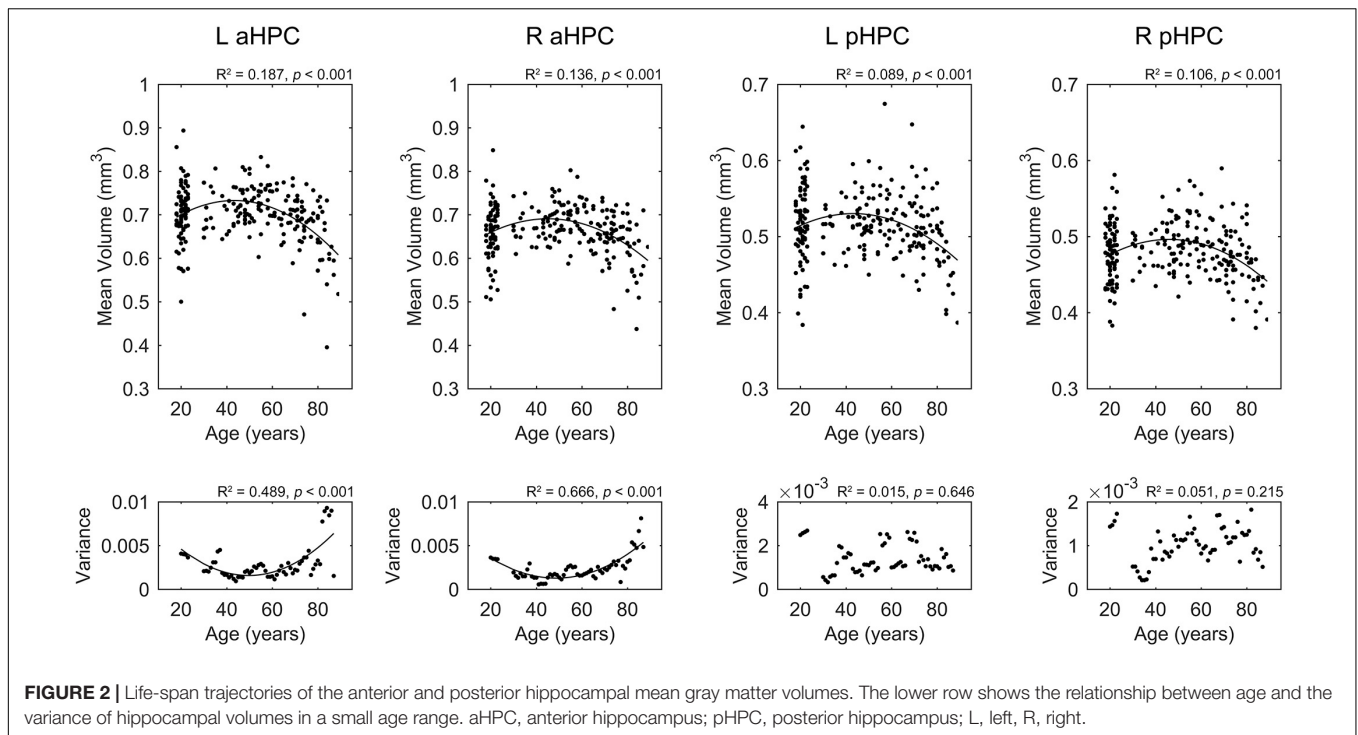
The SCNs seeding from the aHPC and pHPC in the young participants are presented in **Figure 3** ($p < 0.05$, FWE corrected). The aHPC correlated with the bilateral temporal lobe (including the superior, middle and inferior temporal, parahippocampal gyri, entorhinal cortex, fusiform and temporal pole), amygdalae, insula and posterior cingulate gyrus, orbitofrontal cortex, as well as left superior frontal gyrus. For the pHPC, its covariance maps involved the bilateral medial temporal regions (including the parahippocampal gyrus, entorhinal cortex and fusiform), amygdalae and insula. Noted that the regions correlated with both the aHPC and pHPC were mainly located in the medial temporal lobe and insula.

Age-Related Differences Within the Anterior Hippocampal Network

Within the anterior hippocampal network, significant between-group differences were only observed between the young group and the old group ($p < 0.05$, FWE corrected, **Figure 4** and **Table 2**). Specifically, the left and right aHPC showed decreased positive correlation with the ipsilateral parahippocampus and increased positive correlation with the ipsilateral amygdala in the old group relative to the young group. Moreover, compared to the young group, the left aHPC exhibited lower structural covariance with the left precuneus and greater structural covariance with the right putamen in the old group.

Age-Related Differences Within the Posterior Hippocampal Network

Within the posterior hippocampal network, only increased structural associations were found in the old group relative to younger adults (mainly the young group, $p < 0.05$, FWE corrected, see **Figure 5** and **Table 2**). For the left pHPC, the



old group exhibited significantly increased connectivity with the right caudate related to the young group. For the right pHPC, its connection with bilateral putamen was negative in the young group but was positive in the old group. Similarly, the right pHPC and temporal pole was negatively related in the middle-aged group but positively related in the old group.

DISCUSSION

Here, we studied the age-related structural covariance alterations of the aHPC and pHPC using a seed-based SCN approach. We found that the SCNs seeding from the aHPC and pHPC in the young adults were different from each other, but both of them related with the medial temporal lobe and insula. In addition, the structural covariance differences within the anterior hippocampal network were mainly between the young group and the old group with both decreased and increased positive structural associations. While compared to

the younger adults, only increased structural associations were found in the old group within the posterior hippocampal network.

We observed that the volumes of aHPC/pHPC slightly increased from young to middle age, and then decreased sharply with age. In line with this finding, several morphometric studies reported an inverted U pattern of the hippocampal volume changes with age (Walhovd et al., 2005; Li et al., 2014). As the hippocampus is important in memory processing, this pattern may partially explain the similar age-related memory change trajectory (Nyberg et al., 2012). Interestingly, we found that the anterior hippocampal volumes of the young and old subjects are more dispersed than the middle age, may pointing to stronger heterogeneity memory ability in young and old subjects. Whether this age-related dispersion due to the sample selection or other reasons requires further analysis.

Structural covariance analyses suggested that the aHPC connected with temporal lobe, amygdala, insula, and orbitofrontal cortex ($p < 0.05$, FWE corrected), which agree with

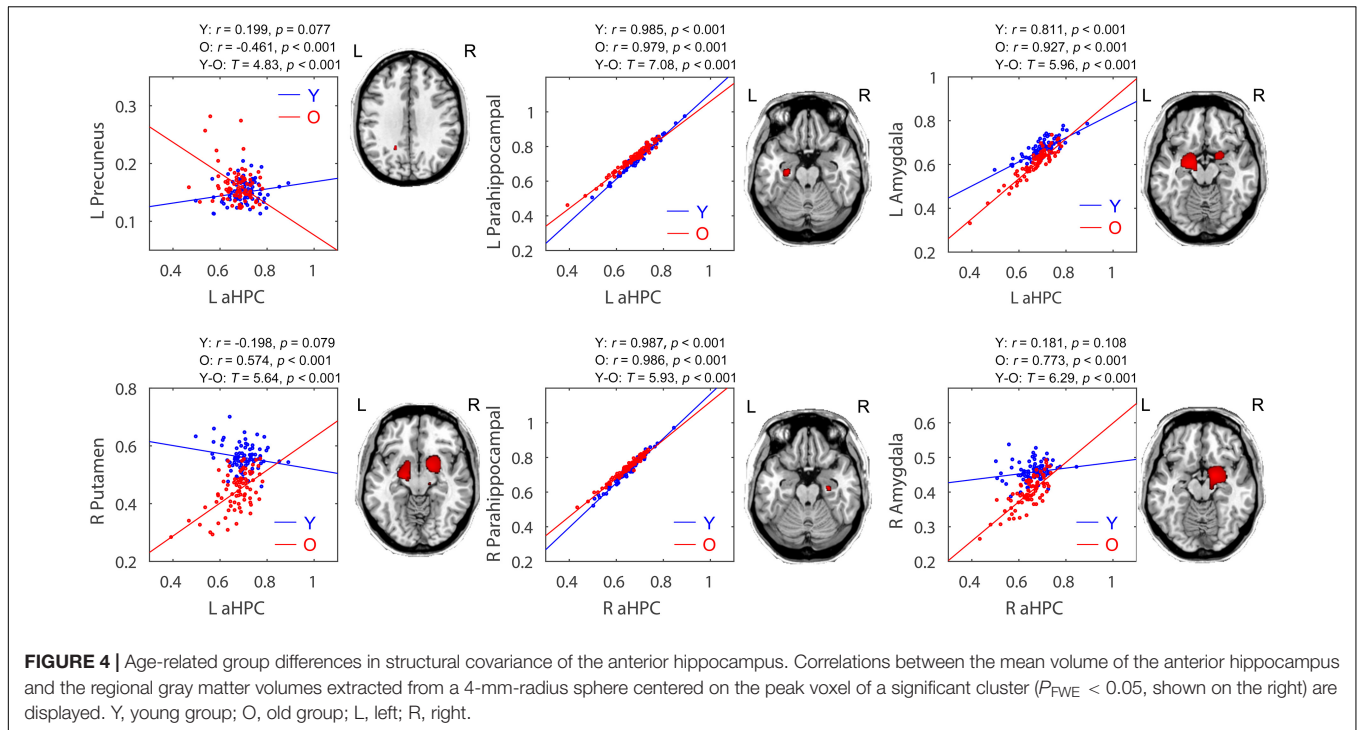


FIGURE 4 | Age-related group differences in structural covariance of the anterior hippocampus. Correlations between the mean volume of the anterior hippocampus and the regional gray matter volumes extracted from a 4-mm-radius sphere centered on the peak voxel of a significant cluster ($P_{FWE} < 0.05$, shown on the right) are displayed. Y, young group; O, old group; L, left; R, right.

TABLE 2 | Significant between-group differences in structural association between hippocampal seeds and other anatomical regions.

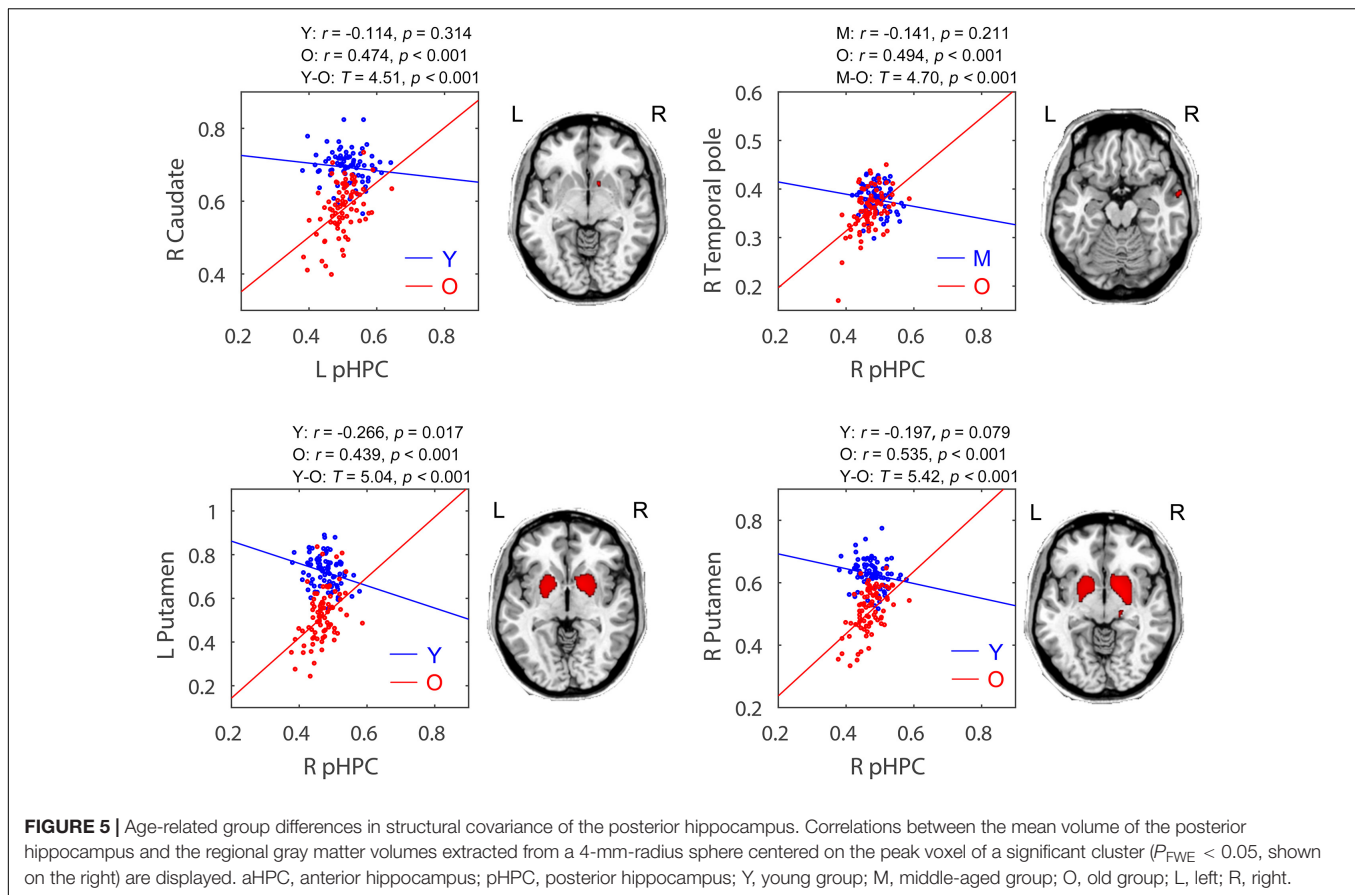
| Seed | Contrast | Anatomical region | MNI coordinates | | | Cluster size | MaxT |
|--------|----------|-------------------|-----------------|-----|-----|--------------|------|
| | | | X | Y | Z | | |
| L aHPC | Y > O | L Parahippocampus | -27 | -16 | -21 | 126 | 7.08 |
| | | L Precuneus | -18 | -52 | 31 | 18 | 4.83 |
| | Y < O | L Amygdala | -21 | -7 | -15 | 1314 | 5.96 |
| R aHPC | | R Putamen | 18 | 3 | -11 | 1096 | 5.64 |
| | Y > O | R Parahippocampus | 27 | -15 | -21 | 36 | 5.93 |
| | Y < O | R Amygdala | 16 | -1 | -14 | 1871 | 6.29 |
| L pHPC | Y < O | R Caudate | 12 | 10 | -6 | 5 | 4.51 |
| R pHPC | M < O | R Temporal pole | 62 | 0 | -17 | 29 | 4.70 |
| | | R Putamen | 14 | 8 | -6 | 1655 | 5.42 |
| | Y < O | L Putamen | -22 | 3 | -3 | 1084 | 5.04 |

$P < 0.05$, FWE corrected. Abbreviations: L, left; R, right; aHPC, anterior hippocampus; pHPC, posterior hippocampus; Y, young group; M, middle-aged group; O, old group.

previous studies (Kier et al., 2004; Smith et al., 2009; Catenoix et al., 2011). And the pHPC was covariant with medial temporal amygdala, and insula ($p < 0.05$, FWE corrected) showing consistent connections with previous studies by using fMRI and tractography (Kahn et al., 2008; Poppenk and Moscovitch, 2011; Poppenk et al., 2013). The common related regions with both aHPC and pHPC were mainly located in the medial temporal lobe where the hippocampus located.

Age-related decrements in structural covariance were observed in the aHPC-related SCNs ($p < 0.05$, FWE corrected). In particular, the parahippocampal gyrus and precuneus showed reduced association with the aHPC seed in old adults relative to young adults. The parahippocampal gyrus is considered as a mediator between the cortical DMN subsystem and the

hippocampus (Ward et al., 2014), and the integrity of the cortico-parahippocampus-hippocampus circuit is important for learning and episodic memory (Witter et al., 2000; Van Strien et al., 2009). Therefore, the weakened parahippocampus-hippocampus connection may lead to memory deficits in normal elderly, and result in decreased structural covariance between the hippocampus and cortical regions, such as the precuneus found in this study. Besides, the decreased connectivity between the precuneus and hippocampus might result from very early beta-amyloid deposition of the precuneus in elderly subjects (Sheline et al., 2010). The abnormal synaptic activity caused by amyloid deposition might disrupt cortico-hippocampal connectivity, which then results in hippocampal atrophy (Mormino et al., 2009).



Note that the parahippocampal gyrus, precuneus, and hippocampus are all components of DMN (Andrews-Hanna et al., 2014). Thus, our findings may indicate that aging is associated with decreased structural covariance within the DMN, which is in keeping with observations from previous SCN studies (Montembeault et al., 2012; Li et al., 2013; Spreng and Turner, 2013). A previous study reported decreased fractal complexity in DMN with age using multifractal analysis of fMRI series (Ni et al., 2014). Moreover, aging-related decrements in functional connectivity (Damoiseaux et al., 2008; Tomasi and Volkow, 2012) and white matter integrity (Damoiseaux et al., 2009; Brown et al., 2015) of DMN were also reported. Since DMN is known to play a role in episodic memory processing (Greicius et al., 2004, 2009), its decreased integrity could underlie memory impairment in senior populations (Salami et al., 2014).

Additionally, our data suggest that the influence of age on the structural connectivity between the hippocampus and cortical DMN nodes may be limited to the anterior portion of the hippocampus. Similarly, Salami et al. (2014) revealed reduced functional connectivity between the cortical DMN subsystems and more anteriorly located hippocampus with advancing age. Several fMRI studies have demonstrated the aHPC as part of DMN was engaged in episodic memory (autobiographical memory) processing (Zeidman and Maguire, 2016). However, some studies found no age-related differences

for the connectivity between the aHPC and DMN regions (Koch et al., 2010; Damoiseaux et al., 2016), while others reported lower connectivity between the pHPC and DMN regions in older adults (Andrews-Hanna et al., 2007; Damoiseaux et al., 2016). These discrepancies may be due to methodological differences, notably in the type of measurements and sample characteristics, which should be further investigated.

Moreover, age-related increments in structural covariance were observed in both the aHPC- and pHPC-related SCNs ($p < 0.05$, FWE corrected). Particularly, compared to young adults, the putamen and amygdala showed increased associations within the aHPC-related SCNs in old adults. Within the pHPC-related SCNs, the putamen, caudate, and temporal pole showed increased associations in old adults relative to younger adults. The putamen and caudate form the dorsal striatum. In fact, the hippocampus, dorsal striatum, and amygdala belong to different memory systems and play different roles in information acquisition (McDonald and White, 1993). The dorsal striatum and hippocampus cooperate to support episodic memory function (Sadeh et al., 2011), while the amygdala plays a role in regulating these two memory systems (Packard and Teather, 1998). We speculated that the age-related increment in hippocampal structural covariance may reflect the compensatory mechanism or dedifferentiation effects of the brain memory systems during aging (Dennis and Cabeza, 2011; Oedekoven et al., 2015).

The greater structural covariance between the hippocampus and dorsal striatum (caudate-putamen) in older adults may also be related to non-optimal dopamine processing. The CA1 area of the hippocampus receives dopaminergic modulation from the ventral tegmental area, which plays a vital role in synaptic plasticity of the hippocampus (Lisman and Grace, 2005). But the ventral tegmental area suffers from dopamine neurons loss (Siddiqi et al., 1999) and reduced dopamine transporter function (Salvatore et al., 2003) with age. However, the dorsal striatum, another area in the dopamine system, increases its dopamine synthesis capacity in aging (Braskie et al., 2008). Thus, the increased connections between the hippocampus and dorsal striatum during aging suggest compensation for deficits in the ventral tegmental area, which may represent non-optimal dopamine system functioning.

The SCN method used in this study provides an effective way to construct brain networks from medical images, which complements the signal analysis methods (Liu et al., 2015). However, since aging is not only characterized by brain deficits but also decline in multiple organ functions, it is interesting to utilize the integrative approaches within the new field of network physiology to study the effects of aging on brain–brain or brain–organ networks in future (Bashan et al., 2012; Bartsch et al., 2015; Ivanov et al., 2016). In addition, it is worth noting that brain networks have a fractal property of hierarchical modularity, which confers robustness of network function (Bullmore and Sporns, 2012). Future studies using fractal analysis approaches (Meunier et al., 2010; Xue and Bogdan, 2017) to study the

complexity and heterogeneity of hippocampal networks could advance our understanding of the brain in normal aging.

AUTHOR CONTRIBUTIONS

XL designed and performed the experiments, analyzed the data, and drafted the manuscript. QL and XW helped to analyze the data and to draft the manuscript. DL and SL contributed to the study design, coordination, and final approval of the manuscript. All authors read and approved this version to be published.

FUNDING

This work was supported by the National Natural Science Foundation of China (Grant Nos. 81622025 and 81471731), the Fundamental Research Funds for the Central Universities (Grant No. YWF-17-BJ-J-11), the Innovation Foundation of BUAA for Ph.D. Students, and Academic Excellence Foundation of BUAA for Ph.D. Students. The OASIS project was supported by the NIH Grant Nos. P50 AG05681, P01 AG03991, R01 AG021910, P50 MH071616, U24 RR021382, and R01 MH56584.

ACKNOWLEDGMENTS

The authors would like to thank the OASIS project for making the MRI data freely available.

REFERENCES

- Alexander-Bloch, A., Giedd, J. N., and Bullmore, E. (2013). Imaging structural co-variance between human brain regions. *Nat. Rev. Neurosci.* 14, 322–336. doi: 10.1038/nrn3465
- Andrews-Hanna, J. R., Snyder, A. Z., Vincent, J. L., Lustig, C., Head, D., Raichle, M. E., et al. (2007). Disruption of large-scale brain systems in advanced aging. *Neuron* 56, 924–935. doi: 10.1016/j.neuron.2007.10.038
- Andrews-Hanna, J. R., Smallwood, J., and Spreng, R. N. (2014). The default network and self-generated thought: component processes, dynamic control, and clinical relevance. *Ann. N. Y. Acad. Sci.* 1316, 29–52. doi: 10.1111/nyas.12360
- Ashburner, J., and Friston, K. J. (2000). Voxel-based morphometry—the methods. *Neuroimage* 11, 805–821. doi: 10.1006/nimg.2000.0582
- Ashburner, J., and Friston, K. J. (2005). Unified segmentation. *Neuroimage* 26, 839–851. doi: 10.1016/j.neuroimage.2005.02.018
- Babb, T. L., Lieb, J. P., Brown, W. J., Pretorius, J., and Crandall, P. H. (1984). Distribution of pyramidal cell density and hyperexcitability in the epileptic human hippocampal formation. *Epilepsia* 25, 721–728. doi: 10.1111/j.1528-1157.1984.tb03483.x
- Bartsch, R. P., Liu, K. K., Bashan, A., and Ivanov, P. C. (2015). Network physiology: how organ systems dynamically interact. *PLoS One* 10:e0142143. doi: 10.1371/journal.pone.0142143
- Bashan, A., Bartsch, R. P., Kantelhardt, J. W., Havlin, S., and Ivanov, P. C. (2012). Network physiology reveals relations between network topology and physiological function. *Nat. Commun.* 3:702. doi: 10.1038/ncomms1705
- Braskie, M. N., Wilcox, C. E., Landau, S. M., O'neil, J. P., Baker, S. L., Madison, C. M., et al. (2008). Relationship of striatal dopamine synthesis capacity to age and cognition. *J. Neurosci.* 28, 14320–14328. doi: 10.1523/JNEUROSCI.3729-08.2008
- Brown, C. A., Hakun, J. G., Zhu, Z. D., Johnson, N. F., and Gold, B. T. (2015). White matter microstructure contributes to age-related declines in task-induced deactivation of the default mode network. *Front. Aging Neurosci.* 7:194. doi: 10.3389/fnagi.2015.00194
- Bullmore, E., and Sporns, O. (2012). The economy of brain network organization. *Nat. Rev. Neurosci.* 13, 336–349. doi: 10.1038/nrn3214
- Buzsáki, G., and Moser, E. I. (2013). Memory, navigation and theta rhythm in the hippocampal-entorhinal system. *Nat. Neurosci.* 16, 130–138. doi: 10.1038/nn.3304
- Catenoix, H., Magnin, M., Manguiere, F., and Rylvlin, P. (2011). Evoked potential study of hippocampal efferent projections in the human brain. *Clin. Neurophysiol.* 122, 2488–2497. doi: 10.1016/j.clinph.2011.05.007
- Chen, K. H., Chuah, L. Y., Sim, S. K., and Chee, M. W. (2010). Hippocampal region-specific contributions to memory performance in normal elderly. *Brain Cogn.* 72, 400–407. doi: 10.1016/j.bandc.2009.11.007
- Damoiseaux, J. S., Beckmann, C. F., Arigita, E. J., Barkhof, F., Scheltens, P., Stam, C. J., et al. (2008). Reduced resting-state brain activity in the “default network” in normal aging. *Cereb. Cortex* 18, 1856–1864. doi: 10.1093/cercor/bhm207
- Damoiseaux, J. S., Smith, S. M., Witter, M. P., Sanz-Arigita, E. J., Barkhof, F., Scheltens, P., et al. (2009). White matter tract integrity in aging and Alzheimer's disease. *Hum. Brain Mapp.* 30, 1051–1059. doi: 10.1002/hbm.20563
- Damoiseaux, J. S., Viviano, R. P., Yuan, P., and Raz, N. (2016). Differential effect of age on posterior and anterior hippocampal functional connectivity. *Neuroimage* 133, 468–476. doi: 10.1016/j.neuroimage.2016.03.047
- de Leon, M. J., Convit, A., Wolf, O. T., Tarshish, C. T., DeSanti, S., Rusinek, H., et al. (2001). Prediction of cognitive decline in normal elderly subjects with 2-[18F] fluoro-2-deoxy-D-glucose/positron-emission tomography (FDG/PET). *Proc. Natl. Acad. Sci. U.S.A.* 98, 10966–10971. doi: 10.1073/pnas.191044198
- DeMaster, D., Pathman, T., Lee, J. K., and Ghetti, S. (2014). Structural Development of the Hippocampus and Episodic Memory: Developmental Differences Along

- the Anterior/Posterior Axis. *Cereb. Cortex* 24, 3036–3045. doi: 10.1093/cercor/bht160
- Dennis, N. A., and Cabeza, R. (2011). Age-related dedifferentiation of learning systems: an fMRI study of implicit and explicit learning. *Neurobiol. Aging* 32, 2318.e17–30. doi: 10.1016/j.neurobiolaging.2010.04.004
- Desikan, R. S., Ségonne, F., Fischl, B., Quinn, B. T., Dickerson, B. C., Blacker, D., et al. (2006). An automated labeling system for subdividing the human cerebral cortex on MRI scans into gyral based regions of interest. *Neuroimage* 31, 968–980. doi: 10.1016/j.neuroimage.2006.01.021
- DuPre, E., and Spreng, R. N. (2017). Structural covariance networks across the lifespan, from 6–94 years of age. *Netw. Neurosci.* 1, 302–323.
- Fjell, A. M., Westlye, L. T., Grydeland, H., Amlien, I., Espeseth, T., Reinvang, I., et al. (2013). Critical ages in the life course of the adult brain: nonlinear subcortical aging. *Neurobiol. Aging* 34, 2239–2247. doi: 10.1016/j.neurobiolaging.2013.04.006
- Folstein, M. F., Folstein, S. E., and McHugh, P. R. (1975). “Mini-mental state”: a practical method for grading the cognitive state of patients for the clinician. *J. Psychiatr. Res.* 12, 189–198. doi: 10.1016/0022-3956(75)90026-6
- Goldberger, A. L., Amaral, L. A., Hausdorff, J. M., Ivanov, P. C., Peng, C.-K., and Stanley, H. E. (2002). Fractal dynamics in physiology: alterations with disease and aging. *Proc. Natl. Acad. Sci. U.S.A.* 99, 2466–2472. doi: 10.1073/pnas.012579499
- Greicius, M. D., Srivastava, G., Reiss, A. L., and Menon, V. (2004). Default-mode network activity distinguishes Alzheimer’s disease from healthy aging: evidence from functional MRI. *Proc. Natl. Acad. Sci. U.S.A.* 101, 4637–4642. doi: 10.1073/pnas.0308627101
- Greicius, M. D., Supekar, K., Menon, V., and Dougherty, R. F. (2009). Resting-state functional connectivity reflects structural connectivity in the default mode network. *Cereb. Cortex* 19, 72–78. doi: 10.1093/cercor/bhn059
- Ivanov, P. C., Liu, K. K., and Bartsch, R. P. (2016). Focus on the emerging new fields of network physiology and network medicine. *N. J. Phys.* 18:100201. doi: 10.1111/ede.12187
- Kahn, I., Andrews-Hanna, J. R., Vincent, J. L., Snyder, A. Z., and Buckner, R. L. (2008). Distinct cortical anatomy linked to subregions of the medial temporal lobe revealed by intrinsic functional connectivity. *J. Neurophysiol.* 100, 129–139. doi: 10.1152/jn.00077.2008
- Kier, E. L., Staib, L. H., Davis, L. M., and Bronen, R. A. (2004). MR imaging of the temporal stem: anatomic dissection tractography of the uncinate fasciculus, inferior occipitofrontal fasciculus, and Meyer’s loop of the optic radiation. *Am. J. Neuroradiol.* 25, 677–691.
- King, K. G., Glodzik, L., Liu, S., Babb, J. S., De Leon, M. J., and Gonen, O. (2008). Anteroposterior hippocampal metabolic heterogeneity: three-dimensional multivoxel proton 1H MR spectroscopic imaging—initial findings. *Radiology* 249, 242–250. doi: 10.1148/radiol.2491071500
- Koch, W., Teipel, S., Mueller, S., Buerger, K., Bokde, A. L., Hampel, H., et al. (2010). Effects of aging on default mode network activity in resting state fMRI: does the method of analysis matter? *Neuroimage* 51, 280–287. doi: 10.1016/j.neuroimage.2009.12.008
- Lerch, J. P., Worsley, K., Shaw, W. P., Greenstein, D. K., Lenroot, R. K., Giedd, J., et al. (2006). Mapping anatomical correlations across cerebral cortex (MACACC) using cortical thickness from MRI. *Neuroimage* 31, 993–1003. doi: 10.1016/j.neuroimage.2006.01.042
- Li, W., Wu, B., Batrachenko, A., Bancroft-Wu, V., Morey, R. A., Shashi, V., et al. (2014). Differential developmental trajectories of magnetic susceptibility in human brain gray and white matter over the lifespan. *Hum. Brain Mapp.* 35, 2698–2713. doi: 10.1002/hbm.22360
- Li, X., Pu, F., Fan, Y., Niu, H., Li, S., and Li, D. (2013). Age-related changes in brain structural covariance networks. *Front. Hum. Neurosci.* 7:98. doi: 10.3389/fnhum.2013.00098
- Lisman, J. E., and Grace, A. A. (2005). The hippocampal-VTA loop: controlling the entry of information into long-term memory. *Neuron* 46, 703–713. doi: 10.1016/j.neuron.2005.05.002
- Liu, K. K., Bartsch, R. P., Lin, A., Mantegna, R. N., and Ivanov, P. C. (2015). Plasticity of brain wave network interactions and evolution across physiologic states. *Front. Neural Circ.* 9:62. doi: 10.3389/fncir.2015.00062
- Malykhin, N. V., Bouchard, T. P., Camicioli, R., and Coupland, N. J. (2008). Aging hippocampus and amygdala. *Neuroreport* 19, 543–547. doi: 10.1097/WNR.0b013e3282f8b18c
- Marcus, D. S., Wang, T. H., Parker, J., Csernansky, J. G., Morris, J. C., and Buckner, R. L. (2007). Open Access Series of Imaging Studies (OASIS): cross-sectional MRI data in young, middle aged, nondemented, and demented older adults. *J. Cogn. Neurosci.* 19, 1498–1507. doi: 10.1162/jocn.2007.19.9.1498
- McDonald, R. J., and White, N. M. (1993). A triple dissociation of memory systems: hippocampus, amygdala, and dorsal striatum. *Behav. Neurosci.* 107, 3–22. doi: 10.1037/0735-7044.107.1.3
- Mechelli, A., Friston, K. J., Frackowiak, R. S., and Price, C. J. (2005). Structural covariance in the human cortex. *J. Neurosci.* 25, 8303–8310. doi: 10.1523/JNEUROSCI.0357-05.2005
- Meunier, D., Lambiotte, R., and Bullmore, E. T. (2010). Modular and hierarchically modular organization of brain networks. *Front. Neuroscience* 4:200. doi: 10.3389/fnins.2010.00200
- Modinos, G., Vercammen, A., Mechelli, A., Knegeting, H., McGuire, P. K., and Aleman, A. (2009). Structural covariance in the hallucinating brain: a voxel-based morphometry study. *J. Psychiatry Neurosci.* 34, 465–469.
- Montembeault, M., Joubert, S., Doyon, J., Carrier, J., Gagnon, J. F., Monchi, O., et al. (2012). The impact of aging on gray matter structural covariance networks. *Neuroimage* 63, 754–759. doi: 10.1016/j.neuroimage.2012.06.052
- Mormino, E., Kluth, J., Madison, C., Rabinovici, G., Baker, S., Miller, B., et al. (2009). Episodic memory loss is related to hippocampal-mediated β -amyloid deposition in elderly subjects. *Brain* 132, 1310–1323. doi: 10.1093/brain/awn320
- Ni, H., Huang, X., Ning, X., Huo, C., Liu, T., and Ben, D. (2014). Multifractal analysis of resting state fMRI series in default mode network: age and gender effects. *Chin. Sci. Bull.* 59, 3107–3113. doi: 10.1007/s11434-014-0355-x
- Nyberg, L., Lövdén, M., Riklund, K., Lindenberger, U., and Bäckman, L. (2012). Memory aging and brain maintenance. *Trends Cogn. Sci.* 16, 292–305. doi: 10.1016/j.tics.2012.04.005
- Oedekoven, C. S., Jansen, A., Keidel, J. L., Kircher, T., and Leube, D. (2015). The influence of age and mild cognitive impairment on associative memory performance and underlying brain networks. *Brain Imaging Behav.* 9, 776–789. doi: 10.1007/s11682-014-9335-7
- Packard, M. G., and Teather, L. A. (1998). Amygdala modulation of multiple memory systems: hippocampus and caudate-putamen. *Neurobiol. Learn. Mem.* 69, 163–203. doi: 10.1006/nlme.1997.3815
- Persson, J., Spreng, R. N., Turner, G., Herlitz, A., Morell, A., Stening, E., et al. (2014). Sex differences in volume and structural covariance of the anterior and posterior hippocampus. *Neuroimage* 99, 215–225. doi: 10.1016/j.neuroimage.2014.05.038
- Poppenk, J., Evensmoen, H. R., Moscovitch, M., and Nadel, L. (2013). Long-axis specialization of the human hippocampus. *Trends Cogn. Sci.* 17, 230–240. doi: 10.1016/j.tics.2013.03.005
- Poppenk, J., and Moscovitch, M. (2011). A hippocampal marker of recollection memory ability among healthy young adults: contributions of posterior and anterior segments. *Neuron* 72, 931–937. doi: 10.1016/j.neuron.2011.10.014
- Pruessner, J., Collins, D., Pruessner, M., and Evans, A. (2001). Age and gender predict volume decline in the anterior and posterior hippocampus in early adulthood. *J. Neurosci.* 21, 194–200. doi: 10.1523/JNEUROSCI.21-01-00194.2001
- Rajah, M. N., Kromas, M., Han, J. E., and Pruessner, J. C. (2010). Group differences in anterior hippocampal volume and in the retrieval of spatial and temporal context memory in healthy young versus older adults. *Neuropsychologia* 48, 4020–4030. doi: 10.1016/j.neuropsychologia.2010.10.010
- Raz, N., Ghisletta, P., Rodrigue, K. M., Kennedy, K. M., and Lindenberger, U. (2010). Trajectories of brain aging in middle-aged and older adults: regional and individual differences. *Neuroimage* 51, 501–511. doi: 10.1016/j.neuroimage.2010.03.020
- Sadeh, T., Shohamy, D., Levy, D. R., Reggev, N., and Maril, A. (2011). Cooperation between the hippocampus and the striatum during episodic encoding. *J. Cogn. Neurosci.* 23, 1597–1608. doi: 10.1162/jocn.2010.21549
- Salami, A., Pudas, S., and Nyberg, L. (2014). Elevated hippocampal resting-state connectivity underlies deficient neurocognitive function in aging. *Proc. Natl. Acad. Sci. U.S.A.* 111, 17654–17659. doi: 10.1073/pnas.1410233111
- Salvatore, M. F., Apparsundaram, S., and Gerhardt, G. A. (2003). Decreased plasma membrane expression of striatal dopamine transporter in aging. *Neurobiol. Aging* 24, 1147–1154. doi: 10.1016/S0197-4580(03)00129-5
- Schuff, N., Tosun, D., Insel, P. S., Chiang, G. C., Truran, D., Aisen, P. S., et al. (2012). Nonlinear time course of brain volume loss in cognitively normal and

- impaired elders. *Neurobiol. Aging* 33, 845–855. doi: 10.1016/j.neurobiolaging.2010.07.012
- Scoville, W. B., and Milner, B. (1957). Loss of recent memory after bilateral hippocampal lesions. *J. Neurol. Neurosurg. Psychiatry* 20, 11–21. doi: 10.1136/jnnp.20.1.11
- Seeley, W. W., Crawford, R. K., Zhou, J., Miller, B. L., and Greicius, M. D. (2009). Neurodegenerative diseases target large-scale human brain networks. *Neuron* 62, 42–52. doi: 10.1016/j.neuron.2009.03.024
- Sheline, Y. I., Raichle, M. E., Snyder, A. Z., Morris, J. C., Head, D., Wang, S., et al. (2010). Amyloid plaques disrupt resting state default mode network connectivity in cognitively normal elderly. *Biol. Psychiatry* 67, 584–587. doi: 10.1016/j.biopsych.2009.08.024
- Siddiqi, Z., Kemper, T. L., and Killiany, R. (1999). Age-related neuronal loss from the substantia nigra-pars compacta and ventral tegmental area of the rhesus monkey. *J. Neuropathol. Exp. Neurol.* 58, 959–971. doi: 10.1097/00005072-199909000-00006
- Smith, C. D., Lori, N. F., Akbudak, E., Sorar, E., Gultepe, E., Shimony, J. S., et al. (2009). MRI diffusion tensor tracking of a new amygdalo-fusiform and hippocampo-fusiform pathway system in humans. *J. Magn. Reson. Imaging* 29, 1248–1261. doi: 10.1002/jmri.21692
- Smith, S. M., Jenkinson, M., Woolrich, M. W., Beckmann, C. F., Behrens, T. E., Johansen-Berg, H., et al. (2004). Advances in functional and structural MR image analysis and implementation as FSL. *Neuroimage* 23, S208–S219. doi: 10.1016/j.neuroimage.2004.07.051
- Spreng, R. N., and Turner, G. R. (2013). Structural covariance of the default network in healthy and pathological aging. *J. Neurosci.* 33, 15226–15234. doi: 10.1523/JNEUROSCI.2261-13.2013
- Tomasi, D., and Volkow, N. D. (2012). Aging and functional brain networks. *Mol. Psychiatry* 17, 471–558. doi: 10.1038/mp.2011.81
- Van Strien, N., Cappaert, N., and Witter, M. (2009). The anatomy of memory: an interactive overview of the parahippocampal–hippocampal network. *Nat. Rev. Neurosci.* 10, 272–282. doi: 10.1038/nrn2614
- Walhovd, K. B., Fjell, A. M., Reinvang, I., Lundervold, A., Dale, A. M., Eilertsen, D. E., et al. (2005). Effects of age on volumes of cortex, white matter and subcortical structures. *Neurobiol. Aging* 26, 1261–1270. doi: 10.1016/j.neurobiolaging.2005.05.020
- Ward, A. M., Schultz, A. P., Huijbers, W., Van Dijk, K. R., Hedden, T., and Sperling, R. A. (2014). The parahippocampal gyrus links the default-mode cortical network with the medial temporal lobe memory system. *Hum. Brain Mapp.* 35, 1061–1073. doi: 10.1002/hbm.22234
- Wink, A. M., Bernard, F., Salvador, R., Bullmore, E., and Suckling, J. (2006). Age and cholinergic effects on hemodynamics and functional coherence of human hippocampus. *Neurobiol. Aging* 27, 1395–1404. doi: 10.1016/j.neurobiolaging.2005.08.011
- Witter, M. P., Naber, P. A., Van Haeften, T., Machielsen, W. C., Rombouts, S. A., Barkhof, F., et al. (2000). Cortico-hippocampal communication by way of parallel parahippocampal-subicular pathways. *Hippocampus* 10, 398–410. doi: 10.1002/1098-1063(2000)10:4<398::AID-HIPO6>3.0.CO;2-K
- Wu, W., Brickman, A. M., Luchsinger, J., Ferrazzano, P., Pichiule, P., Yoshita, M., et al. (2008). The brain in the age of old: the hippocampal formation is targeted differentially by diseases of late life. *Ann. Neurol.* 64, 698–706. doi: 10.1002/ana.21557
- Xia, M., Wang, J., and He, Y. (2013). BrainNet viewer: a network visualization tool for human brain connectomics. *PLoS One* 8:e68910. doi: 10.1371/journal.pone.0068910
- Xue, Y., and Bogdan, P. (2017). Reliable multi-fractal characterization of weighted complex networks: algorithms and implications. *Sci. Rep.* 7:7487. doi: 10.1038/s41598-017-07209-5
- Zeidman, P., and Maguire, E. A. (2016). Anterior hippocampus: the anatomy of perception, imagination and episodic memory. *Nat. Rev. Neurosci.* 17, 173–182. doi: 10.1038/nrn.2015.24
- Zielinski, B. A., Gennatas, E. D., Zhou, J., and Seeley, W. W. (2010). Network-level structural covariance in the developing brain. *Proc. Natl. Acad. Sci. U.S.A.* 107, 18191–18196. doi: 10.1073/pnas.1003109107
- Conflict of Interest Statement:** The authors declare that the research was conducted in the absence of any commercial or financial relationships that could be construed as a potential conflict of interest.
- Copyright © 2018 Li, Li, Wang, Li and Li. This is an open-access article distributed under the terms of the Creative Commons Attribution License (CC BY). The use, distribution or reproduction in other forums is permitted, provided the original author(s) and the copyright owner are credited and that the original publication in this journal is cited, in accordance with accepted academic practice. No use, distribution or reproduction is permitted which does not comply with these terms.



Individual Morphological Brain Network Construction Based on Multivariate Euclidean Distances Between Brain Regions

Kaixin Yu^{1,2}, Xuotong Wang^{1,2}, Qionglin Li^{1,2}, Xiaohui Zhang^{1,2}, Xinwei Li^{1,2}, Shuyu Li^{1,2*} for the Alzheimer's Disease Neuroimaging Initiative[†]

OPEN ACCESS

Edited by:

Jinhui Wang,
Hangzhou Normal University, China

Reviewed by:

Chong-Yaw Wee,
National University of Singapore,
Singapore
Mingrui Xia,
Beijing Normal University, China

*Correspondence:

Shuyu Li
shuyuli@buaa.edu.cn

[†]Data used in preparing this article were obtained from the Alzheimer's Disease Neuroimaging Initiative (ADNI) database (adni.loni.usc.edu). As such, the investigators within the ADNI contributed to the design and implementation of ADNI and/or provided data but most of them did not participate in this analysis or writing this report. A complete list of ADNI investigators can be found at: http://adni.loni.usc.edu/wp-content/uploads/how_to_apply/ADNI_Acknowledgement_List.pdf

Received: 09 March 2018

Accepted: 01 May 2018

Published: 24 May 2018

Citation:

Yu K, Wang X, Li Q, Zhang X, Li X, Li S for the Alzheimer's Disease Neuroimaging Initiative (2018) Individual Morphological Brain Network Construction Based on Multivariate Euclidean Distances Between Brain Regions. *Front. Hum. Neurosci.* 12:204. doi: 10.3389/fnhum.2018.00204

¹ School of Biological Science & Medical Engineering, Beihang University, Beijing, China, ² Beijing Advanced Innovation Centre for Biomedical Engineering, Beihang University, Beijing, China

Morphological brain network plays a key role in investigating abnormalities in neurological diseases such as mild cognitive impairment (MCI) and Alzheimer's disease (AD). However, most of the morphological brain network construction methods only considered a single morphological feature. Each type of morphological feature has specific neurological and genetic underpinnings. A combination of morphological features has been proven to have better diagnostic performance compared with a single feature, which suggests that an individual morphological brain network based on multiple morphological features would be beneficial in disease diagnosis. Here, we proposed a novel method to construct individual morphological brain networks for two datasets by calculating the exponential function of multivariate Euclidean distance as the evaluation of similarity between two regions. The first dataset included 24 healthy subjects who were scanned twice within a 3-month period. The topological properties of these brain networks were analyzed and compared with previous studies that used different methods and modalities. Small world property was observed in all of the subjects, and the high reproducibility indicated the robustness of our method. The second dataset included 170 patients with MCI (86 stable MCI and 84 progressive MCI cases) and 169 normal controls (NC). The edge features extracted from the individual morphological brain networks were used to distinguish MCI from NC and separate MCI subgroups (progressive vs. stable) through the support vector machine in order to validate our method. The results showed that our method achieved an accuracy of 79.65% (MCI vs. NC) and 70.59% (stable MCI vs. progressive MCI) in a one-dimension situation. In a multiple-dimension situation, our method improved the classification performance with an accuracy of 80.53% (MCI vs. NC) and 77.06% (stable MCI vs. progressive MCI) compared with the method using a single feature. The results indicated that our method could effectively construct an individual morphological brain network based on multiple morphological features and could accurately discriminate MCI from NC and stable MCI from progressive MCI, and may provide a valuable tool for the investigation of individual morphological brain networks.

Keywords: individual morphological brain network, multivariate Euclidean distance, mild cognitive impairment, multiple morphological features, classification

INTRODUCTION

Morphological brain network refers to the intracortical similarities in gray matter morphology (He et al., 2007) which plays a key role in investigating brain abnormalities in neurological diseases. By analyzing morphological brain network features, the abnormalities in connectivity parameters can be found in patients (Yao et al., 2010; Tijms et al., 2013). More importantly, sensitive biomarkers for clinical diagnosis can be detected in brain networks from cases of Alzheimer's disease (He et al., 2008, 2009), schizophrenia (Bassett et al., 2008; Zhang et al., 2012) and epilepsy (Bernhardt et al., 2008, 2009).

Although previous morphological brain network studies achieved significant breakthroughs, they largely depended on group-level anatomical correlations of cortical morphology (He et al., 2007; Zhang et al., 2012). For example, He et al. (2007) constructed a network for each group by quantifying morphological relations characterized by the Pearson correlation coefficient between averaged regional morphological measures among participants. However, this method only works with a relatively large number of participants (Kong et al., 2014). In addition, it remains unclear if there are changes in brain networks at the individual level (Saggar et al., 2015). Therefore, it is necessary to construct morphological brain networks at the individual level for the direct analysis of individual differences.

Recently, several methods have been proposed to construct individual morphological brain networks either using a single feature or multiple morphological features. By using gray matter volume as the morphological measure, Tijms et al. (2012) proposed an individual morphological brain network by computing the correlation between two 27-voxel sets from two rigid cubes. There were some studies constructing individual brain networks by averaging the vertex value (e.g., cortical thickness) within regions of interest (ROI) (Dai et al., 2013; Wee et al., 2013; Kim et al., 2016) or by estimating interregional similarity in the distribution of regional morphological measures (e.g., cortical thickness or volume) (Kong et al., 2014; Zheng et al., 2015). Wang et al. (2016) employed graph-based analyses to support individual morphological network analysis as a meaningful and reliable method when characterizing brain structural organization. Some recent studies (Li et al., 2017; Seidlitz et al., 2017) built individual morphological networks with multiple morphological features extracted from the cortical surface. Each type of morphological feature has specific neurological and genetic underpinnings. Volumetric measures (i.e., cortical thickness, gray matter volume) reflect the size, density and arrangement of cells (neurons, neuroglia, and nerve fibers) (Parent and Carpenter, 1996) and surface area is linked to the number of mini columns in the cortical layer (Rakic, 1988). Geometric measures (i.e., sulcal depth, curvature, and metric distortion) mainly reflect the cortical folding pattern (Van Essen, 1997; Cachia et al., 2003; Lohmann et al., 2008). Li et al. (2014) found that various morphological features had unique contributions to the classification of the amnesic MCI (aMCI) and NC. In the two studies (Li et al., 2017; Seidlitz et al., 2017), a morphological feature vector was used to represent one region and pairwise inter-regional Pearson correlations were used to

construct brain network, while not considering the distribution of the intra-regional morphological features.

In this paper, we proposed a novel individual morphological brain network method by defining multivariate Euclidean distance to describe the inter-regional similarity based on multiple morphological features. First, multivariate Euclidean distance was calculated by using the six morphological features of all of the vertices within each region. Second, the Min-Max normalization for Euclidean distance was performed to minimize possible bias in different ranges of different subjects. Finally, the normalized Euclidean distance was converted to a similarity measurement using an exponential function. Then, we validated the proposed method by computing the topological properties of individual brain networks, i.e., small-world, hubs and intraclass correlation coefficient (ICC) in 24 healthy subjects. In addition, we applied the edges of each individual morphological network as features to discriminate the MCI and NC in the AD Neuroimaging Initiative (ADNI) dataset. The accuracy of classification was used to assess the effectiveness of our method.

MATERIALS AND METHODS

Participants

The first dataset used in this study consisted of 24 right-handed healthy subjects (12 men with ages ranging from 25 to 29 years with mean = 27.17 years, and standard deviation = 1.40; 12 women with ages ranging from 26 to 30 years with mean = 27.83 years, and standard deviation = 1.11). All subjects were native Chinese speakers who had grown up in China. All subjects provided written informed consent; in addition, the local ethics committee approved this study.

The subjects were scanned twice within a 3-month period. All of the MRI data were obtained using a SIEMENS Trio Tim 3.0T scanner with a 12-channel phased array head coil in the Imaging Center for Brain Research, Beijing Normal University. The brain structural images were acquired using T1-weighted, sagittal 3D magnetization prepared rapid gradient echo (MPRAGE) sequences. The sequence parameters had a repetition time (TR) = 2,530 ms, echo time (TE) = 3.39 ms, inversion time (TI) = 1,100 ms, flip angle = 7°, FOV = 256 * 256 mm, in-plane resolution = 256 * 256, slice thickness = 1.33 mm, and 144 sagittal slices covering the whole brain.

The second dataset used in this study was obtained from the ADNI database (adni.loni.usc.edu). The ADNI was launched in 2003 as a public-private partnership, led by Principal Investigator Michael W. Weiner, MD. The primary goal of ADNI has been to test whether serial MRI, positron emission tomography (PET), other biological markers, and clinical and neuropsychological assessment can be combined to measure the progression of MCI and early Alzheimer's disease (AD). This study was carried out in accordance with the recommendations of the ADNI database with written informed consent from all subjects. The protocol was approved by the ADNI coordinating committee.

The eligibility criteria for inclusion of subjects are described at http://adni.loni.usc.edu/wp-content/uploads/2010/09/ADNI_GeneralProceduresManual.pdf. General criteria for MCI were

as follows: (1) Mini-Mental-State-Examination (MMSE) scores between 24 and 30 (inclusive), (2) a memory complaint, objective memory loss measured by education adjusted scores on the Wechsler Memory Scale Logical Memory II, (3) a Clinical Dementia Rating (CDR) ≥ 0.5 , and (4) absence of significant levels of impairment in other cognitive domains, essentially preserved activities of daily living, and an absence of dementia.

Three hundred and thirty-nine subjects, which included 170 MCI patients and 169 NC subjects were analyzed in this study. Age, gender and education in the MCI group were matched with the NC group. All subjects received the baseline clinical/cognitive examinations including 1.5T structural MRI scan and were reevaluated at specified intervals (6 or 12 months). The baseline scans were used in our experiments. The 170 MCI subjects included two subcategories: 86 stable MCI (sMCI) and 84 progressive MCI (pMCI). Subjects who converted to AD within 24 months were classified as pMCI, and those not converting into AD within the same period were classified as sMCI. The 169 NC subjects were not converted to MCI or AD within 24 months. The demographic information and clinical characteristics of the participants involved in this study are shown in **Table 1**.

Image Processing

The same pre-processing pipeline was applied in the two datasets by using the FreeSurfer image analysis suite v4.3 (<http://surfer.nmr.mgh.harvard.edu/>). For the second dataset, the pre-processed images were downloaded from the public ADNI site. The pipeline for T1-weighted scans contained (1) registration to the Talairach space, (2) correction for intensity bias, (3) skull stripped from the intensity normalized image, (4) segmentation into white matter, gray matter or cerebrospinal fluid, (5) cutting planes to sphere the hemispheres and remove the cerebellum and brain stem, (6) generation of a single connected mass representing the white matter structure of each hemisphere, and (7) surface tessellation, refinement, and deformation for each hemisphere (Dale et al., 1999). A variety of morphological features such as volumetric (cortical thickness, surface area, and gray matter volume) and geometric (sulcal depth, metric distortion, and mean curvature) measures at each vertex on the pial surface were extracted after the preprocessing. Then, the surface data were resampled to a common subject (usually an average subject) and smoothed with a Gaussian filter (FWHM = 5 mm).

Construction of Individual Morphological Brain Network

A brain network is typically defined as $G = (V, E)$, where V denotes the set of nodes (or vertices) and E denotes the set of edges (or links). In this paper, we parceled the cortical cortex into 68 cortical ROIs based on the Desikan-Killiany Atlas (Desikan et al., 2006). Here, we assumed that nodes represent cortical regions and edges represent the similarity of two cortical regions. Each individual network shares the same set of 68 nodes, which facilitates the comparisons using the edges. Dissimilarity connectivity is measured by the formula below (Székely and Rizzo, 2004). Let A and B denote the ROIs of the

TABLE 1 | Subject demographic and clinical characteristics.

| | MCI (<i>n</i> = 170) | sMCI (<i>n</i> = 86) | pMCI (<i>n</i> = 84) | Control (<i>n</i> = 169) |
|--------------|---------------------------------|---------------------------------|---------------------------------|-------------------------------------|
| Gender (M/F) | 104/66 | 53/33 | 51/33 | 88/81 |
| Age | 74.8 ± 6.7 | 74.6 ± 6.4 | 75.1 ± 7.2 | 75.7 ± 5.1 |
| Education | 15.7 ± 3.0 | 15.8 ± 3.1 | 15.7 ± 3.0 | 16.0 ± 2.7 |
| MMSE | 26.9 ± 1.7 | 27.4 ± 1.8 | 26.4 ± 1.7 | 29.1 ± 0.9 |
| CDR | 1.6 ± 0.8 | 1.5 ± 0.7 | 1.8 ± 1.0 | 0 ± 0.1 |

Age, education, MMSE and CDR are expressed as the mean ± SD. There were no significant differences between the MCI and the control group and between the sMCI and pMCI group in gender, age and education years. The MCI with control groups, and sMCI with pMCI group showed significant differences in the MMSE and CDR. MCI, mild cognitive impairment; sMCI, stable mild cognitive impairment; pMCI, progressive mild cognitive impairment; M/F, Male/Female; MMSE, Mini-Mental-State-Examination; CDR, Clinical Dementia Rating.

k th subject, and then the combined Euclidean distance $e_k(A, B)$ is defined as:

$$e_k(A, B) = \frac{n_1 n_2}{n_1 + n_2} \left(\frac{2}{n_1 n_2} \sum_{i=1}^{n_1} \sum_{j=1}^{n_2} \|a_i - b_j\|_2 - \frac{1}{n_1^2} \sum_{i=1}^{n_1} \sum_{j=1}^{n_1} \|a_i - a_j\|_2 - \frac{1}{n_2^2} \sum_{i=1}^{n_2} \sum_{j=1}^{n_2} \|b_i - b_j\|_2 \right) \tag{1}$$

Let $A = \{a_1, \dots, a_{n_1}\}$ and $B = \{b_1, \dots, b_{n_2}\}$, where a and b denote vertices in A and B , respectively. These elements represent morphological features, which could be either one-dimensional or multi-dimensional. n_1 and n_2 are the numbers of vertices in A and B . Euclidean distance is computed by the 2-norm ($\|\cdot\|_2$).

The first part of the formula $\frac{2}{n_1 n_2} \sum_{i=1}^{n_1} \sum_{j=1}^{n_2} \|a_i - b_j\|_2$ describes the Euclidean distance for any pair of vertices between A and B . $\frac{1}{n_1^2} \sum_{i=1}^{n_1} \sum_{j=1}^{n_1} \|a_i - a_j\|_2$ and $\frac{1}{n_2^2} \sum_{i=1}^{n_2} \sum_{j=1}^{n_2} \|b_i - b_j\|_2$ are the Euclidean distances for any pair of vertices within A and B , respectively.

A smaller intra-regional Euclidean distance indicating uniform morphological feature distribution within ROI results in a distance $e(A, B)$ is more dependent on the Euclidean distance between pairs of vertices in A and B . Moreover, the distance $e(A, B)$ will be influenced if the morphological feature distribution within the ROI is unequal. When A and B have the same morphological feature distribution, the combined Euclidean distance $e(A, B) = 0$.

After calculation of the combined Euclidean distance matrix that reflected the dissimilarity between brain regions, Min-Max normalization was proposed to minimize possible bias in different ranges of different subjects. We chose the Min-Max normalization because of its boundness and direct reflection of the dissimilarity. The Min-Max normalization between regions A and B of the k th subject is computed as:

$$e_{k-n}(A, B) = \frac{e_k(A, B) - e_{k_min}}{e_{k_max} - e_{k_min}} \tag{2}$$

where e_{k_min} and e_{k_max} are the minimum and maximal value in the dissimilarity connectivity of the k th subject, respectively. The value of $e_{k_n}(A, B)$ can be converted to a similarity measurement using the following equation:

$$c_k(A, B) = \exp(-e_{k_n}(A, B)) \tag{3}$$

Based on the above calculation, a 68*68 diagonal symmetry correlation matrix of each subject was obtained. The $c_k(A, B)$ ranges from 0 to 1, and 1 represents that the two morphological feature distributions are identical.

Method Validation

We validated the above method by computing the topological properties of the individual brain network, i.e., small-world, hubs and intraclass correlation coefficient (ICC) in the first dataset. In addition, we applied the edges of each individual morphological network as features to discriminate the MCI and NC in the ADNI dataset. The accuracy of classification was used to assess the effectiveness of our method.

Topological Properties of Networks

We constructed the individual morphological brain network based on the proposed method in a six-dimension situation in the first dataset. The small-world configurations, hubs and reproducibility of individual brain network were calculated and analyzed. The network properties were computed using the Graph-theoretical Network Analysis (GRETNA) toolkit (Wang et al., 2015).

For small-world configurations, the clustering coefficient (C_p), minimum path length (L_p), γ , λ and σ were calculated. Small-worldness (Watts and Strogatz, 1998; Humphries et al., 2006) can be demonstrated mathematically as:

$$\gamma = \frac{C_p}{C_p^{random}} > 1, \lambda = \frac{L_p}{L_p^{random}} \approx 1 \text{ and } \sigma = \frac{\gamma}{\lambda} > 1$$

where *random* represents a random network that consists of the same number of nodes and edges.

The betweenness centrality (BC) is defined as the number of shortest paths between any two nodes running through the given node (Freeman, 1977) and measures the nodal ability of information flow throughout the network. The hubs were defined as the nodes that achieved a higher BC than the sum of the mean and standard deviation for the entire network.

The intraclass correlation coefficient (ICC) was used to estimate the reproducibility of the topological properties of the network (Shrout and Fleiss, 1979). ICC was defined as the fraction of the variance of the chosen graphic property between subjects to the total variance, which is the summation variance of between and within subjects of that property:

$$ICC = \frac{\sigma_{between}^2}{\sigma_{between}^2 + \sigma_{within}^2} \tag{4}$$

If the measurements of repeated scans are consistent for each subject, the ICC would be close to one. An ICC value above 0.75 is considered excellent, and one ranging from 0.59 to 0.75 is considered good (Cicchetti and Sparrow, 1981).

Classification Between MCI and NC Groups

For the second dataset, we used the support vector machine (SVM) classifiers with leave-one-out cross validation (LOOCV) to test the effectiveness of our method. Additionally, feature selection is employed for each individual morphological brain network before classification regarding the curse of dimensionality.

Feature selection

Each network has $p = V \times (V - 1)/2 = 2278$ edges. Due to the high dimensionality of the network features and a small number of samples, also namely, the curse of dimensionality, the classification model often confronts problems such as overfitting and under generalization. Feature selection is considered to reduce the irrelevant or redundant features and improve the performance of classifiers. The least absolute shrinkage and selection operator (Lasso) (Tibshirani, 1996) was applied for feature selection.

Specifically, Lasso was put forward by Tibshirani (1996) for parameter estimation and feature selection in regression analysis. The Lasso algorithm does not focus on selection of subsets but rather on defining a continuous shrinking operation that can produce coefficients of redundant components to zero. It has been shown in the literature (Yamada et al., 2012; Kamkar et al., 2015) that the algorithm can effectively select the relevant features in high dimensional data space. Sparse linear regression is applied for Lasso features calculation with L_1 -norm regularization. In the training set, let matrix $X = [x_1, x_2, \dots, x_n]^T \in \mathbb{R}^{n \times m}$ represent m features of n subjects, $y = [y_1, y_2, \dots, y_n]^T \in \mathbb{R}^{n \times 1}$ be an n dimension corresponding to sample labels ($y_i = 1$ for MCI and $y_i = -1$ for NC) and m denotes the number of edges except the duplicated part in the individual brain network. The linear regression model is defined as follows:

$$\hat{y} = Xw \tag{5}$$

where $w = [w_1, w_2, \dots, w_n]^T \in \mathbb{R}^{n \times 1}$ denotes the regression coefficient vector and \hat{y} denotes the predicted label vector. The objective function is minimized as follows to estimate w :

$$\min_w \frac{1}{2} \|Xw - y\|_2^2 + \lambda \|w\|_1 \tag{6}$$

where $\lambda > 0$ is a regularization parameter in control of the sparsity of the model, i.e., many entries of w are zeros. $\|w\|_1$ is the L_1 -norm of w defined as $\sum_{i=1}^n |w_i|$. The SLEP package (Liu et al., 2009) was used for solving sparse linear regression. If an edge is selected as a feature in each iteration of the LOOCV classification, the edge is considered as discriminative in the brain network.

Classification

According to the selected features described above, a commonly used classifier SVM was implemented using the LIBSVM library (Chang and Lin, 2011) in MATLAB, with a radial basis function (RBF) kernel and an optimal value for the penalized coefficient C (a constant determining the tradeoff between training error and model flatness). The RBF kernel was utilized for its good

performance especially on small sample problems (Hertz et al., 2006) and defined as follows:

$$K(x_1, x_2) = \exp\left(-\frac{\|x_1 - x_2\|^2}{2\sigma^2}\right) \quad (7)$$

where x_1 and x_2 are two feature vectors and σ is the width of the Gaussian kernel. To obtain the optimal SVM model, we selected the optimal hyperparameters (C and σ) through a grid-search. Specifically, the classification was performed via a LOOCV in which one subject was selected as the testing set and the rest were used as the training set. The parameters were changed after all samples were classified to estimate the LOOCV accuracy. In the end, the average accuracy across all subjects was computed as a performance measurement. The hyperparameter values that lead to the highest performance are then selected. The pipeline of our classification framework for MCI and NC is presented in **Figure 1**. The pipeline of classification framework for sMCI and pMCI is same as the classification framework for MCI and NC.

RESULTS

Small-World Configurations

As shown in **Figure 2**, γ is larger than one (max = 1.86, min = 1.25) throughout the whole sparsity range, while λ is close to one (max = 1.15, min = 1.02) by our method. Hence, the individual morphological brain networks exhibit a higher C_p than the random network, while maintaining a similar L_p . As expected, σ was found to be larger than one (max = 1.62, min = 1.23) throughout the entire sparsity range. The results showed the existence of small world property in the constructed individual morphological brain network by using six features. Moreover, as the sparsity increased, the increase of C_p and decrease of L_p , λ , σ , and γ in **Figure 2** are in accordance with the variation tendency of previous reports (Kong et al., 2015; Li et al., 2017).

Furthermore, the sparsity of 23% is highlighted for convenient comparison with previous studies (Tijms et al., 2012; Kong et al., 2015). As listed in **Table 2**, our results are similar to previous individual-based morphological brain network studies, whereas the population-based morphological brain networks and functional networks exhibit smaller results than our method in most small world configurations.

Hubs

Hubs were investigated for all subjects and sparsities. A total of four hub regions were identified throughout the entire sparsity range across all subjects, including the left and right frontal pole, right rostral anterior cingulate and right transverse temporal cortex.

Reproducibility

The reproducibility of our method was evaluated by measuring the ICCs of network properties for scans with acquisitions of two different time points in the same subjects. The ICC was investigated throughout the entire sparsity range. The C_p , L_p , and BC were examined in this study.

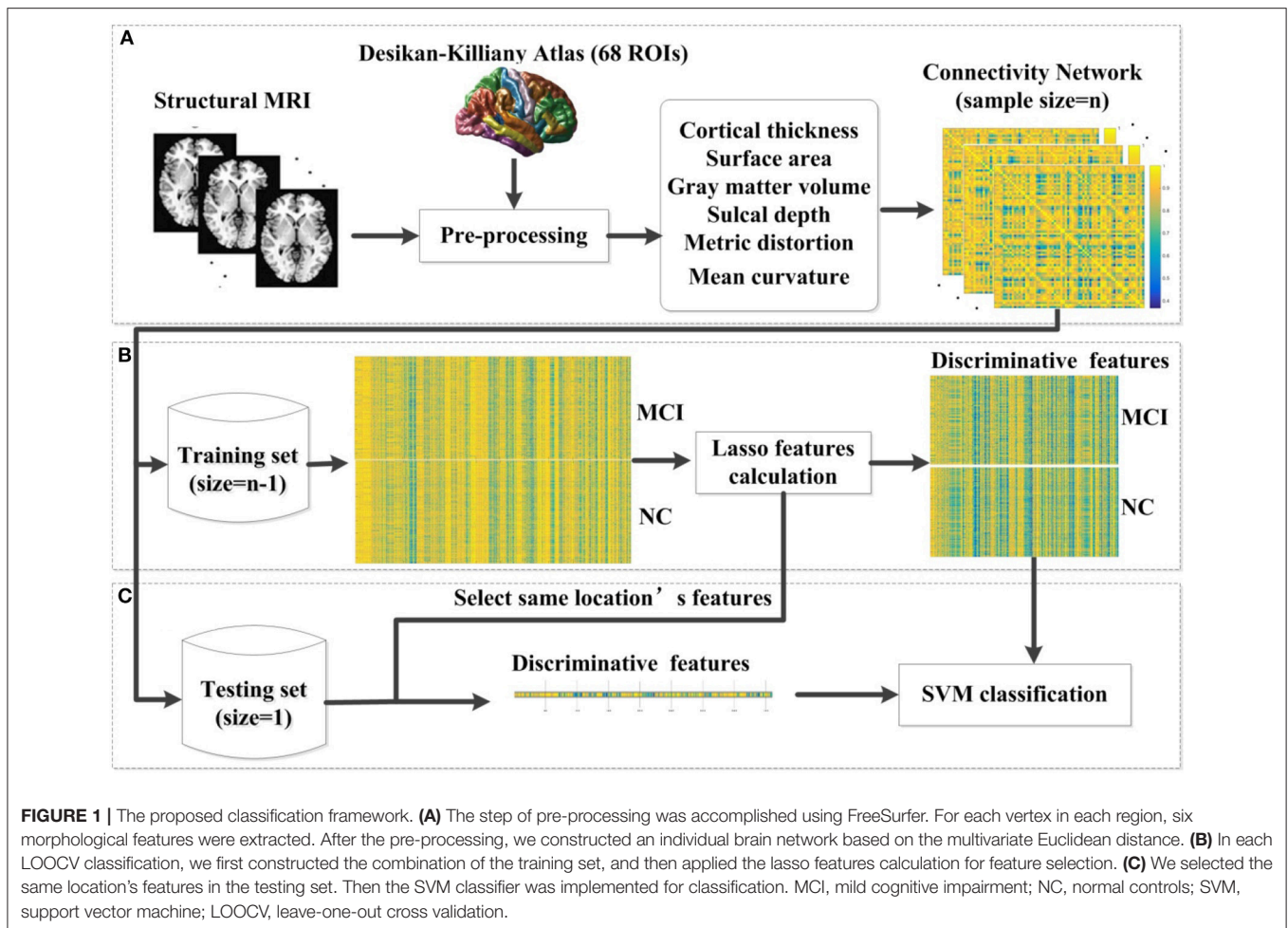
The results indicated that C_p is highly reproducible (minimum ICC = 0.72, average ICC = 0.83), as shown in **Figure 3A**. Moreover, the reproducibility of L_p (minimum ICC = 0.62, average ICC = 0.82) and BC (minimum ICC = 0.82, average ICC = 0.87) are shown in **Figures 3B,C**. Most results of ICC were significant, except for L_p at sparsity of 20, 21, and 22% ($p = 0.098, 0.13$ and 0.10 , separately). The reliability of our method performed well in accordance with previous studies (Cicchetti and Sparrow, 1981; Li et al., 2017). For example, the reproducibility of C_p and L_p are similar to Li's results (minimum C_p ICC = 0.71, average C_p ICC = 0.83; minimum L_p ICC = 0.63, average L_p ICC = 0.81) and the reproducibility of BC was better than Li's result (minimum BC ICC = 0.629, average BC ICC = 0.78).

Classification Performance

In this subsection, we made a comparison of classification accuracies between our method and other methods as reported in previous studies, which included Kong's method (Kong et al., 2014), Kim's method (Kim et al., 2016), Zheng's method (Zheng et al., 2015), Dai's method (Dai et al., 2013), and Wee's method (Wee et al., 2013). The details of these methods are described in **Table 3**.

Like other papers, we selected cortical thickness as the single dimension feature to construct individual brain network. All methods employed an identical feature selection method after the constructions of each individual brain network and optimization of the parameters in SVM. The accuracy, sensitivity, specificity and area under receiver operating characteristic (ROC) curve (AUC) values of each method were calculated as evaluation metrics for the performance. The results are summarized in **Tables 4, 5**. It can be clearly observed that our method performed well compared with previous methods in the classification task. In particular, our method achieved an accuracy of 79.65% in distinguishing MCI patients from NC with a sensitivity of 78.82% and achieved an accuracy of 70.59% in distinguishing sMCI from pMCI with a sensitivity of 75.58%.

Although accuracy is commonly used for an evaluation of classification, it may provide a biased description due to its dependency on the decision threshold selection in SVM. The ROC curve is shown to be a simple but completely empirical description of this decision threshold effect, indicating all possible combinations of the relative frequencies of the various kinds of correct and incorrect decisions. In ROC space, the (0, 1) point represents a perfect classifier (all samples are correctly predicted). Thus, the nearer a point is to the (0, 1) point (closer to the upper left corner), the better a classifier is (Prati et al., 2011). **Figures 4, 5** show the ROC graphs of classification using different methods to construct individual brain networks, from which we can see that the ROC curve of our method is closer to the upper left corner than some conventional methods. In addition, a single measure of classification performance can be derived from the area under the ROC curve (AUC). A larger AUC indicates a better classifier. In **Tables 4, 5** the AUC for all methods are listed and it can be seen that our method achieved AUC scores of 0.84 for MCI vs. NC, and 0.73 for sMCI vs. pMCI, while most other methods slightly underperformed.



Comparison of Our Method Using One Dimension and Six Dimensions in Classification

In this experiment, we compared the performance of the proposed method by using one dimension and six dimensions. We used cortical thickness as the single dimension and used cortical thickness, surface areas, gray matter volume, sulcal depth, metric distortion and mean curvature as the six dimensions. **Tables 4,5** show that our method of applying six dimensions outperforms the one only using a single cortical thickness feature, which achieved 80.53% and 77.06% for accuracy in distinguishing MCI from NC and distinguishing sMCI from pMCI, respectively. The ROC graphs in **Figures 6,7** illustrate the classification performance based on brain networks that were constructed using one dimension and six dimensions. We also list the AUC score in **Tables 4,5**. It can be noticed that compared with the univariate situation, individual brain network construction based on multivariate performs better in classification with an AUC score of 0.86 and 0.74, respectively.

Most Discriminative Features of Individual Brain Networks

The most discriminative features demonstrate the edges selected in each time of cross-validation for classification based on multivariate connectivity. Here, we selected the most discriminative features under the best condition. In **Figure 8**, the blocks of the circle represent ROIs. As shown in **Figures 8A,B** the most discriminative edges connected most ROIs in the brain.

Based on the selected edges, pairs of regions that contribute to classification are not only within the same hemisphere and the same lobe but also across different hemispheres and lobes, which indicates the abnormalities caused by MCI involve the entire brain rather than certain areas. The number of discriminative edges that connect the two hemispheres was 115. Conversely, the number of discriminative edges that are the connections within a single hemisphere was relatively low, with quantities of 64 and 43 for the left and right hemisphere, respectively. We correlated the most discriminative edges with MMSE and CDR scores. In **Figures 8C,D**, the selected edges that were significant correlated ($p < 0.05$) with MMSE and CDR are shown. As seen, these edges

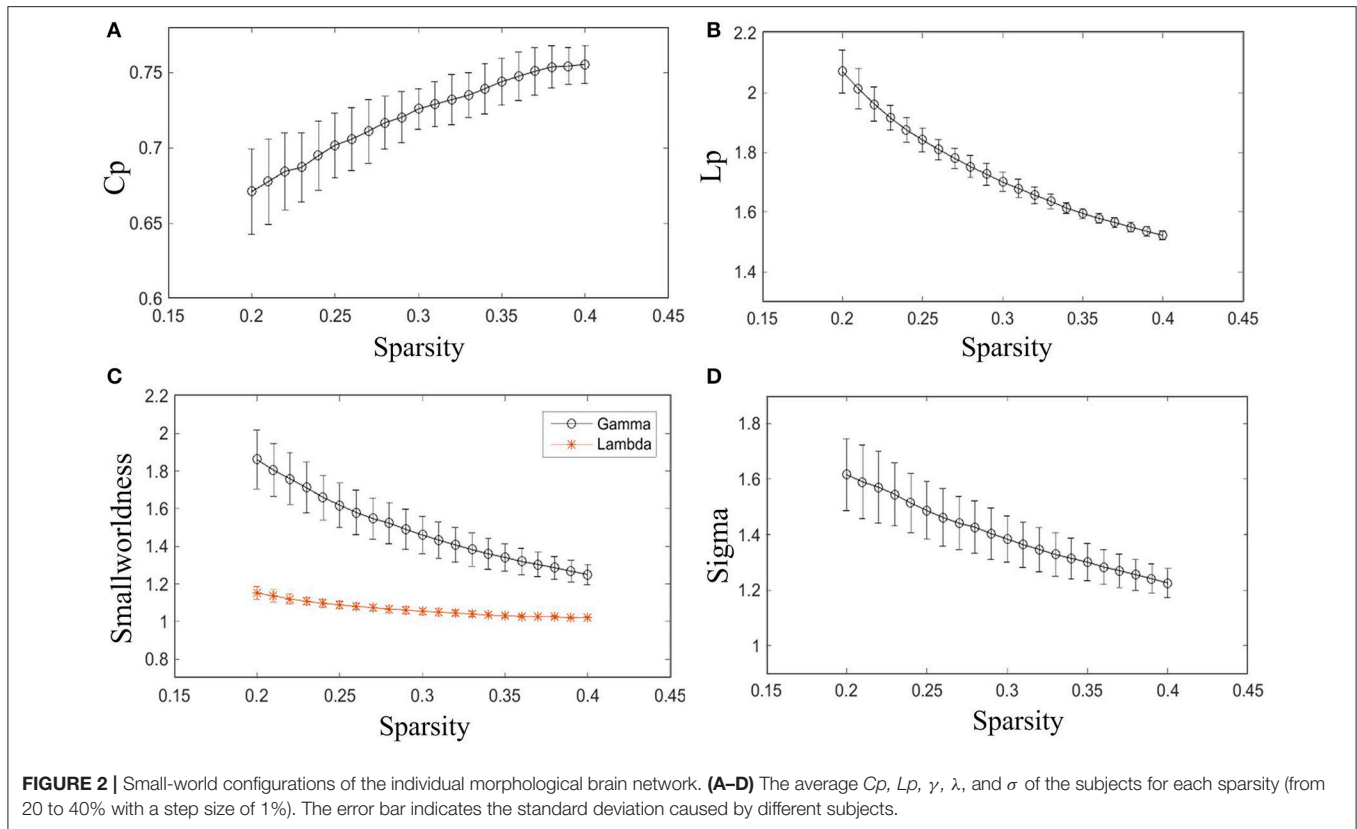


TABLE 2 | Comparison of small world configurations between the present study and previous studies.

| Method | N | C_p | L_p | γ | λ | σ | S (%) |
|-----------------------------------------------------|--------|-------|-------|----------|-----------|----------|---------|
| INDIVIDUAL-BASED MORPHOLOGICAL BRAIN NETWORK | | | | | | | |
| Our method | 68 | 0.69 | 1.92 | 1.71 | 1.10 | 1.54 | 23 |
| Li's method (Li et al., 2017) | 68 | 0.62 | 2.23 | 1.81 | 1.22 | 1.52 | 23 |
| Kong's method (Kong et al., 2015) | 90 | 0.66 | 1.92 | 1.74 | 1.15 | 1.50 | 23 |
| Tijms's method (Tijms et al., 2012) | 6,982 | 0.53 | 1.86 | 1.35 | 1.05 | 1.28 | 23 |
| POPULATION-BASED MORPHOLOGICAL BRAIN NETWORK | | | | | | | |
| He's method (He et al., 2007) | 54 | ≈0.3 | ≈1.6 | ≈1.35 | ≈1 | ≈1.35 | 23 |
| Yao's method (Yao et al., 2010) | 90 | ≈0.49 | ≈1.89 | ≈1.62 | ≈1.1 | ≈1.47 | 23 |
| Zhu's method (Zhu et al., 2012) | 90 | ≈0.26 | NR | ≈1.20 | ≈1.03 | ≈1.17 | 23 |
| FUNCTIONAL BRAIN NETWORK | | | | | | | |
| Van's method (Van Essen, 1997) | 10,000 | ≈0.52 | ≈1.75 | ≈1.9 | ≈1.03 | ≈1.85 | 20 |
| Zhang's method (Zhang et al., 2011) | 90 | ≈0.33 | ≈1.65 | ≈1.3 | ≈1 | ≈1.4 | 23 |

N , C_p , and L_p denote the number of nodes in the networks, the average clustering coefficient and the average shortest path length, respectively. γ represents the ratio of the clustering coefficient of the network over that of the random network. λ represents the ratio of the average shortest path length of the network over that of the random network. σ indicates the small-worldness. The small world attributes of previous studies are inferred (with ≈). NR, not reported.

are predominately in the frontal, temporal, parietal, and insula parts.

DISCUSSION

In the present study, we introduced a new method to construct individual morphological brain network. The combination of inter-regional Euclidean distance and intra-regional Euclidean

distance was used to quantify the inter-regional relations. Through the small-world configurations analysis, our method confirmed the existence of small world property. In addition, as listed in **Table 2**, the population-based morphological brain networks and functional networks exhibit smaller results than our results in most small world configurations, which may suggest that the individual morphological brain networks demonstrate a stronger integration and segregation because

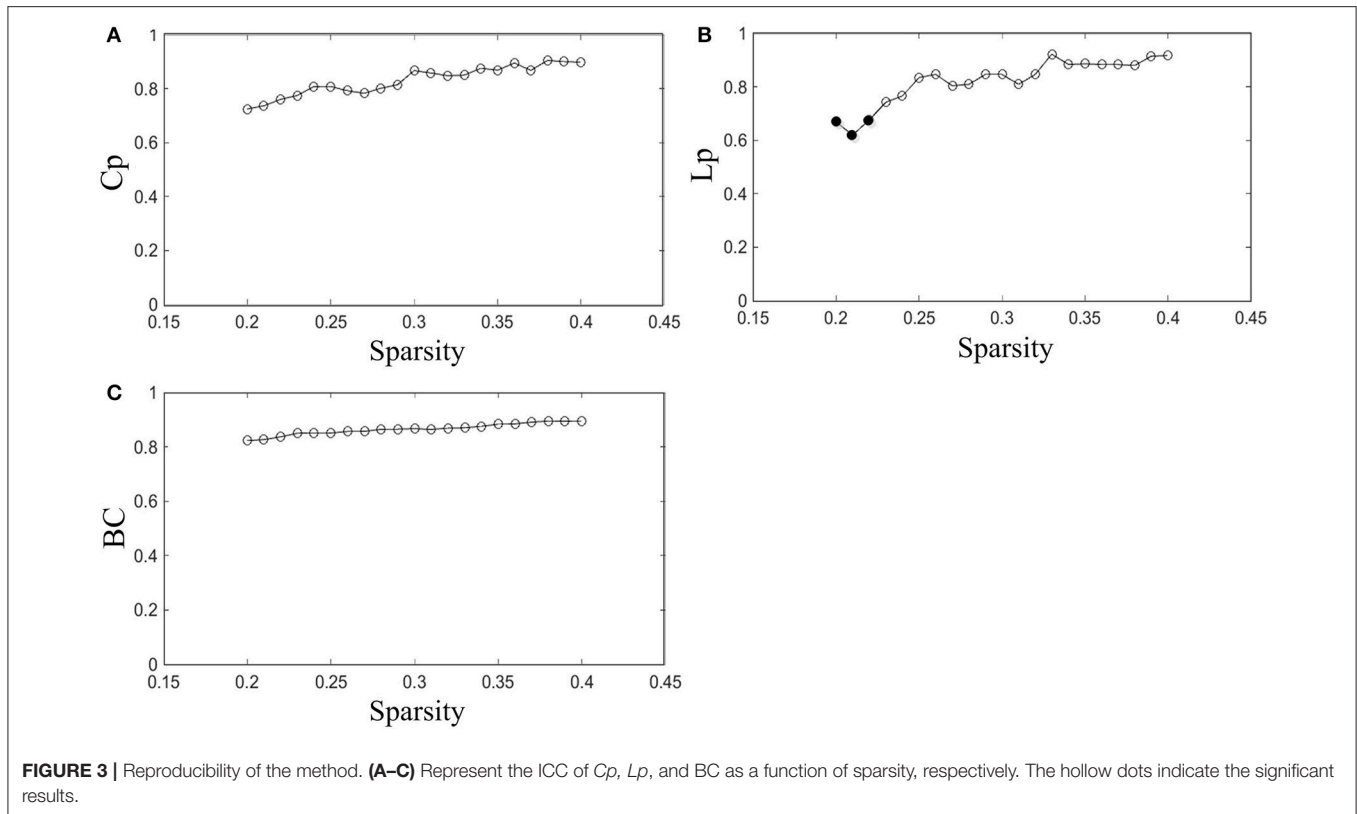


FIGURE 3 | Reproducibility of the method. (A–C) Represent the ICC of C_p , L_p , and BC as a function of sparsity, respectively. The hollow dots indicate the significant results.

TABLE 3 | The methods of constructing individual morphological brain networks in previous studies.

| Author | Methods | Explanation |
|----------------------------|-----------------------------------------------------------------------------------------------------------------------------------------------|------------------------------------------------------------------------------------------------------------------------------------------------------------------------------------------------------------|
| Kong (Kong et al., 2014) | $KL(i, j) = \int_x (i(x) \log(\frac{i(x)}{j(x)}) + j(x) \log(\frac{j(x)}{i(x)}))$, $c(i, j) = e^{-KL(i, j)}$ | $i(x)$ and $j(x)$ denote the probability density functions (PDF) of i and j respectively. |
| Kim (Kim et al., 2016) | $Z(i, j) = \frac{T(i) - T(j)}{\sigma_j}$, $c(i, j) = \frac{Z(i, j) + Z(j, i)}{2}$ | $T(i)$ and $T(j)$ denote the mean value of cortical thickness in i and j respectively, σ_i and σ_j denote the standard deviation of regional cortical thickness of regions i and j . |
| Wee (Wee et al., 2013) | $d(i, j) = [T(i) - T(j)]^2$, $\sigma = \sqrt{\sigma_i + \sigma_j}$, $c(i, j) = \exp(-\frac{d(i, j)}{2\sigma^2})$ | η is an input parameter. |
| Dai (Dai et al., 2013) | $d(i, j) = [T(i) - T(j)]^2$, $c(i, j) = \exp(-\frac{d(i, j)}{\eta})$ | |
| Zheng (Zheng et al., 2015) | $C_{precision}(i, j) = \frac{1}{m} \sum_{p=1}^m t_i^p - T(i) \frac{1}{n} \sum_{q=1}^n t_j^q - T(j) $, $C_{rough}(i, j) = T(i) - T(j) ^2$ | t denotes the vertex's cortical thickness, m and n are the number of points in i and j , respectively. |

In these formulas, i and j denote two brain regions; $c(i, j)$ denotes the correlation between i and j .

the inter-individual variability is highly reserved (Kanai and Rees, 2011). Hubs such as left and right frontal pole and right rostral anterior cingulate have been reported in previous studies (Hagmann et al., 2008; Van den Heuvel and Sporns, 2013). The ICC was used to estimate the reproducibility of graph theoretical measures. The results indicated that the reliability of our method performed well in accordance with previous studies. In addition, compared with other conventional methods, which average the vertices within ROIs, our method improves the classification performance in univariate situation. Here, we explained the rationality of our method from two aspects. (1) In previous

studies, the individual morphological brain networks were mostly constructed based on the average value of morphological features within the ROI. However, the abnormal region for pathology might be only a fraction of the defined ROI and the abnormal change of brain region may be ignored by taking the average, which potentially reduces the discriminative power. In our proposed method, we directly used the morphological features of vertices to retain more detailed information. The results of Kong's method (Kong et al., 2014) and Zheng's method (Zheng et al., 2015) in **Table 4** also demonstrated the importance of detailed information. (2) In previous studies, the

TABLE 4 | Classification performance of different methods to distinguish MCI and NC.

| Method | Accuracy (%) | Sensitivity (%) | Specificity (%) | AUC |
|----------------------------------------|--------------|-----------------|-----------------|-------------|
| Our method using six dimensions | 80.53 | 79.41 | 81.66 | 0.86 |
| Our method using one dimension | 79.65 | 78.82 | 80.47 | 0.84 |
| Kong's Method | 77.88 | 74.12 | 81.66 | 0.84 |
| Kim's Method | 75.81 | 71.18 | 80.47 | 0.79 |
| Dai's Method | 76.70 | 73.53 | 79.88 | 0.82 |
| Zheng's Method | 79.94 | 76.47 | 83.43 | 0.84 |
| Wee's Method | 77.29 | 73.53 | 81.07 | 0.83 |

One dimension denotes cortical thickness; six dimensions include cortical thickness, surface areas, gray matter volume, sulcal depth, metric distortion, and mean curvature. The lower bold values mean the best performance (accuracy, sensitivity, specificity and AUC) among different methods in one dimension situation. The upper bold values mean the best performance of our method in one and six dimension. AUC, area under the curve.

TABLE 5 | Classification performance of different methods to distinguish sMCI and pMCI.

| Method | Accuracy (%) | Sensitivity (%) | Specificity (%) | AUC |
|----------------------------------------|--------------|-----------------|-----------------|-------------|
| Our method using six dimensions | 77.06 | 77.91 | 76.19 | 0.74 |
| Our method using one dimension | 70.59 | 75.58 | 65.48 | 0.73 |
| Kong's Method | 65.89 | 67.44 | 64.29 | 0.67 |
| Kim's Method | 67.06 | 63.95 | 70.24 | 0.65 |
| Dai's Method | 63.53 | 70.93 | 55.95 | 0.64 |
| Zheng's Method | 67.65 | 63.95 | 71.43 | 0.68 |
| Wee's Method | 65.89 | 67.44 | 64.29 | 0.69 |

One dimension denotes cortical thickness; six dimensions include cortical thickness, surface areas, gray matter volume, sulcal depth, metric distortion, and mean curvature. The lower bold values mean the best performance (accuracy, sensitivity, specificity and AUC) among different methods in one dimension situation. The upper bold values mean the best performance of our method in one and six dimension. AUC, area under curve.

morphological distribution within an ROI was not considered, which may influence the strength of edges between ROIs. In our method, the dissimilarity connectivity was the combination of inter-regional Euclidean distance and intra-regional Euclidean distance, while previous methods only considered the relation between two ROIs.

An inherent advantage of our method is that it can be applied to multi-dimensional situations. In previous studies, researchers have found the small-world properties were disrupted for brain networks that were constructed based on cortical thickness in MCI patients (Zhou and Lui, 2013), and the brain network based on the surface area can reveal topological properties of the networks resulting from the concurrent changes between different anatomical regions (Sanabriadiaz et al., 2010). The sulcal depth, curvature, and metric distortion related to cortical folding vary and could be more suitable descriptors for finding the anatomical-axonal and morphological connectivity correlation

(Van Essen, 1997). Previous studies have reported that brain networks based on both the volumetric measures and geometric measures showed significant differences in graphical properties between aMCI and NC (Li et al., 2016). These results may suggest that brain network construction based on multiple features is beneficial to the diagnosis and analysis of neurological diseases. However, most previous approaches (Dai et al., 2013; Wee et al., 2013; Kong et al., 2014; Zheng et al., 2015; Kim et al., 2016) that constructed individual brain networks only considered one morphological feature (e.g., cortical thickness or gray matter volume) between two brain regions. The first paper involved in building morphological brain networks based on multiple morphological features demonstrated that multiple morphometric features can be applied to form a rational reproducible individual-based morphological brain network (Li et al., 2017), but it averaged the morphological features within each ROI, such as the mean cortical thickness, which may neglect some detailed information. In our method, every vertex's different kinds of cortical features within each ROI were considered and the relations between brain regions were determined based on these features. In this paper, the multiple morphological features including cortical thickness, surface areas, gray matter volume, sulcal depth, metric distortion and mean curvature as well as the cortical thickness as a single feature were used for individual brain network construction. The results show (Tables 4,5) that the brain network constructed from the combination of morphological features outperforms the one only considering cortical thickness. The resulting high AUC value proves the excellent classification power and generalizability of our proposed method on an unseen data set, as well as the ability to construct an accurate and credible individual morphological brain network. Moreover, the classification performance of our method in a multivariate situation revealed the existence of useful information within these morphological features. The abnormal connectivity across various regions can be located within different morphological features, which greatly benefits the detection of neurological diseases.

An interesting finding shown in Figures 8A,B is that the majority of the selected correlative features in the MCI and NC classification task are the edges connecting the left and right hemisphere. This might suggest that the most significant differences between MCI subjects and health subjects are changes in the connections between the left and the right hemisphere. The connection alterations caused by MCI pathological attacks are not restricted to certain brain areas but are widely spread over the whole brain. What's more, the most discriminative edges connecting the regions in our study are consistent with previous publications, such as the lingual gyrus, postcentral gyrus, middle temporal gyrus, pars opercularis, and superior frontal sulcus (Li et al., 2014; Wei et al., 2016). Previous studies have found that subjects with MCI have abnormal network patterns in the lingual gyrus and middle temporal gyrus (Yao et al., 2010). He et al. (2008) demonstrated an abnormal correlation between the bilateral postcentral gyrus in AD. From Figures 8C,D we can see the selected edges are predominately connected to the regions of the frontal, temporal,

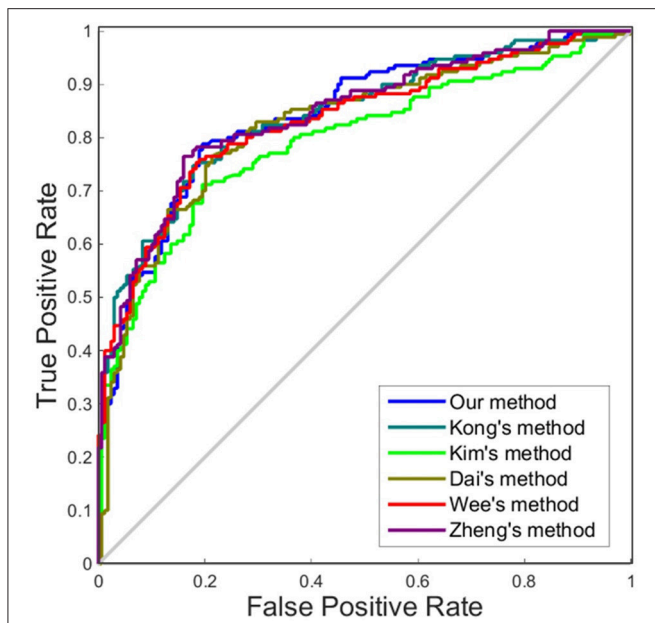


FIGURE 4 | ROC curves of different methods using one dimension to distinguish MCI and NC. The different line colors represent different methods to construct individual morphological brain networks based on cortical thickness. ROC, receiver operating characteristic.

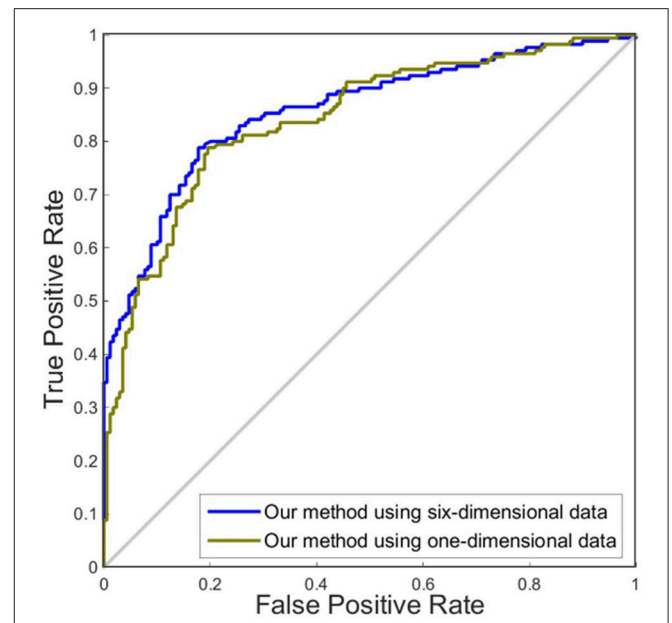


FIGURE 6 | ROC curves of our method using different dimensions of original features to distinguish MCI and NC. The different line colors represent ROC curves of our methods of constructing individual morphological brain networks based on different dimensional features. ROC, receiver operating characteristic.

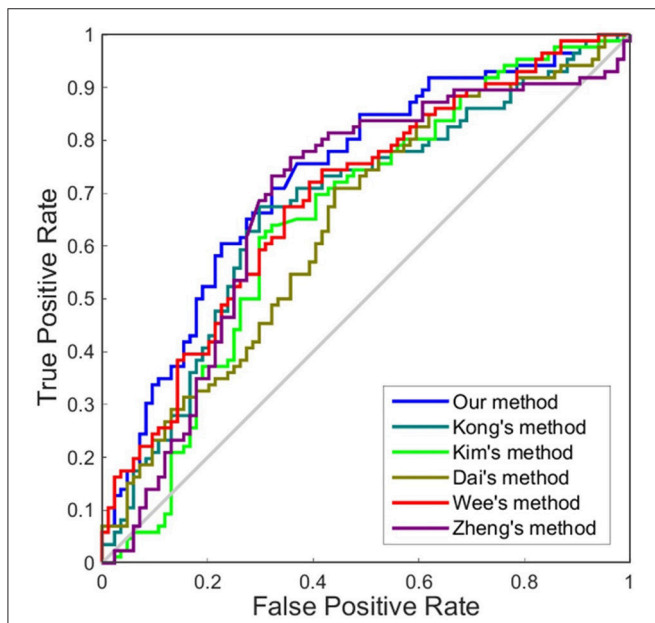


FIGURE 5 | ROC curves of different methods using one dimension to distinguish sMCI and pMCI. The different line colors represent different methods to construct individual morphological brain networks based on cortical thickness. ROC, receiver operating characteristic.

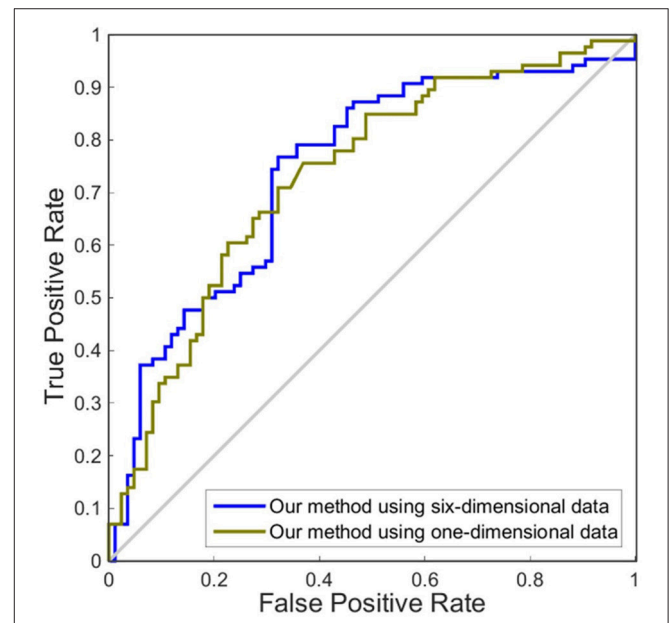


FIGURE 7 | ROC curves of our method using different dimensions of original features to distinguish sMCI and pMCI. The different line colors represent ROC curves of our method of constructing individual morphological brain networks based on different dimensional features. ROC, receiver operating characteristic.

parietal, and insula parts. These regions have been reported that retain more hubs which are considered to be the substrates of human cognition and consciousness (Yao et al., 2010). In

addition, some regions are associated with changes in different morphological features in MCI subjects, such as the middle frontal gyrus with cortical thickness, the postcentral gyrus with

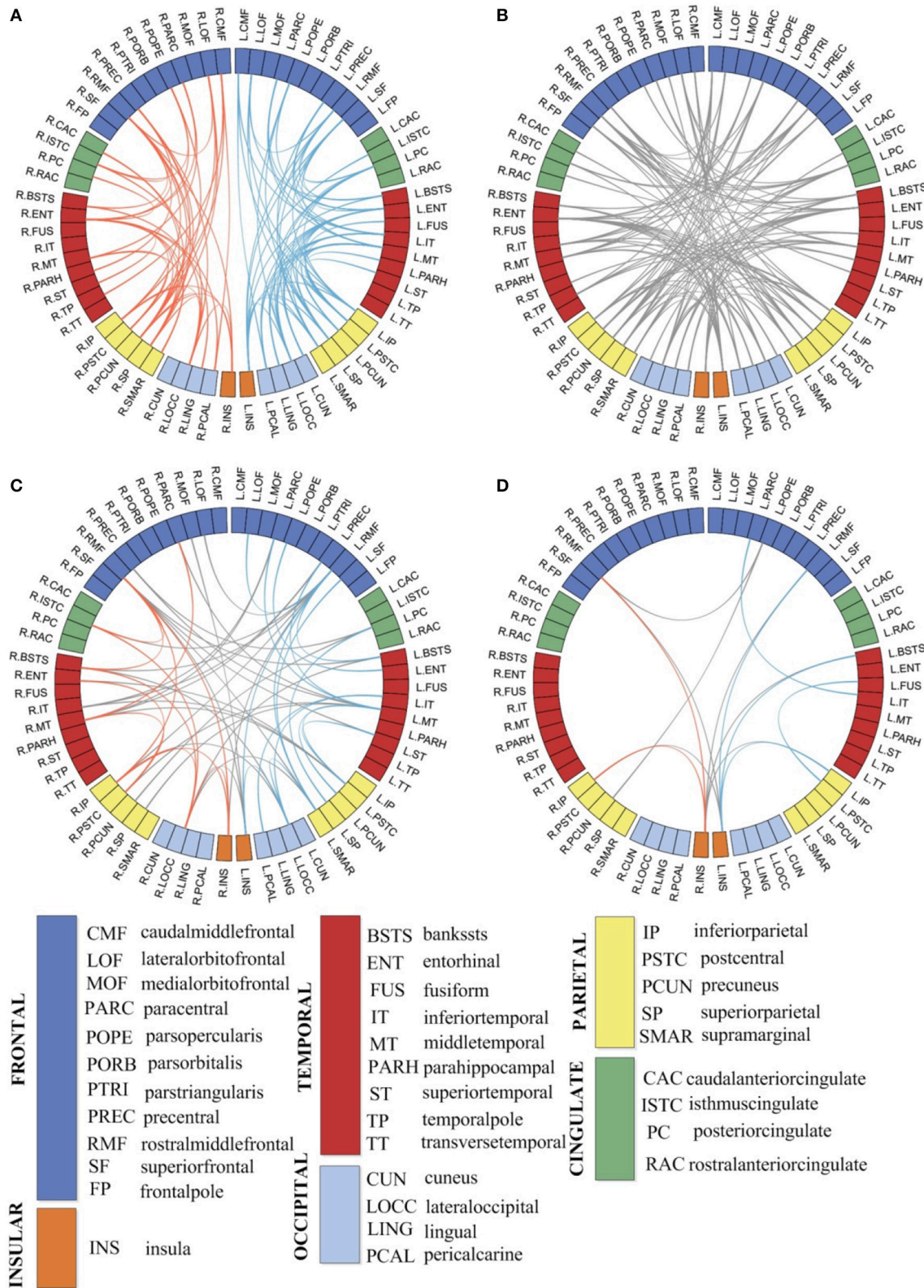


FIGURE 8 | The most discriminative edges of individual morphological brain networks in classification (A,B) and the significant correlation of the most discriminative edges with MMSE (C) and CDR (D) scores. L, left hemisphere; R, right hemisphere; the different colors of the blocks represent ROIs in different areas of the cortical surface. The blue lines represent the discriminative edges in the left hemisphere; the red lines represent the discriminative edges in the right hemisphere. The gray lines represent the discriminative edges between the left and right hemisphere.

metric distortion, the pars opercularis with mean curvature, the lingual gyrus with surface area, and the superior frontal sulcus with sulcal depth (Li et al., 2014). In conclusion, our results suggest that changes in the cortical regions may be associated with mechanisms underlying the conversion of MCI to AD, and the changes were displayed in multiple morphological features. These findings illustrate the potential application of our proposed method.

There are still some limitations in this study. First, the selection of the brain atlas could affect the organization of the individual brain network (Wang et al., 2016). In the future, it is important to validate our proposed method in different atlases. Second, in the current study, we combined multiple morphological features to construct the individual network, and we validated the effectiveness of our method. However, it is noticeable that the physiological explanation of this network is difficult. Third, a recent study (Seidlitz et al., 2017) proposed an individual brain network method by estimating the inter-regional correlation based on multiple macro- and micro-structural multimodal MR variables. And this network could capture cellular, molecular and functional features of the brain and even predict inter-individual differences in cognition. In future, it would be interesting to employ multiple morphometric parameters measured using multimodal MRI. Last, each feature type had its distinct contribution when discriminating between two groups. In the future, we may first select the most discriminant features and then construct the individual network, which could improve its classification performance.

AUTHOR CONTRIBUTIONS

KY, XW, and SL designed the experiments. XL assembled the data. KY performed the experiments and prepared the manuscript. XW, QL, and XZ helped in manuscript writing. SL

was in charge of manuscript verification. All authors reviewed the manuscript.

ACKNOWLEDGMENTS

This work was supported by the National Natural Science Foundation of China (Grant No. 81471731, 81622025).

Data collection and sharing for this project was funded by the Alzheimer's Disease Neuroimaging Initiative (ADNI) (National Institutes of Health Grant U01 AG024904) and DOD ADNI (Department of Defense award number W81XWH-12-2-0012). ADNI is funded by the National Institute on Aging, the National Institute of Biomedical Imaging and Bioengineering, and through generous contributions from the following: AbbVie, Alzheimer's Association; Alzheimer's Drug Discovery Foundation; Araclon Biotech; BioClinica, Inc.; Biogen; Bristol-Myers Squibb Company; CereSpir, Inc.; Eisai Inc.; Elan Pharmaceuticals, Inc.; Eli Lilly and Company; EuroImmun; F.Hoffmann-La Roche Ltd. and its affiliated company Genentech, Inc.; Fujirebio; GE Healthcare; IXICO Ltd.; Janssen Alzheimer Immunotherapy Research & Development, LLC.; Johnson & Johnson Pharmaceutical Research & Development LLC.; Lumosity; Lundbeck; Merck & Co., Inc.; Meso Scale Diagnostics, LLC.; NeuroRx Research; Neurotrack Technologies; Novartis Pharmaceuticals Corporation; Pfizer Inc.; Piramal Imaging; Servier; Takeda Pharmaceutical Company; and Transition Therapeutics. The Canadian Institutes of Health Research is providing funds to support ADNI clinical sites in Canada. Private sector contributions are facilitated by the Foundation for the National Institutes of Health (www.fnih.org). The grantee organization is the Northern California Institute for Research and Education, and the study is coordinated by the Alzheimer's Disease Cooperative Study at the University of California, San Diego. ADNI data are disseminated by the Laboratory for NeuroImaging at the University of Southern California.

REFERENCES

- Bassett, D. S., Bullmore, E., Verchinski, B. A., Mattay, V. S., Weinberger, D. R., and Meyer-lindenberg, A. (2008). Hierarchical organization of human cortical networks in health and schizophrenia. *J. Neurosci.* 28, 9239–9248. doi: 10.1523/JNEUROSCI.1929-08.2008
- Bernhardt, B. C., Rozen, D. A., Worsley, K. J., Evans, A. C., Bernasconi, N., and Bernasconi, A. (2009). Thalamo-cortical network pathology in idiopathic generalized epilepsy: insights from MRI-based morphometric correlation analysis. *Neuroimage* 46, 373–381. doi: 10.1016/j.neuroimage.2009.01.055
- Bernhardt, B. C., Worsley, K. J., Besson, P., Concha, L., Lerch, J. P., Evans, A. C., et al. (2008). Mapping limbic network organization in temporal lobe epilepsy using morphometric correlations: insights on the relation between mesiotemporal connectivity and cortical atrophy. *Neuroimage* 42, 515–524. doi: 10.1016/j.neuroimage.2008.04.261
- Cachia, A., Mangin, J. F., Rivière, D., Kherif, F., Bodaert, N., Andrade, A., et al. (2003). A primal sketch of the cortex mean curvature: a morphogenesis based approach to study the variability of the folding patterns. *IEEE Trans. Med. Imaging* 22, 754–765. doi: 10.1109/TMI.2003.814781
- Chang, C. C., and Lin, C. J. (2011). LIBSVM: a library for support vector machines. *ACM Trans. Intell. Syst. Technol.* 2, 1–27. doi: 10.1145/1961189.1961199
- Cicchetti, D. V., and Sparrow, S. A. (1981). Developing criteria for establishing interrater reliability of specific items: applications to assessment of adaptive behavior. *Am. J. Ment. Defic.* 86, 127–137.
- Dai, D., He, H., Vogelstein, J. T., and Hou, Z. (2013). Accurate prediction of AD patients using cortical thickness networks. *Mach. Vis. Appl.* 24, 1445–1457. doi: 10.1007/s00138-012-0462-0
- Dale, A. M., Fischl, B., and Sereno, M. I. (1999). Cortical surface-based analysis. I. Segmentation and surface reconstruction. *Neuroimage* 9, 179–194. doi: 10.1006/nimg.1998.0395
- Desikan, R. S., Ségonne, F., Fischl, B., Quinn, B. T., Dickerson, B. C., Blacker, D., et al. (2006). An automated labeling system for subdividing the human cerebral cortex on MRI scans into gyral based regions of interest. *Neuroimage* 31, 968–980. doi: 10.1016/j.neuroimage.2006.01.021
- Freeman, L. C. (1977). A set of measures of centrality based on betweenness. *Sociometry* 40, 35–41. doi: 10.2307/3033543
- Hagmann, P., Cammoun, L., Gigandet, X., Meuli, R., Honey, C. J., Wedeen, V. J., et al. (2008). Mapping the structural core of human cerebral cortex. *PLoS Biol.* 6:e159. doi: 10.1371/journal.pbio.0060159
- He, Y., Chen, Z., and Evans, A. (2007). Small-world anatomical networks in the human brain revealed by cortical thickness from MRI. *Cereb. Cortex* 17, 2407–2419. doi: 10.1093/cercor/bhl149


- He, Y., Chen, Z., and Evans, A. (2008). Structural insights into aberrant topological patterns of large-scale cortical networks in Alzheimer's disease. *J. Neurosci.* 28, 4756–4766. doi: 10.1523/JNEUROSCI.0141-08.2008
- He, Y., Chen, Z., Gong, G., and Evans, A. (2009). Neuronal networks in Alzheimer's disease. *Neuroscientist* 15, 333–350. doi: 10.1177/1073858409334423
- Hertz, T., Hillel, A. B., and Weinshall, D. (2006). "Learning a kernel function for classification with small training samples", in *Proceedings. 23rd International Conference on Machine Learning*. (Pittsburgh, PA: ACM), 401–408.
- Humphries, M. D., Gurney, K., and Prescott, T. J. (2006). The brainstem reticular formation is a small-world, not scale-free, network. *Proc. Biol. Sci.* 273, 503–511. doi: 10.1098/rspb.2005.3354
- Kamkar, I., Gupta, S. K., Phung, D., and Venkatesh, S. (2015). Stable feature selection for clinical prediction: exploiting ICD tree structure using Tree-Lasso. *J. Biomed. Inform.* 53, 277–290. doi: 10.1016/j.jbi.2014.11.013
- Kanai, R., and Rees, G. (2011). The structural basis of inter-individual differences in human behaviour and cognition. *Nat. Rev. Neurosci.* 12, 231–242. doi: 10.1038/nrn3000
- Kim, H. J., Shin, J. H., Han, C. E., Kim, H. J., Na, D. L., Sang, W. S., et al. (2016). Using individualized brain network for analyzing structural covariance of the cerebral cortex in alzheimer's patients. *Front. Neurosci.* 10:394. doi: 10.3389/fnins.2016.00394
- Kong, X. Z., Liu, Z., Huang, L., Wang, X., Yang, Z., Zhou, G., et al. (2015). Mapping individual brain networks using statistical similarity in regional morphology from MRI. *PLoS ONE* 10:e0141840. doi: 10.1371/journal.pone.0141840
- Kong, X. Z., Wang, X., Huang, L., Pu, Y., Yang, Z., Dang, X., et al. (2014). Measuring individual morphological relationship of cortical regions. *J. Neurosci. Methods* 237, 103–107. doi: 10.1016/j.jneumeth.2014.09.003
- Li, Q., Li, X., Wang, X., Li, Y., Li, K., Yu, Y., et al. (2016). Topological properties of large-scale cortical networks based on multiple morphological features in amnesic mild cognitive impairment. *Neural Plast.* 2016:3462309. doi: 10.1155/2016/3462309
- Li, S., Yuan, X., Pu, F., Li, D., Fan, Y., Wu, L., et al. (2014). Abnormal changes of multidimensional surface features using multivariate pattern classification in amnesic mild cognitive impairment patients. *J. Neurosci.* 34, 10541–10553. doi: 10.1523/JNEUROSCI.4356-13.2014
- Li, W., Yang, C., Shi, F., Wu, S., Wang, Q., Nie, Y., et al. (2017). Construction of individual morphological brain networks with multiple morphometric features. *Front. Neuroanat.* 11:34. doi: 10.3389/fnana.2017.00034
- Liu, J., Ji, S., and Ye, J. (2009). *SLEP: Sparse Learning with Efficient Projections*. Arizona State University. Available online at: <http://www.public.asu.edu/~jye02/Software/SLEP/download.htm>
- Lohmann, G., von Cramon, D. Y., and Colchester, A. C. (2008). Deep sulcal landmarks provide an organizing framework for human cortical folding. *Cereb. Cortex* 18, 1415–1420. doi: 10.1093/cercor/bhm174
- Parent, A., and Carpenter, M. B. (1996). *Carpenter's Human Neuroanatomy*. Tokyo: Williams & Wilkins.
- Prati, R. C., Batista, G. E. A. P. A., and Monard, M. C. (2011). A survey on graphical methods for classification predictive performance evaluation. *IEEE Trans. Knowl. Data Eng.* 23, 1601–1618. doi: 10.1109/TKDE.2011.59
- Rakic, P. (1988). Defects of neuronal migration and the pathogenesis of cortical malformations. *Prog. Brain Res.* 73, 15–37. doi: 10.1016/S0079-6123(08)60494-X
- Saggar, M., Hosseini, S. M., Bruno, J. L., Quintin, E. M., Raman, M. M., Kesler, S. R., et al. (2015). Estimating individual contribution from group-based structural correlation networks. *Neuroimage* 120, 274–284. doi: 10.1016/j.neuroimage.2015.07.006
- Sanabriadiáz, G., Meliegarcía, L., Iturriamedina, Y., Alemángómez, Y., Hernándezgonzález, G., Valdésurrutia, L., et al. (2010). Surface area and cortical thickness descriptors reveal different attributes of the structural human brain networks. *Neuroimage* 50, 1497–1510. doi: 10.1016/j.neuroimage.2010.01.028
- Seidlitz, J., Shinn, M., Romero-Garcia, R., Whitaker, K. J., Vértes, P. E., Wagstyl, K., et al. (2017). Morphometric similarity networks detect microscale cortical organization and predict inter-individual cognitive variation. *Neuron* 97, 231.e7–247.e7. doi: 10.1016/j.neuron.2017.11.039
- Shrout, P. E., and Fleiss, J. L. (1979). Intraclass correlations: uses in assessing rater reliability. *Psychol. Bull.* 86, 420–428. doi: 10.1037/0033-2909.86.2.420
- Székely, G. J., and Rizzo, M. L. (2004). Testing for equal distributions in high dimension. *Interstat* 5, 1–16.
- Tibshirani, R. (1996). Regression shrinkage and selection via the lasso. *J. R. Stat. Soc. Ser. B Methodol* 58, 267–288.
- Tijms, B. M., Seriès, P., Willshaw, D. J., and Lawrie, S. M. (2012). Similarity-based extraction of individual networks from gray matter MRI scans. *Cereb. Cortex* 22, 1530–1541. doi: 10.1093/cercor/bhr221
- Tijms, B. M., Wink, A. M., De, H. W., Wm, V. D. F., Stam, C. J., Scheltens, P., et al. (2013). Alzheimer's disease: connecting findings from graph theoretical studies of brain networks. *Neurobiol. Aging* 34, 2023–2036. doi: 10.1016/j.neurobiolaging.2013.02.020
- Van den Heuvel, M. P., and Sporns, O. (2013). Network hubs in the human brain. *Trends Cogn. Sci.* 17, 683–696. doi: 10.1016/j.tics.2013.09.012
- Van Essen, D. C. (1997). A tension-based theory of morphogenesis and compact wiring in the central nervous system. *Nature* 385, 313–318. doi: 10.1038/385313a0
- Wang, H., Jin, X., Zhang, Y., and Wang, J. (2016). Single-subject morphological brain networks: connectivity mapping, topological characterization and test-retest reliability. *Brain Behav.* 6:e00448. doi: 10.1002/brb3.448
- Wang, J., Wang, X., Xia, M., Liao, X., Evans, A., and He, Y. (2015). GRENA: a graph theoretical network analysis toolbox for imaging connectomics. *Front. Hum. Neurosci.* 9:386. doi: 10.3389/fnhum.2015.00386
- Watts, D. J., and Strogatz, S. H. (1998). Collective dynamics of 'small-world' networks. *Nature* 393, 440.
- Wee, C. Y., Yap, P. T., and Shen, D. (2013). Prediction of Alzheimer's disease and mild cognitive impairment using cortical morphological patterns. *Hum. Brain Mapp.* 34, 3411–3425. doi: 10.1002/hbm.22156
- Wei, R., Li, C., Noa, F., and Ling, L. (2016). Prediction of Conversion from mild cognitive impairment to alzheimer's disease using MRI and structural network features. *Front. Aging Neurosci.* 8:76. doi: 10.3389/fnagi.2016.00076
- Yamada, M., Jitkrittum, W., Sigal, L., Xing, E. P., and Sugiyama, M. (2012). High-dimensional feature selection by feature-wise non-linear lasso. *Neural Comput.* 26, 185–207. doi: 10.1162/NECO_a_00537
- Yao, Z., Zhang, Y., Lin, L., Zhou, Y., Xu, C., and Jiang, T. (2010). Abnormal cortical networks in mild cognitive impairment and Alzheimer's disease. *PLoS Comput. Biol.* 6:e1001006. doi: 10.1371/journal.pcbi.1001006
- Zhang, J., Wang, J., Wu, Q., Kuang, W., Huang, X., He, Y., et al. (2011). Disrupted brain connectivity networks in drug-naive, first-episode major depressive disorder. *Biol. Psychiatry* 70, 334–342. doi: 10.1016/j.biopsych.2011.05.018
- Zhang, Y., Lin, L., Lin, C. P., Zhou, Y., Chou, K. H., Lo, C. Y., et al. (2012). Abnormal topological organization of structural brain networks in schizophrenia. *Schizophr. Res.* 141, 109–118. doi: 10.1016/j.schres.2012.08.021
- Zheng, W., Yao, Z., Hu, B., Gao, X., Cai, H., and Moore, P. (2015). Novel cortical thickness pattern for accurate detection of alzheimer's disease. *J. Alzheimers Dis.* 48, 995–1008. doi: 10.3233/JAD-150311
- Zhou, Y., and Lui, Y. W. (2013). Small-world properties in mild cognitive impairment and early alzheimer's disease: a cortical thickness MRI Study. *ISRN Geriatr.* 2013:542080. doi: 10.1155/2013/542080
- Zhu, W., Wen, W., He, Y., Xia, A., Anstey, K. J., and Sachdev, P. (2012). Changing topological patterns in normal aging using large-scale structural networks. *Neurobiol. Aging* 33, 899–913. doi: 10.1016/j.neurobiolaging.2010.06.022

Conflict of Interest Statement: The authors declare that the research was conducted in the absence of any commercial or financial relationships that could be construed as a potential conflict of interest.

Copyright © 2018 Yu, Wang, Li, Zhang, Li, Li for the Alzheimer's Disease Neuroimaging Initiative. This is an open-access article distributed under the terms of the Creative Commons Attribution License (CC BY). The use, distribution or reproduction in other forums is permitted, provided the original author(s) and the copyright owner are credited and that the original publication in this journal is cited, in accordance with accepted academic practice. No use, distribution or reproduction is permitted which does not comply with these terms.

RESEARCH ARTICLE

Musical training induces functional and structural auditory-motor network plasticity in young adults

Qionglin Li^{1,2} | Xuotong Wang^{1,2} | Shaoyi Wang^{1,2} | Yongqi Xie^{1,2} |
Xinwei Li^{1,2} | Yachao Xie^{3,4} | Shuyu Li^{1,2} 

¹School of Biological Science & Medical Engineering, Beihang University, Beijing 100083, China

²Beijing Advanced Innovation Centre for Biomedical Engineering, Beihang University, Beijing 102402, China

³State Key Laboratory of Cognitive Neuroscience and Learning & IDG/McGovern Institute for Brain Research, Beijing Normal University, Beijing 100875, China

⁴Center for Collaboration and Innovation in Brain and Learning Sciences, Beijing Normal University, Beijing 100875, China

Correspondence

Shuyu Li, PhD, School of Biological Science & Medical Engineering, Beihang University, Beijing 100083, China.
Email: shuyuli@buaa.edu.cn

Funding information

National Natural Science Foundation of China, Grant/Award Numbers: 81171403, 81471731; National Natural Science Foundation of China Excellent Youth Fund, Grant/Award Number: 81622025

Abstract

Playing music requires a strong coupling of perception and action mediated by multimodal integration of brain regions, which can be described as network connections measured by anatomical and functional correlations between regions. However, the structural and functional connectivities within and between the auditory and sensorimotor networks after long-term musical training remain largely uninvestigated. Here, we compared the structural connectivity (SC) and resting-state functional connectivity (rs-FC) within and between the two networks in 29 novice healthy young adults before and after musical training (piano) with those of another 27 novice participants who were evaluated longitudinally but with no intervention. In addition, a correlation analysis was performed between the changes in FC or SC with practice time in the training group. As expected, participants in the training group showed increased FC within the sensorimotor network and increased FC and SC of the auditory-motor network after musical training. Interestingly, we further found that the changes in FC within the sensorimotor network and SC of the auditory-motor network were positively correlated with practice time. Our results indicate that musical training could induce enhanced local interaction and global integration between musical performance-related regions, which provides insights into the mechanism of brain plasticity in young adults.

KEYWORDS

auditory-motor network, brain plasticity, functional connectivity, musical training, structural connectivity

1 | INTRODUCTION

Musical performance is complex requiring a strong coupling of perception and action (Schlaug, 2015) which intensive training can induce structural and functional changes in the brain (Boyke, Driemeyer, Gaser, Büchel, & May, 2008; Herdener et al., 2010; Klein, Liem, Hänggi, Elmer, & Jäncke, 2016), even in a short-term training (Song, Skoe, Banai, & Kraus, 2012). Musical training is an excellent model to study training-related plasticity in auditory and motor areas. Previous studies have reported that acquiring musical performance skills is associated with functional and structural changes in the auditory and motor cortices (Elmer, Hänggi, Meyer, & Jäncke, 2013; Putkinen, Tervaniemi, Saarikivi, de Vent, & Huotilainen, 2014). Morphological changes (such as grey matter volume and cortical thickness) in different parts of the auditory and motor cortices due to musical training have been reported in the whole-

brain analysis in cross-sectional (Bermudez, Lerch, Evans, & Zatorre, 2009; Gaser & Schlaug, 2003) and longitudinal (Hyde et al., 2009) studies. In addition to morphological alterations, musical training has also been associated with functional and structural connectivity between cortices.

The human brain is organized in a form of network architecture in which local interactions (short-range connections) are integrated by long-range connections to support diverse brain high-order cognitive function (Park & Friston, 2013). String players, when playing their musical instruments, require information integration between different brain regions supporting auditory, somatosensory, motor, and cognitive function. Resting-state functional MRI usually measures the spontaneous low frequency fluctuations (<0.1 Hz) in the blood oxygen level-dependent (BOLD) signals which reflects patterns of brain activity in the absence of an external task. The functional connectivity measured by rs-fMRI is generally inferred by the correlations of BOLD signals

which reflect the synchronization of brain activity between distant brain areas in the absence of an external task. Using independent component analysis, the resting-state BOLD signals can be decomposed into a limited number of brain networks called intrinsic connectivity networks (ICNs). Functional communication between these networks was considered to be important in performing cognitive processes that integrate information across different brain regions (Guerra-Carrillo, Mackey, & Bunge, 2014; Harmelech & Malach, 2013). Structural connectivity (SC) usually reflects large-range fiber bundles inferred from diffusion tensor MRI, which can derive a structural brain network in terms of fiber bundles according to the regions in which they are connected (Basser, Mattiello, & LeBihan, 1994; Hagmann et al., 2007; Park et al., 2004). On a relatively short time scale in which the effects of neuronal growth and learning can be ignored, the structural networks constructed on the basis of anatomical architectures can be considered relatively fixed during different cognitive performances (Stam et al., 2016). However, it has been demonstrated that functional connectivity is task-related and state-dependent (Laird et al., 2013; Smith et al., 2009), which changes with task when comparing the functional connectivity statistics during the performance of visual attention and memory tasks (Hermundstad et al., 2013). Dynamic functional networks are intrinsically dependent on the static structural architecture of the connections that enable fast and efficient hierarchical functional integration (Park & Friston, 2013). Playing music depends on a strong coupling of perception and action mediated by multimodal integration regions distributed throughout the brain, especially the auditory and motor regions. Will SC of training-related regions be modulated in young adults after long-term musical training? If the FC is intrinsically constrained by the relatively static SC, how does it change after this training? In addition, does musical training have effects on the relationship between SC and FC? These are important questions that require answers to reveal the nature of training-induced plasticity and to provide new evidence regarding brain mechanisms to explore the changes in SC and FC between those training-related regions.

In this study, we compared the most relevant auditory and sensorimotor networks of the rs-FC and SC in 29 novice healthy young adults before and after musical training with those of another 27 novice participants who were evaluated longitudinally but with no intervention. We hypothesized that participants after training, as opposed to the controls with no intervention, would exhibit (1) FC changes in the ICNs within the auditory and motor networks and changes in the auditory-motor interaction, (2) diffusion parameter (fractional anisotropy, (FA)) changes in the SC within the auditory and motor structural network, and changed FA of the probabilistic tract pathway between the auditory and motor areas, and (3) changes of FC would be related to FA changes in the training group.

2 | MATERIALS AND METHODS

2.1 | Longitudinal experiment

2.1.1 | Participants

Sixty young healthy volunteers (29 males and 31 females) participated in this study. Participants with neurological or psychiatric disorders,

such as schizophrenia, health problems affecting dexterity, and most importantly, any experience of musical performance, were excluded following a questionnaire. Depressed persons, which were identified by a score >14 on the Beck Depression Inventory (BDI) (Beck & Steer, 1987), were excluded. Participants who were left-handers or mixed-handers, as identified via a handedness questionnaire (a modified version of the Edinburgh Handedness Inventory) (Oldfield, 1971), were also excluded. All participants were native Chinese speakers who had grown up in China and provided written informed consent; in addition, the local ethics committee approved this study.

2.1.2 | Assessment

The initial assessment included tests of overall cognitive and musical abilities. Measures of overall cognitive and musical abilities were presented to confirm that the training group and control group had similar cognitive and musical abilities and to compare possible training-related changes with these abilities. All participants were given the Advanced Measures of Music Audiation (1989) which was developed by Edwin E. Gordon to measure musical aptitude or the potential to learn in the musical domain. In the measurement, a series of 30 taped melodic excerpts were played, and participants listened and distinguished potential rhythmic and melodic alterations by choosing the appropriate answer. The percentile rank scores were acquired based on Gordon's table for individuals with a minimum of 12 years of education. In addition, an IQ score containing a performance IQ (PIQ) and a verbal IQ (VIQ) for each participant was acquired by employing the Wechsler Adult Intelligence Scale-Revised Chinese revised version (WAIS-RC) (Gong, 1992). Moreover, the trail making tests (parts A and B) (Reitan & Wolfson, 1985) were also performed to assess the visual processing and motor abilities.

The participants, who lacked a musical background (AMMA score: 20~80) and had normal intelligence (IQ score: 115~140), were randomly divided into a training group, which received 24 weeks piano training, and a control group without any training. Initially, 30 (14 males) participants were enrolled in the training group and 30 (15 males) participants were enrolled in the control group. Four persons (3 males and 1 female) dropped out due to a failure to comply with the training rules or due to health problems not related to the study design, which resulted in 29 participants (13 males) in the training group and 27 participants (13 males) in the control group.

We used a within-subject design comprising a training group in which participants received 24 weeks piano training, and a control group without any training. Participants were all tested at three time points: at the beginning (Tp1) and the end (Tp2) of 24 weeks training and at 12 weeks after training (Tp3) as shown in Figure 1a. At each time point, the participants received behavioral tests and scanning sessions. Three subtests (block design, digit symbol, and digit span) of the WAIS-RC and trail making tests were repeated at all the three time points. These tests were chosen as repeated measures based on their potential sensitivity to piano instruction with respect to motor, spatial, visual, and sequential memory. Assessments and scans in the control group were similar to those of the training group without receiving any musical training between Tp1 and Tp2.

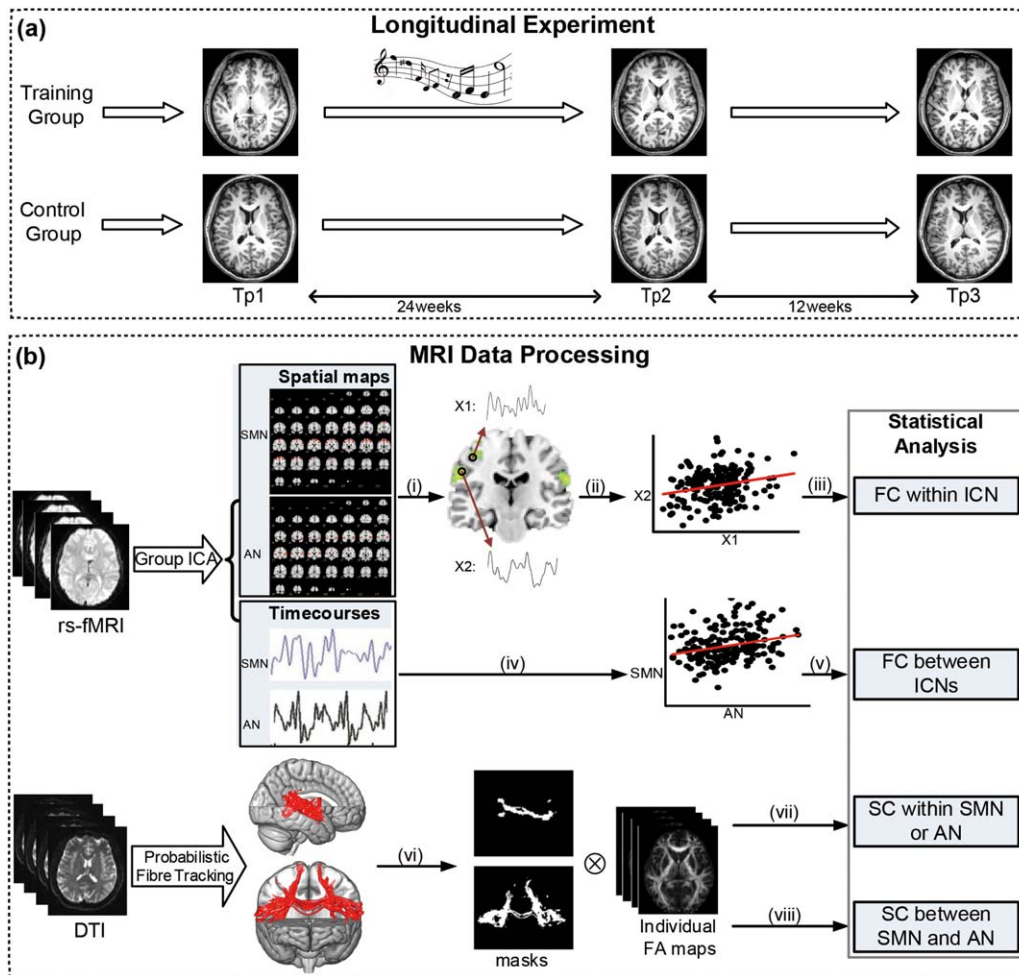


FIGURE 1 Framework for the investigation. (a) Longitudinal experiment: we used a within-subject design comprising a training group in which participants received 24-weeks piano training, and a control group with no intervention. Participants were all tested at 3-time points: at the beginning (Tp1) and the end (Tp2) of 24 weeks training and at 12 weeks after training (Tp3). At each time point, the participants all received musical assessments, behavioral tests, and scanning sessions. (b) MRI data processing: group ICA was used to acquire the auditory network (AN) and sensorimotor network (SMN) and its corresponding time courses. Probabilistic fiber tracking was conducted to acquire the WM tracts within and between the auditory and sensorimotor cortices: (i) voxel-wise ANOVA of AN and SMN; (ii) extraction of the time series from the significant clusters; (iii) correlation analysis between the time series of the significant clusters; (iv) extraction of the time courses from group ICA; (v) correlation analysis between the time series of AN and SMN; (vi) thresholded and binarized the WM tracts; (vii) calculation of the mean FA of the pathways within the auditory or sensorimotor regions; (viii) calculation of the mean FA of the pathway between the auditory and sensorimotor regions. Notes: Tp1, time point 1; Tp2, time point 2; Tp3, time point 3; ICA, independent component analysis; AN, auditory network; SMN, sensorimotor network; FC, functional connectivity; SC, structural connectivity; ANOVA, analysis of variance [Color figure can be viewed at wileyonlinelibrary.com]

A two-sample t test implemented in SPSS (SPSS version 22) was used to test the demographic data and musical performance between the two groups at baseline, except for gender (Chi-squared test). Two-sample t tests were also used to examine whether there were any differences between the two groups of these cognitive abilities at baseline. A mixed ANOVA with a between-subject factor group (training group and control group) and within-subject factor time (Tp1, Tp2, and Tp3) was performed to determine the group effects on the assessments of cognitive and musical abilities, including age, gender, and education as covariates of no interest. Significant interactions were followed by a post hoc pairwise t test between the factor of time to determine which of the time points differ from each other.

2.1.3 | Procedures

The musical training program was designed to include professional instruction, practice with the instruction, and a final musical performance. The program required participants to attend a one-hour music course once a week in the form of one-to-two lessons by professional musicians. The professional musicians provided instructions regarding music theory, progressive difficulty in musical performance, and technical motor exercises. The music theory taught in the weekly one-hour course took about 10 min. The time spent on the music theory learning was nearly the same for each participant and about 4 h for the whole training program. Instructions of music theory and progressive difficulty in musical performance referred to the *Bastien Piano for Adults-Book 1*

(Bastien, Bastien, & Bastien, 2000), and technical motor exercises referred to as *Hanon Piano Fingering Practice*. A typical course began with correcting errors in the weekly music theory assignment and explaining new theoretical concepts for study. From the beginning of the 18th week, in addition to the exercises in Bastien, one Hanon exercise was assigned every week, and these often required one week to complete at a moderate tempo. Specifically, a minimum practice time of five 30-min sessions (i.e., five days, each day at least 30-min practice) and a maximum practice time of seven 60-min sessions (i.e., seven days, each day at most one-hour practice) per week in the assigned room was also required, and the practice time was logged. Exercises for participants were also presented in the *Bastien Piano for Adults-Book 1* (Bastien et al., 2000) and the *Hanon Piano Fingering Practice*. Finally, the participants performed selected pieces from *Bastien Piano for Adults-Book 1* and were assessed by professional musicians. In addition, everyone who finished the program could individually and skillfully perform the selected pieces, which was equivalent to being certified by the Central Conservatory of Music piano level 4.

2.2 | Image acquisition

MRI scans were collected at each of the 3 measurement time points in the study. All the MRI data were obtained using a SIEMENS Trio Tim 3.0T scanner with a 12-channel phased array head coil in the Imaging Center for Brain Research, Beijing Normal University. The 3D high-resolution brain structural images were acquired using T1-weighted, sagittal 3D magnetization prepared rapid gradient echo (MPRAGE) sequences. The sequence parameters had a repetition time (TR) = 2,530 ms, echo time (TE) = 3.39 ms, inversion time (TI) = 1,100 ms, flip angle = 7°, FOV = 256 mm × 256 mm, in-plane resolution = 256 × 256, slice thickness = 1.33 mm, and 144 sagittal slices covering the whole brain. The diffusion-weighted imaging data were acquired using a single-shot twice-refocused spin-echo diffusion echo-planar imaging (EPI) sequence. The sequence parameters were TR/TE = 8,000 ms/89 ms, 30 nonlinear diffusion directions with $b = 1,000$ s/mm², and an additional volume with $b = 0$ s/mm², data matrix = 128 × 128, field of view (FOV) = 282 mm × 282 mm, 2.2 mm slice thickness, isotropic voxel size (2.2 mm)³, bandwidth (BW) = 1,562 Hz/pixel, and 62 transverse slices without gaps covering the whole brain and two averages. During the resting-state session, the participants were instructed to hold still, stay relaxed, and keep their eyes closed but not fall asleep. The functional MRI data were obtained using an echo-planar imaging (EPI) sequence with the following parameters: 33 axial slices, thickness/gap = 3.5/0.7 mm, in-plane resolution = 64 × 64, repeat time (TR) = 2,000 ms, echo time (TE) = 30 ms, flip angle = 90°, and a field of view (FOV) = 200 × 200 mm. None of the participants fell asleep according to a simple questionnaire after the scan.

2.3 | Functional connectivity analysis

Data processing was conducted using the Data Processing Assistant for the Resting-State Toolbox (DPARSF, <http://fmri.org/DPARSF>; Yan

& Zang, 2010)). Preprocessing included the following steps: (a) slice-timing correction for interleaved acquisitions; (b) head motion correction where the images are registered to the mean of the images after registering to the first image in the series; (c) T1 structural image coregistration to the functional image; (d) segmentation of the transformed structural image into grey matter, white matter, and cerebrospinal fluid; (e) spatial normalization for motion corrected functional images to the MNI space; and (f) spatial smoothing with a 4-mm Gaussian Kernel.

The spontaneous brain activity measured by rs-fMRI is typically organized in a limited number of brain networks, which are often referred to as ICNs (Beckmann, DeLuca, Devlin, & Smith, 2005; Damoiseaux et al., 2006; Shehzad et al., 2009). According to our hypotheses, the two most relevant networks were selected: auditory network (AN) and sensorimotor network (SMN). The group ICA algorithm from the fMRI toolbox (GIFT) software (<http://icatb.sourceforge.net/groupica.htm>) was used to extract the spatially independent but temporally coherent components (ICs). Data sets were temporally concatenated through subjects for one session and then concatenated through all sessions, and the data dimensions were reduced to the number of ICs using principal component analysis (PCA) (Calhoun, Adali, Pearlson, & Pekar, 2001). The optimal number of ICs in the dataset was 29 as estimated by the minimum length description (MLD) criteria implemented in the GIFT (Li, Adali, & Calhoun, 2007). Accordingly, 29 ICs were acquired using the Infomax algorithm to decompose the data from all subjects (Bell & Sejnowski, 1995), which generated a spatial map and a time course for each IC. To determine the repeatability of the ICs, 50 ICA iterations were performed using ICASSO, and the best estimate for each IC was utilized (Himberg, Hyvärinen, & Esposito, 2004). Finally, the individual IC maps and time courses were computed by back reconstruction using both aggregate components and the results from the data reduction step (Calhoun et al., 2001; Erhardt et al., 2011). The ICNs were classified by visually examining the spatial pattern (by rejecting the ICs related with physiological artifacts) and the spectral frequency (<0.1 Hz) (Lowe, Mock, & Sorenson, 1998).

A mixed ANOVA (i.e., flexible factorial model in SPM12) with a between-subject factor group (training group and control group) and a within-subject factor time (Tp1, Tp2, and Tp3) was performed to determine the group effects on SMN and AN including age, sex, and education as covariates of no interest. Significant interactions were followed by a post hoc pairwise *t* test between the factors of time. In the case of a significant test, we applied the family-wise error (FWE, $p < .05$) correction to the *p* values of the comparison of interest. Then, average time series were extracted from spherical ROIs centering on the local maxima peak of significant clusters with a radius of 8 mm. Functional connectivity within each ICN was acquired by calculating the correlation between any two of the average time series. In addition, the FC between SMN and AN was also estimated by calculating the correlation of their corresponding time courses. Statistical analyses of FC within and between SMN and AN were performed using a mixed ANOVA with post hoc tests implemented in SPSS. Finally, a correlation analysis was performed using linear regression between the changes in FC (only for those in which the post hoc pairwise *t* test was significant) with the practice time in the training group.

TABLE 1 The participant characteristics and demographics

| | Control group (n = 27) | Training group (n = 29) | p value |
|--------------------------------|---------------------------|----------------------------|---------|
| Gender (M/F) | 13/14 | 13/16 | .803 |
| Age (years) | 23.33 (1.39) | 23.10 (1.37) | .536 |
| Education | 16.70 (1.26) | 16.59 (1.09) | .709 |
| BDI | 5.15 (3.87) | 4.71 (3.62) | .646 |
| IQ | 128.19 (7.33) | 129.11 (5.65) | .598 |
| AMMA tonal percentile rank | 54.26 (14.78) | 59.34 (10.78) | .145 |
| AMMA rhythm percentile rank | 46.90 (14.54) | 53.83 (11.61) | .116 |
| AMMA composite percentile rank | 51.93 (15.31) | 57.28 (11.08) | .351 |

Note. Abbreviations: AMMA = Advanced Measures of Music Audiation; BDI = Beck Depression Inventory; M/F, male/female.

Age, education, BDI, IQ, and AMMA scores of participants in both groups at baseline are expressed as the mean (SD), and *p* values for demographics were shown in the right column.

2.4 | Structural connectivity analysis

All tensor calculations and probabilistic fiber tracking were conducted using FSL (<https://fsl.fmrib.ox.ac.uk/fsl/fslwiki/FSL>) (Smith et al., 2004). First, the raw 4D data were corrected for distortions due to eddy currents and the head motion between volumes by using an affine registration to the first $b = 0$ volume by means of FLIRT (Jenkinson & Smith, 2001). In addition, a brain extraction tool (BET) (Smith, 2002) was used to extract the brain and exclude dura, skull, scalp, and other nonbrain tissue. Second, the diffusion tensor model was built to obtain the FA, eigenvector, and eigenvalue maps for each subject. Then, the linear affine and nonlinear transform registrations were used to register individual FA map to an FMRIB FA template in the MNI space. The resulting warping transformations were then applied to resample the images of FA into the MNI space with a $2 \times 2 \times 2$ mm spatial resolution. The normalized images were then smoothed with a Gaussian kernel of 6 mm to reduce image noise and misalignment between the subjects.

Probabilistic fiber tracking was conducted between 2 ROIs: sensorimotor and auditory cortices created in the AAL template, which involved the bilateral precentral/postcentral gyrus, supplementary motor area (SMA), superior temporal gyrus, and Heschl's gyrus. The fiber tracking algorithm was performed from all voxels within each seed mask and generated 5,000 streamline samples per seed voxel with a curvature threshold of 0.2, a step length of 0.5 mm, and a maximum number of 2,000 steps. One ROI was used as the seed mask and a connection distribution was calculated between the pair of masks with another ROI as the target mask, and this process was repeatedly computed with another ROI as the seed mask. Finally, the probability of a given voxel on the pathway was represented by the sum of these samples that reached a target voxel from a given seed voxel. The results of the probabilistic tractography for each subject were thresholded and binarized to create a probabilistic fiber mask within which the mean FA for each subject was computed. The threshold was the sum of the samples sent out from the 2 ROIs and multiplied by the same percentage of 0.2%. The SC between the sensorimotor and auditory cortices was estimated by the mean FA of the tracts between the two cortices. The WM tracts within the auditory or

sensorimotor cortex were reconstructed by performing probabilistic fiber tracking in which the seed mask and target mask were both the auditory or sensorimotor regions in the AAL template. SC within the sensorimotor or auditory cortex was respectively calculated by the mean FA of the tracts within each of the cortex.

Statistical analyses of SCs within and between the sensorimotor and auditory networks were performed using mixed ANOVA with post hoc tests implemented in SPSS. In addition, a correlation analysis was performed using linear regression between the changes in SC (only those for which the post hoc pairwise *t* test was significant) with practice time in the training group.

2.5 | Relationship between FC and SC

FC is intrinsically dependent on SC for fast and efficient transfer of information, but it is unknown what degree FC is constrained by or related to characteristics of SC (Fjell et al., 2017). Due to the complex relationship between SC and FC, we explored the relationship between FC change and SC change (Tp2–Tp1) induced by musical training in the training group, which was tested by regression analysis with SC change as the independent variable and FC change as the dependent variable.

3 | RESULTS

3.1 | Participants and demographics

Twenty-nine participants in the training group (13 males, age 23.10 ± 1.37) and 27 participants in the control group (13 males, age 23.33 ± 1.39) completed the study. Moreover, the groups did not differ in terms of gender, age, education, BDI, IQ, and AMMA scores ($p > .05$) at baseline as shown in Table 1.

The mean scores and standard variances of the repeated cognitive ability assessments were shown in Table 2. No significant differences were found in any of these cognitive abilities between the two groups at baseline. A mixed ANOVA suggested that no significant interactions of the group over time were found in trail making test part A ($p = .914$) and part B ($p = .424$). In addition, no significant interactions of the

TABLE 2 Cognitive assessment data for training and control participants

| | Control group (n = 27) | | | Training group (n = 29) | | | *p value |
|--------------------|------------------------|--------------|---------------|-------------------------|---------------|---------------|----------|
| | Tp1 | Tp2 | Tp3 | Tp1 | Tp2 | Tp3 | |
| Trail making tests | | | | | | | |
| Part A | 23.37 (5.89) | 19.94 (4.39) | 17.95 (3.14) | 27.76 (10.27) | 24.10 (8.95) | 21.32 (8.15) | 0.057 |
| Part B | 54.75 (16.68) | 43.43 (9.25) | 47.45 (22.92) | 60.11 (35.04) | 45.18 (12.55) | 41.94 (13.72) | 0.474 |
| WAIS-RC subtests | | | | | | | |
| Digit span | 15.1 (2.50) | 15.7 (2.27) | 16.1 (2.30) | 14.5 (2.52) | 15.6 (2.48) | 16.3 (2.27) | 0.299 |
| Digit symbol | 17.1 (1.59) | 17.4 (1.40) | 17.6 (1.25) | 17.5 (1.57) | 18.1 (1.10) | 18.2 (1.05) | 0.338 |
| Block design | 14.1 (1.23) | 14.6 (0.97) | 14.5 (0.98) | 14.1 (1.22) | 14.5 (0.95) | 14.7 (0.75) | 0.975 |

Note. Abbreviations: Tp1 = time point 1; Tp2 = time point 2; Tp3 = time point 3; WAIS-RC = Wechsler Adult Intelligence Scale-Revised Chinese revised version.

Cognitive assessment data for training and control participants are expressed as mean (SD) for all the three time points and *p* values for these cognitive assessments at the baseline were shown in the right column (**p* value).

group over time were found in any of the repeated WAIS-RC subtests: digit span ($p = .995$), digit symbol ($p = .757$), and block design ($p = .440$). However, mixed ANOVA showed a significant main effect for time on all these cognitive tests: digit span ($F = 6.695$, $p = .002$), digit symbol ($F = 7.97$, $p = .001$), block design ($F = 6.568$, $p = .002$), trail making test part A ($F = 12.19$, $p < .001$), and part B ($F = 7.807$, $p = .01$).

3.2 | Functional connectivity

The auditory network was formed by the bilateral middle and superior temporal gyrus and Heschl's gyrus, whereas the SMN was formed by the bilateral precentral/postcentral gyrus and the bilateral SMA, as shown in Figure 2. The results showed no significant interaction of the group over time in the auditory network. However, for SMN, a significant interaction of the group over time has been found in areas of the

bilateral postcentral, left superior parietal gyrus, right inferior parietal gyrus, right precentral gyrus, and right superior frontal gyrus. The local maxima peak coordinates in the MNI space and cluster size are shown in Table 3. No significant interaction of the group over time has been found except for the FC between the right postcentral and right precentral ($F = 5.410$, $p = .006$). In addition, post hoc pairwise comparisons showed increased FC between the right postcentral and right precentral gyri when compared after (Tp2) with before musical training (Tp1) (** $p < .001$) and decreased FC when comparing Tp3 with Tp2 (* $p = .001$) in the training group, whereas there was no significant change in the control group as shown in Figure 3a.

In addition to FC within ICN, significant interaction of the group over time has been found ($F = 5.588$, $p = .005$) in FC of auditory-motor network and post hoc pairwise comparisons showed increased FC of the auditory-motor network when Tp2 was compared with Tp1

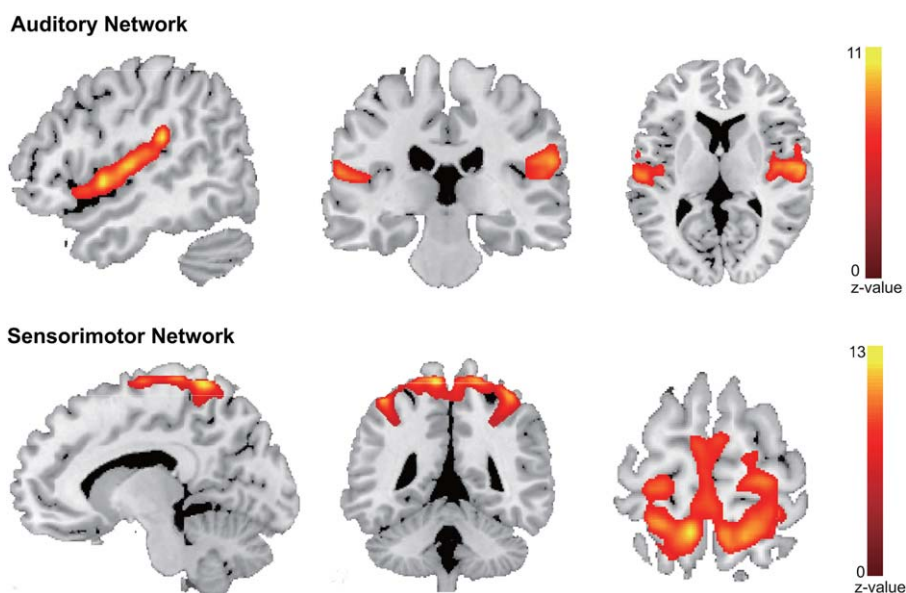


FIGURE 2 The functional auditory network and sensorimotor network. The auditory network and sensorimotor network were identified by group ICA. The AN was formed by the bilateral middle and superior temporal gyrus, and Heschl's gyrus; the SMN was formed by the bilateral precentral/postcentral gyrus and bilateral SMA. Note: AN, auditory network; SMN, sensorimotor network; SMA, supplementary motor area [Color figure can be viewed at wileyonlinelibrary.com]

TABLE 3 Clusters with a significant interaction of group over time in sensorimotor network

| Index | Number of voxels | Peak MNI coordinate | Peak MNI coordinate region (AAL) |
|-------|------------------|---------------------|----------------------------------|
| 1 | 73 | -63 -21 24 | Postcentral_L |
| 2 | 93 | 60 -24 27 | Postcentral_R |
| 3 | 101 | -18 -60 60 | Parietal_Sup_L |
| 4 | 52 | 36 -42 39 | Parietal_Inf_R |
| 5 | 50 | 42 -21 51 | Precentral_R |
| 6 | 24 | 21 3 54 | Frontal_Sup_R |

Note. Abbreviations: Postcentral_L = left postcentral gyrus; Postcentral_R = right postcentral gyrus; Parietal_Sup_L = left superior parietal gyrus; Parietal_Inf_R = right inferior parietal gyrus; Precentral_R = right precentral gyrus; Frontal_Sup_R = right superior frontal gyrus.

(** $p < .001$), decreased FC when Tp3 was compared with Tp2 ($*p = .003$) and increased FC when Tp3 was compared with Tp1 ($*p = .02$) in the training group, whereas there was no significant change in the control group as shown in Figure 3c.

3.3 | Structural connectivity

The WM tracts within sensorimotor and auditory cortices and between the sensorimotor and auditory cortices are displayed in Figure 4a and 4b, and the two areas are mainly connected by the corticospinal tract (CST), the superior longitudinal fasciculus (SLF), and the corpus callosum (CC), of which the mean FA was calculated. A significant interaction of the group over time in the WM tracts between these two areas has been found ($F = 5.643$, $p = .005$) and post hoc pairwise comparisons showed increased mean FA of the WM tracts when Tp2 was compared with Tp1 (** $p < .001$) and decreased mean FA when Tp3 was compared with Tp2 (** $p < .001$) in the training group, whereas there was no significant change in the control group as shown in Figure 5a. However, no significant interactions of the group over time have been found in any of the four structural networks within the auditory and sensorimotor areas.

3.4 | Correlation analysis

In Figure 3b, the correlation analysis revealed that the increased FC within SMN (between right postcentral and right precentral gyri) when comparing after with before training, was positively correlated with

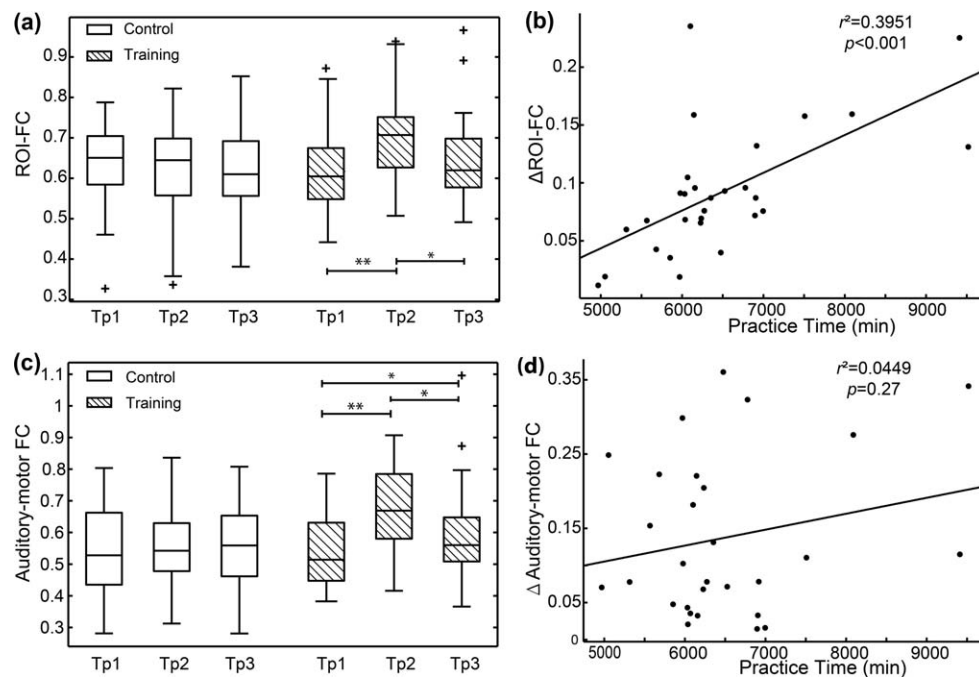


FIGURE 3 Functional connectivity comparisons and correlation analyses. (a) Comparisons showed increased functional connectivity between the right postcentral and right precentral gyri (regions within SMN) when Tp2 (at the end of training) was compared with Tp1 (at the beginning of training) (** $p < .001$) and decreased functional connectivity when Tp3 (at 12 weeks after training) was compared with Tp2 ($*p = .001$) in the training group, whereas there was no significant change in the control group. (b) The scatter plot shows that participants in the training group who practiced for longer time showed greater increased functional connectivity (Tp2–Tp1) between right postcentral and precentral gyri ($r^2 = .395$, $p < .001$). (c) Comparisons showed increased functional connectivity between SMN and AN when Tp2 (at the end of training) was compared with Tp1 (at the beginning of training) (** $p < .001$), decreased functional connectivity when Tp3 (at 12 weeks after training) was compared with Tp2 ($*p = .003$), and increased functional connectivity when Tp3 was compared with Tp1 ($*p = .02$) in the training group, whereas there was no significant change in the control group. (d) No significant correlation was found between the changes of functional connectivity (Tp2–Tp1) between the auditory and sensorimotor cortices and the practice time in the training group ($r^2 = .045$, $p = .27$). Note: Tp1, time point 1; Tp2, time point 2; Tp3, time point 3; FC, functional connectivity; SMN, sensorimotor network; AN, auditory network

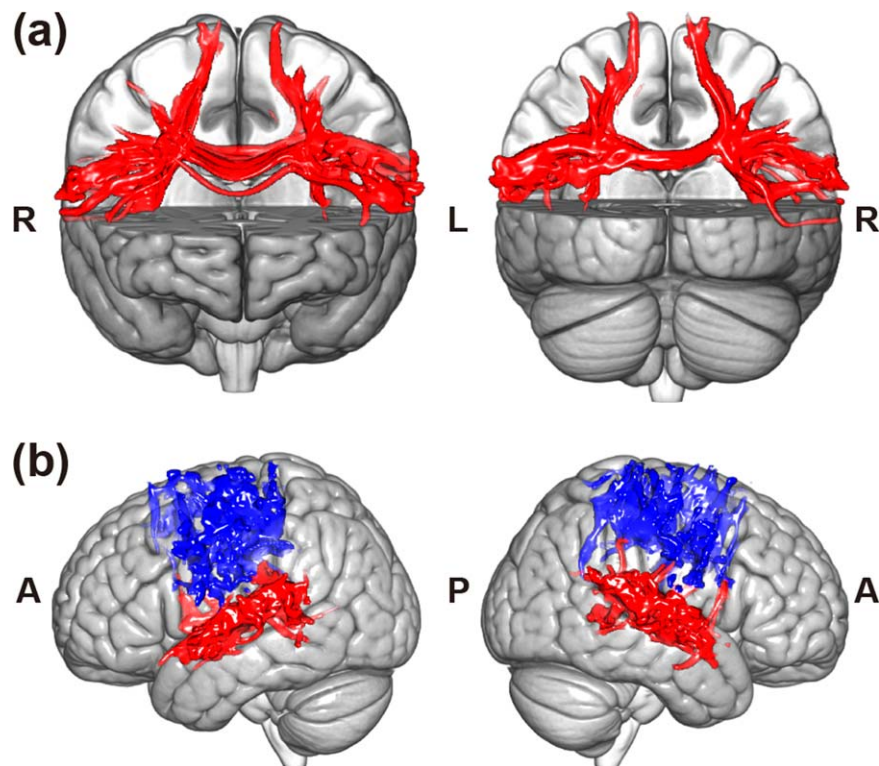


FIGURE 4 White matter fiber pathway within and between auditory and sensorimotor regions. (a) The WM tracts between auditory and sensorimotor regions were reconstructed by performing probabilistic fiber tracking between two ROI masks (auditory and sensorimotor regions). The two ROIs were connected by the corticospinal tract, superior longitudinal fasciculus, and corpus callosum. (b) The WM tracts within the auditory or sensorimotor regions were reconstructed by performing a probabilistic fiber tracking in which the seed mask and target mask were both the auditory and sensorimotor regions in the AAL template. Note: L, left side of the brain; R, right side of the brain; A, anterior side of the brain; P, posterior side of the brain [Color figure can be viewed at wileyonlinelibrary.com]

practice time ($r^2 = .395$, $p < .001$) such that participants who practiced for longer time showed greater increased FC. In addition, the mean FA of the WM tracts between auditory and sensorimotor cortices correlated positively with practice time in the training group ($r^2 = 0.370$, $p < .001$) as shown in Figure 5b. That is, participants who

practiced longer showed greater enhanced SC of the auditory-motor network. However, as seen in Figure 3d, there was no significant relationship between practice time and the changes in FC between the auditory and sensorimotor cortices in the training group ($r^2 = .045$, $p = .27$). Moreover, we have also analyzed the relationship

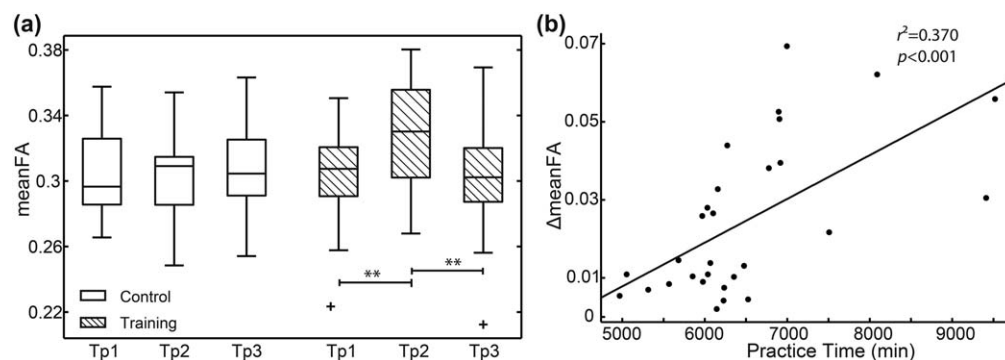


FIGURE 5 Structural connectivity comparisons and correlation analysis. (a) Structural connectivity between auditory and sensorimotor regions was evaluated by the mean FA of the WM tracts between the two regions in which probabilistic tracking was obtained. Comparisons showed increased mean FA of the WM tracts between sensorimotor and auditory cortices when Tp2 (at the end of training) was compared with Tp1 (at the beginning of training) (** $p < .001$) and decreased mean FA when Tp3 (at 12 weeks after training) was compared with Tp2 (** $p < .001$) in the training group, whereas there was no significant change in the control group. (b) Correlation analysis showed that increased mean FA of the WM tracts (Tp2–Tp1) between sensorimotor and auditory cortices was positively correlated with practice time in the training group ($r^2 = .370$, $p < .001$). Note: Tp1, time point 1; Tp2, time point 2; Tp3, time point 3; FA, fractional anisotropy; WM, white matter

between the decrease in Tp3 of structural and functional connectivity changes and the training hours in the training group. The results showed that the decreased functional connectivity within the sensorimotor network (Tp2–Tp3) was positively correlated with the practice time ($r^2 = .146, p = .041$). However, there were no significant correlations between the practice time and the decreased functional or structural connectivity of the auditory-motor network ($p > .05$).

3.5 | Relationship between functional and structural connectivity

It can be seen from Figures 3c and 5a that both FC and SC of the auditory-motor network were increased in the training group when Tp2 was compared with Tp1, showing good correspondence between FC and SC. For connectivity within the two regions, only increased FC within the sensorimotor area (between right postcentral and right precentral gyri) was found in the training group as shown in Figure 3a but with no significant changes of SC. In addition, the relationship between the significant changes of FC and SC of the auditory-motor network was explored by performing regression analysis in the training group. No significant correlation between changes of FC and SC of the auditory-motor network was found in the training group ($p = .933$).

4 | DISCUSSION

In this study, we investigated the impact of musical training on the structural and functional connectivity of the auditory and sensorimotor regions. Besides, we also analyzed the relationship between SC and FC of the two regions. Notably, we targeted at the auditory and sensorimotor regions, the most related regions during the musical performance, and demonstrated that musical training affects FC within the sensorimotor regions, whereas no effects were found within the auditory regions. In addition, we also found that musical training was associated with increased FC of the auditory-motor network and increased SC between the two regions. Moreover, the effects on FC within the sensorimotor regions and SC between the auditory and sensorimotor regions were stronger in participants with longer training time.

4.1 | Functional connectivity within and between the auditory and sensorimotor networks

The obtained ICNs in our resting-state fMRI analysis were consistent with the main networks found in previous studies (Allen et al., 2014). In this study, the ICNs showed significant training-related changes in the SMN but not the AN. Previous studies used magnetoencephalographic (MEG) measurements of the mismatch negativity (MMNm) with brain sources within the auditory cortex to evaluate the training-induced cortical response changes not the functional connectivity within the auditory cortex (Lappe, Herholz, Trainor, & Pantev, 2008; Lappe, Trainor, Herholz, & Pantev, 2011). They found differential training effects between mere auditory musical training and sensorimotor-auditory training. While there was a significant increase in the mismatch negativity after sensorimotor piano training, there was no

functional increase in the mismatch negativity after mere auditory training. The SMN, which showed the significant interaction of the group over time included regions of bilateral postcentral gyrus, left superior parietal gyrus, right inferior parietal gyrus, right precentral gyrus, and right superior frontal gyrus. In line with previous studies (Palomar-García, Zatorre, Ventura-Campos, Bueichekú, & Ávila, 2017), we also found enhanced FC within sensorimotor areas. In contrast to increased activities in motor areas (Herholz, Coffey, Pantev, & Zatorre, 2016), enhanced FC between subareas in sensorimotor cortex (right precentral and postcentral gyri), that is, FC within the sensorimotor network, was found in the present study. Previous fMRI studies have suggested that the activity of the subareas of the primary motor cortex, which was mentioned above, was related to voluntary finger movements (Indovina & Sanes, 2001). In addition to the motor areas, increases in the magnitude of the task-evoked BOLD response in the primary somatosensory cortex have also proven to be associated with long-term motor skill learning (Floyer-Lea & Matthews, 2005). It has been suggested that somatosensory feedback is also important in motor task learning (Asanuma & Pavlides, 1997; Kaelin-Lang et al., 2002; Pavlides, Miyashita, & Asanuma, 1993), which is a major source of afferents to the primary motor cortex (Asanuma, Stoney, & Abzug, 1968). Activation of both the somatosensory and motor cortices in hand movements (Kleinschmidt, Nitschke, & Frahm, 1997) suggests the importance of afferent feedback in full movement. The results of this study are compatible with this concept of afferent feedback because we found higher functional connectivity between primary motor and somatosensory cortices after musical training. Thus, we can infer that the information interaction of the local somatosensory and motor areas can be modulated by long-term musical training in young adults.

In addition to increased FC within the sensorimotor network, our results also showed increased rs-FC of the auditory-motor network after long-term musical training. Feedback interactions are particularly relevant in playing an instrument, where performers must listen to each note they produce and perform appropriate action adjustments in due course. It has been proven that musicians can still perform prehearsed pieces when auditory feedback is blocked, but expressive aspects of performance are affected (Repp, 1999). More importantly, when auditory feedback is experimentally manipulated by the introduction of delays or distortions, the motor performance is significantly altered (Pfordresher & Palmer, 2006). Thus, information integration between auditory and sensorimotor cortices is of particular importance in musical performance, which indicates that the FC of the auditory-motor network increased after long-term musical training.

Perfect musical performance requires the interaction of local information within the auditory and sensorimotor cortices and global integration between the two areas. The results of this study showed enhanced local interaction within the sensorimotor cortex and global integration between the auditory and sensorimotor cortices after long-term musical training. Interestingly, in this study, participants in the training group with more hours of practice showed a greater increase in FC within the sensorimotor network. This finding indicates the possibility of brain plasticity in local interaction within the sensorimotor

cortex. Our findings provide new evidence for revealing the mechanism of brain functional organization modulated by musical training.

4.2 | Structural connectivity within and between auditory and sensorimotor networks

In contrast to focusing on white matter architectures, we used probabilistic fiber tracking to construct the structural connectivity within and between auditory and sensorimotor areas. Consistent with the increased FA reported in previous studies (Halwani, Loui, Rueber, & Schlaug, 2011; Rüber, Lindenber, & Schlaug, 2015; Steele, Bailey, Zatorre, & Penhune, 2013), we also found increased mean FA of WM tracts between the sensorimotor and auditory cortices after long-term musical training and receded when exercise stopped, whereas no significant changes in mean FA were found within the auditory or sensorimotor cortex in this study. Auditory and sensorimotor cortices are mainly connected by the corticospinal tract (CST), superior longitudinal fasciculus (SLF), and corpus callosum (CC). Both CST and SLF are part of the sensorimotor system. The fiber of the CST plays a key role in the control of voluntary movement which projects from the sensorimotor and premotor cortices to the motor-neurons in the spinal cord. The SLF links posterior sensory to the frontal regions, which involves the integration of sensory and motor information for action (Hecht et al., 2013; Rodriguez-Herreros et al., 2015). The body of CC connects premotor and sensorimotor regions, whereas the splenium connects the visual, parietal, and auditory regions (Hofer & Frahm, 2006; Knyazeva, 2013). The lateral portions of the CC are crossed by other fiber tracts, including the SLF and the CST. The FA changes of these pathways have been shown to be related to musical performance (Giacosa, Karpati, Foster, Penhune, & Hyde, 2016; Steele et al., 2013). Children with 15 months musical training showed larger deformation changes of CC compared with the controls which supported the findings in this study (Hyde et al., 2009). Increases in FA are thought to be associated with changes in axon diameter, the fanning of primary fibers or the density and coherence of secondary fibers in crossing regions (Douaud et al., 2009, 2011; Zatorre, Fields, & Johansen-Berg, 2012). Playing the piano requires the coordinated action of two hands, auditory feedback and interhemispheric interactions, and may place greater demands on interactions between auditory and sensorimotor regions (Zatorre, Chen, & Penhune, 2007), thus promoting the enhanced connections that are indexed by increased FA. In addition, the increased FA of fibers between auditory and sensorimotor cortices was correlated with the practice time in the training group. That is, participants who practiced for longer time showed greater enhanced structural connectivity between the musical performance related regions. Thus, it can be suggested that musical training could induce modulation of long-range brain structural connectivity, which mediates submodules of the brain.

4.3 | Relationship between functional and structural connectivity

In this study, we found increased FC of the auditory-motor network and increased SC between the two regions in the training group after a

long-term musical training, showing good correspondence between FC and SC. However, the relationship between change in FC and change in SC of auditory-motor network was not significant in the training group, showing different modulation of FC and SC induced by musical training. Besides increased FC and SC of auditory-motor network, enhanced FC within the sensorimotor area but no significant changes in SC within sensorimotor or auditory were found.

The human brain is organized by global integration of local interaction in which global integration via long-range weak connections facilitate diverse cognitive function mediated by short-range dense connectivity (Park & Friston, 2013). The long-range weak connections are relatively flexible and facilitate diverse integration for various functional demands (Ekman, Derrfuss, Tittgemeyer, & Fiebach, 2012; Hermundstad et al., 2013). Furthermore, the coupling between different local interactions may be more dynamic and task-related, which is plausibly mediated by long-range structural connections, such as commissural fibers for bilateral submodules and longitudinal fibers within a hemisphere (Allen et al., 2014; Park et al., 2012), than the strong coupling within local interactions. Thus, it can be interpreted that both the relatively static SC and the dynamic FC between training related regions could be induced changes after long-term intensive musical training but changes in FC and SC are not necessarily strongly correlated.

In this study, the FC within the sensorimotor network and SC between auditory and sensorimotor cortices changes degraded nearly to baseline without training over 12 weeks. However, increased FC of the auditory-motor network lasted for 12 weeks without further training (even though lower than Tp2). The lasting increased long-range functional connectivity between auditory and sensorimotor cortices may underlie a brain optimization strategy that may reduce the need for the equivalent dedicated structural networks and avoid the incremental metabolic costs in terms of modifying physical connections (Sami & Miall, 2013). Functional connectivity within sensorimotor network was significantly increased after the musical training but decreased to the baseline when training ended. Interestingly, participants in the training group who practiced for a longer time showed greater increased functional connectivity within the sensorimotor network during the training period and also greater decrease after the training period. The transient changes of the functional connectivity within the sensorimotor network could be explained by the perspective that the local connectivity was more task-related and may only characterize patterns of activity during training (Park & Friston, 2013). However, there were no significant correlations between the practice time and the decrease of the functional and structural connectivity between sensorimotor and auditory cortices. Therefore, in future, the longitudinal study in which imaging data are acquired at multiple time points could help for revealing the different dynamic properties of training-related plastic changes in structural connectivity and functional connectivity.

4.4 | Limitations and future directions

This study still has some limitations. First, the relationship between FC and SC is complex and the alignment of FC and SC seems restricted to specific regions (Fjell et al., 2017), thus an appropriate approach which

can qualitatively and quantitatively characterize the SC–FC coupling is needed to examine the effects of musical training on SC–FC relationships of auditory and sensorimotor cortices. Second, we explored the relationship between practice time and changes of connectivity. Even though longer practice time may be linked with an increase in proficiency (Sloboda, Davidson, Howe, & Moore, 1996), in future, the measures of the piano efficiency deserve to be recorded to investigate the relationship between training and changes of connectivity. Third, SC was estimated by tractography and based on diffusion imaging treating the bilateral auditory or sensorimotor as a whole seed. Musical training has been associated with increased hemispheric asymmetries (Boemio, Fromm, Braun, & Poeppel, 2005; Zatorre, Belin, & Penhune, 2002), and investigating the interhemispheric and intrahemispheric SC between auditory and sensorimotor areas is of great importance. Fourth, participants in the training group received instructions in music theory while the controls did not get any cognitive instructions at all, which may be confounding in the analysis of training-induced auditory and sensorimotor changes. Future studies are needed to shed more light on these issues.

ACKNOWLEDGMENTS

This work was supported by the National Natural Science Foundation of China (Grant No. 81171403, 81471731), National Natural Science Foundation of China Excellent Youth Fund (Grant No. 81622025).

CONFLICT OF INTERESTS

The authors declare that there are no conflicts of interest regarding the publication of this article.

ORCID

Shuyu Li  <http://orcid.org/0000-0002-3459-6821>

REFERENCES

- Allen, E. A., Damaraju, E., Plis, S. M., Erhardt, E. B., Eichele, T., & Calhoun, V. D. (2014). Tracking whole-brain connectivity dynamics in the resting state. *Cerebral Cortex*, *24*, 663–676.
- Asanuma, H., & Pavlides, C. (1997). Neurobiological basis of motor learning in mammals. *Neuroreport: An International Journal for the Rapid Communication of Research in Neuroscience*, *8*, i–vi.
- Asanuma, H., Stoney, S., & Abzug, C. (1968). Relationship between afferent input and motor outflow in cat motor sensory cortex. *Journal of Neurophysiology*, *31*, 670–681.
- Basser, P. J., Mattiello, J., & LeBihan, D. (1994). MR diffusion tensor spectroscopy and imaging. *Biophysical Journal*, *66*, 259–267.
- Bastien, J. S., Bastien, L., & Bastien, L. (2000). *Piano for adults*. Kjos Music Press.
- Beck, A., & Steer, R. (1987). *Beck depression inventory manual*. New York: The Psychological Corporation Harcourt Brace Jovanovich Inc.
- Beckmann, C. F., DeLuca, M., Devlin, J. T., & Smith, S. M. (2005). Investigations into resting-state connectivity using independent component analysis. *Philosophical Transactions of the Royal Society of London B: Biological Sciences*, *360*, 1001–1013.
- Bell, A. J., & Sejnowski, T. J. (1995). An information-maximization approach to blind separation and blind deconvolution. *Neural Computation*, *7*, 1129–1159.
- Bermudez, P., Lerch, J. P., Evans, A. C., & Zatorre, R. J. (2009). Neuroanatomical correlates of musicianship as revealed by cortical thickness and voxel-based morphometry. *Cerebral Cortex*, *19*, 1583–1596.
- Boemio, A., Fromm, S., Braun, A., & Poeppel, D. (2005). Hierarchical and asymmetric temporal sensitivity in human auditory cortices. *Nature Neuroscience*, *8*, 389–395.
- Boyke, J., Driemeyer, J., Gaser, C., Büchel, C., & May, A. (2008). Training-induced brain structure changes in the elderly. *Journal of Neuroscience*, *28*, 7031–7035.
- Calhoun, V., Adali, T., Pearlson, G., & Pekar, J. (2001). A method for making group inferences from functional MRI data using independent component analysis. *Human Brain Mapping*, *14*, 140–151.
- Damoiseaux, J., Rombouts, S., Barkhof, F., Scheltens, P., Stam, C., Smith, S. M., & Beckmann, C. (2006). Consistent resting-state networks across healthy subjects. *Proceedings of the National Academy of Sciences*, *103*, 13848–13853.
- Douaud, G., Behrens, T. E., Poupon, C., Cointepas, Y., Jbabdi, S., Gaura, V., ... Damier, P. (2009). In vivo evidence for the selective subcortical degeneration in Huntington's disease. *NeuroImage*, *46*, 958–966.
- Douaud, G., Jbabdi, S., Behrens, T. E., Menke, R. A., Gass, A., Monsch, A. U., ... Matthews, P. M. (2011). DTI measures in crossing-fibre areas: Increased diffusion anisotropy reveals early white matter alteration in MCI and mild Alzheimer's disease. *NeuroImage*, *55*, 880–890.
- Ekman, M., Derrfuss, J., Tittgemeyer, M., & Fiebach, C. J. (2012). Predicting errors from reconfiguration patterns in human brain networks. *Proceedings of the National Academy of Sciences*, *109*, 16714–16719.
- Elmer, S., Hänggi, J., Meyer, M., & Jäncke, L. (2013). Increased cortical surface area of the left planum temporale in musicians facilitates the categorization of phonetic and temporal speech sounds. *Cortex*, *49*, 2812–2821.
- Erhardt, E. B., Rachakonda, S., Bedrick, E. J., Allen, E. A., Adali, T., & Calhoun, V. D. (2011). Comparison of multi-subject ICA methods for analysis of fMRI data. *Human Brain Mapping*, *32*, 2075–2095.
- Fjell, A. M., Sneve, M. H., Grydeland, H., Storsve, A. B., Amlien, I. K., Yendiki, A., & Walhovd, K. B. (2017). Relationship between structural and functional connectivity change across the adult lifespan: A longitudinal investigation. *Human Brain Mapping*, *38*, 561–573.
- Floyer-Lea, A., & Matthews, P. M. (2005). Distinguishable brain activation networks for short- and long-term motor skill learning. *Journal of Neurophysiology*, *94*, 512–518.
- Gaser, C., & Schlaug, G. (2003). Brain structures differ between musicians and non-musicians. *Journal of Neuroscience*, *23*, 9240–9245.
- Giacosa, C., Karpati, F. J., Foster, N. E., Penhune, V. B., & Hyde, K. L. (2016). Dance and music training have different effects on white matter diffusivity in sensorimotor pathways. *NeuroImage*, *135*, 273–286.
- Gong, Y. (1992). *Wechsler Adult Intelligence Scale-revised (Chinese revised version)*. Hunan Medical Institute.
- Guerra-Carrillo, B., Mackey, A. P., & Bunge, S. A. (2014). Resting-state fMRI A window into human brain plasticity. *Neuroscientist*, *20*, 522–533.
- Hagmann, P., Kurant, M., Gigandet, X., Thiran, P., Wedeen, V. J., Meuli, R., & Thiran, J.-P. (2007). Mapping human whole-brain structural networks with diffusion MRI. *PLoS One*, *2*, e597.
- Halwani, G., Loui, P., Rueber, T., & Schlaug, G. (2011). Effects of practice and experience on the arcuate fasciculus: Comparing singers, instrumentalists, and non-musicians. *Frontiers in Psychology*, *2*,

- Harmelech, T., & Malach, R. (2013). Neurocognitive biases and the patterns of spontaneous correlations in the human cortex. *Trends in Cognitive Sciences*, 17, 606–615.
- Hecht, E. E., Gutman, D. A., Preuss, T. M., Sanchez, M. M., Parr, L. A., & Rilling, J. K. (2013). Process versus product in social learning: Comparative diffusion tensor imaging of neural systems for action execution—Observation matching in macaques, chimpanzees, and humans. *Cerebral Cortex*, 23, 1014–1024.
- Herdener, M., Esposito, F., di Salle, F., Boller, C., Hilti, C. C., Habermeyer, B., ... Cattapan-Ludewig, K. (2010). Musical training induces functional plasticity in human hippocampus. *Journal of Neuroscience*, 30, 1377–1384.
- Herholz, S. C., Coffey, E. B. J., Pantev, C., & Zatorre, R. J. (2016). Dissociation of neural networks for predisposition and for training-related plasticity in auditory-motor learning. *Cerebral Cortex*, 26, 3125–3134.
- Hermundstad, A. M., Bassett, D. S., Brown, K. S., Aminoff, E. M., Clewett, D., Freeman, S., ... Miller, M. B. (2013). Structural foundations of resting-state and task-based functional connectivity in the human brain. *Proceedings of the National Academy of Sciences*, 110, 6169–6174.
- Himberg, J., Hyvärinen, A., & Esposito, F. (2004). Validating the independent components of neuroimaging time series via clustering and visualization. *NeuroImage*, 22, 1214–1222.
- Hofer, S., & Frahm, J. (2006). Topography of the human corpus callosum revisited—comprehensive fiber tractography using diffusion tensor magnetic resonance imaging. *NeuroImage*, 32, 989–994.
- Hyde, K. L., Lerch, J., Norton, A., Forgeard, M., Winner, E., Evans, A. C., & Schlaug, G. (2009). Musical training shapes structural brain development. *Journal of Neuroscience*, 29, 3019–3025.
- Indovina, I., & Sanes, J. N. (2001). On somatotopic representation centers for finger movements in human primary motor cortex and supplementary motor area. *NeuroImage*, 13, 1027–1034.
- Jenkinson, M., & Smith, S. (2001). A global optimisation method for robust affine registration of brain images. *Medical Image Analysis*, 5, 143–156.
- Kaelin-Lang, A., Luft, A. R., Sawaki, L., Burstein, A. H., Sohn, Y. H., & Cohen, L. G. (2002). Modulation of human corticomotor excitability by somatosensory input. *Journal of Physiology*, 540, 623–633.
- Klein, C., Liem, F., Hänggi, J., Elmer, S., Jäncke, L. (2016). The “silent” imprint of musical training. *Human Brain Mapping*, 37, 536–546.
- Kleinschmidt, A., Nitschke, M. F., & Frahm, J. (1997). Somatotopy in the human motor cortex hand area. A high-resolution functional MRI study. *European Journal of Neuroscience*, 9, 2178–2186.
- Knyazeva, M. G. (2013). Splenium of corpus callosum: Patterns of inter-hemispheric interaction in children and adults. *Neural Plasticity*, 2013, 1–10.
- Laird, A. R., Eickhoff, S. B., Rotzschy, C., Bzdok, D., Ray, K. L., & Fox, P. T. (2013). Networks of task co-activations. *NeuroImage*, 80, 505–514.
- Lappe, C., Herholz, S. C., Trainor, L. J., & Pantev, C. (2008). Cortical plasticity induced by short-term unimodal and multimodal musical training. *Journal of Neuroscience*, 28, 9632–9639.
- Lappe, C., Trainor, L. J., Herholz, S. C., & Pantev, C. (2011). Cortical plasticity induced by short-term multimodal musical rhythm training. *PLoS One*, 6, e21493.
- Li, Y. O., Adali, T., & Calhoun, V. D. (2007). Estimating the number of independent components for functional magnetic resonance imaging data. *Human Brain Mapping*, 28, 1251–1266.
- Lowe, M., Mock, B., & Sorenson, J. (1998). Functional connectivity in single and multislice echoplanar imaging using resting-state fluctuations. *NeuroImage*, 7, 119–132.
- Oldfield, R. C. (1971). The assessment and analysis of handedness: The Edinburgh inventory. *Neuropsychologia*, 9, 97–113.
- Palomar-García, M.-Á., Zatorre, R. J., Ventura-Campos, N., Bueichekú, E., & Ávila, C. (2017). Modulation of functional connectivity in auditory-motor networks in musicians compared with nonmusicians. *Cerebral Cortex*, 27, 2768–2778.
- Park, B., Kim, J. I., Lee, D., Jeong, S.-O., Lee, J. D., & Park, H.-J. (2012). Are brain networks stable during a 24-hour period? *NeuroImage*, 59, 456–466.
- Park, H.-J., Kubicki, M., Westin, C.-F., Talos, I.-F., Brun, A., Peiper, S., ... Shenton, M. E. (2004). Method for combining information from white matter fiber tracking and gray matter parcellation. *American Journal of Neuroradiology*, 25, 1318–1324.
- Park, H. J., & Friston, K. (2013). Structural and functional brain networks: From connections to cognition. *Science (New York, N.Y.)*, 342, 1238411.
- Pavlidis, C., Miyashita, E., & Asanuma, H. (1993). Projection from the sensory to the motor cortex is important in learning motor skills in the monkey. *Journal of Neurophysiology*, 70, 733–741.
- Pfordresher, P. Q., & Palmer, C. (2006). Effects of hearing the past, present, or future during music performance. *Attention, Perception, & Psychophysics*, 68, 362–376.
- Putkinen, V., Tervaniemi, M., Saarikivi, K., de Vent, N., & Huotilainen, M. (2014). Investigating the effects of musical training on functional brain development with a novel melodic MMN paradigm. *Neurobiology of Learning and Memory*, 110, 8–15.
- Reitan, R. M., & Wolfson, D. (1985). *The Halstead-Reitan neuropsychological test battery: Theory and clinical interpretation*. Reitan Neuropsychology.
- Repp, B. H. (1999). Effects of auditory feedback deprivation on expressive piano performance. *Music Perception: An Interdisciplinary Journal*, 16, 409–438.
- Rodriguez-Herreros, B., Amengual, J. L., Gurtubay-Antolín, A., Richter, L., Jauer, P., Erdmann, C., ... Münte, T. F. (2015). Microstructure of the superior longitudinal fasciculus predicts stimulation-induced interference with on-line motor control. *NeuroImage*, 120, 254–265.
- Rüber, T., Lindenberg, R., & Schlaug, G. (2015). Differential adaptation of descending motor tracts in musicians. *Cerebral Cortex*, 25, 1490–1498.
- Sami, S., & Miall, R. (2013). Graph network analysis of immediate motor-learning induced changes in resting state BOLD. *Frontiers in Human Neuroscience*, 7, 1–10.
- Schlaug, G. (2015). Musicians and music making as a model for the study of brain plasticity. *Progress in Brain Research*, 217, 37–55.
- Shehzad, Z., Kelly, A. C., Reiss, P. T., Gee, D. G., Gotimer, K., Uddin, L. Q., ... Biswal, B. B. (2009). The resting brain: Unconstrained yet reliable. *Cerebral Cortex*, 19, 2209–2229.
- Sloboda, J. A., Davidson, J. W., Howe, M. J., & Moore, D. G. (1996). The role of practice in the development of performing musicians. *British Journal of Psychology*, 87, 287–309.
- Smith, S. M. (2002). Fast robust automated brain extraction. *Human Brain Mapping*, 17, 143–155.
- Smith, S. M., Fox, P. T., Miller, K. L., Glahn, D. C., Fox, P. M., Mackay, C. E., ... Laird, A. R. (2009). Correspondence of the brain's functional architecture during activation and rest. *Proceedings of the National Academy of Sciences*, 106, 13040–13045.
- Smith, S. M., Jenkinson, M., Woolrich, M. W., Beckmann, C. F., Behrens, T. E., Johansen-Berg, H., ... Flitney, D. E. (2004). Advances in functional and structural MR image analysis and implementation as FSL. *NeuroImage*, 23, S208–S219.
- Song, J. H., Skoe, E., Banai, K., & Kraus, N. (2012). Training to improve hearing speech in noise: Biological mechanisms. *Cerebral Cortex*, 22, 1180.

- Stam, C. J., van Straaten, E. C. W., Van Dellen, E., Tewarie, P., Gong, G., Hillebrand, A., . . . Van Mieghem, P. (2016). The relation between structural and functional connectivity patterns in complex brain networks. *International Journal of Psychophysiology*, *103*, 149–160.
- Steele, C. J., Bailey, J. A., Zatorre, R. J., & Penhune, V. B. (2013). Early musical training and white-matter plasticity in the corpus callosum: Evidence for a sensitive period. *Journal of Neuroscience*, *33*, 1282–1290.
- Yan, C., & Zang, Y. (2010). DPARSF: A MATLAB toolbox for “pipeline” data analysis of resting-state fMRI. *Frontiers in Systems Neuroscience*, *4*, 13.
- Zatorre, R. J., Belin, P., & Penhune, V. B. (2002). Structure and function of auditory cortex: Music and speech. *Trends in Cognitive Sciences*, *6*, 37–46.
- Zatorre, R. J., Chen, J. L., & Penhune, V. B. (2007). When the brain plays music: Auditory–motor interactions in music perception and production. *Nature Reviews Neuroscience*, *8*, 547–558.
- Zatorre, R. J., Fields, R. D., & Johansen-Berg, H. (2012). Plasticity in gray and white: Neuroimaging changes in brain structure during learning. *Nature Neuroscience*, *15*, 528–536.

How to cite this article: Li Q, Wang X, Wang S, et al. Musical training induces functional and structural auditory-motor network plasticity in young adults. *Hum Brain Mapp.* 2018;39:2098–2110. <https://doi.org/10.1002/hbm.23989>

北京航空航天大学四年级博士生和五年级直博生 学校奖学金申报表


(请按填表说明填写, 本表填写的内容必须为非涉密可公开!)

| | | | | | | |
|----------------------------------------|---------------------------------------------------------------------------------------------------------------------|----------|-----------|---------------------------------|-----------|--|
| 姓 名 | 王雪彤 | 学 号 | BY1510117 | 指导教师 | 李淑宇 | |
| 类 别 | <input checked="" type="checkbox"/> 三年级博士生 <input type="checkbox"/> 四年级直博生 | | 学科/专业 | 生物与医学工程 | | |
| 承担 科研 任务 情况 | 项目名称 | 课题来源 | 课题负责人 | 本人承担的具体工作 | | |
| | 基于音乐训练的老年人脑可塑造功能区多模态影像研究 | 国家自然科学基金 | 李淑宇 | 影像数据采集、筛查 | | |
| | 海马亚区的结构与功能连接方法的研究及在轻度认知障碍疾病中的应用 | 国家自然科学基金 | 李淑宇 | 海马亚区在 aMCI、svMCI 应用 | | |
| | 计算神经解剖 | 国家自然科学基金 | 李淑宇 | 大脑网络构建方法研究 | | |
| 已取得 研究成 果(论 文、专 利、获 奖等) | 论文题目 | 本人排名 | 发表年月 | 期刊(会议)名称 | 被检索 类型 | |
| | Altered whole-brain structural covariance of the hippocampal subfields in svMCI and aMCI patients | 1 | 2018 | Frontiers in Neurology | SCI 源 | |
| | Individual Morphological Brain Network Construction Based on Multivariate Euclidean Distances Between Brain Regions | 2 | 2018 | Frontiers in Human Neuroscience | SCI 源 | |
| | Musical training induces functional and structural auditory - motor network plasticity in young adults. | 2 | 2018 | Human brain mapping | SCI 源 | |
| | Differential age-related changes in structural covariance networks of human anterior and posterior hippocampus | 3 | 2018 | Frontiers in Physiology | SCI 源 | |

| | | | | | |
|--------------|---------------------------------------------------------------------------------------------------------------------------------------|------|------|-------------------|-------|
| | Topological properties of large-scale cortical networks based on multiple morphological features in amnesic mild cognitive impairment | 3 | 2016 | Neural Plasticity | SCI 源 |
| | 专利名称 | 本人排名 | 发布年月 | 专利号 | 专利类型 |
| | | | | | |
| | | | | | |
| | 获科技成果奖励名称 | 本人排名 | 获奖年月 | 证书编号 | 奖励级别 |
| | | | | | |
| | | | | | |
| 本人承诺 | 本人所填写的以上内容均为真实情况。 本人签字：_____ 年 月 日 | | | | |
| 导师意见 | 同意 / 不同意 该同学申报学校奖学金。 导师签字：_____ 年 月 日 | | | | |
| 学院学位评定分委员会意见 | 同意 / 不同意 该同学获得学校奖学金。 签字：_____ (学院代盖) 年 月 日 | | | | |

RESEARCH ARTICLE

Musical training induces functional and structural auditory-motor network plasticity in young adults

Qionglin Li^{1,2} | Xuotong Wang^{1,2} | Shaoyi Wang^{1,2} | Yongqi Xie^{1,2} |
Xinwei Li^{1,2} | Yachao Xie^{3,4} | Shuyu Li^{1,2} 

¹School of Biological Science & Medical Engineering, Beihang University, Beijing 100083, China

²Beijing Advanced Innovation Centre for Biomedical Engineering, Beihang University, Beijing 102402, China

³State Key Laboratory of Cognitive Neuroscience and Learning & IDG/McGovern Institute for Brain Research, Beijing Normal University, Beijing 100875, China

⁴Center for Collaboration and Innovation in Brain and Learning Sciences, Beijing Normal University, Beijing 100875, China

Correspondence

Shuyu Li, PhD, School of Biological Science & Medical Engineering, Beihang University, Beijing 100083, China.
Email: shuyuli@buaa.edu.cn

Funding information

National Natural Science Foundation of China, Grant/Award Numbers: 81171403, 81471731; National Natural Science Foundation of China Excellent Youth Fund, Grant/Award Number: 81622025

Abstract

Playing music requires a strong coupling of perception and action mediated by multimodal integration of brain regions, which can be described as network connections measured by anatomical and functional correlations between regions. However, the structural and functional connectivities within and between the auditory and sensorimotor networks after long-term musical training remain largely uninvestigated. Here, we compared the structural connectivity (SC) and resting-state functional connectivity (rs-FC) within and between the two networks in 29 novice healthy young adults before and after musical training (piano) with those of another 27 novice participants who were evaluated longitudinally but with no intervention. In addition, a correlation analysis was performed between the changes in FC or SC with practice time in the training group. As expected, participants in the training group showed increased FC within the sensorimotor network and increased FC and SC of the auditory-motor network after musical training. Interestingly, we further found that the changes in FC within the sensorimotor network and SC of the auditory-motor network were positively correlated with practice time. Our results indicate that musical training could induce enhanced local interaction and global integration between musical performance-related regions, which provides insights into the mechanism of brain plasticity in young adults.

KEYWORDS

auditory-motor network, brain plasticity, functional connectivity, musical training, structural connectivity

1 | INTRODUCTION

Musical performance is complex requiring a strong coupling of perception and action (Schlaug, 2015) which intensive training can induce structural and functional changes in the brain (Boyke, Driemeyer, Gaser, Büchel, & May, 2008; Herdener et al., 2010; Klein, Liem, Hänggi, Elmer, & Jäncke, 2016), even in a short-term training (Song, Skoe, Banai, & Kraus, 2012). Musical training is an excellent model to study training-related plasticity in auditory and motor areas. Previous studies have reported that acquiring musical performance skills is associated with functional and structural changes in the auditory and motor cortices (Elmer, Hänggi, Meyer, & Jäncke, 2013; Putkinen, Tervaniemi, Saarikivi, de Vent, & Huotilainen, 2014). Morphological changes (such as grey matter volume and cortical thickness) in different parts of the auditory and motor cortices due to musical training have been reported in the whole-

brain analysis in cross-sectional (Bermudez, Lerch, Evans, & Zatorre, 2009; Gaser & Schlaug, 2003) and longitudinal (Hyde et al., 2009) studies. In addition to morphological alterations, musical training has also been associated with functional and structural connectivity between cortices.

The human brain is organized in a form of network architecture in which local interactions (short-range connections) are integrated by long-range connections to support diverse brain high-order cognitive function (Park & Friston, 2013). String players, when playing their musical instruments, require information integration between different brain regions supporting auditory, somatosensory, motor, and cognitive function. Resting-state functional MRI usually measures the spontaneous low frequency fluctuations (<0.1 Hz) in the blood oxygen level-dependent (BOLD) signals which reflects patterns of brain activity in the absence of an external task. The functional connectivity measured by rs-fMRI is generally inferred by the correlations of BOLD signals

which reflect the synchronization of brain activity between distant brain areas in the absence of an external task. Using independent component analysis, the resting-state BOLD signals can be decomposed into a limited number of brain networks called intrinsic connectivity networks (ICNs). Functional communication between these networks was considered to be important in performing cognitive processes that integrate information across different brain regions (Guerra-Carrillo, Mackey, & Bunge, 2014; Harmelech & Malach, 2013). Structural connectivity (SC) usually reflects large-range fiber bundles inferred from diffusion tensor MRI, which can derive a structural brain network in terms of fiber bundles according to the regions in which they are connected (Basser, Mattiello, & LeBihan, 1994; Hagmann et al., 2007; Park et al., 2004). On a relatively short time scale in which the effects of neuronal growth and learning can be ignored, the structural networks constructed on the basis of anatomical architectures can be considered relatively fixed during different cognitive performances (Stam et al., 2016). However, it has been demonstrated that functional connectivity is task-related and state-dependent (Laird et al., 2013; Smith et al., 2009), which changes with task when comparing the functional connectivity statistics during the performance of visual attention and memory tasks (Hermundstad et al., 2013). Dynamic functional networks are intrinsically dependent on the static structural architecture of the connections that enable fast and efficient hierarchical functional integration (Park & Friston, 2013). Playing music depends on a strong coupling of perception and action mediated by multimodal integration regions distributed throughout the brain, especially the auditory and motor regions. Will SC of training-related regions be modulated in young adults after long-term musical training? If the FC is intrinsically constrained by the relatively static SC, how does it change after this training? In addition, does musical training have effects on the relationship between SC and FC? These are important questions that require answers to reveal the nature of training-induced plasticity and to provide new evidence regarding brain mechanisms to explore the changes in SC and FC between those training-related regions.

In this study, we compared the most relevant auditory and sensorimotor networks of the rs-FC and SC in 29 novice healthy young adults before and after musical training with those of another 27 novice participants who were evaluated longitudinally but with no intervention. We hypothesized that participants after training, as opposed to the controls with no intervention, would exhibit (1) FC changes in the ICNs within the auditory and motor networks and changes in the auditory-motor interaction, (2) diffusion parameter (fractional anisotropy, (FA)) changes in the SC within the auditory and motor structural network, and changed FA of the probabilistic tract pathway between the auditory and motor areas, and (3) changes of FC would be related to FA changes in the training group.

2 | MATERIALS AND METHODS

2.1 | Longitudinal experiment

2.1.1 | Participants

Sixty young healthy volunteers (29 males and 31 females) participated in this study. Participants with neurological or psychiatric disorders,

such as schizophrenia, health problems affecting dexterity, and most importantly, any experience of musical performance, were excluded following a questionnaire. Depressed persons, which were identified by a score >14 on the Beck Depression Inventory (BDI) (Beck & Steer, 1987), were excluded. Participants who were left-handers or mixed-handers, as identified via a handedness questionnaire (a modified version of the Edinburgh Handedness Inventory) (Oldfield, 1971), were also excluded. All participants were native Chinese speakers who had grown up in China and provided written informed consent; in addition, the local ethics committee approved this study.

2.1.2 | Assessment

The initial assessment included tests of overall cognitive and musical abilities. Measures of overall cognitive and musical abilities were presented to confirm that the training group and control group had similar cognitive and musical abilities and to compare possible training-related changes with these abilities. All participants were given the Advanced Measures of Music Audiation (1989) which was developed by Edwin E. Gordon to measure musical aptitude or the potential to learn in the musical domain. In the measurement, a series of 30 taped melodic excerpts were played, and participants listened and distinguished potential rhythmic and melodic alterations by choosing the appropriate answer. The percentile rank scores were acquired based on Gordon's table for individuals with a minimum of 12 years of education. In addition, an IQ score containing a performance IQ (PIQ) and a verbal IQ (VIQ) for each participant was acquired by employing the Wechsler Adult Intelligence Scale-Revised Chinese revised version (WAIS-RC) (Gong, 1992). Moreover, the trail making tests (parts A and B) (Reitan & Wolfson, 1985) were also performed to assess the visual processing and motor abilities.

The participants, who lacked a musical background (AMMA score: 20~80) and had normal intelligence (IQ score: 115~140), were randomly divided into a training group, which received 24 weeks piano training, and a control group without any training. Initially, 30 (14 males) participants were enrolled in the training group and 30 (15 males) participants were enrolled in the control group. Four persons (3 males and 1 female) dropped out due to a failure to comply with the training rules or due to health problems not related to the study design, which resulted in 29 participants (13 males) in the training group and 27 participants (13 males) in the control group.

We used a within-subject design comprising a training group in which participants received 24 weeks piano training, and a control group without any training. Participants were all tested at three time points: at the beginning (Tp1) and the end (Tp2) of 24 weeks training and at 12 weeks after training (Tp3) as shown in Figure 1a. At each time point, the participants received behavioral tests and scanning sessions. Three subtests (block design, digit symbol, and digit span) of the WAIS-RC and trail making tests were repeated at all the three time points. These tests were chosen as repeated measures based on their potential sensitivity to piano instruction with respect to motor, spatial, visual, and sequential memory. Assessments and scans in the control group were similar to those of the training group without receiving any musical training between Tp1 and Tp2.

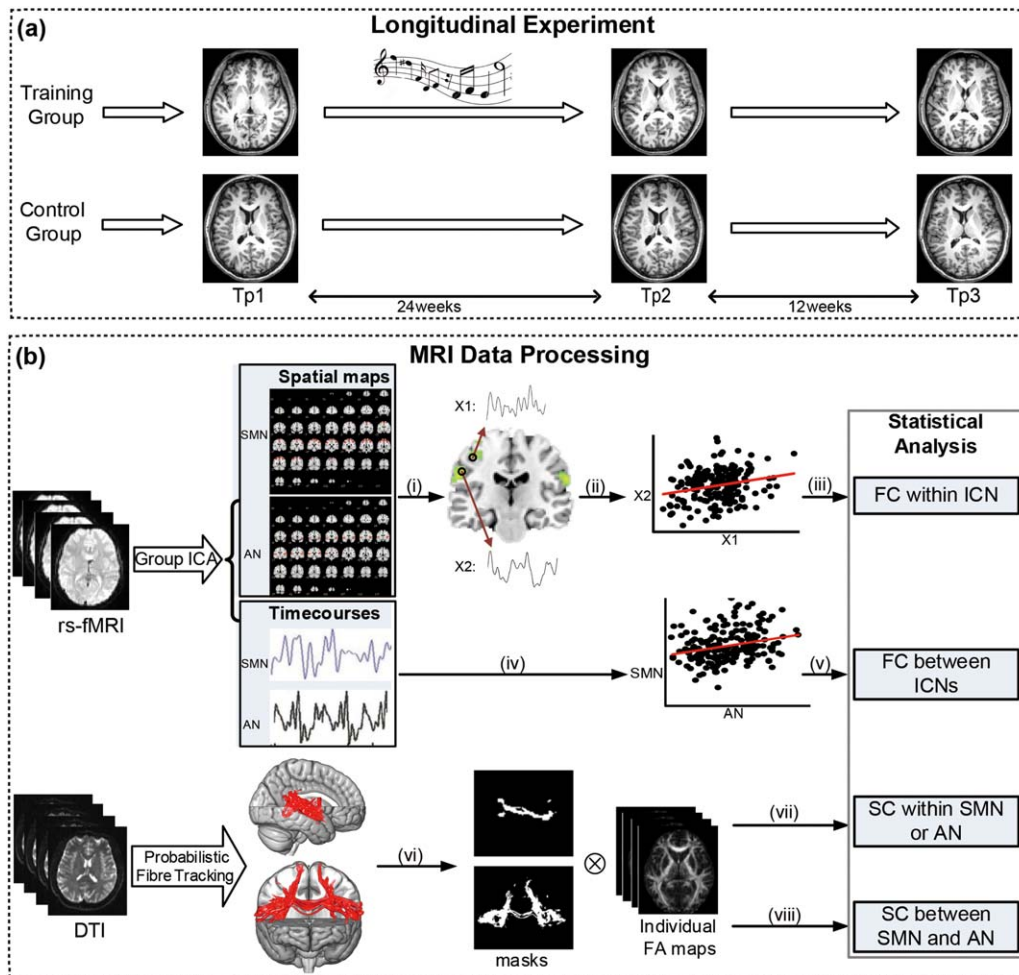


FIGURE 1 Framework for the investigation. (a) Longitudinal experiment: we used a within-subject design comprising a training group in which participants received 24-weeks piano training, and a control group with no intervention. Participants were all tested at 3-time points: at the beginning (Tp1) and the end (Tp2) of 24 weeks training and at 12 weeks after training (Tp3). At each time point, the participants all received musical assessments, behavioral tests, and scanning sessions. (b) MRI data processing: group ICA was used to acquire the auditory network (AN) and sensorimotor network (SMN) and its corresponding time courses. Probabilistic fiber tracking was conducted to acquire the WM tracts within and between the auditory and sensorimotor cortices: (i) voxel-wise ANOVA of AN and SMN; (ii) extraction of the time series from the significant clusters; (iii) correlation analysis between the time series of the significant clusters; (iv) extraction of the time courses from group ICA; (v) correlation analysis between the time series of AN and SMN; (vi) thresholded and binarized the WM tracts; (vii) calculation of the mean FA of the pathways within the auditory or sensorimotor regions; (viii) calculation of the mean FA of the pathway between the auditory and sensorimotor regions. Notes: Tp1, time point 1; Tp2, time point 2; Tp3, time point 3; ICA, independent component analysis; AN, auditory network; SMN, sensorimotor network; FC, functional connectivity; SC, structural connectivity; ANOVA, analysis of variance [Color figure can be viewed at wileyonlinelibrary.com]

A two-sample t test implemented in SPSS (SPSS version 22) was used to test the demographic data and musical performance between the two groups at baseline, except for gender (Chi-squared test). Two-sample t tests were also used to examine whether there were any differences between the two groups of these cognitive abilities at baseline. A mixed ANOVA with a between-subject factor group (training group and control group) and within-subject factor time (Tp1, Tp2, and Tp3) was performed to determine the group effects on the assessments of cognitive and musical abilities, including age, gender, and education as covariates of no interest. Significant interactions were followed by a post hoc pairwise t test between the factor of time to determine which of the time points differ from each other.

2.1.3 | Procedures

The musical training program was designed to include professional instruction, practice with the instruction, and a final musical performance. The program required participants to attend a one-hour music course once a week in the form of one-to-two lessons by professional musicians. The professional musicians provided instructions regarding music theory, progressive difficulty in musical performance, and technical motor exercises. The music theory taught in the weekly one-hour course took about 10 min. The time spent on the music theory learning was nearly the same for each participant and about 4 h for the whole training program. Instructions of music theory and progressive difficulty in musical performance referred to the *Bastien Piano for Adults-Book 1*

(Bastien, Bastien, & Bastien, 2000), and technical motor exercises referred to as *Hanon Piano Fingering Practice*. A typical course began with correcting errors in the weekly music theory assignment and explaining new theoretical concepts for study. From the beginning of the 18th week, in addition to the exercises in Bastien, one Hanon exercise was assigned every week, and these often required one week to complete at a moderate tempo. Specifically, a minimum practice time of five 30-min sessions (i.e., five days, each day at least 30-min practice) and a maximum practice time of seven 60-min sessions (i.e., seven days, each day at most one-hour practice) per week in the assigned room was also required, and the practice time was logged. Exercises for participants were also presented in the *Bastien Piano for Adults-Book 1* (Bastien et al., 2000) and the *Hanon Piano Fingering Practice*. Finally, the participants performed selected pieces from *Bastien Piano for Adults-Book 1* and were assessed by professional musicians. In addition, everyone who finished the program could individually and skillfully perform the selected pieces, which was equivalent to being certified by the Central Conservatory of Music piano level 4.

2.2 | Image acquisition

MRI scans were collected at each of the 3 measurement time points in the study. All the MRI data were obtained using a SIEMENS Trio Tim 3.0T scanner with a 12-channel phased array head coil in the Imaging Center for Brain Research, Beijing Normal University. The 3D high-resolution brain structural images were acquired using T1-weighted, sagittal 3D magnetization prepared rapid gradient echo (MPRAGE) sequences. The sequence parameters had a repetition time (TR) = 2,530 ms, echo time (TE) = 3.39 ms, inversion time (TI) = 1,100 ms, flip angle = 7°, FOV = 256 mm × 256 mm, in-plane resolution = 256 × 256, slice thickness = 1.33 mm, and 144 sagittal slices covering the whole brain. The diffusion-weighted imaging data were acquired using a single-shot twice-refocused spin-echo diffusion echo-planar imaging (EPI) sequence. The sequence parameters were TR/TE = 8,000 ms/89 ms, 30 nonlinear diffusion directions with $b = 1,000$ s/mm², and an additional volume with $b = 0$ s/mm², data matrix = 128 × 128, field of view (FOV) = 282 mm × 282 mm, 2.2 mm slice thickness, isotropic voxel size (2.2 mm)³, bandwidth (BW) = 1,562 Hz/pixel, and 62 transverse slices without gaps covering the whole brain and two averages. During the resting-state session, the participants were instructed to hold still, stay relaxed, and keep their eyes closed but not fall asleep. The functional MRI data were obtained using an echo-planar imaging (EPI) sequence with the following parameters: 33 axial slices, thickness/gap = 3.5/0.7 mm, in-plane resolution = 64 × 64, repeat time (TR) = 2,000 ms, echo time (TE) = 30 ms, flip angle = 90°, and a field of view (FOV) = 200 × 200 mm. None of the participants fell asleep according to a simple questionnaire after the scan.

2.3 | Functional connectivity analysis

Data processing was conducted using the Data Processing Assistant for the Resting-State Toolbox (DPARSF, <http://fmri.org/DPARSF>; Yan

& Zang, 2010)). Preprocessing included the following steps: (a) slice-timing correction for interleaved acquisitions; (b) head motion correction where the images are registered to the mean of the images after registering to the first image in the series; (c) T1 structural image coregistration to the functional image; (d) segmentation of the transformed structural image into grey matter, white matter, and cerebrospinal fluid; (e) spatial normalization for motion corrected functional images to the MNI space; and (f) spatial smoothing with a 4-mm Gaussian Kernel.

The spontaneous brain activity measured by rs-fMRI is typically organized in a limited number of brain networks, which are often referred to as ICNs (Beckmann, DeLuca, Devlin, & Smith, 2005; Damoiseaux et al., 2006; Shehzad et al., 2009). According to our hypotheses, the two most relevant networks were selected: auditory network (AN) and sensorimotor network (SMN). The group ICA algorithm from the fMRI toolbox (GIFT) software (<http://icatb.sourceforge.net/groupica.htm>) was used to extract the spatially independent but temporally coherent components (ICs). Data sets were temporally concatenated through subjects for one session and then concatenated through all sessions, and the data dimensions were reduced to the number of ICs using principal component analysis (PCA) (Calhoun, Adali, Pearlson, & Pekar, 2001). The optimal number of ICs in the dataset was 29 as estimated by the minimum length description (MLD) criteria implemented in the GIFT (Li, Adali, & Calhoun, 2007). Accordingly, 29 ICs were acquired using the Infomax algorithm to decompose the data from all subjects (Bell & Sejnowski, 1995), which generated a spatial map and a time course for each IC. To determine the repeatability of the ICs, 50 ICA iterations were performed using ICASSO, and the best estimate for each IC was utilized (Himberg, Hyvärinen, & Esposito, 2004). Finally, the individual IC maps and time courses were computed by back reconstruction using both aggregate components and the results from the data reduction step (Calhoun et al., 2001; Erhardt et al., 2011). The ICNs were classified by visually examining the spatial pattern (by rejecting the ICs related with physiological artifacts) and the spectral frequency (<0.1 Hz) (Lowe, Mock, & Sorenson, 1998).

A mixed ANOVA (i.e., flexible factorial model in SPM12) with a between-subject factor group (training group and control group) and a within-subject factor time (Tp1, Tp2, and Tp3) was performed to determine the group effects on SMN and AN including age, sex, and education as covariates of no interest. Significant interactions were followed by a post hoc pairwise *t* test between the factors of time. In the case of a significant test, we applied the family-wise error (FWE, $p < .05$) correction to the *p* values of the comparison of interest. Then, average time series were extracted from spherical ROIs centering on the local maxima peak of significant clusters with a radius of 8 mm. Functional connectivity within each ICN was acquired by calculating the correlation between any two of the average time series. In addition, the FC between SMN and AN was also estimated by calculating the correlation of their corresponding time courses. Statistical analyses of FC within and between SMN and AN were performed using a mixed ANOVA with post hoc tests implemented in SPSS. Finally, a correlation analysis was performed using linear regression between the changes in FC (only for those in which the post hoc pairwise *t* test was significant) with the practice time in the training group.

TABLE 1 The participant characteristics and demographics

| | Control group (n = 27) | Training group (n = 29) | p value |
|--------------------------------|---------------------------|----------------------------|---------|
| Gender (M/F) | 13/14 | 13/16 | .803 |
| Age (years) | 23.33 (1.39) | 23.10 (1.37) | .536 |
| Education | 16.70 (1.26) | 16.59 (1.09) | .709 |
| BDI | 5.15 (3.87) | 4.71 (3.62) | .646 |
| IQ | 128.19 (7.33) | 129.11 (5.65) | .598 |
| AMMA tonal percentile rank | 54.26 (14.78) | 59.34 (10.78) | .145 |
| AMMA rhythm percentile rank | 46.90 (14.54) | 53.83 (11.61) | .116 |
| AMMA composite percentile rank | 51.93 (15.31) | 57.28 (11.08) | .351 |

Note. Abbreviations: AMMA = Advanced Measures of Music Audiation; BDI = Beck Depression Inventory; M/F, male/female.

Age, education, BDI, IQ, and AMMA scores of participants in both groups at baseline are expressed as the mean (SD), and *p* values for demographics were shown in the right column.

2.4 | Structural connectivity analysis

All tensor calculations and probabilistic fiber tracking were conducted using FSL (<https://fsl.fmrib.ox.ac.uk/fsl/fslwiki/FSL>) (Smith et al., 2004). First, the raw 4D data were corrected for distortions due to eddy currents and the head motion between volumes by using an affine registration to the first $b = 0$ volume by means of FLIRT (Jenkinson & Smith, 2001). In addition, a brain extraction tool (BET) (Smith, 2002) was used to extract the brain and exclude dura, skull, scalp, and other nonbrain tissue. Second, the diffusion tensor model was built to obtain the FA, eigenvector, and eigenvalue maps for each subject. Then, the linear affine and nonlinear transform registrations were used to register individual FA map to an FMRIB FA template in the MNI space. The resulting warping transformations were then applied to resample the images of FA into the MNI space with a $2 \times 2 \times 2$ mm spatial resolution. The normalized images were then smoothed with a Gaussian kernel of 6 mm to reduce image noise and misalignment between the subjects.

Probabilistic fiber tracking was conducted between 2 ROIs: sensorimotor and auditory cortices created in the AAL template, which involved the bilateral precentral/postcentral gyrus, supplementary motor area (SMA), superior temporal gyrus, and Heschl's gyrus. The fiber tracking algorithm was performed from all voxels within each seed mask and generated 5,000 streamline samples per seed voxel with a curvature threshold of 0.2, a step length of 0.5 mm, and a maximum number of 2,000 steps. One ROI was used as the seed mask and a connection distribution was calculated between the pair of masks with another ROI as the target mask, and this process was repeatedly computed with another ROI as the seed mask. Finally, the probability of a given voxel on the pathway was represented by the sum of these samples that reached a target voxel from a given seed voxel. The results of the probabilistic tractography for each subject were thresholded and binarized to create a probabilistic fiber mask within which the mean FA for each subject was computed. The threshold was the sum of the samples sent out from the 2 ROIs and multiplied by the same percentage of 0.2%. The SC between the sensorimotor and auditory cortices was estimated by the mean FA of the tracts between the two cortices. The WM tracts within the auditory or

sensorimotor cortex were reconstructed by performing probabilistic fiber tracking in which the seed mask and target mask were both the auditory or sensorimotor regions in the AAL template. SC within the sensorimotor or auditory cortex was respectively calculated by the mean FA of the tracts within each of the cortex.

Statistical analyses of SCs within and between the sensorimotor and auditory networks were performed using mixed ANOVA with post hoc tests implemented in SPSS. In addition, a correlation analysis was performed using linear regression between the changes in SC (only those for which the post hoc pairwise *t* test was significant) with practice time in the training group.

2.5 | Relationship between FC and SC

FC is intrinsically dependent on SC for fast and efficient transfer of information, but it is unknown what degree FC is constrained by or related to characteristics of SC (Fjell et al., 2017). Due to the complex relationship between SC and FC, we explored the relationship between FC change and SC change (Tp2–Tp1) induced by musical training in the training group, which was tested by regression analysis with SC change as the independent variable and FC change as the dependent variable.

3 | RESULTS

3.1 | Participants and demographics

Twenty-nine participants in the training group (13 males, age 23.10 ± 1.37) and 27 participants in the control group (13 males, age 23.33 ± 1.39) completed the study. Moreover, the groups did not differ in terms of gender, age, education, BDI, IQ, and AMMA scores ($p > .05$) at baseline as shown in Table 1.

The mean scores and standard variances of the repeated cognitive ability assessments were shown in Table 2. No significant differences were found in any of these cognitive abilities between the two groups at baseline. A mixed ANOVA suggested that no significant interactions of the group over time were found in trail making test part A ($p = .914$) and part B ($p = .424$). In addition, no significant interactions of the

TABLE 2 Cognitive assessment data for training and control participants

| | Control group (n = 27) | | | Training group (n = 29) | | | *p value |
|--------------------|------------------------|--------------|---------------|-------------------------|---------------|---------------|----------|
| | Tp1 | Tp2 | Tp3 | Tp1 | Tp2 | Tp3 | |
| Trail making tests | | | | | | | |
| Part A | 23.37 (5.89) | 19.94 (4.39) | 17.95 (3.14) | 27.76 (10.27) | 24.10 (8.95) | 21.32 (8.15) | 0.057 |
| Part B | 54.75 (16.68) | 43.43 (9.25) | 47.45 (22.92) | 60.11 (35.04) | 45.18 (12.55) | 41.94 (13.72) | 0.474 |
| WAIS-RC subtests | | | | | | | |
| Digit span | 15.1 (2.50) | 15.7 (2.27) | 16.1 (2.30) | 14.5 (2.52) | 15.6 (2.48) | 16.3 (2.27) | 0.299 |
| Digit symbol | 17.1 (1.59) | 17.4 (1.40) | 17.6 (1.25) | 17.5 (1.57) | 18.1 (1.10) | 18.2 (1.05) | 0.338 |
| Block design | 14.1 (1.23) | 14.6 (0.97) | 14.5 (0.98) | 14.1 (1.22) | 14.5 (0.95) | 14.7 (0.75) | 0.975 |

Note. Abbreviations: Tp1 = time point 1; Tp2 = time point 2; Tp3 = time point 3; WAIS-RC = Wechsler Adult Intelligence Scale-Revised Chinese revised version.

Cognitive assessment data for training and control participants are expressed as mean (SD) for all the three time points and *p* values for these cognitive assessments at the baseline were shown in the right column (**p* value).

group over time were found in any of the repeated WAIS-RC subtests: digit span ($p = .995$), digit symbol ($p = .757$), and block design ($p = .440$). However, mixed ANOVA showed a significant main effect for time on all these cognitive tests: digit span ($F = 6.695$, $p = .002$), digit symbol ($F = 7.97$, $p = .001$), block design ($F = 6.568$, $p = .002$), trail making test part A ($F = 12.19$, $p < .001$), and part B ($F = 7.807$, $p = .01$).

3.2 | Functional connectivity

The auditory network was formed by the bilateral middle and superior temporal gyrus and Heschl's gyrus, whereas the SMN was formed by the bilateral precentral/postcentral gyrus and the bilateral SMA, as shown in Figure 2. The results showed no significant interaction of the group over time in the auditory network. However, for SMN, a significant interaction of the group over time has been found in areas of the

bilateral postcentral, left superior parietal gyrus, right inferior parietal gyrus, right precentral gyrus, and right superior frontal gyrus. The local maxima peak coordinates in the MNI space and cluster size are shown in Table 3. No significant interaction of the group over time has been found except for the FC between the right postcentral and right precentral ($F = 5.410$, $p = .006$). In addition, post hoc pairwise comparisons showed increased FC between the right postcentral and right precentral gyri when compared after (Tp2) with before musical training (Tp1) (** $p < .001$) and decreased FC when comparing Tp3 with Tp2 (* $p = .001$) in the training group, whereas there was no significant change in the control group as shown in Figure 3a.

In addition to FC within ICN, significant interaction of the group over time has been found ($F = 5.588$, $p = .005$) in FC of auditory-motor network and post hoc pairwise comparisons showed increased FC of the auditory-motor network when Tp2 was compared with Tp1

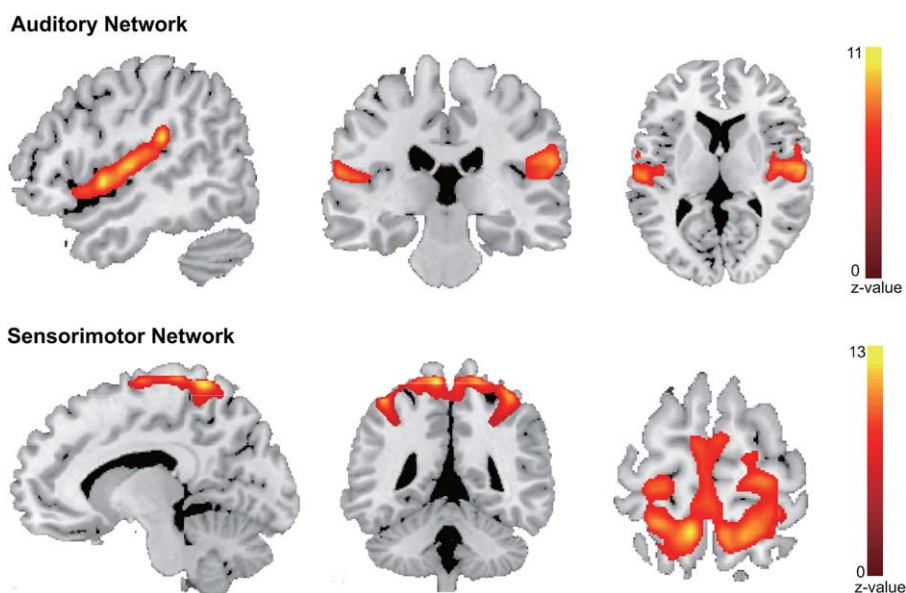


FIGURE 2 The functional auditory network and sensorimotor network. The auditory network and sensorimotor network were identified by group ICA. The AN was formed by the bilateral middle and superior temporal gyrus, and Heschl's gyrus; the SMN was formed by the bilateral precentral/postcentral gyrus and bilateral SMA. Note: AN, auditory network; SMN, sensorimotor network; SMA, supplementary motor area [Color figure can be viewed at wileyonlinelibrary.com]

TABLE 3 Clusters with a significant interaction of group over time in sensorimotor network

| Index | Number of voxels | Peak MNI coordinate | Peak MNI coordinate region (AAL) |
|-------|------------------|---------------------|----------------------------------|
| 1 | 73 | -63 -21 24 | Postcentral_L |
| 2 | 93 | 60 -24 27 | Postcentral_R |
| 3 | 101 | -18 -60 60 | Parietal_Sup_L |
| 4 | 52 | 36 -42 39 | Parietal_Inf_R |
| 5 | 50 | 42 -21 51 | Precentral_R |
| 6 | 24 | 21 3 54 | Frontal_Sup_R |

Note. Abbreviations: Postcentral_L = left postcentral gyrus; Postcentral_R = right postcentral gyrus; Parietal_Sup_L = left superior parietal gyrus; Parietal_Inf_R = right inferior parietal gyrus; Precentral_R = right precentral gyrus; Frontal_Sup_R = right superior frontal gyrus.

(** $p < .001$), decreased FC when Tp3 was compared with Tp2 ($*p = .003$) and increased FC when Tp3 was compared with Tp1 ($*p = .02$) in the training group, whereas there was no significant change in the control group as shown in Figure 3c.

3.3 | Structural connectivity

The WM tracts within sensorimotor and auditory cortices and between the sensorimotor and auditory cortices are displayed in Figure 4a and 4b, and the two areas are mainly connected by the corticospinal tract (CST), the superior longitudinal fasciculus (SLF), and the corpus callosum (CC), of which the mean FA was calculated. A significant interaction of the group over time in the WM tracts between these two areas has been found ($F = 5.643$, $p = .005$) and post hoc pairwise comparisons showed increased mean FA of the WM tracts when Tp2 was compared with Tp1 (** $p < .001$) and decreased mean FA when Tp3 was compared with Tp2 (** $p < .001$) in the training group, whereas there was no significant change in the control group as shown in Figure 5a. However, no significant interactions of the group over time have been found in any of the four structural networks within the auditory and sensorimotor areas.

3.4 | Correlation analysis

In Figure 3b, the correlation analysis revealed that the increased FC within SMN (between right postcentral and right precentral gyri) when comparing after with before training, was positively correlated with

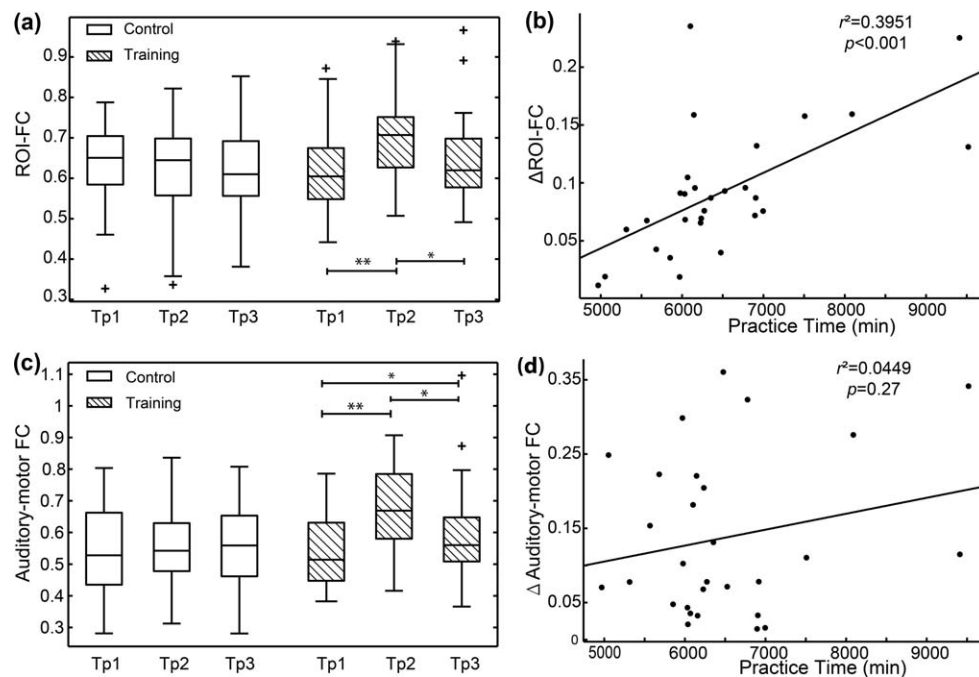


FIGURE 3 Functional connectivity comparisons and correlation analyses. (a) Comparisons showed increased functional connectivity between the right postcentral and right precentral gyri (regions within SMN) when Tp2 (at the end of training) was compared with Tp1 (at the beginning of training) (** $p < .001$) and decreased functional connectivity when Tp3 (at 12 weeks after training) was compared with Tp2 ($*p = .001$) in the training group, whereas there was no significant change in the control group. (b) The scatter plot shows that participants in the training group who practiced for longer time showed greater increased functional connectivity (Tp2–Tp1) between right postcentral and precentral gyri ($r^2 = .395$, $p < .001$). (c) Comparisons showed increased functional connectivity between SMN and AN when Tp2 (at the end of training) was compared with Tp1 (at the beginning of training) (** $p < .001$), decreased functional connectivity when Tp3 (at 12 weeks after training) was compared with Tp2 ($*p = .003$), and increased functional connectivity when Tp3 was compared with Tp1 ($*p = .02$) in the training group, whereas there was no significant change in the control group. (d) No significant correlation was found between the changes of functional connectivity (Tp2–Tp1) between the auditory and sensorimotor cortices and the practice time in the training group ($r^2 = .045$, $p = .27$). Note: Tp1, time point 1; Tp2, time point 2; Tp3, time point 3; FC, functional connectivity; SMN, sensorimotor network; AN, auditory network

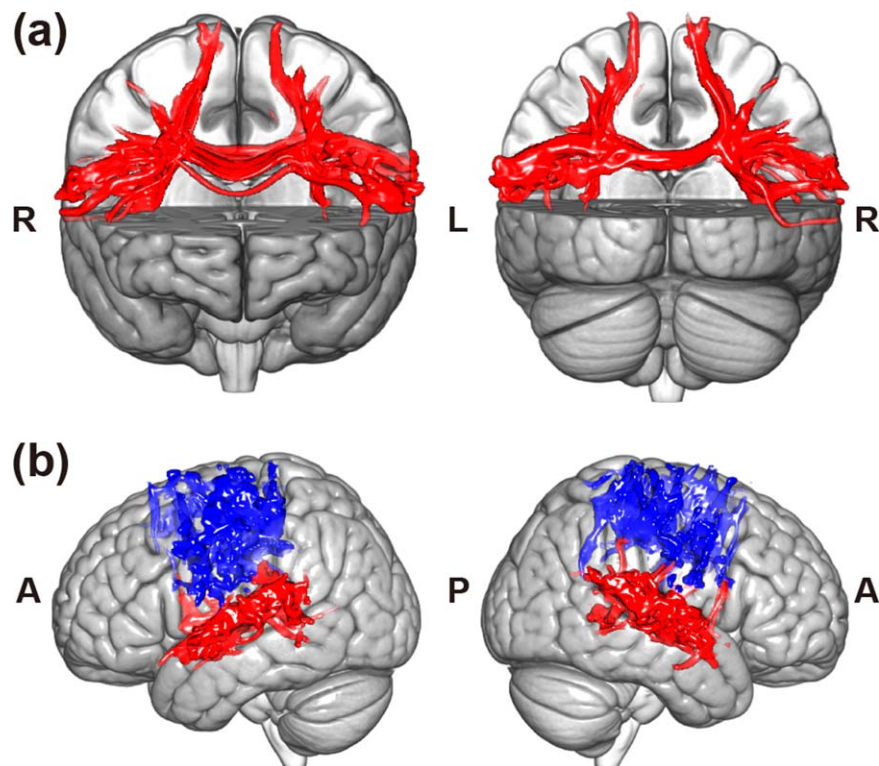


FIGURE 4 White matter fiber pathway within and between auditory and sensorimotor regions. (a) The WM tracts between auditory and sensorimotor regions were reconstructed by performing probabilistic fiber tracking between two ROI masks (auditory and sensorimotor regions). The two ROIs were connected by the corticospinal tract, superior longitudinal fasciculus, and corpus callosum. (b) The WM tracts within the auditory or sensorimotor regions were reconstructed by performing a probabilistic fiber tracking in which the seed mask and target mask were both the auditory and sensorimotor regions in the AAL template. Note: L, left side of the brain; R, right side of the brain; A, anterior side of the brain; P, posterior side of the brain [Color figure can be viewed at wileyonlinelibrary.com]

practice time ($r^2 = .395$, $p < .001$) such that participants who practiced for longer time showed greater increased FC. In addition, the mean FA of the WM tracts between auditory and sensorimotor cortices correlated positively with practice time in the training group ($r^2 = 0.370$, $p < .001$) as shown in Figure 5b. That is, participants who

practiced longer showed greater enhanced SC of the auditory-motor network. However, as seen in Figure 3d, there was no significant relationship between practice time and the changes in FC between the auditory and sensorimotor cortices in the training group ($r^2 = .045$, $p = .27$). Moreover, we have also analyzed the relationship

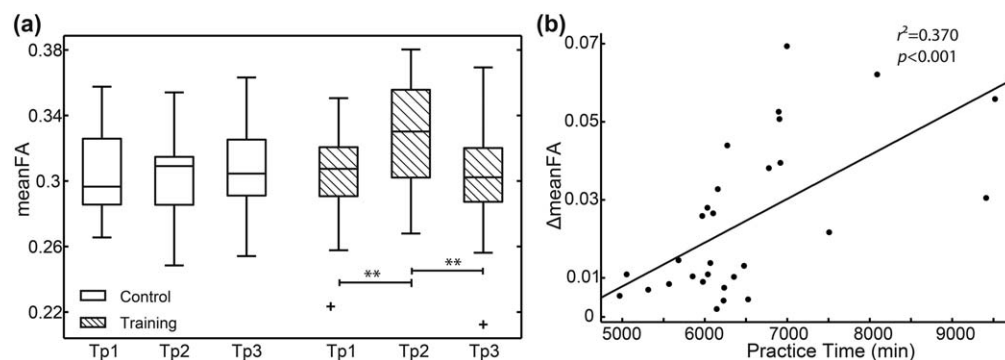


FIGURE 5 Structural connectivity comparisons and correlation analysis. (a) Structural connectivity between auditory and sensorimotor regions was evaluated by the mean FA of the WM tracts between the two regions in which probabilistic tracking was obtained. Comparisons showed increased mean FA of the WM tracts between sensorimotor and auditory cortices when Tp2 (at the end of training) was compared with Tp1 (at the beginning of training) (** $p < .001$) and decreased mean FA when Tp3 (at 12 weeks after training) was compared with Tp2 (** $p < .001$) in the training group, whereas there was no significant change in the control group. (b) Correlation analysis showed that increased mean FA of the WM tracts (Tp2–Tp1) between sensorimotor and auditory cortices was positively correlated with practice time in the training group ($r^2 = .370$, $p < .001$). Note: Tp1, time point 1; Tp2, time point 2; Tp3, time point 3; FA, fractional anisotropy; WM, white matter

between the decrease in Tp3 of structural and functional connectivity changes and the training hours in the training group. The results showed that the decreased functional connectivity within the sensorimotor network (Tp2–Tp3) was positively correlated with the practice time ($r^2 = .146, p = .041$). However, there were no significant correlations between the practice time and the decreased functional or structural connectivity of the auditory-motor network ($p > .05$).

3.5 | Relationship between functional and structural connectivity

It can be seen from Figures 3c and 5a that both FC and SC of the auditory-motor network were increased in the training group when Tp2 was compared with Tp1, showing good correspondence between FC and SC. For connectivity within the two regions, only increased FC within the sensorimotor area (between right postcentral and right precentral gyri) was found in the training group as shown in Figure 3a but with no significant changes of SC. In addition, the relationship between the significant changes of FC and SC of the auditory-motor network was explored by performing regression analysis in the training group. No significant correlation between changes of FC and SC of the auditory-motor network was found in the training group ($p = .933$).

4 | DISCUSSION

In this study, we investigated the impact of musical training on the structural and functional connectivity of the auditory and sensorimotor regions. Besides, we also analyzed the relationship between SC and FC of the two regions. Notably, we targeted at the auditory and sensorimotor regions, the most related regions during the musical performance, and demonstrated that musical training affects FC within the sensorimotor regions, whereas no effects were found within the auditory regions. In addition, we also found that musical training was associated with increased FC of the auditory-motor network and increased SC between the two regions. Moreover, the effects on FC within the sensorimotor regions and SC between the auditory and sensorimotor regions were stronger in participants with longer training time.

4.1 | Functional connectivity within and between the auditory and sensorimotor networks

The obtained ICNs in our resting-state fMRI analysis were consistent with the main networks found in previous studies (Allen et al., 2014). In this study, the ICNs showed significant training-related changes in the SMN but not the AN. Previous studies used magnetoencephalographic (MEG) measurements of the mismatch negativity (MMNm) with brain sources within the auditory cortex to evaluate the training-induced cortical response changes not the functional connectivity within the auditory cortex (Lappe, Herholz, Trainor, & Pantev, 2008; Lappe, Trainor, Herholz, & Pantev, 2011). They found differential training effects between mere auditory musical training and sensorimotor-auditory training. While there was a significant increase in the mismatch negativity after sensorimotor piano training, there was no

functional increase in the mismatch negativity after mere auditory training. The SMN, which showed the significant interaction of the group over time included regions of bilateral postcentral gyrus, left superior parietal gyrus, right inferior parietal gyrus, right precentral gyrus, and right superior frontal gyrus. In line with previous studies (Palomar-García, Zatorre, Ventura-Campos, Bueichekú, & Ávila, 2017), we also found enhanced FC within sensorimotor areas. In contrast to increased activities in motor areas (Herholz, Coffey, Pantev, & Zatorre, 2016), enhanced FC between subareas in sensorimotor cortex (right precentral and postcentral gyri), that is, FC within the sensorimotor network, was found in the present study. Previous fMRI studies have suggested that the activity of the subareas of the primary motor cortex, which was mentioned above, was related to voluntary finger movements (Indovina & Sanes, 2001). In addition to the motor areas, increases in the magnitude of the task-evoked BOLD response in the primary somatosensory cortex have also proven to be associated with long-term motor skill learning (Floyer-Lea & Matthews, 2005). It has been suggested that somatosensory feedback is also important in motor task learning (Asanuma & Pavlides, 1997; Kaelin-Lang et al., 2002; Pavlides, Miyashita, & Asanuma, 1993), which is a major source of afferents to the primary motor cortex (Asanuma, Stoney, & Abzug, 1968). Activation of both the somatosensory and motor cortices in hand movements (Kleinschmidt, Nitschke, & Frahm, 1997) suggests the importance of afferent feedback in full movement. The results of this study are compatible with this concept of afferent feedback because we found higher functional connectivity between primary motor and somatosensory cortices after musical training. Thus, we can infer that the information interaction of the local somatosensory and motor areas can be modulated by long-term musical training in young adults.

In addition to increased FC within the sensorimotor network, our results also showed increased rs-FC of the auditory-motor network after long-term musical training. Feedback interactions are particularly relevant in playing an instrument, where performers must listen to each note they produce and perform appropriate action adjustments in due course. It has been proven that musicians can still perform prehearsed pieces when auditory feedback is blocked, but expressive aspects of performance are affected (Repp, 1999). More importantly, when auditory feedback is experimentally manipulated by the introduction of delays or distortions, the motor performance is significantly altered (Pfordresher & Palmer, 2006). Thus, information integration between auditory and sensorimotor cortices is of particular importance in musical performance, which indicates that the FC of the auditory-motor network increased after long-term musical training.

Perfect musical performance requires the interaction of local information within the auditory and sensorimotor cortices and global integration between the two areas. The results of this study showed enhanced local interaction within the sensorimotor cortex and global integration between the auditory and sensorimotor cortices after long-term musical training. Interestingly, in this study, participants in the training group with more hours of practice showed a greater increase in FC within the sensorimotor network. This finding indicates the possibility of brain plasticity in local interaction within the sensorimotor

cortex. Our findings provide new evidence for revealing the mechanism of brain functional organization modulated by musical training.

4.2 | Structural connectivity within and between auditory and sensorimotor networks

In contrast to focusing on white matter architectures, we used probabilistic fiber tracking to construct the structural connectivity within and between auditory and sensorimotor areas. Consistent with the increased FA reported in previous studies (Halwani, Loui, Rueber, & Schlaug, 2011; Rüber, Lindenberg, & Schlaug, 2015; Steele, Bailey, Zatorre, & Penhune, 2013), we also found increased mean FA of WM tracts between the sensorimotor and auditory cortices after long-term musical training and receded when exercise stopped, whereas no significant changes in mean FA were found within the auditory or sensorimotor cortex in this study. Auditory and sensorimotor cortices are mainly connected by the corticospinal tract (CST), superior longitudinal fasciculus (SLF), and corpus callosum (CC). Both CST and SLF are part of the sensorimotor system. The fiber of the CST plays a key role in the control of voluntary movement which projects from the sensorimotor and premotor cortices to the motor-neurons in the spinal cord. The SLF links posterior sensory to the frontal regions, which involves the integration of sensory and motor information for action (Hecht et al., 2013; Rodriguez-Herreros et al., 2015). The body of CC connects premotor and sensorimotor regions, whereas the splenium connects the visual, parietal, and auditory regions (Hofer & Frahm, 2006; Knyazeva, 2013). The lateral portions of the CC are crossed by other fiber tracts, including the SLF and the CST. The FA changes of these pathways have been shown to be related to musical performance (Giacosa, Karpati, Foster, Penhune, & Hyde, 2016; Steele et al., 2013). Children with 15 months musical training showed larger deformation changes of CC compared with the controls which supported the findings in this study (Hyde et al., 2009). Increases in FA are thought to be associated with changes in axon diameter, the fanning of primary fibers or the density and coherence of secondary fibers in crossing regions (Douaud et al., 2009, 2011; Zatorre, Fields, & Johansen-Berg, 2012). Playing the piano requires the coordinated action of two hands, auditory feedback and interhemispheric interactions, and may place greater demands on interactions between auditory and sensorimotor regions (Zatorre, Chen, & Penhune, 2007), thus promoting the enhanced connections that are indexed by increased FA. In addition, the increased FA of fibers between auditory and sensorimotor cortices was correlated with the practice time in the training group. That is, participants who practiced for longer time showed greater enhanced structural connectivity between the musical performance related regions. Thus, it can be suggested that musical training could induce modulation of long-range brain structural connectivity, which mediates submodules of the brain.

4.3 | Relationship between functional and structural connectivity

In this study, we found increased FC of the auditory-motor network and increased SC between the two regions in the training group after a

long-term musical training, showing good correspondence between FC and SC. However, the relationship between change in FC and change in SC of auditory-motor network was not significant in the training group, showing different modulation of FC and SC induced by musical training. Besides increased FC and SC of auditory-motor network, enhanced FC within the sensorimotor area but no significant changes in SC within sensorimotor or auditory were found.

The human brain is organized by global integration of local interaction in which global integration via long-range weak connections facilitate diverse cognitive function mediated by short-range dense connectivity (Park & Friston, 2013). The long-range weak connections are relatively flexible and facilitate diverse integration for various functional demands (Ekman, Derrfuss, Tittgemeyer, & Fiebach, 2012; Hermundstad et al., 2013). Furthermore, the coupling between different local interactions may be more dynamic and task-related, which is plausibly mediated by long-range structural connections, such as commissural fibers for bilateral submodules and longitudinal fibers within a hemisphere (Allen et al., 2014; Park et al., 2012), than the strong coupling within local interactions. Thus, it can be interpreted that both the relatively static SC and the dynamic FC between training related regions could be induced changes after long-term intensive musical training but changes in FC and SC are not necessarily strongly correlated.

In this study, the FC within the sensorimotor network and SC between auditory and sensorimotor cortices changes degraded nearly to baseline without training over 12 weeks. However, increased FC of the auditory-motor network lasted for 12 weeks without further training (even though lower than Tp2). The lasting increased long-range functional connectivity between auditory and sensorimotor cortices may underlie a brain optimization strategy that may reduce the need for the equivalent dedicated structural networks and avoid the incremental metabolic costs in terms of modifying physical connections (Sami & Miall, 2013). Functional connectivity within sensorimotor network was significantly increased after the musical training but decreased to the baseline when training ended. Interestingly, participants in the training group who practiced for a longer time showed greater increased functional connectivity within the sensorimotor network during the training period and also greater decrease after the training period. The transient changes of the functional connectivity within the sensorimotor network could be explained by the perspective that the local connectivity was more task-related and may only characterize patterns of activity during training (Park & Friston, 2013). However, there were no significant correlations between the practice time and the decrease of the functional and structural connectivity between sensorimotor and auditory cortices. Therefore, in future, the longitudinal study in which imaging data are acquired at multiple time points could help for revealing the different dynamic properties of training-related plastic changes in structural connectivity and functional connectivity.

4.4 | Limitations and future directions

This study still has some limitations. First, the relationship between FC and SC is complex and the alignment of FC and SC seems restricted to specific regions (Fjell et al., 2017), thus an appropriate approach which

can qualitatively and quantitatively characterize the SC–FC coupling is needed to examine the effects of musical training on SC–FC relationships of auditory and sensorimotor cortices. Second, we explored the relationship between practice time and changes of connectivity. Even though longer practice time may be linked with an increase in proficiency (Sloboda, Davidson, Howe, & Moore, 1996), in future, the measures of the piano efficiency deserve to be recorded to investigate the relationship between training and changes of connectivity. Third, SC was estimated by tractography and based on diffusion imaging treating the bilateral auditory or sensorimotor as a whole seed. Musical training has been associated with increased hemispheric asymmetries (Boemio, Fromm, Braun, & Poeppel, 2005; Zatorre, Belin, & Penhune, 2002), and investigating the interhemispheric and intrahemispheric SC between auditory and sensorimotor areas is of great importance. Fourth, participants in the training group received instructions in music theory while the controls did not get any cognitive instructions at all, which may be confounding in the analysis of training-induced auditory and sensorimotor changes. Future studies are needed to shed more light on these issues.

ACKNOWLEDGMENTS

This work was supported by the National Natural Science Foundation of China (Grant No. 81171403, 81471731), National Natural Science Foundation of China Excellent Youth Fund (Grant No. 81622025).

CONFLICT OF INTERESTS

The authors declare that there are no conflicts of interest regarding the publication of this article.

ORCID

Shuyu Li  <http://orcid.org/0000-0002-3459-6821>

REFERENCES

- Allen, E. A., Damaraju, E., Plis, S. M., Erhardt, E. B., Eichele, T., & Calhoun, V. D. (2014). Tracking whole-brain connectivity dynamics in the resting state. *Cerebral Cortex*, *24*, 663–676.
- Asanuma, H., & Pavlides, C. (1997). Neurobiological basis of motor learning in mammals. *Neuroreport: An International Journal for the Rapid Communication of Research in Neuroscience*, *8*, i–vi.
- Asanuma, H., Stoney, S., & Abzug, C. (1968). Relationship between afferent input and motor outflow in cat motor sensory cortex. *Journal of Neurophysiology*, *31*, 670–681.
- Basser, P. J., Mattiello, J., & LeBihan, D. (1994). MR diffusion tensor spectroscopy and imaging. *Biophysical Journal*, *66*, 259–267.
- Bastien, J. S., Bastien, L., & Bastien, L. (2000). *Piano for adults*. Kjos Music Press.
- Beck, A., & Steer, R. (1987). *Beck depression inventory manual*. New York: The Psychological Corporation Harcourt Brace Jovanovich Inc.
- Beckmann, C. F., DeLuca, M., Devlin, J. T., & Smith, S. M. (2005). Investigations into resting-state connectivity using independent component analysis. *Philosophical Transactions of the Royal Society of London B: Biological Sciences*, *360*, 1001–1013.
- Bell, A. J., & Sejnowski, T. J. (1995). An information-maximization approach to blind separation and blind deconvolution. *Neural Computation*, *7*, 1129–1159.
- Bermudez, P., Lerch, J. P., Evans, A. C., & Zatorre, R. J. (2009). Neuroanatomical correlates of musicianship as revealed by cortical thickness and voxel-based morphometry. *Cerebral Cortex*, *19*, 1583–1596.
- Boemio, A., Fromm, S., Braun, A., & Poeppel, D. (2005). Hierarchical and asymmetric temporal sensitivity in human auditory cortices. *Nature Neuroscience*, *8*, 389–395.
- Boyke, J., Driemeyer, J., Gaser, C., Büchel, C., & May, A. (2008). Training-induced brain structure changes in the elderly. *Journal of Neuroscience*, *28*, 7031–7035.
- Calhoun, V., Adali, T., Pearlson, G., & Pekar, J. (2001). A method for making group inferences from functional MRI data using independent component analysis. *Human Brain Mapping*, *14*, 140–151.
- Damoiseaux, J., Rombouts, S., Barkhof, F., Scheltens, P., Stam, C., Smith, S. M., & Beckmann, C. (2006). Consistent resting-state networks across healthy subjects. *Proceedings of the National Academy of Sciences*, *103*, 13848–13853.
- Douaud, G., Behrens, T. E., Poupon, C., Cointepas, Y., Jbabdi, S., Gaura, V., ... Damier, P. (2009). In vivo evidence for the selective subcortical degeneration in Huntington's disease. *NeuroImage*, *46*, 958–966.
- Douaud, G., Jbabdi, S., Behrens, T. E., Menke, R. A., Gass, A., Monsch, A. U., ... Matthews, P. M. (2011). DTI measures in crossing-fibre areas: Increased diffusion anisotropy reveals early white matter alteration in MCI and mild Alzheimer's disease. *NeuroImage*, *55*, 880–890.
- Ekman, M., Derrfuss, J., Tittgemeyer, M., & Fiebach, C. J. (2012). Predicting errors from reconfiguration patterns in human brain networks. *Proceedings of the National Academy of Sciences*, *109*, 16714–16719.
- Elmer, S., Hänggi, J., Meyer, M., & Jäncke, L. (2013). Increased cortical surface area of the left planum temporale in musicians facilitates the categorization of phonetic and temporal speech sounds. *Cortex*, *49*, 2812–2821.
- Erhardt, E. B., Rachakonda, S., Bedrick, E. J., Allen, E. A., Adali, T., & Calhoun, V. D. (2011). Comparison of multi-subject ICA methods for analysis of fMRI data. *Human Brain Mapping*, *32*, 2075–2095.
- Fjell, A. M., Sneve, M. H., Grydeland, H., Storsve, A. B., Amlien, I. K., Yendiki, A., & Walhovd, K. B. (2017). Relationship between structural and functional connectivity change across the adult lifespan: A longitudinal investigation. *Human Brain Mapping*, *38*, 561–573.
- Floyer-Lea, A., & Matthews, P. M. (2005). Distinguishable brain activation networks for short- and long-term motor skill learning. *Journal of Neurophysiology*, *94*, 512–518.
- Gaser, C., & Schlaug, G. (2003). Brain structures differ between musicians and non-musicians. *Journal of Neuroscience*, *23*, 9240–9245.
- Giacosa, C., Karpati, F. J., Foster, N. E., Penhune, V. B., & Hyde, K. L. (2016). Dance and music training have different effects on white matter diffusivity in sensorimotor pathways. *NeuroImage*, *135*, 273–286.
- Gong, Y. (1992). *Wechsler Adult Intelligence Scale-revised (Chinese revised version)*. Hunan Medical Institute.
- Guerra-Carrillo, B., Mackey, A. P., & Bunge, S. A. (2014). Resting-state fMRI A window into human brain plasticity. *Neuroscientist*, *20*, 522–533.
- Hagmann, P., Kurant, M., Gigandet, X., Thiran, P., Wedeen, V. J., Meuli, R., & Thiran, J.-P. (2007). Mapping human whole-brain structural networks with diffusion MRI. *PLoS One*, *2*, e597.
- Halwani, G., Loui, P., Rueber, T., & Schlaug, G. (2011). Effects of practice and experience on the arcuate fasciculus: Comparing singers, instrumentalists, and non-musicians. *Frontiers in Psychology*, *2*,

- Harmelech, T., & Malach, R. (2013). Neurocognitive biases and the patterns of spontaneous correlations in the human cortex. *Trends in Cognitive Sciences*, 17, 606–615.
- Hecht, E. E., Gutman, D. A., Preuss, T. M., Sanchez, M. M., Parr, L. A., & Rilling, J. K. (2013). Process versus product in social learning: Comparative diffusion tensor imaging of neural systems for action execution—Observation matching in macaques, chimpanzees, and humans. *Cerebral Cortex*, 23, 1014–1024.
- Herdener, M., Esposito, F., di Salle, F., Boller, C., Hilti, C. C., Habermeyer, B., ... Cattapan-Ludewig, K. (2010). Musical training induces functional plasticity in human hippocampus. *Journal of Neuroscience*, 30, 1377–1384.
- Herholz, S. C., Coffey, E. B. J., Pantev, C., & Zatorre, R. J. (2016). Dissociation of neural networks for predisposition and for training-related plasticity in auditory-motor learning. *Cerebral Cortex*, 26, 3125–3134.
- Hermundstad, A. M., Bassett, D. S., Brown, K. S., Aminoff, E. M., Clewett, D., Freeman, S., ... Miller, M. B. (2013). Structural foundations of resting-state and task-based functional connectivity in the human brain. *Proceedings of the National Academy of Sciences*, 110, 6169–6174.
- Himberg, J., Hyvärinen, A., & Esposito, F. (2004). Validating the independent components of neuroimaging time series via clustering and visualization. *NeuroImage*, 22, 1214–1222.
- Hofer, S., & Frahm, J. (2006). Topography of the human corpus callosum revisited—comprehensive fiber tractography using diffusion tensor magnetic resonance imaging. *NeuroImage*, 32, 989–994.
- Hyde, K. L., Lerch, J., Norton, A., Forgeard, M., Winner, E., Evans, A. C., & Schlaug, G. (2009). Musical training shapes structural brain development. *Journal of Neuroscience*, 29, 3019–3025.
- Indovina, I., & Sanes, J. N. (2001). On somatotopic representation centers for finger movements in human primary motor cortex and supplementary motor area. *NeuroImage*, 13, 1027–1034.
- Jenkinson, M., & Smith, S. (2001). A global optimisation method for robust affine registration of brain images. *Medical Image Analysis*, 5, 143–156.
- Kaelin-Lang, A., Luft, A. R., Sawaki, L., Burstein, A. H., Sohn, Y. H., & Cohen, L. G. (2002). Modulation of human corticomotor excitability by somatosensory input. *Journal of Physiology*, 540, 623–633.
- Klein, C., Liem, F., Hänggi, J., Elmer, S., Jäncke, L. (2016). The “silent” imprint of musical training. *Human Brain Mapping*, 37, 536–546.
- Kleinschmidt, A., Nitschke, M. F., & Frahm, J. (1997). Somatotopy in the human motor cortex hand area. A high-resolution functional MRI study. *European Journal of Neuroscience*, 9, 2178–2186.
- Knyazeva, M. G. (2013). Splenium of corpus callosum: Patterns of inter-hemispheric interaction in children and adults. *Neural Plasticity*, 2013, 1–10.
- Laird, A. R., Eickhoff, S. B., Rotzsch, C., Bzdok, D., Ray, K. L., & Fox, P. T. (2013). Networks of task co-activations. *NeuroImage*, 80, 505–514.
- Lappe, C., Herholz, S. C., Trainor, L. J., & Pantev, C. (2008). Cortical plasticity induced by short-term unimodal and multimodal musical training. *Journal of Neuroscience*, 28, 9632–9639.
- Lappe, C., Trainor, L. J., Herholz, S. C., & Pantev, C. (2011). Cortical plasticity induced by short-term multimodal musical rhythm training. *PLoS One*, 6, e21493.
- Li, Y. O., Adali, T., & Calhoun, V. D. (2007). Estimating the number of independent components for functional magnetic resonance imaging data. *Human Brain Mapping*, 28, 1251–1266.
- Lowe, M., Mock, B., & Sorenson, J. (1998). Functional connectivity in single and multislice echoplanar imaging using resting-state fluctuations. *NeuroImage*, 7, 119–132.
- Oldfield, R. C. (1971). The assessment and analysis of handedness: The Edinburgh inventory. *Neuropsychologia*, 9, 97–113.
- Palomar-García, M.-Á., Zatorre, R. J., Ventura-Campos, N., Bueichekú, E., & Ávila, C. (2017). Modulation of functional connectivity in auditory-motor networks in musicians compared with nonmusicians. *Cerebral Cortex*, 27, 2768–2778.
- Park, B., Kim, J. I., Lee, D., Jeong, S.-O., Lee, J. D., & Park, H.-J. (2012). Are brain networks stable during a 24-hour period? *NeuroImage*, 59, 456–466.
- Park, H.-J., Kubicki, M., Westin, C.-F., Talos, I.-F., Brun, A., Peiper, S., ... Shenton, M. E. (2004). Method for combining information from white matter fiber tracking and gray matter parcellation. *American Journal of Neuroradiology*, 25, 1318–1324.
- Park, H. J., & Friston, K. (2013). Structural and functional brain networks: From connections to cognition. *Science (New York, N.Y.)*, 342, 1238411.
- Pavlidis, C., Miyashita, E., & Asanuma, H. (1993). Projection from the sensory to the motor cortex is important in learning motor skills in the monkey. *Journal of Neurophysiology*, 70, 733–741.
- Pfordresher, P. Q., & Palmer, C. (2006). Effects of hearing the past, present, or future during music performance. *Attention, Perception, & Psychophysics*, 68, 362–376.
- Putkinen, V., Tervaniemi, M., Saarikivi, K., de Vent, N., & Huotilainen, M. (2014). Investigating the effects of musical training on functional brain development with a novel melodic MMN paradigm. *Neurobiology of Learning and Memory*, 110, 8–15.
- Reitan, R. M., & Wolfson, D. (1985). *The Halstead-Reitan neuropsychological test battery: Theory and clinical interpretation*. Reitan Neuropsychology.
- Repp, B. H. (1999). Effects of auditory feedback deprivation on expressive piano performance. *Music Perception: An Interdisciplinary Journal*, 16, 409–438.
- Rodriguez-Herreros, B., Amengual, J. L., Gurtubay-Antolín, A., Richter, L., Jauer, P., Erdmann, C., ... Münte, T. F. (2015). Microstructure of the superior longitudinal fasciculus predicts stimulation-induced interference with on-line motor control. *NeuroImage*, 120, 254–265.
- Rüber, T., Lindenberg, R., & Schlaug, G. (2015). Differential adaptation of descending motor tracts in musicians. *Cerebral Cortex*, 25, 1490–1498.
- Sami, S., & Miall, R. (2013). Graph network analysis of immediate motor-learning induced changes in resting state BOLD. *Frontiers in Human Neuroscience*, 7, 1–10.
- Schlaug, G. (2015). Musicians and music making as a model for the study of brain plasticity. *Progress in Brain Research*, 217, 37–55.
- Shehzad, Z., Kelly, A. C., Reiss, P. T., Gee, D. G., Gotimer, K., Uddin, L. Q., ... Biswal, B. B. (2009). The resting brain: Unconstrained yet reliable. *Cerebral Cortex*, 19, 2209–2229.
- Sloboda, J. A., Davidson, J. W., Howe, M. J., & Moore, D. G. (1996). The role of practice in the development of performing musicians. *British Journal of Psychology*, 87, 287–309.
- Smith, S. M. (2002). Fast robust automated brain extraction. *Human Brain Mapping*, 17, 143–155.
- Smith, S. M., Fox, P. T., Miller, K. L., Glahn, D. C., Fox, P. M., Mackay, C. E., ... Laird, A. R. (2009). Correspondence of the brain's functional architecture during activation and rest. *Proceedings of the National Academy of Sciences*, 106, 13040–13045.
- Smith, S. M., Jenkinson, M., Woolrich, M. W., Beckmann, C. F., Behrens, T. E., Johansen-Berg, H., ... Flitney, D. E. (2004). Advances in functional and structural MR image analysis and implementation as FSL. *NeuroImage*, 23, S208–S219.
- Song, J. H., Skoe, E., Banai, K., & Kraus, N. (2012). Training to improve hearing speech in noise: Biological mechanisms. *Cerebral Cortex*, 22, 1180.

- Stam, C. J., van Straaten, E. C. W., Van Dellen, E., Tewarie, P., Gong, G., Hillebrand, A., . . . Van Mieghem, P. (2016). The relation between structural and functional connectivity patterns in complex brain networks. *International Journal of Psychophysiology*, *103*, 149–160.
- Steele, C. J., Bailey, J. A., Zatorre, R. J., & Penhune, V. B. (2013). Early musical training and white-matter plasticity in the corpus callosum: Evidence for a sensitive period. *Journal of Neuroscience*, *33*, 1282–1290.
- Yan, C., & Zang, Y. (2010). DPARSF: A MATLAB toolbox for “pipeline” data analysis of resting-state fMRI. *Frontiers in Systems Neuroscience*, *4*, 13.
- Zatorre, R. J., Belin, P., & Penhune, V. B. (2002). Structure and function of auditory cortex: Music and speech. *Trends in Cognitive Sciences*, *6*, 37–46.
- Zatorre, R. J., Chen, J. L., & Penhune, V. B. (2007). When the brain plays music: Auditory–motor interactions in music perception and production. *Nature Reviews Neuroscience*, *8*, 547–558.
- Zatorre, R. J., Fields, R. D., & Johansen-Berg, H. (2012). Plasticity in gray and white: Neuroimaging changes in brain structure during learning. *Nature Neuroscience*, *15*, 528–536.

How to cite this article: Li Q, Wang X, Wang S, et al. Musical training induces functional and structural auditory-motor network plasticity in young adults. *Hum Brain Mapp.* 2018;39:2098–2110. <https://doi.org/10.1002/hbm.23989>



Individual Morphological Brain Network Construction Based on Multivariate Euclidean Distances Between Brain Regions

Kaixin Yu^{1,2}, Xuotong Wang^{1,2}, Qionglin Li^{1,2}, Xiaohui Zhang^{1,2}, Xinwei Li^{1,2}, Shuyu Li^{1,2*} for the Alzheimer's Disease Neuroimaging Initiative[†]

OPEN ACCESS

Edited by:

Jinhui Wang,
Hangzhou Normal University, China

Reviewed by:

Chong-Yaw Wee,
National University of Singapore,
Singapore
Mingrui Xia,
Beijing Normal University, China

*Correspondence:

Shuyu Li
shuyuli@buaa.edu.cn

[†]Data used in preparing this article were obtained from the Alzheimer's Disease Neuroimaging Initiative (ADNI) database (adni.loni.usc.edu). As such, the investigators within the ADNI contributed to the design and implementation of ADNI and/or provided data but most of them did not participate in this analysis or writing this report. A complete list of ADNI investigators can be found at: http://adni.loni.usc.edu/wp-content/uploads/how_to_apply/ADNI_Acknowledgement_List.pdf

Received: 09 March 2018

Accepted: 01 May 2018

Published: 24 May 2018

Citation:

Yu K, Wang X, Li Q, Zhang X, Li X, Li S for the Alzheimer's Disease Neuroimaging Initiative (2018) Individual Morphological Brain Network Construction Based on Multivariate Euclidean Distances Between Brain Regions. *Front. Hum. Neurosci.* 12:204. doi: 10.3389/fnhum.2018.00204

¹ School of Biological Science & Medical Engineering, Beihang University, Beijing, China, ² Beijing Advanced Innovation Centre for Biomedical Engineering, Beihang University, Beijing, China

Morphological brain network plays a key role in investigating abnormalities in neurological diseases such as mild cognitive impairment (MCI) and Alzheimer's disease (AD). However, most of the morphological brain network construction methods only considered a single morphological feature. Each type of morphological feature has specific neurological and genetic underpinnings. A combination of morphological features has been proven to have better diagnostic performance compared with a single feature, which suggests that an individual morphological brain network based on multiple morphological features would be beneficial in disease diagnosis. Here, we proposed a novel method to construct individual morphological brain networks for two datasets by calculating the exponential function of multivariate Euclidean distance as the evaluation of similarity between two regions. The first dataset included 24 healthy subjects who were scanned twice within a 3-month period. The topological properties of these brain networks were analyzed and compared with previous studies that used different methods and modalities. Small world property was observed in all of the subjects, and the high reproducibility indicated the robustness of our method. The second dataset included 170 patients with MCI (86 stable MCI and 84 progressive MCI cases) and 169 normal controls (NC). The edge features extracted from the individual morphological brain networks were used to distinguish MCI from NC and separate MCI subgroups (progressive vs. stable) through the support vector machine in order to validate our method. The results showed that our method achieved an accuracy of 79.65% (MCI vs. NC) and 70.59% (stable MCI vs. progressive MCI) in a one-dimension situation. In a multiple-dimension situation, our method improved the classification performance with an accuracy of 80.53% (MCI vs. NC) and 77.06% (stable MCI vs. progressive MCI) compared with the method using a single feature. The results indicated that our method could effectively construct an individual morphological brain network based on multiple morphological features and could accurately discriminate MCI from NC and stable MCI from progressive MCI, and may provide a valuable tool for the investigation of individual morphological brain networks.

Keywords: individual morphological brain network, multivariate Euclidean distance, mild cognitive impairment, multiple morphological features, classification

INTRODUCTION

Morphological brain network refers to the intracortical similarities in gray matter morphology (He et al., 2007) which plays a key role in investigating brain abnormalities in neurological diseases. By analyzing morphological brain network features, the abnormalities in connectivity parameters can be found in patients (Yao et al., 2010; Tijms et al., 2013). More importantly, sensitive biomarkers for clinical diagnosis can be detected in brain networks from cases of Alzheimer's disease (He et al., 2008, 2009), schizophrenia (Bassett et al., 2008; Zhang et al., 2012) and epilepsy (Bernhardt et al., 2008, 2009).

Although previous morphological brain network studies achieved significant breakthroughs, they largely depended on group-level anatomical correlations of cortical morphology (He et al., 2007; Zhang et al., 2012). For example, He et al. (2007) constructed a network for each group by quantifying morphological relations characterized by the Pearson correlation coefficient between averaged regional morphological measures among participants. However, this method only works with a relatively large number of participants (Kong et al., 2014). In addition, it remains unclear if there are changes in brain networks at the individual level (Saggar et al., 2015). Therefore, it is necessary to construct morphological brain networks at the individual level for the direct analysis of individual differences.

Recently, several methods have been proposed to construct individual morphological brain networks either using a single feature or multiple morphological features. By using gray matter volume as the morphological measure, Tijms et al. (2012) proposed an individual morphological brain network by computing the correlation between two 27-voxel sets from two rigid cubes. There were some studies constructing individual brain networks by averaging the vertex value (e.g., cortical thickness) within regions of interest (ROI) (Dai et al., 2013; Wee et al., 2013; Kim et al., 2016) or by estimating interregional similarity in the distribution of regional morphological measures (e.g., cortical thickness or volume) (Kong et al., 2014; Zheng et al., 2015). Wang et al. (2016) employed graph-based analyses to support individual morphological network analysis as a meaningful and reliable method when characterizing brain structural organization. Some recent studies (Li et al., 2017; Seidlitz et al., 2017) built individual morphological networks with multiple morphological features extracted from the cortical surface. Each type of morphological feature has specific neurological and genetic underpinnings. Volumetric measures (i.e., cortical thickness, gray matter volume) reflect the size, density and arrangement of cells (neurons, neuroglia, and nerve fibers) (Parent and Carpenter, 1996) and surface area is linked to the number of mini columns in the cortical layer (Rakic, 1988). Geometric measures (i.e., sulcal depth, curvature, and metric distortion) mainly reflect the cortical folding pattern (Van Essen, 1997; Cachia et al., 2003; Lohmann et al., 2008). Li et al. (2014) found that various morphological features had unique contributions to the classification of the amnesic MCI (aMCI) and NC. In the two studies (Li et al., 2017; Seidlitz et al., 2017), a morphological feature vector was used to represent one region and pairwise inter-regional Pearson correlations were used to

construct brain network, while not considering the distribution of the intra-regional morphological features.

In this paper, we proposed a novel individual morphological brain network method by defining multivariate Euclidean distance to describe the inter-regional similarity based on multiple morphological features. First, multivariate Euclidean distance was calculated by using the six morphological features of all of the vertices within each region. Second, the Min-Max normalization for Euclidean distance was performed to minimize possible bias in different ranges of different subjects. Finally, the normalized Euclidean distance was converted to a similarity measurement using an exponential function. Then, we validated the proposed method by computing the topological properties of individual brain networks, i.e., small-world, hubs and intraclass correlation coefficient (ICC) in 24 healthy subjects. In addition, we applied the edges of each individual morphological network as features to discriminate the MCI and NC in the AD Neuroimaging Initiative (ADNI) dataset. The accuracy of classification was used to assess the effectiveness of our method.

MATERIALS AND METHODS

Participants

The first dataset used in this study consisted of 24 right-handed healthy subjects (12 men with ages ranging from 25 to 29 years with mean = 27.17 years, and standard deviation = 1.40; 12 women with ages ranging from 26 to 30 years with mean = 27.83 years, and standard deviation = 1.11). All subjects were native Chinese speakers who had grown up in China. All subjects provided written informed consent; in addition, the local ethics committee approved this study.

The subjects were scanned twice within a 3-month period. All of the MRI data were obtained using a SIEMENS Trio Tim 3.0T scanner with a 12-channel phased array head coil in the Imaging Center for Brain Research, Beijing Normal University. The brain structural images were acquired using T1-weighted, sagittal 3D magnetization prepared rapid gradient echo (MPRAGE) sequences. The sequence parameters had a repetition time (TR) = 2,530 ms, echo time (TE) = 3.39 ms, inversion time (TI) = 1,100 ms, flip angle = 7°, FOV = 256 * 256 mm, in-plane resolution = 256 * 256, slice thickness = 1.33 mm, and 144 sagittal slices covering the whole brain.

The second dataset used in this study was obtained from the ADNI database (adni.loni.usc.edu). The ADNI was launched in 2003 as a public-private partnership, led by Principal Investigator Michael W. Weiner, MD. The primary goal of ADNI has been to test whether serial MRI, positron emission tomography (PET), other biological markers, and clinical and neuropsychological assessment can be combined to measure the progression of MCI and early Alzheimer's disease (AD). This study was carried out in accordance with the recommendations of the ADNI database with written informed consent from all subjects. The protocol was approved by the ADNI coordinating committee.

The eligibility criteria for inclusion of subjects are described at http://adni.loni.usc.edu/wp-content/uploads/2010/09/ADNI_GeneralProceduresManual.pdf. General criteria for MCI were

as follows: (1) Mini-Mental-State-Examination (MMSE) scores between 24 and 30 (inclusive), (2) a memory complaint, objective memory loss measured by education adjusted scores on the Wechsler Memory Scale Logical Memory II, (3) a Clinical Dementia Rating (CDR) ≥ 0.5 , and (4) absence of significant levels of impairment in other cognitive domains, essentially preserved activities of daily living, and an absence of dementia.

Three hundred and thirty-nine subjects, which included 170 MCI patients and 169 NC subjects were analyzed in this study. Age, gender and education in the MCI group were matched with the NC group. All subjects received the baseline clinical/cognitive examinations including 1.5T structural MRI scan and were reevaluated at specified intervals (6 or 12 months). The baseline scans were used in our experiments. The 170 MCI subjects included two subcategories: 86 stable MCI (sMCI) and 84 progressive MCI (pMCI). Subjects who converted to AD within 24 months were classified as pMCI, and those not converting into AD within the same period were classified as sMCI. The 169 NC subjects were not converted to MCI or AD within 24 months. The demographic information and clinical characteristics of the participants involved in this study are shown in **Table 1**.

Image Processing

The same pre-processing pipeline was applied in the two datasets by using the FreeSurfer image analysis suite v4.3 (<http://surfer.nmr.mgh.harvard.edu/>). For the second dataset, the pre-processed images were downloaded from the public ADNI site. The pipeline for T1-weighted scans contained (1) registration to the Talairach space, (2) correction for intensity bias, (3) skull stripped from the intensity normalized image, (4) segmentation into white matter, gray matter or cerebrospinal fluid, (5) cutting planes to sphere the hemispheres and remove the cerebellum and brain stem, (6) generation of a single connected mass representing the white matter structure of each hemisphere, and (7) surface tessellation, refinement, and deformation for each hemisphere (Dale et al., 1999). A variety of morphological features such as volumetric (cortical thickness, surface area, and gray matter volume) and geometric (sulcal depth, metric distortion, and mean curvature) measures at each vertex on the pial surface were extracted after the preprocessing. Then, the surface data were resampled to a common subject (usually an average subject) and smoothed with a Gaussian filter (FWHM = 5 mm).

Construction of Individual Morphological Brain Network

A brain network is typically defined as $G = (V, E)$, where V denotes the set of nodes (or vertices) and E denotes the set of edges (or links). In this paper, we parceled the cortical cortex into 68 cortical ROIs based on the Desikan-Killiany Atlas (Desikan et al., 2006). Here, we assumed that nodes represent cortical regions and edges represent the similarity of two cortical regions. Each individual network shares the same set of 68 nodes, which facilitates the comparisons using the edges. Dissimilarity connectivity is measured by the formula below (Székelly and Rizzo, 2004). Let A and B denote the ROIs of the

TABLE 1 | Subject demographic and clinical characteristics.

| | MCI (<i>n</i> = 170) | sMCI (<i>n</i> = 86) | pMCI (<i>n</i> = 84) | Control (<i>n</i> = 169) |
|--------------|---------------------------------|---------------------------------|---------------------------------|-------------------------------------|
| Gender (M/F) | 104/66 | 53/33 | 51/33 | 88/81 |
| Age | 74.8 ± 6.7 | 74.6 ± 6.4 | 75.1 ± 7.2 | 75.7 ± 5.1 |
| Education | 15.7 ± 3.0 | 15.8 ± 3.1 | 15.7 ± 3.0 | 16.0 ± 2.7 |
| MMSE | 26.9 ± 1.7 | 27.4 ± 1.8 | 26.4 ± 1.7 | 29.1 ± 0.9 |
| CDR | 1.6 ± 0.8 | 1.5 ± 0.7 | 1.8 ± 1.0 | 0 ± 0.1 |

Age, education, MMSE and CDR are expressed as the mean ± SD. There were no significant differences between the MCI and the control group and between the sMCI and pMCI group in gender, age and education years. The MCI with control groups, and sMCI with pMCI group showed significant differences in the MMSE and CDR. MCI, mild cognitive impairment; sMCI, stable mild cognitive impairment; pMCI, progressive mild cognitive impairment; M/F, Male/Female; MMSE, Mini-Mental-State-Examination; CDR, Clinical Dementia Rating.

k th subject, and then the combined Euclidean distance $e_k(A, B)$ is defined as:

$$e_k(A, B) = \frac{n_1 n_2}{n_1 + n_2} \left(\frac{2}{n_1 n_2} \sum_{i=1}^{n_1} \sum_{j=1}^{n_2} \|a_i - b_j\|_2 - \frac{1}{n_1^2} \sum_{i=1}^{n_1} \sum_{j=1}^{n_1} \|a_i - a_j\|_2 - \frac{1}{n_2^2} \sum_{i=1}^{n_2} \sum_{j=1}^{n_2} \|b_i - b_j\|_2 \right) \tag{1}$$

Let $A = \{a_1, \dots, a_{n_1}\}$ and $B = \{b_1, \dots, b_{n_2}\}$, where a and b denote vertices in A and B , respectively. These elements represent morphological features, which could be either one-dimensional or multi-dimensional. n_1 and n_2 are the numbers of vertices in A and B . Euclidean distance is computed by the 2-norm ($\|\cdot\|_2$).

The first part of the formula $\frac{2}{n_1 n_2} \sum_{i=1}^{n_1} \sum_{j=1}^{n_2} \|a_i - b_j\|_2$ describes the Euclidean distance for any pair of vertices between A and B . $\frac{1}{n_1^2} \sum_{i=1}^{n_1} \sum_{j=1}^{n_1} \|a_i - a_j\|_2$ and $\frac{1}{n_2^2} \sum_{i=1}^{n_2} \sum_{j=1}^{n_2} \|b_i - b_j\|_2$ are the Euclidean distances for any pair of vertices within A and B , respectively.

A smaller intra-regional Euclidean distance indicating uniform morphological feature distribution within ROI results in a distance $e(A, B)$ is more dependent on the Euclidean distance between pairs of vertices in A and B . Moreover, the distance $e(A, B)$ will be influenced if the morphological feature distribution within the ROI is unequal. When A and B have the same morphological feature distribution, the combined Euclidean distance $e(A, B) = 0$.

After calculation of the combined Euclidean distance matrix that reflected the dissimilarity between brain regions, Min-Max normalization was proposed to minimize possible bias in different ranges of different subjects. We chose the Min-Max normalization because of its boundness and direct reflection of the dissimilarity. The Min-Max normalization between regions A and B of the k th subject is computed as:

$$e_{k-n}(A, B) = \frac{e_k(A, B) - e_{k_min}}{e_{k_max} - e_{k_min}} \tag{2}$$

where e_{k_min} and e_{k_max} are the minimum and maximal value in the dissimilarity connectivity of the k th subject, respectively. The value of $e_{k_n}(A, B)$ can be converted to a similarity measurement using the following equation:

$$c_k(A, B) = \exp(-e_{k_n}(A, B)) \tag{3}$$

Based on the above calculation, a 68*68 diagonal symmetry correlation matrix of each subject was obtained. The $c_k(A, B)$ ranges from 0 to 1, and 1 represents that the two morphological feature distributions are identical.

Method Validation

We validated the above method by computing the topological properties of the individual brain network, i.e., small-world, hubs and intraclass correlation coefficient (ICC) in the first dataset. In addition, we applied the edges of each individual morphological network as features to discriminate the MCI and NC in the ADNI dataset. The accuracy of classification was used to assess the effectiveness of our method.

Topological Properties of Networks

We constructed the individual morphological brain network based on the proposed method in a six-dimension situation in the first dataset. The small-world configurations, hubs and reproducibility of individual brain network were calculated and analyzed. The network properties were computed using the Graph-theoretical Network Analysis (GRETNA) toolkit (Wang et al., 2015).

For small-world configurations, the clustering coefficient (C_p), minimum path length (L_p), γ , λ and σ were calculated. Small-worldness (Watts and Strogatz, 1998; Humphries et al., 2006) can be demonstrated mathematically as:

$$\gamma = \frac{C_p}{C_p^{random}} > 1, \lambda = \frac{L_p}{L_p^{random}} \approx 1 \text{ and } \sigma = \frac{\gamma}{\lambda} > 1$$

where *random* represents a random network that consists of the same number of nodes and edges.

The betweenness centrality (BC) is defined as the number of shortest paths between any two nodes running through the given node (Freeman, 1977) and measures the nodal ability of information flow throughout the network. The hubs were defined as the nodes that achieved a higher BC than the sum of the mean and standard deviation for the entire network.

The intraclass correlation coefficient (ICC) was used to estimate the reproducibility of the topological properties of the network (Shrout and Fleiss, 1979). ICC was defined as the fraction of the variance of the chosen graphic property between subjects to the total variance, which is the summation variance of between and within subjects of that property:

$$ICC = \frac{\sigma_{between}^2}{\sigma_{between}^2 + \sigma_{within}^2} \tag{4}$$

If the measurements of repeated scans are consistent for each subject, the ICC would be close to one. An ICC value above 0.75 is considered excellent, and one ranging from 0.59 to 0.75 is considered good (Cicchetti and Sparrow, 1981).

Classification Between MCI and NC Groups

For the second dataset, we used the support vector machine (SVM) classifiers with leave-one-out cross validation (LOOCV) to test the effectiveness of our method. Additionally, feature selection is employed for each individual morphological brain network before classification regarding the curse of dimensionality.

Feature selection

Each network has $p = V \times (V - 1)/2 = 2278$ edges. Due to the high dimensionality of the network features and a small number of samples, also namely, the curse of dimensionality, the classification model often confronts problems such as overfitting and under generalization. Feature selection is considered to reduce the irrelevant or redundant features and improve the performance of classifiers. The least absolute shrinkage and selection operator (Lasso) (Tibshirani, 1996) was applied for feature selection.

Specifically, Lasso was put forward by Tibshirani (1996) for parameter estimation and feature selection in regression analysis. The Lasso algorithm does not focus on selection of subsets but rather on defining a continuous shrinking operation that can produce coefficients of redundant components to zero. It has been shown in the literature (Yamada et al., 2012; Kamkar et al., 2015) that the algorithm can effectively select the relevant features in high dimensional data space. Sparse linear regression is applied for Lasso features calculation with L_1 -norm regularization. In the training set, let matrix $X = [x_1, x_2, \dots, x_n]^T \in \mathbb{R}^{n \times m}$ represent m features of n subjects, $y = [y_1, y_2, \dots, y_n]^T \in \mathbb{R}^{n \times 1}$ be an n dimension corresponding to sample labels ($y_i = 1$ for MCI and $y_i = -1$ for NC) and m denotes the number of edges except the duplicated part in the individual brain network. The linear regression model is defined as follows:

$$\hat{y} = Xw \tag{5}$$

where $w = [w_1, w_2, \dots, w_n]^T \in \mathbb{R}^{n \times 1}$ denotes the regression coefficient vector and \hat{y} denotes the predicted label vector. The objective function is minimized as follows to estimate w :

$$\min_w \frac{1}{2} \|Xw - y\|_2^2 + \lambda \|w\|_1 \tag{6}$$

where $\lambda > 0$ is a regularization parameter in control of the sparsity of the model, i.e., many entries of w are zeros. $\|w\|_1$ is the L_1 -norm of w defined as $\sum_{i=1}^n |w_i|$. The SLEP package (Liu et al., 2009) was used for solving sparse linear regression. If an edge is selected as a feature in each iteration of the LOOCV classification, the edge is considered as discriminative in the brain network.

Classification

According to the selected features described above, a commonly used classifier SVM was implemented using the LIBSVM library (Chang and Lin, 2011) in MATLAB, with a radial basis function (RBF) kernel and an optimal value for the penalized coefficient C (a constant determining the tradeoff between training error and model flatness). The RBF kernel was utilized for its good

performance especially on small sample problems (Hertz et al., 2006) and defined as follows:

$$K(x_1, x_2) = \exp\left(-\frac{\|x_1 - x_2\|^2}{2\sigma^2}\right) \quad (7)$$

where x_1 and x_2 are two feature vectors and σ is the width of the Gaussian kernel. To obtain the optimal SVM model, we selected the optimal hyperparameters (C and σ) through a grid-search. Specifically, the classification was performed via a LOOCV in which one subject was selected as the testing set and the rest were used as the training set. The parameters were changed after all samples were classified to estimate the LOOCV accuracy. In the end, the average accuracy across all subjects was computed as a performance measurement. The hyperparameter values that lead to the highest performance are then selected. The pipeline of our classification framework for MCI and NC is presented in **Figure 1**. The pipeline of classification framework for sMCI and pMCI is same as the classification framework for MCI and NC.

RESULTS

Small-World Configurations

As shown in **Figure 2**, γ is larger than one (max = 1.86, min = 1.25) throughout the whole sparsity range, while λ is close to one (max = 1.15, min = 1.02) by our method. Hence, the individual morphological brain networks exhibit a higher C_p than the random network, while maintaining a similar L_p . As expected, σ was found to be larger than one (max = 1.62, min = 1.23) throughout the entire sparsity range. The results showed the existence of small world property in the constructed individual morphological brain network by using six features. Moreover, as the sparsity increased, the increase of C_p and decrease of L_p , λ , σ , and γ in **Figure 2** are in accordance with the variation tendency of previous reports (Kong et al., 2015; Li et al., 2017).

Furthermore, the sparsity of 23% is highlighted for convenient comparison with previous studies (Tijms et al., 2012; Kong et al., 2015). As listed in **Table 2**, our results are similar to previous individual-based morphological brain network studies, whereas the population-based morphological brain networks and functional networks exhibit smaller results than our method in most small world configurations.

Hubs

Hubs were investigated for all subjects and sparsities. A total of four hub regions were identified throughout the entire sparsity range across all subjects, including the left and right frontal pole, right rostral anterior cingulate and right transverse temporal cortex.

Reproducibility

The reproducibility of our method was evaluated by measuring the ICCs of network properties for scans with acquisitions of two different time points in the same subjects. The ICC was investigated throughout the entire sparsity range. The C_p , L_p , and BC were examined in this study.

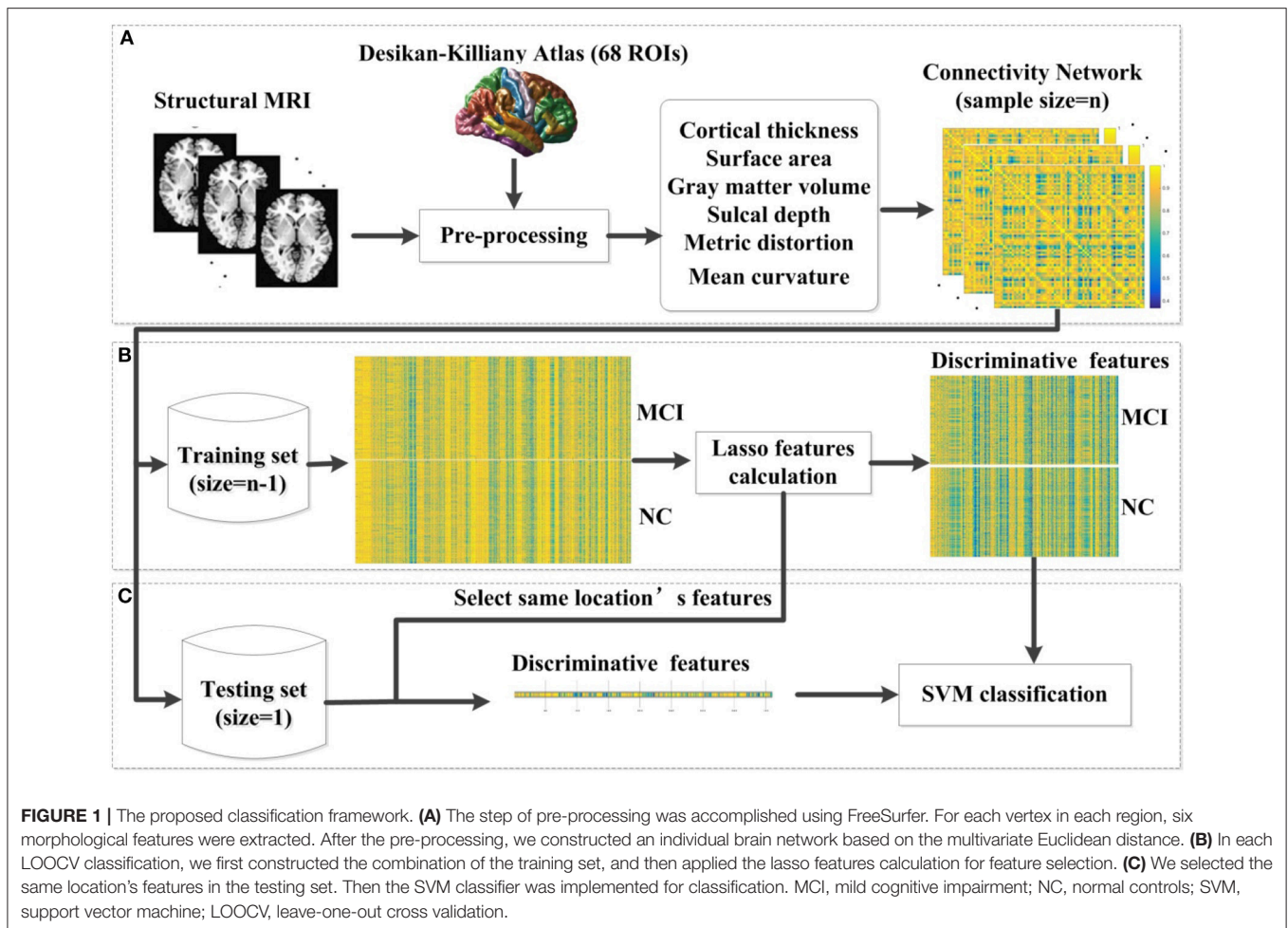
The results indicated that C_p is highly reproducible (minimum ICC = 0.72, average ICC = 0.83), as shown in **Figure 3A**. Moreover, the reproducibility of L_p (minimum ICC = 0.62, average ICC = 0.82) and BC (minimum ICC = 0.82, average ICC = 0.87) are shown in **Figures 3B,C**. Most results of ICC were significant, except for L_p at sparsity of 20, 21, and 22% ($p = 0.098, 0.13$ and 0.10 , separately). The reliability of our method performed well in accordance with previous studies (Cicchetti and Sparrow, 1981; Li et al., 2017). For example, the reproducibility of C_p and L_p are similar to Li's results (minimum C_p ICC = 0.71, average C_p ICC = 0.83; minimum L_p ICC = 0.63, average L_p ICC = 0.81) and the reproducibility of BC was better than Li's result (minimum BC ICC = 0.629, average BC ICC = 0.78).

Classification Performance

In this subsection, we made a comparison of classification accuracies between our method and other methods as reported in previous studies, which included Kong's method (Kong et al., 2014), Kim's method (Kim et al., 2016), Zheng's method (Zheng et al., 2015), Dai's method (Dai et al., 2013), and Wee's method (Wee et al., 2013). The details of these methods are described in **Table 3**.

Like other papers, we selected cortical thickness as the single dimension feature to construct individual brain network. All methods employed an identical feature selection method after the constructions of each individual brain network and optimization of the parameters in SVM. The accuracy, sensitivity, specificity and area under receiver operating characteristic (ROC) curve (AUC) values of each method were calculated as evaluation metrics for the performance. The results are summarized in **Tables 4, 5**. It can be clearly observed that our method performed well compared with previous methods in the classification task. In particular, our method achieved an accuracy of 79.65% in distinguishing MCI patients from NC with a sensitivity of 78.82% and achieved an accuracy of 70.59% in distinguishing sMCI from pMCI with a sensitivity of 75.58%.

Although accuracy is commonly used for an evaluation of classification, it may provide a biased description due to its dependency on the decision threshold selection in SVM. The ROC curve is shown to be a simple but completely empirical description of this decision threshold effect, indicating all possible combinations of the relative frequencies of the various kinds of correct and incorrect decisions. In ROC space, the (0, 1) point represents a perfect classifier (all samples are correctly predicted). Thus, the nearer a point is to the (0, 1) point (closer to the upper left corner), the better a classifier is (Prati et al., 2011). **Figures 4, 5** show the ROC graphs of classification using different methods to construct individual brain networks, from which we can see that the ROC curve of our method is closer to the upper left corner than some conventional methods. In addition, a single measure of classification performance can be derived from the area under the ROC curve (AUC). A larger AUC indicates a better classifier. In **Tables 4, 5** the AUC for all methods are listed and it can be seen that our method achieved AUC scores of 0.84 for MCI vs. NC, and 0.73 for sMCI vs. pMCI, while most other methods slightly underperformed.



Comparison of Our Method Using One Dimension and Six Dimensions in Classification

In this experiment, we compared the performance of the proposed method by using one dimension and six dimensions. We used cortical thickness as the single dimension and used cortical thickness, surface areas, gray matter volume, sulcal depth, metric distortion and mean curvature as the six dimensions. **Tables 4,5** show that our method of applying six dimensions outperforms the one only using a single cortical thickness feature, which achieved 80.53% and 77.06% for accuracy in distinguishing MCI from NC and distinguishing sMCI from pMCI, respectively. The ROC graphs in **Figures 6,7** illustrate the classification performance based on brain networks that were constructed using one dimension and six dimensions. We also list the AUC score in **Tables 4,5**. It can be noticed that compared with the univariate situation, individual brain network construction based on multivariate performs better in classification with an AUC score of 0.86 and 0.74, respectively.

Most Discriminative Features of Individual Brain Networks

The most discriminative features demonstrate the edges selected in each time of cross-validation for classification based on multivariate connectivity. Here, we selected the most discriminative features under the best condition. In **Figure 8**, the blocks of the circle represent ROIs. As shown in **Figures 8A,B** the most discriminative edges connected most ROIs in the brain.

Based on the selected edges, pairs of regions that contribute to classification are not only within the same hemisphere and the same lobe but also across different hemispheres and lobes, which indicates the abnormalities caused by MCI involve the entire brain rather than certain areas. The number of discriminative edges that connect the two hemispheres was 115. Conversely, the number of discriminative edges that are the connections within a single hemisphere was relatively low, with quantities of 64 and 43 for the left and right hemisphere, respectively. We correlated the most discriminative edges with MMSE and CDR scores. In **Figures 8C,D**, the selected edges that were significant correlated ($p < 0.05$) with MMSE and CDR are shown. As seen, these edges

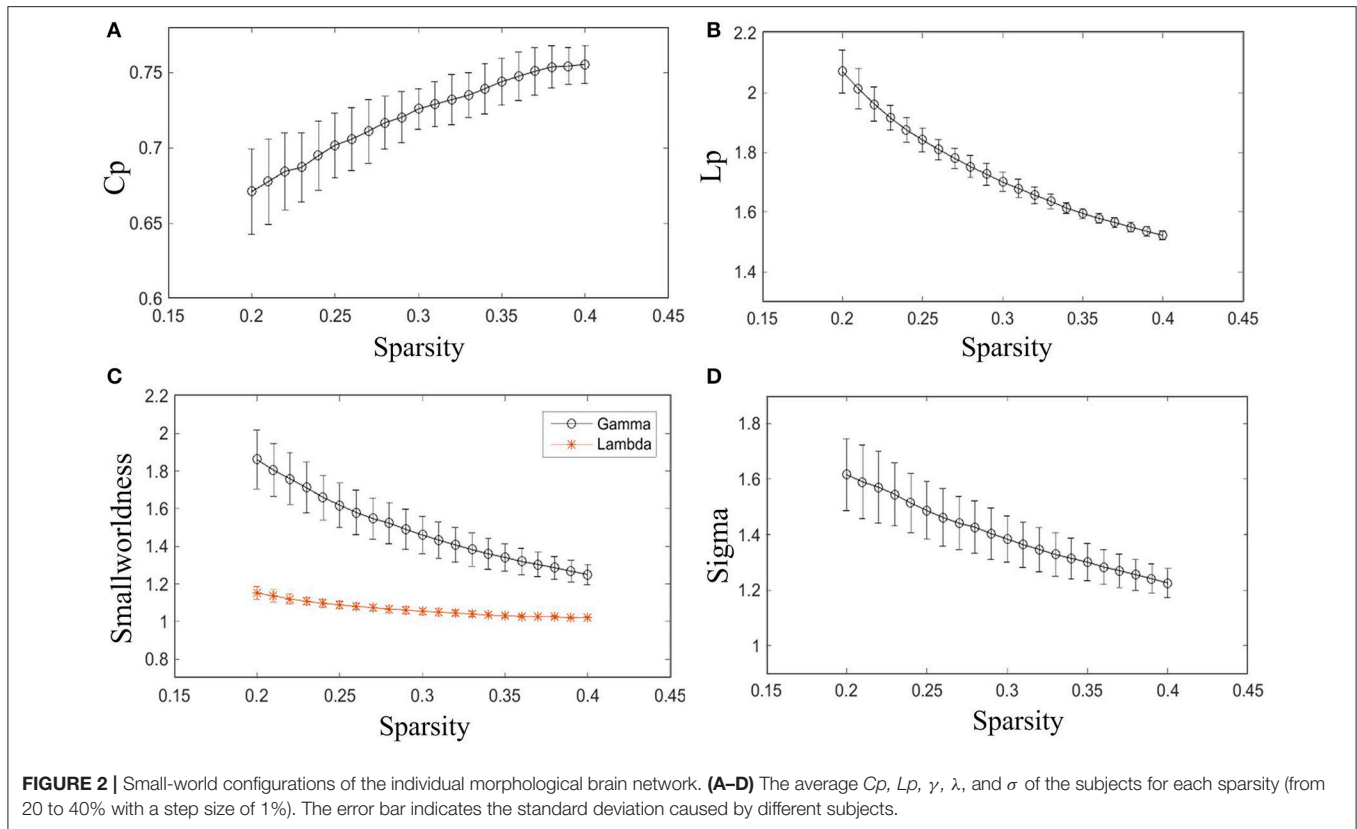


TABLE 2 | Comparison of small world configurations between the present study and previous studies.

| Method | N | C_p | L_p | γ | λ | σ | S (%) |
|-----------------------------------------------------|--------|-------|-------|----------|-----------|----------|---------|
| INDIVIDUAL-BASED MORPHOLOGICAL BRAIN NETWORK | | | | | | | |
| Our method | 68 | 0.69 | 1.92 | 1.71 | 1.10 | 1.54 | 23 |
| Li's method (Li et al., 2017) | 68 | 0.62 | 2.23 | 1.81 | 1.22 | 1.52 | 23 |
| Kong's method (Kong et al., 2015) | 90 | 0.66 | 1.92 | 1.74 | 1.15 | 1.50 | 23 |
| Tijms's method (Tijms et al., 2012) | 6,982 | 0.53 | 1.86 | 1.35 | 1.05 | 1.28 | 23 |
| POPULATION-BASED MORPHOLOGICAL BRAIN NETWORK | | | | | | | |
| He's method (He et al., 2007) | 54 | ≈0.3 | ≈1.6 | ≈1.35 | ≈1 | ≈1.35 | 23 |
| Yao's method (Yao et al., 2010) | 90 | ≈0.49 | ≈1.89 | ≈1.62 | ≈1.1 | ≈1.47 | 23 |
| Zhu's method (Zhu et al., 2012) | 90 | ≈0.26 | NR | ≈1.20 | ≈1.03 | ≈1.17 | 23 |
| FUNCTIONAL BRAIN NETWORK | | | | | | | |
| Van's method (Van Essen, 1997) | 10,000 | ≈0.52 | ≈1.75 | ≈1.9 | ≈1.03 | ≈1.85 | 20 |
| Zhang's method (Zhang et al., 2011) | 90 | ≈0.33 | ≈1.65 | ≈1.3 | ≈1 | ≈1.4 | 23 |

N , C_p , and L_p denote the number of nodes in the networks, the average clustering coefficient and the average shortest path length, respectively. γ represents the ratio of the clustering coefficient of the network over that of the random network. λ represents the ratio of the average shortest path length of the network over that of the random network. σ indicates the small-worldness. The small world attributes of previous studies are inferred (with ≈). NR, not reported.

are predominately in the frontal, temporal, parietal, and insula parts.

DISCUSSION

In the present study, we introduced a new method to construct individual morphological brain network. The combination of inter-regional Euclidean distance and intra-regional Euclidean

distance was used to quantify the inter-regional relations. Through the small-world configurations analysis, our method confirmed the existence of small world property. In addition, as listed in **Table 2**, the population-based morphological brain networks and functional networks exhibit smaller results than our results in most small world configurations, which may suggest that the individual morphological brain networks demonstrate a stronger integration and segregation because

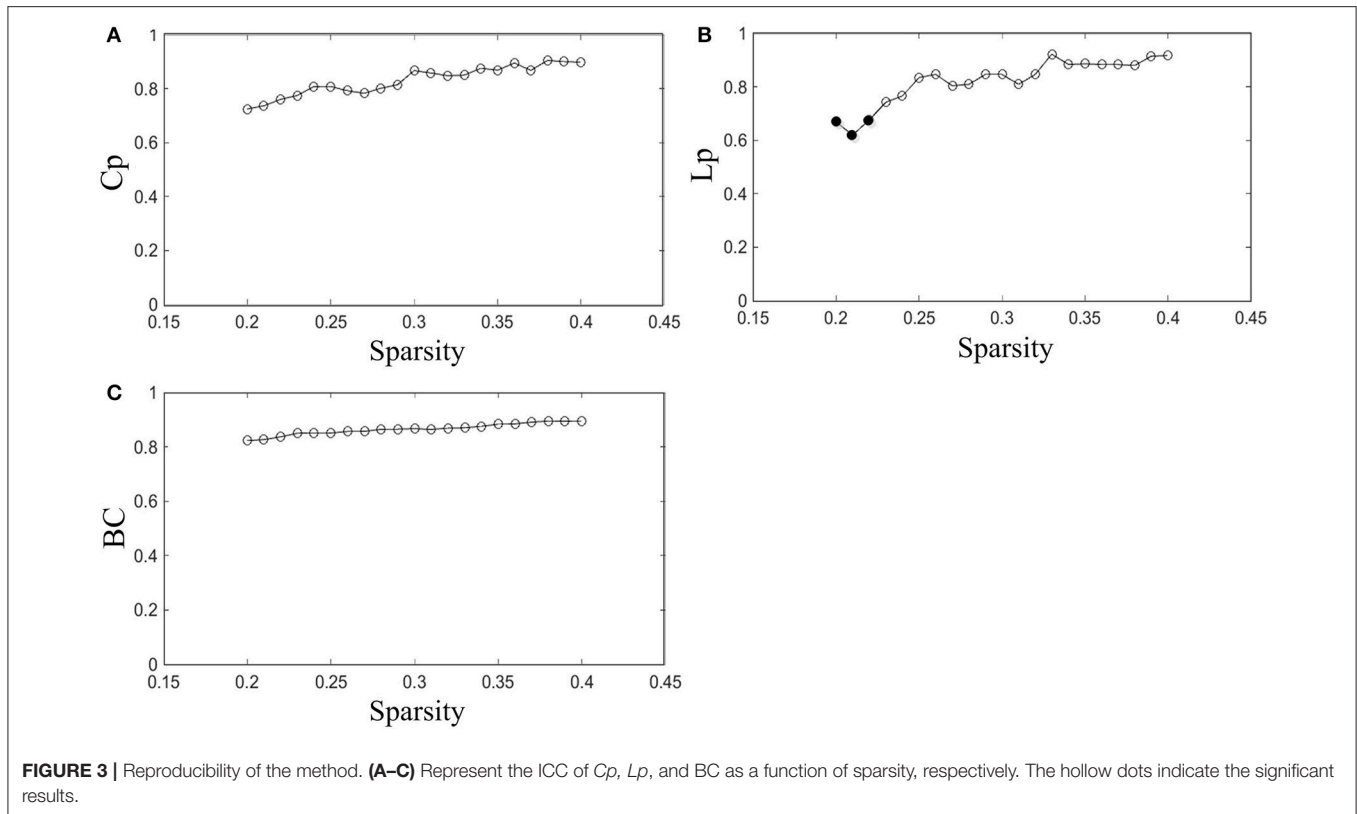


FIGURE 3 | Reproducibility of the method. (A–C) Represent the ICC of C_p , L_p , and BC as a function of sparsity, respectively. The hollow dots indicate the significant results.

TABLE 3 | The methods of constructing individual morphological brain networks in previous studies.

| Author | Methods | Explanation |
|----------------------------|-----------------------------------------------------------------------------------------------------------------------------------------------|------------------------------------------------------------------------------------------------------------------------------------------------------------------------------------------------------------|
| Kong (Kong et al., 2014) | $KL(i, j) = \int_x (i(x) \log(\frac{i(x)}{j(x)}) + j(x) \log(\frac{j(x)}{i(x)}))$, $c(i, j) = e^{-KL(i, j)}$ | $i(x)$ and $j(x)$ denote the probability density functions (PDF) of i and j respectively. |
| Kim (Kim et al., 2016) | $Z(i, j) = \frac{T(i) - T(j)}{\sigma_j}$, $c(i, j) = \frac{Z(i, j) + Z(j, i)}{2}$ | $T(i)$ and $T(j)$ denote the mean value of cortical thickness in i and j respectively, σ_i and σ_j denote the standard deviation of regional cortical thickness of regions i and j . |
| Wee (Wee et al., 2013) | $d(i, j) = [T(i) - T(j)]^2$, $\sigma = \sqrt{\sigma_i + \sigma_j}$, $c(i, j) = \exp(-\frac{d(i, j)}{2\sigma^2})$ | η is an input parameter. |
| Dai (Dai et al., 2013) | $d(i, j) = [T(i) - T(j)]^2$, $c(i, j) = \exp(-\frac{d(i, j)}{\eta})$ | |
| Zheng (Zheng et al., 2015) | $C_{precision}(i, j) = \frac{1}{m} \sum_{p=1}^m t_i^p - T(i) \frac{1}{n} \sum_{q=1}^n t_j^q - T(j) $, $C_{rough}(i, j) = T(i) - T(j) ^2$ | t denotes the vertex's cortical thickness, m and n are the number of points in i and j , respectively. |

In these formulas, i and j denote two brain regions; $c(i, j)$ denotes the correlation between i and j .

the inter-individual variability is highly reserved (Kanai and Rees, 2011). Hubs such as left and right frontal pole and right rostral anterior cingulate have been reported in previous studies (Hagmann et al., 2008; Van den Heuvel and Sporns, 2013). The ICC was used to estimate the reproducibility of graph theoretical measures. The results indicated that the reliability of our method performed well in accordance with previous studies. In addition, compared with other conventional methods, which average the vertices within ROIs, our method improves the classification performance in univariate situation. Here, we explained the rationality of our method from two aspects. (1) In previous

studies, the individual morphological brain networks were mostly constructed based on the average value of morphological features within the ROI. However, the abnormal region for pathology might be only a fraction of the defined ROI and the abnormal change of brain region may be ignored by taking the average, which potentially reduces the discriminative power. In our proposed method, we directly used the morphological features of vertices to retain more detailed information. The results of Kong's method (Kong et al., 2014) and Zheng's method (Zheng et al., 2015) in **Table 4** also demonstrated the importance of detailed information. (2) In previous studies, the

TABLE 4 | Classification performance of different methods to distinguish MCI and NC.

| Method | Accuracy (%) | Sensitivity (%) | Specificity (%) | AUC |
|----------------------------------------|--------------|-----------------|-----------------|-------------|
| Our method using six dimensions | 80.53 | 79.41 | 81.66 | 0.86 |
| Our method using one dimension | 79.65 | 78.82 | 80.47 | 0.84 |
| Kong's Method | 77.88 | 74.12 | 81.66 | 0.84 |
| Kim's Method | 75.81 | 71.18 | 80.47 | 0.79 |
| Dai's Method | 76.70 | 73.53 | 79.88 | 0.82 |
| Zheng's Method | 79.94 | 76.47 | 83.43 | 0.84 |
| Wee's Method | 77.29 | 73.53 | 81.07 | 0.83 |

One dimension denotes cortical thickness; six dimensions include cortical thickness, surface areas, gray matter volume, sulcal depth, metric distortion, and mean curvature. The lower bold values mean the best performance (accuracy, sensitivity, specificity and AUC) among different methods in one dimension situation. The upper bold values mean the best performance of our method in one and six dimension. AUC, area under the curve.

TABLE 5 | Classification performance of different methods to distinguish sMCI and pMCI.

| Method | Accuracy (%) | Sensitivity (%) | Specificity (%) | AUC |
|----------------------------------------|--------------|-----------------|-----------------|-------------|
| Our method using six dimensions | 77.06 | 77.91 | 76.19 | 0.74 |
| Our method using one dimension | 70.59 | 75.58 | 65.48 | 0.73 |
| Kong's Method | 65.89 | 67.44 | 64.29 | 0.67 |
| Kim's Method | 67.06 | 63.95 | 70.24 | 0.65 |
| Dai's Method | 63.53 | 70.93 | 55.95 | 0.64 |
| Zheng's Method | 67.65 | 63.95 | 71.43 | 0.68 |
| Wee's Method | 65.89 | 67.44 | 64.29 | 0.69 |

One dimension denotes cortical thickness; six dimensions include cortical thickness, surface areas, gray matter volume, sulcal depth, metric distortion, and mean curvature. The lower bold values mean the best performance (accuracy, sensitivity, specificity and AUC) among different methods in one dimension situation. The upper bold values mean the best performance of our method in one and six dimension. AUC, area under curve.

morphological distribution within an ROI was not considered, which may influence the strength of edges between ROIs. In our method, the dissimilarity connectivity was the combination of inter-regional Euclidean distance and intra-regional Euclidean distance, while previous methods only considered the relation between two ROIs.

An inherent advantage of our method is that it can be applied to multi-dimensional situations. In previous studies, researchers have found the small-world properties were disrupted for brain networks that were constructed based on cortical thickness in MCI patients (Zhou and Lui, 2013), and the brain network based on the surface area can reveal topological properties of the networks resulting from the concurrent changes between different anatomical regions (Sanabriadiaz et al., 2010). The sulcal depth, curvature, and metric distortion related to cortical folding vary and could be more suitable descriptors for finding the anatomical-axonal and morphological connectivity correlation

(Van Essen, 1997). Previous studies have reported that brain networks based on both the volumetric measures and geometric measures showed significant differences in graphical properties between aMCI and NC (Li et al., 2016). These results may suggest that brain network construction based on multiple features is beneficial to the diagnosis and analysis of neurological diseases. However, most previous approaches (Dai et al., 2013; Wee et al., 2013; Kong et al., 2014; Zheng et al., 2015; Kim et al., 2016) that constructed individual brain networks only considered one morphological feature (e.g., cortical thickness or gray matter volume) between two brain regions. The first paper involved in building morphological brain networks based on multiple morphological features demonstrated that multiple morphometric features can be applied to form a rational reproducible individual-based morphological brain network (Li et al., 2017), but it averaged the morphological features within each ROI, such as the mean cortical thickness, which may neglect some detailed information. In our method, every vertex's different kinds of cortical features within each ROI were considered and the relations between brain regions were determined based on these features. In this paper, the multiple morphological features including cortical thickness, surface areas, gray matter volume, sulcal depth, metric distortion and mean curvature as well as the cortical thickness as a single feature were used for individual brain network construction. The results show (Tables 4,5) that the brain network constructed from the combination of morphological features outperforms the one only considering cortical thickness. The resulting high AUC value proves the excellent classification power and generalizability of our proposed method on an unseen data set, as well as the ability to construct an accurate and credible individual morphological brain network. Moreover, the classification performance of our method in a multivariate situation revealed the existence of useful information within these morphological features. The abnormal connectivity across various regions can be located within different morphological features, which greatly benefits the detection of neurological diseases.

An interesting finding shown in Figures 8A,B is that the majority of the selected correlative features in the MCI and NC classification task are the edges connecting the left and right hemisphere. This might suggest that the most significant differences between MCI subjects and health subjects are changes in the connections between the left and the right hemisphere. The connection alterations caused by MCI pathological attacks are not restricted to certain brain areas but are widely spread over the whole brain. What's more, the most discriminative edges connecting the regions in our study are consistent with previous publications, such as the lingual gyrus, postcentral gyrus, middle temporal gyrus, pars opercularis, and superior frontal sulcus (Li et al., 2014; Wei et al., 2016). Previous studies have found that subjects with MCI have abnormal network patterns in the lingual gyrus and middle temporal gyrus (Yao et al., 2010). He et al. (2008) demonstrated an abnormal correlation between the bilateral postcentral gyrus in AD. From Figures 8C,D we can see the selected edges are predominately connected to the regions of the frontal, temporal,

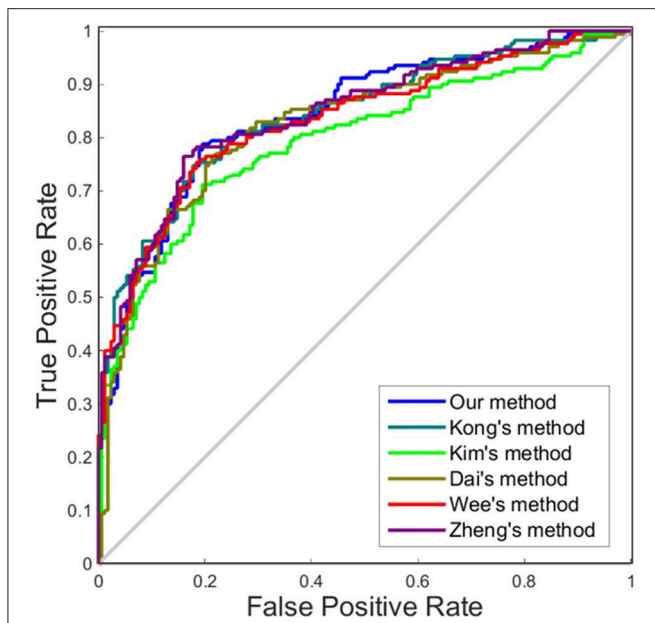


FIGURE 4 | ROC curves of different methods using one dimension to distinguish MCI and NC. The different line colors represent different methods to construct individual morphological brain networks based on cortical thickness. ROC, receiver operating characteristic.

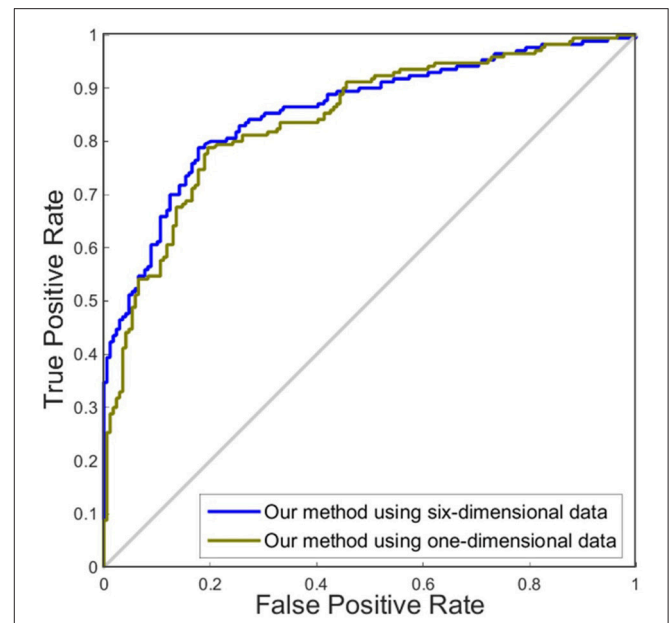


FIGURE 6 | ROC curves of our method using different dimensions of original features to distinguish MCI and NC. The different line colors represent ROC curves of our methods of constructing individual morphological brain networks based on different dimensional features. ROC, receiver operating characteristic.

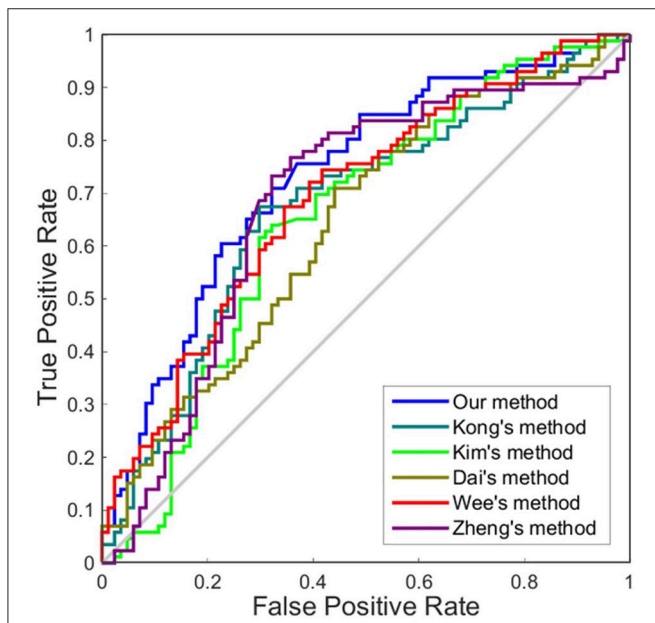


FIGURE 5 | ROC curves of different methods using one dimension to distinguish sMCI and pMCI. The different line colors represent different methods to construct individual morphological brain networks based on cortical thickness. ROC, receiver operating characteristic.

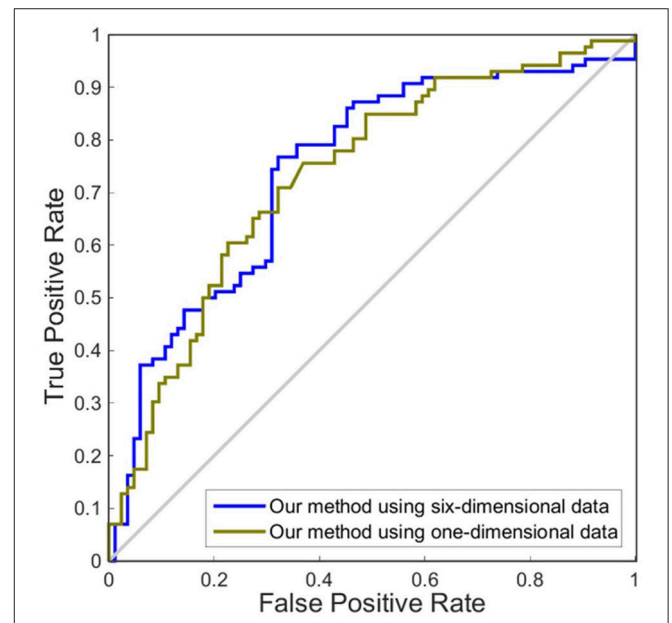


FIGURE 7 | ROC curves of our method using different dimensions of original features to distinguish sMCI and pMCI. The different line colors represent ROC curves of our method of constructing individual morphological brain networks based on different dimensional features. ROC, receiver operating characteristic.

parietal, and insula parts. These regions have been reported that retain more hubs which are considered to be the substrates of human cognition and consciousness (Yao et al., 2010). In

addition, some regions are associated with changes in different morphological features in MCI subjects, such as the middle frontal gyrus with cortical thickness, the postcentral gyrus with

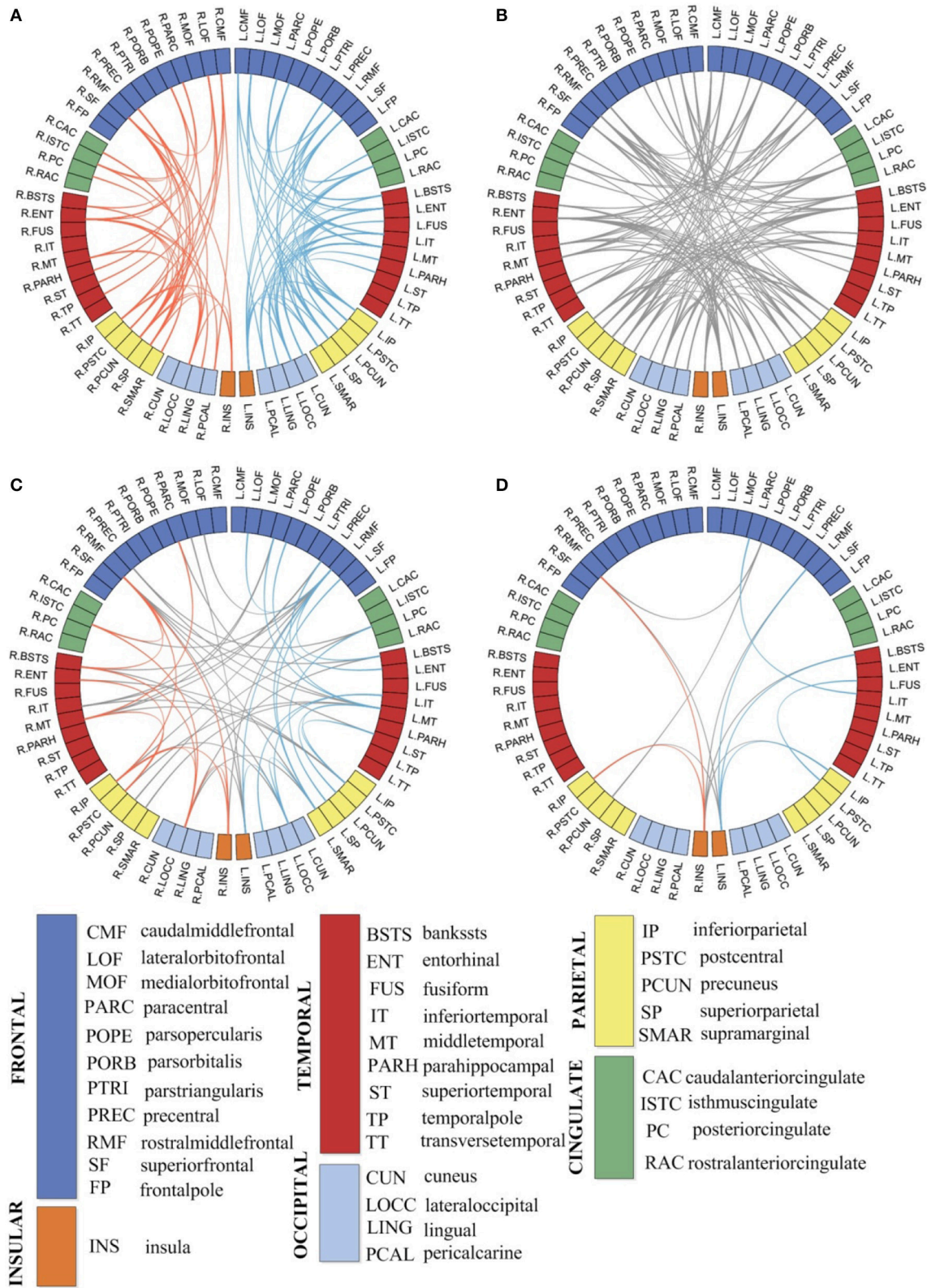


FIGURE 8 | The most discriminative edges of individual morphological brain networks in classification (A,B) and the significant correlation of the most discriminative edges with MMSE (C) and CDR (D) scores. L, left hemisphere; R, right hemisphere; the different colors of the blocks represent ROIs in different areas of the cortical surface. The blue lines represent the discriminative edges in the left hemisphere; the red lines represent the discriminative edges in the right hemisphere. The gray lines represent the discriminative edges between the left and right hemisphere.

metric distortion, the pars opercularis with mean curvature, the lingual gyrus with surface area, and the superior frontal sulcus with sulcal depth (Li et al., 2014). In conclusion, our results suggest that changes in the cortical regions may be associated with mechanisms underlying the conversion of MCI to AD, and the changes were displayed in multiple morphological features. These findings illustrate the potential application of our proposed method.

There are still some limitations in this study. First, the selection of the brain atlas could affect the organization of the individual brain network (Wang et al., 2016). In the future, it is important to validate our proposed method in different atlases. Second, in the current study, we combined multiple morphological features to construct the individual network, and we validated the effectiveness of our method. However, it is noticeable that the physiological explanation of this network is difficult. Third, a recent study (Seidlitz et al., 2017) proposed an individual brain network method by estimating the inter-regional correlation based on multiple macro- and micro-structural multimodal MR variables. And this network could capture cellular, molecular and functional features of the brain and even predict inter-individual differences in cognition. In future, it would be interesting to employ multiple morphometric parameters measured using multimodal MRI. Last, each feature type had its distinct contribution when discriminating between two groups. In the future, we may first select the most discriminant features and then construct the individual network, which could improve its classification performance.

AUTHOR CONTRIBUTIONS

KY, XW, and SL designed the experiments. XL assembled the data. KY performed the experiments and prepared the manuscript. XW, QL, and XZ helped in manuscript writing. SL

was in charge of manuscript verification. All authors reviewed the manuscript.

ACKNOWLEDGMENTS

This work was supported by the National Natural Science Foundation of China (Grant No. 81471731, 81622025).

Data collection and sharing for this project was funded by the Alzheimer's Disease Neuroimaging Initiative (ADNI) (National Institutes of Health Grant U01 AG024904) and DOD ADNI (Department of Defense award number W81XWH-12-2-0012). ADNI is funded by the National Institute on Aging, the National Institute of Biomedical Imaging and Bioengineering, and through generous contributions from the following: AbbVie, Alzheimer's Association; Alzheimer's Drug Discovery Foundation; Araclon Biotech; BioClinica, Inc.; Biogen; Bristol-Myers Squibb Company; CereSpir, Inc.; Eisai Inc.; Elan Pharmaceuticals, Inc.; Eli Lilly and Company; EuroImmun; F.Hoffmann-La Roche Ltd. and its affiliated company Genentech, Inc.; Fujirebio; GE Healthcare; IXICO Ltd.; Janssen Alzheimer Immunotherapy Research & Development, LLC.; Johnson & Johnson Pharmaceutical Research & Development LLC.; Lumosity; Lundbeck; Merck & Co., Inc.; Meso Scale Diagnostics, LLC.; NeuroRx Research; Neurotrack Technologies; Novartis Pharmaceuticals Corporation; Pfizer Inc.; Piramal Imaging; Servier; Takeda Pharmaceutical Company; and Transition Therapeutics. The Canadian Institutes of Health Research is providing funds to support ADNI clinical sites in Canada. Private sector contributions are facilitated by the Foundation for the National Institutes of Health (www.fnih.org). The grantee organization is the Northern California Institute for Research and Education, and the study is coordinated by the Alzheimer's Disease Cooperative Study at the University of California, San Diego. ADNI data are disseminated by the Laboratory for NeuroImaging at the University of Southern California.

REFERENCES

- Bassett, D. S., Bullmore, E., Verchinski, B. A., Mattay, V. S., Weinberger, D. R., and Meyer-lindenberg, A. (2008). Hierarchical organization of human cortical networks in health and schizophrenia. *J. Neurosci.* 28, 9239–9248. doi: 10.1523/JNEUROSCI.1929-08.2008
- Bernhardt, B. C., Rozen, D. A., Worsley, K. J., Evans, A. C., Bernasconi, N., and Bernasconi, A. (2009). Thalamo-cortical network pathology in idiopathic generalized epilepsy: insights from MRI-based morphometric correlation analysis. *Neuroimage* 46, 373–381. doi: 10.1016/j.neuroimage.2009.01.055
- Bernhardt, B. C., Worsley, K. J., Besson, P., Concha, L., Lerch, J. P., Evans, A. C., et al. (2008). Mapping limbic network organization in temporal lobe epilepsy using morphometric correlations: insights on the relation between mesiotemporal connectivity and cortical atrophy. *Neuroimage* 42, 515–524. doi: 10.1016/j.neuroimage.2008.04.261
- Cachia, A., Mangin, J. F., Rivière, D., Kherif, F., Boddart, N., Andrade, A., et al. (2003). A primal sketch of the cortex mean curvature: a morphogenesis based approach to study the variability of the folding patterns. *IEEE Trans. Med. Imaging* 22, 754–765. doi: 10.1109/TMI.2003.814781
- Chang, C. C., and Lin, C. J. (2011). LIBSVM: a library for support vector machines. *ACM Trans. Intell. Syst. Technol.* 2, 1–27. doi: 10.1145/1961189.1961199
- Cicchetti, D. V., and Sparrow, S. A. (1981). Developing criteria for establishing interrater reliability of specific items: applications to assessment of adaptive behavior. *Am. J. Ment. Defic.* 86, 127–137.
- Dai, D., He, H., Vogelstein, J. T., and Hou, Z. (2013). Accurate prediction of AD patients using cortical thickness networks. *Mach. Vis. Appl.* 24, 1445–1457. doi: 10.1007/s00138-012-0462-0
- Dale, A. M., Fischl, B., and Sereno, M. I. (1999). Cortical surface-based analysis. I. Segmentation and surface reconstruction. *Neuroimage* 9, 179–194. doi: 10.1006/nimg.1998.0395
- Desikan, R. S., Ségonne, F., Fischl, B., Quinn, B. T., Dickerson, B. C., Blacker, D., et al. (2006). An automated labeling system for subdividing the human cerebral cortex on MRI scans into gyral based regions of interest. *Neuroimage* 31, 968–980. doi: 10.1016/j.neuroimage.2006.01.021
- Freeman, L. C. (1977). A set of measures of centrality based on betweenness. *Sociometry* 40, 35–41. doi: 10.2307/3033543
- Hagmann, P., Cammoun, L., Gigandet, X., Meuli, R., Honey, C. J., Wedeen, V. J., et al. (2008). Mapping the structural core of human cerebral cortex. *PLoS Biol.* 6:e159. doi: 10.1371/journal.pbio.0060159
- He, Y., Chen, Z., and Evans, A. (2007). Small-world anatomical networks in the human brain revealed by cortical thickness from MRI. *Cere. Cortex* 17, 2407–2419. doi: 10.1093/cercor/bhl149

- He, Y., Chen, Z., and Evans, A. (2008). Structural insights into aberrant topological patterns of large-scale cortical networks in Alzheimer's disease. *J. Neurosci.* 28, 4756–4766. doi: 10.1523/JNEUROSCI.0141-08.2008
- He, Y., Chen, Z., Gong, G., and Evans, A. (2009). Neuronal networks in Alzheimer's disease. *Neuroscientist* 15, 333–350. doi: 10.1177/1073858409334423
- Hertz, T., Hillel, A. B., and Weinshall, D. (2006). "Learning a kernel function for classification with small training samples", in *Proceedings. 23rd International Conference on Machine Learning*. (Pittsburgh, PA: ACM), 401–408.
- Humphries, M. D., Gurney, K., and Prescott, T. J. (2006). The brainstem reticular formation is a small-world, not scale-free, network. *Proc. Biol. Sci.* 273, 503–511. doi: 10.1098/rspb.2005.3354
- Kamkar, I., Gupta, S. K., Phung, D., and Venkatesh, S. (2015). Stable feature selection for clinical prediction: exploiting ICD tree structure using Tree-Lasso. *J. Biomed. Inform.* 53, 277–290. doi: 10.1016/j.jbi.2014.11.013
- Kanai, R., and Rees, G. (2011). The structural basis of inter-individual differences in human behaviour and cognition. *Nat. Rev. Neurosci.* 12, 231–242. doi: 10.1038/nrn3000
- Kim, H. J., Shin, J. H., Han, C. E., Kim, H. J., Na, D. L., Sang, W. S., et al. (2016). Using individualized brain network for analyzing structural covariance of the cerebral cortex in alzheimer's patients. *Front. Neurosci.* 10:394. doi: 10.3389/fnins.2016.00394
- Kong, X. Z., Liu, Z., Huang, L., Wang, X., Yang, Z., Zhou, G., et al. (2015). Mapping individual brain networks using statistical similarity in regional morphology from MRI. *PLoS ONE* 10:e0141840. doi: 10.1371/journal.pone.0141840
- Kong, X. Z., Wang, X., Huang, L., Pu, Y., Yang, Z., Dang, X., et al. (2014). Measuring individual morphological relationship of cortical regions. *J. Neurosci. Methods* 237, 103–107. doi: 10.1016/j.jneumeth.2014.09.003
- Li, Q., Li, X., Wang, X., Li, Y., Li, K., Yu, Y., et al. (2016). Topological properties of large-scale cortical networks based on multiple morphological features in amnesic mild cognitive impairment. *Neural Plast.* 2016:3462309. doi: 10.1155/2016/3462309
- Li, S., Yuan, X., Pu, F., Li, D., Fan, Y., Wu, L., et al. (2014). Abnormal changes of multidimensional surface features using multivariate pattern classification in amnesic mild cognitive impairment patients. *J. Neurosci.* 34, 10541–10553. doi: 10.1523/JNEUROSCI.4356-13.2014
- Li, W., Yang, C., Shi, F., Wu, S., Wang, Q., Nie, Y., et al. (2017). Construction of individual morphological brain networks with multiple morphometric features. *Front. Neuroanat.* 11:34. doi: 10.3389/fnana.2017.00034
- Liu, J., Ji, S., and Ye, J. (2009). *SLEP: Sparse Learning with Efficient Projections*. Arizona State University. Available online at: <http://www.public.asu.edu/~jye02/Software/SLEP/download.htm>
- Lohmann, G., von Cramon, D. Y., and Colchester, A. C. (2008). Deep sulcal landmarks provide an organizing framework for human cortical folding. *Cereb. Cortex* 18, 1415–1420. doi: 10.1093/cercor/bhm174
- Parent, A., and Carpenter, M. B. (1996). *Carpenter's Human Neuroanatomy*. Tokyo: Williams & Wilkins.
- Prati, R. C., Batista, G. E. A. P.A., and Monard, M. C. (2011). A survey on graphical methods for classification predictive performance evaluation. *IEEE Trans. Knowl. Data Eng.* 23, 1601–1618. doi: 10.1109/TKDE.2011.59
- Rakic, P. (1988). Defects of neuronal migration and the pathogenesis of cortical malformations. *Prog. Brain Res.* 73, 15–37. doi: 10.1016/S0079-6123(08)60494-X
- Saggar, M., Hosseini, S. M., Bruno, J. L., Quintin, E. M., Raman, M. M., Kesler, S. R., et al. (2015). Estimating individual contribution from group-based structural correlation networks. *Neuroimage* 120, 274–284. doi: 10.1016/j.neuroimage.2015.07.006
- Sanabriadiáz, G., Meliegarcía, L., Iturriamedina, Y., Alemángómez, Y., Hernándezgonzález, G., Valdésurrutia, L., et al. (2010). Surface area and cortical thickness descriptors reveal different attributes of the structural human brain networks. *Neuroimage* 50, 1497–1510. doi: 10.1016/j.neuroimage.2010.01.028
- Seidlitz, J., Shinn, M., Romero-Garcia, R., Whitaker, K. J., Vértes, P. E., Wagstyl, K., et al. (2017). Morphometric similarity networks detect microscale cortical organization and predict inter-individual cognitive variation. *Neuron* 97, 231.e7–247.e7. doi: 10.1016/j.neuron.2017.11.039
- Shrout, P. E., and Fleiss, J. L. (1979). Intraclass correlations: uses in assessing rater reliability. *Psychol. Bull.* 86, 420–428. doi: 10.1037/0033-2909.86.2.420
- Székely, G. J., and Rizzo, M. L. (2004). Testing for equal distributions in high dimension. *Interstat* 5, 1–16.
- Tibshirani, R. (1996). Regression shrinkage and selection via the lasso. *J. R. Stat. Soc. Ser. B Methodol* 58, 267–288.
- Tijms, B. M., Serié, P., Willshaw, D. J., and Lawrie, S. M. (2012). Similarity-based extraction of individual networks from gray matter MRI scans. *Cereb. Cortex* 22, 1530–1541. doi: 10.1093/cercor/bhr221
- Tijms, B. M., Wink, A. M., De, H. W., Wm, V. D. F., Stam, C. J., Scheltens, P., et al. (2013). Alzheimer's disease: connecting findings from graph theoretical studies of brain networks. *Neurobiol. Aging* 34, 2023–2036. doi: 10.1016/j.neurobiolaging.2013.02.020
- Van den Heuvel, M. P., and Sporns, O. (2013). Network hubs in the human brain. *Trends Cogn. Sci.* 17, 683–696. doi: 10.1016/j.tics.2013.09.012
- Van Essen, D. C. (1997). A tension-based theory of morphogenesis and compact wiring in the central nervous system. *Nature* 385, 313–318. doi: 10.1038/385313a0
- Wang, H., Jin, X., Zhang, Y., and Wang, J. (2016). Single-subject morphological brain networks: connectivity mapping, topological characterization and test-retest reliability. *Brain Behav.* 6:e00448. doi: 10.1002/brb3.448
- Wang, J., Wang, X., Xia, M., Liao, X., Evans, A., and He, Y. (2015). GREtNA: a graph theoretical network analysis toolbox for imaging connectomics. *Front. Hum. Neurosci.* 9:386. doi: 10.3389/fnhum.2015.00386
- Watts, D. J., and Strogatz, S. H. (1998). Collective dynamics of 'small-world' networks. *Nature* 393, 440.
- Wee, C. Y., Yap, P. T., and Shen, D. (2013). Prediction of Alzheimer's disease and mild cognitive impairment using cortical morphological patterns. *Hum. Brain Mapp.* 34, 3411–3425. doi: 10.1002/hbm.22156
- Wei, R., Li, C., Noa, F., and Ling, L. (2016). Prediction of Conversion from mild cognitive impairment to alzheimer's disease using MRI and structural network features. *Front. Aging Neurosci.* 8:76. doi: 10.3389/fnagi.2016.00076
- Yamada, M., Jitkrittum, W., Sigal, L., Xing, E. P., and Sugiyama, M. (2012). High-dimensional feature selection by feature-wise non-linear lasso. *Neural Comput.* 26, 185–207. doi: 10.1162/NECO_a_00537
- Yao, Z., Zhang, Y., Lin, L., Zhou, Y., Xu, C., and Jiang, T. (2010). Abnormal cortical networks in mild cognitive impairment and Alzheimer's disease. *PLoS Comput. Biol.* 6:e1001006. doi: 10.1371/journal.pcbi.1001006
- Zhang, J., Wang, J., Wu, Q., Kuang, W., Huang, X., He, Y., et al. (2011). Disrupted brain connectivity networks in drug-naive, first-episode major depressive disorder. *Biol. Psychiatry* 70, 334–342. doi: 10.1016/j.biopsych.2011.05.018
- Zhang, Y., Lin, L., Lin, C. P., Zhou, Y., Chou, K. H., Lo, C. Y., et al. (2012). Abnormal topological organization of structural brain networks in schizophrenia. *Schizophr. Res.* 141, 109–118. doi: 10.1016/j.schres.2012.08.021
- Zheng, W., Yao, Z., Hu, B., Gao, X., Cai, H., and Moore, P. (2015). Novel cortical thickness pattern for accurate detection of alzheimer's disease. *J. Alzheimers Dis.* 48, 995–1008. doi: 10.3233/JAD-150311
- Zhou, Y., and Lui, Y. W. (2013). Small-world properties in mild cognitive impairment and early alzheimer's disease: a cortical thickness MRI Study. *ISRN Geriatr.* 2013:542080. doi: 10.1155/2013/542080
- Zhu, W., Wen, W., He, Y., Xia, A., Anstey, K. J., and Sachdev, P. (2012). Changing topological patterns in normal aging using large-scale structural networks. *Neurobiol. Aging* 33, 899–913. doi: 10.1016/j.neurobiolaging.2010.06.022

Conflict of Interest Statement: The authors declare that the research was conducted in the absence of any commercial or financial relationships that could be construed as a potential conflict of interest.

Copyright © 2018 Yu, Wang, Li, Zhang, Li, Li for the Alzheimer's Disease Neuroimaging Initiative. This is an open-access article distributed under the terms of the Creative Commons Attribution License (CC BY). The use, distribution or reproduction in other forums is permitted, provided the original author(s) and the copyright owner are credited and that the original publication in this journal is cited, in accordance with accepted academic practice. No use, distribution or reproduction is permitted which does not comply with these terms.

Research Article

Topological Properties of Large-Scale Cortical Networks Based on Multiple Morphological Features in Amnestic Mild Cognitive Impairment

Qionglng Li,¹ Xinwei Li,¹ Xuotong Wang,¹ Yuxia Li,^{2,3,4} Kuncheng Li,⁵
Yang Yu,⁶ Changhao Yin,⁶ Shuyu Li,¹ and Ying Han^{2,3}

¹Key Laboratory for Biomechanics and Mechanobiology of Ministry of Education, School of Biological Science & Medical Engineering, Beihang University, Beijing 100191, China

²Center of Alzheimer's Disease, Beijing Institute for Brain Disorders, Beijing 100053, China

³Department of Neurology, Xuanwu Hospital, Capital Medical University, Beijing 100053, China

⁴Department of Neurology, Tangshan Gongren Hospital, Tangshan 063000, China

⁵Department of Radiology, Xuanwu Hospital, Capital Medical University, Beijing 100053, China

⁶Department of Neurology, Hongqi Hospital, Mudanjiang Medical University, Mudanjiang 157011, China

Correspondence should be addressed to Shuyu Li; shuyuli@buaa.edu.cn and Ying Han; 13621011941@163.com

Received 26 July 2015; Revised 20 December 2015; Accepted 30 December 2015

Academic Editor: Stuart C. Mangel

Copyright © 2016 Qionglng Li et al. This is an open access article distributed under the Creative Commons Attribution License, which permits unrestricted use, distribution, and reproduction in any medium, provided the original work is properly cited.

Previous studies have demonstrated that amnestic mild cognitive impairment (aMCI) has disrupted properties of large-scale cortical networks based on cortical thickness and gray matter volume. However, it is largely unknown whether the topological properties of cortical networks based on geometric measures (i.e., sulcal depth, curvature, and metric distortion) change in aMCI patients compared with normal controls because these geometric features of cerebral cortex may be related to its intrinsic connectivity. Here, we compare properties in cortical networks constructed by six different morphological features in 36 aMCI participants and 36 normal controls. Six cortical features (3 volumetric and 3 geometric features) were extracted for each participant, and brain abnormalities in aMCI were identified by cortical network based on graph theory method. All the cortical networks showed small-world properties. Regions showing significant differences mainly located in the medial temporal lobe and supramarginal and right inferior parietal lobe. In addition, we also found that the cortical networks constructed by cortical thickness and sulcal depth showed significant differences between the two groups. Our results indicated that geometric measure (i.e., sulcal depth) can be used to construct network to discriminate individuals with aMCI from controls besides volumetric measures.

1. Introduction

Mild cognitive impairment (MCI) is considered to be a transitional period between normal aging and Alzheimer's disease (AD), which is a progressive, neurodegenerative disease characterized by cognitive decline greater than expected for one's age and educational level yet not fulfilling the criteria of AD [1]. Amnestic MCI (aMCI), as the most common subtype of MCI, is characterized by primary memory impairments with single or multiple cognitive domains impaired and likely progresses to AD [2–4]. Current studies of aMCI have shown disrupted functional integration [5] and abnormal structural

connections between regions [6]. Morphological features have been widely used to characterize brain structures [7, 8] and also served as structural measures to investigate topological properties in large-scale cortical networks [9–11]. Previous studies on large-scale cortical network in MCI mostly used cortical thickness and gray matter volume as descriptors to construct structural network of the human cortex [12, 13].

However, different morphological features reveal different intrinsic properties of cerebral cortex. For example, volumetric measures (i.e., cortical thickness, gray matter volume) reflect the size, density, and arrangement of cells

(neurons, neuroglia, and nerve fibers) [14, 15], and surface area is linked to the number of mini columns in the cortical layer [16]. Using large-scale cortical network analysis based on cortical thickness, several studies have found disrupted small-world properties (i.e., lower clustering coefficient and shorter path length) in MCI patients compared to normal controls [13, 17, 18]. A cortical network study using surface area can reveal topological properties of the networks resulting from the concurrent changes between different anatomical regions [10]. In addition, geometric measures (i.e., sulcal depth, curvature, and metric distortion) mainly reflect cortical folding pattern [19–21]. For instance, sulcal depth and curvature measure specific aspects of the cortical geometry, and metric distortion is a wider measure of the overall degree of cortical folding [22]. These geometric measures related to cortical folding may vary with the changes of intrinsic as well as extrinsic connectivity according to the tension theory of the cerebral cortex morphogenesis [19] and could be more suitable descriptors for finding the anatomical-axonal and morphological connectivity correlation [10]. Thus, we assume that geometric measures can be used to construct cortical network that may detect the alterations from structural disconnection in aMCI and show different topological properties compared with volumetric measures (i.e., cortical thickness, gray matter volume, and surface area).

Here, we investigated topological properties of large-scale human cortical network based on graph theory analysis method by employing multiple morphological features in aMCI patients. Then we compared the topological properties of different cortical networks constructed by different morphological features. We expected that topological properties of cortical networks based on geometric measures in aMCI patients may be different from normal controls and can be used to discriminate individuals with aMCI from controls.

2. Materials and Methods

2.1. Participants. Seventy-two right-handed participants, including thirty-six aMCI and demography matched healthy normal controls, participated in this study. The aMCI participants were recruited from a clinical research program at Xuanwu Hospital, Beijing, China. The healthy normal controls were recruited from the local community through advertisements. This study was approved by the Research Ethics Review Board of Xuanwu Hospital, and written informed consent was obtained from each participant.

All the aMCI participants were identified according to the criteria for amnesic MCI [23–26], which included (a) memory complaint, preferably confirmed by an informant; (b) objective memory impairment, adjusted for age and education; (c) normal or near-normal performance on general cognitive functioning and no or minimum impairment of daily life activities; (d) the Clinical Dementia Rating (CDR) score of 0.5; and (e) not meeting the criteria for dementia according to the DSM-IV (Diagnostic and Statistical Manual of Mental Disorders, 4th Edition, revised). Participants with aMCI were diagnosed by experienced neurologists. Participants were excluded if they met the following clinical characteristics: (a) a clear history of stroke; (b) severe depression that led

TABLE 1: Subject demographics.

| | aMCI ($n = 36$) | Control ($n = 36$) | p value |
|--------------|------------------------|------------------------|-----------|
| Gender (M/F) | 14/22 | 15/21 | 0.813 |
| Age | 66.0 ± 8.7 (50–83) | 63.9 ± 6.1 (56–79) | 0.258 |
| Education | 10.2 ± 4.4 (2–21) | 10.7 ± 3.2 (5–17) | 0.651 |
| MMSE | 24.4 ± 3.2 (17–30) | 28.1 ± 1.7 (20–30) | <0.001 |
| MoCA | 20.6 ± 3.7 (15–27) | 26.4 ± 2.4 (18–30) | <0.001 |

Age, education, MMSE, and MoCA data are expressed as mean \pm SD (range). No significant differences were between two groups in gender, age, and education years. Groups for aMCI and NC showed significant differences in MMSE and MoCA scores ($p < 0.01$). Statistical p value was analyzed using two-sample t -test, in which gender was converted into a virtual variable.

to mild cognitive impairment (Hamilton Depression Rating Scale score >24 points); (c) other nervous system diseases, which can cause cognitive impairment (such as brain tumors, Parkinson’s disease, encephalitis, and epilepsy); (d) cognitive impairment caused by traumatic brain injury; (e) other systemic diseases, which can cause cognitive impairment, such as thyroid dysfunction, severe anemia, syphilis, and HIV; and (f) a history of psychosis or congenital mental growth retardation. Clinical and demographic data for the participants are shown in Table 1.

2.2. MRI Data Acquisition. MRI data acquisition was performed on a 3.0 T Siemens scanner by employing a sagittal magnetization-prepared rapid gradient echo (MP-RAGE) sequence with the following imaging parameters: repetition time (T_R) = 1900 ms; echo time (T_E) = 2.2 ms; inversion time = 900 ms; flip angle = 90° ; field of view (FOV) = 250 mm \times 250 mm; matrix = 256 \times 256; 176 slices, thickness = 1.0 mm. Brain MR images were inspected by an experienced neuroradiologist, and no gross abnormalities were observed for any subject.

2.3. Cortical Reconstruction and Morphological Features Extraction. Both the cortical reconstruction and morphological features extraction were obtained by using the FreeSurfer software (<http://surfer.nmr.mgh.harvard.edu/>) with a standard cortical automatic handling protocol. First, the data were normalized to a standard anatomical template [27] and corrected for bias-field inhomogeneity. Then the images were skull-stripped using a watershed algorithm [28] and subsequently segmented into subcortical white matter and deep gray matter volumetric structures [29, 30]. The initial tessellation was formed by reconstructing the gray matter/white matter boundary (white surface) and the outer cortical surface (pial surface) [31, 32]. Subsequently, a series of deformable procedures were performed, including surface inflation [31], registration to a spherical atlas [33], and parcellation of the cerebral cortex into units based on gyral and sulcal structures [30]. All reconstructed surfaces were visually inspected for gross-anatomical topological defects. Finally, a variety of morphological features at each vertex on the pial surface were computed, including volumetric

(cortical thickness, surface area, and GM volume) and geometric (sulcal depth, metric distortion, and mean curvature) measures, more details seen in this paper [34]. The thickness maps of both NC and aMCI groups are shown in Figure 1(a).

2.4. Cortical Network Construction. We employed a cortical scheme comprised of 148 regions from Destrieux Atlas. Cortical networks were built from partial correlation of interregional cortical morphological features. Prior to the correlation analysis, a linear regression was performed at every region to remove the effects of age, gender, and the total morphological feature value for each measure. And the resulting residuals were used to substitute for the raw morphological feature values. In this experimental design, the number of observations (participants, $N = 36$) is smaller than the number of dependent variables (regions, $P = 148$). “Small N , large P ” lead to inaccurate estimations of the covariance matrix [35]. A method based on the Ledoit-Wolf lemma was used to shrink the covariance estimates [36]. Finally, the partial correlation coefficients were computed with R software (<http://www.r-project.org/>). The partial correlation matrixes (adjacent matrix) of cortical networks constructed by thickness are shown in Figure 1(b).

The adjacent matrix was then binarized to an undirected and unweighted graph as shown in Figure 1(c) (at the sparsity of 5%) using a wide range of sparsity values (from 5% to 35%, step = 0.01). Sparsity of 5% meant that only the strongest 5% of the connections remained and 95% of the connectivity matrixes were removed. If the sparsity was less than 5%, the small-world properties were not estimable. And if the sparsity was greater than 35%, more noise would be included in the graph and it would be more like random network [37, 38]. The same sparsity range was applied for all network analyses.

2.5. Graph Theoretical Characterization. Graph theory is usually considered an attractive model for the mathematical treatment of cortical network connectivity [39]. In general, a complex network can be represented as a graph G , which consists of a set of nodes and a set of edges. Several important parameters of the graph G for the connectivity matrixes were estimated in this study.

Degree is the number of links connected to the node. Degree of a node “ i ” is defined as

$$k_i = \sum_{j \in N} a_{ij}, \quad (1)$$

where N is the set of all nodes in the network; a_{ij} is the connection status between nodes “ i ” and “ j ” and $a_{ij} = 1$ when link exists; otherwise $a_{ij} = 0$.

The clustering coefficient C_i of a node “ i ” with degree k_i is defined as the ratio of the existing connections (e_i) between the node’s neighbors and the maximum possible connections between neighbors of the node. The clustering coefficient of node “ i ” is given as

$$C_i = \frac{2e_i}{k_i(k_i - 1)}. \quad (2)$$

The clustering coefficient is an index of local structure, while the clustering coefficient of the whole network is the average C_i over all nodes

$$C = \frac{1}{N} \sum_{i=1}^N C_i. \quad (3)$$

The shortest path length $L_{i,j}$ between two nodes “ i ” and “ j ” of the graph G is the smallest number of edges that is required to connect “ i ” and “ j .” The shortest path length of a node “ i ” can be calculated as the distance between a node “ i ” and all other nodes [37]:

$$L_i = \frac{1}{N} \sum_{j=1, j \neq i}^N L_{i,j}. \quad (4)$$

The characteristic path length is defined as the mean of path length $L_{i,j}$ over all pairs of nodes:

$$L = \frac{1}{N} \sum_{i=1}^N L_i. \quad (5)$$

The small-worldness network parameter σ is defined as those with small path length, like random network, and high clustering coefficient networks, much higher than random network. Small-world properties of a given network may be influenced by its intrinsic features, such as the number of nodes, edges, and the degree distribution. Thus, 1000 random networks were generated by using a random rewiring process [40], which preserves the number of nodes, mean degree, and degree distribution. This results in a normalized clustering coefficient $\gamma = C_p/C_{\text{rand}} \gg 1$ and a normalized path length $\lambda = L_p/L_{\text{rand}} \approx 1$. Then a simple quantitative measurement of small-worldness σ is acquired [41]:

$$\sigma = \frac{\gamma}{\lambda}. \quad (6)$$

The real cortical network G is considered to be a small-world network if it meets the following criteria [37]:

$$\sigma = \frac{\gamma}{\lambda} > 1. \quad (7)$$

Betweenness centrality is a measure of network hubs that are crucial to efficient communication. BC is defined as the ratio of the number of shortest path passing through node “ i ” to the total number of shortest paths between pairs of nodes “ j ” and “ k ”:

$$BC_i = \sum_{\substack{j, k \in N \\ j \neq k}} \frac{\rho_{j,k(i)}}{\rho_{j,k}}, \quad (8)$$

where $\rho_{j,k}$ is the number of shortest paths between “ j ” and “ k ” and $\rho_{j,k(i)}$ is the number of shortest path between “ j ” and “ k ” that passes through “ i .” For further comparison, the betweenness BC_i would be normalized as $bc_i = BC_i/BC$, where BC is the average betweenness of the network. Cortex regions were defined as hubs, whose betweenness values were more than twice the average betweenness of the network ($bc_i > 2$).

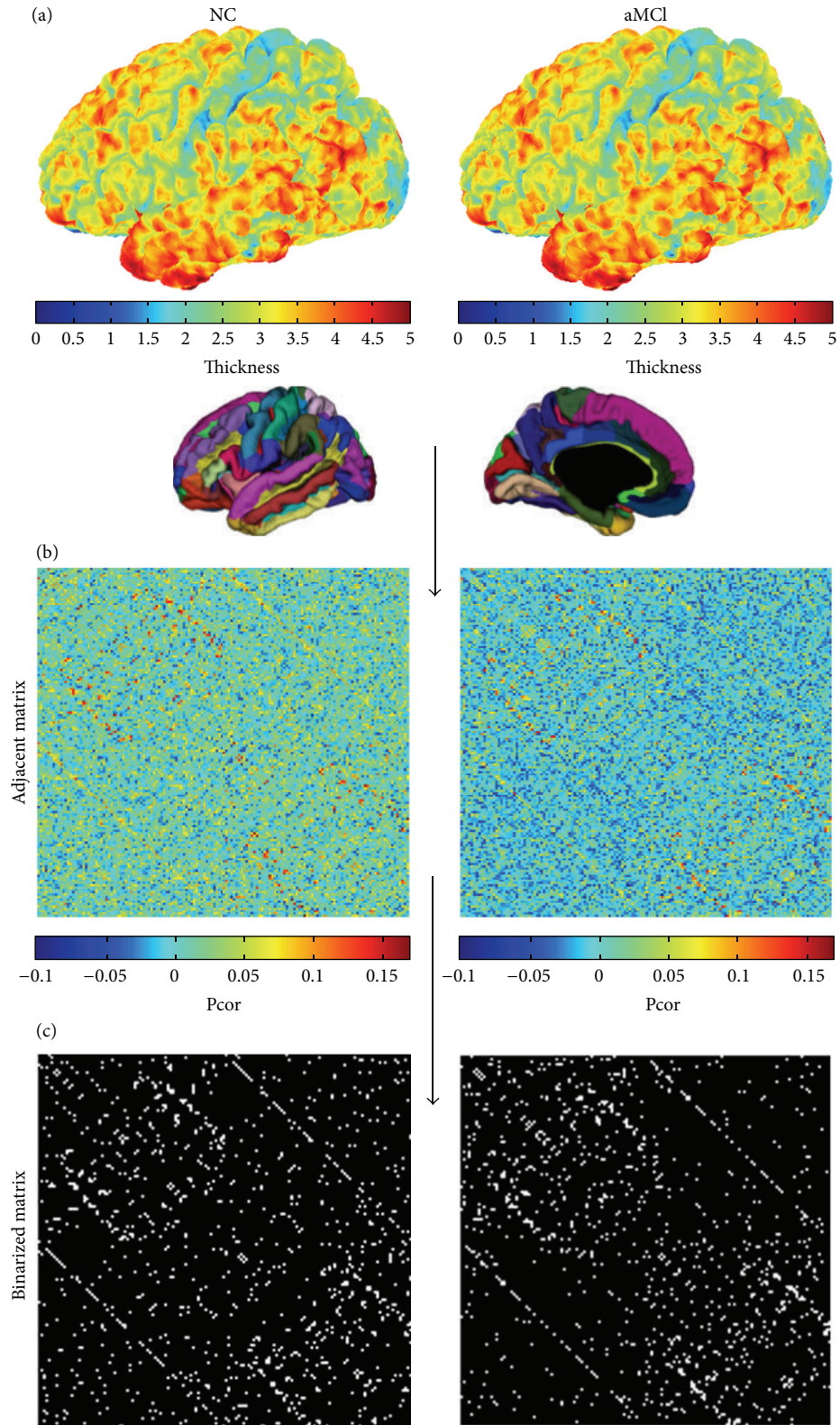


FIGURE 1: Flowchart for the construction of structural cortical networks. (a) Two representative cortical thickness maps (left for a control subject and right for an aMCI subject) were obtained from anatomical MRI. The color bar indicating the range of thickness is shown on the right. (b) The cortical thickness was mapped into 148 regions and the partial correlation matrices were obtained between regional thicknesses across subjects within each group (left for NC and right for aMCI). The color bar indicating the partial correlation coefficient between regions is shown on the right. (c) The correlation matrices of (b) were thresholded into the binarized matrices (left for NC and right for aMCI) by sparsity of 5%. NC, normal controls.

2.6. Statistical Analysis. Two-sample t -test was used to test the demographics, in which gender was converted into a virtual variable. To test the statistical significance of the between-group differences in the parameters of the cortical networks, a nonparametric permutation test was employed [42]. In this permutation test, we calculated possible values of the test statistic on a reference distribution after repeatedly rearranging the observed data from NC and aMCI groups. First, characteristics of the cortical network, such as C_p , L_p , and bc_i , were calculated for NC and aMCI groups, respectively. Then NC and aMCI data were mixed. From the mixed data, the same number of subjects as aMCI patients was randomly chosen to be considered as aMCIs and the rest to be NCs. Next, partial correlation matrix for each randomized group was recalculated and corresponding binarized matrix was obtained using the same sparsity as in the real cortical networks. Third, network parameters for each randomized group were computed. This process was repeated 1000 times and the 95 percentile points of each distribution used as the critical values for a one-tailed procedure were repeated at every sparsity value of the cortical networks.

3. Results

3.1. Demographics. Two-sample t -test was used to test the demographics, in which gender was converted into a virtual variable, and results are shown in Table 1. There were no significant differences in gender, age, or years of education between aMCI and NC. Groups for aMCI and NC showed significant differences in MMSE and MoCA scores ($p < 0.01$).

3.2. Small-World Properties of Cortical Networks. Compared with random networks, small-world networks had higher clustering coefficients and similar characteristic path length. Over a range of sparsity values ($5\% \leq \text{sparsity} \leq 35\%$), clustering coefficient and characteristic path length were calculated for both the NC and aMCI networks based on different morphological features. The small-world attributes of the networks are shown in Figure 2. Compared with matched random networks which had the same number of nodes and degree distribution, all morphological networks had similarly characteristic path length ($\lambda \approx 1$) and larger clustering coefficients ($\gamma \gg 1$) in both NC and aMCI networks. Compared with NC, aMCI showed slightly larger small-world characteristics (larger σ) in the cortical networks obtained for volumetric measures (cortical thickness and GM volume) and there were no great differences between NC and aMCI cortical networks based on surface area and geometric measures (mean curvature, metric distortion, and sulcal depth).

3.3. Abnormal Changes in Nodal Betweenness Centrality. As crucial components required for efficient communication in a network, hubs regulated information flow and played a key role in network resilience against attacks. To study the nodal characteristics, the cortical networks were constructed at certain sparsity of 11%. This sparsity ensured that all regions

were included in the cortical networks while minimizing the number of false-positive paths. Based on the results, some regions were identified as hubs in the cortical network of both the NC and aMCI groups. Details of the hub regions in the cortical networks are shown in Table 2.

In this study, the identified hub in networks based on volumetric measures, as shown in Figures 3(a) and 3(b), was involved in the frontal, temporal, parietal, and insula association cortex in the NC and temporal lobe, superior parietal lobule, cingulate cortex, precentral sulcus, callosum, and insula in the aMCI. High betweenness in network based on geometric measures was similar to volumetric measures. It was worth noting that hubs in networks using sulcal depth as descriptor included frontal polar, lingual sulcus, medial occipitotemporal sulcus, precentral sulcus, temporal gyrus (Heschl), and corpus callosum in NC group. And in aMCI group, regions included collateral sulcus, precentral sulcus, postcentral sulcus, temporal-occipital incisures, frontal gyrus, and corpus callosum (Figure 3(c)).

Permutation test was used to detect the significant differences in betweenness between NC and aMCI. Regions showing significant increase ($p < 0.05$) in the betweenness of cortical networks using volumetric measures in aMCI patients included collateral sulcus, occipital gyrus, temporal gyrus, temporal pole, parietooccipital sulcus, postcentral gyrus, and subcallosal gyrus. And decreased betweenness ($p < 0.05$) regions were located in subparietal sulcus, middle occipital gyrus, precuneus, and superior temporal sulcus as shown in Figures 4(a) and 4(b). Betweenness in inferior temporal gyrus, superior temporal gyrus, inferior frontal gyrus, and pericallosal sulcus showed significant increase ($p < 0.05$) in network constructed by sulcal depth in aMCI patients. And betweenness in lateral sulcus, medial occipitotemporal sulcus, lateral occipitotemporal sulcus, cingulate sulcus, and short insular gyri significantly decreased ($p < 0.05$).

3.4. Comparing Networks from Different Morphological Features between Groups

3.4.1. Volumetric Measures. As shown in Figures 5(a) and 5(b), clustering coefficient and characteristic path length were higher in the structural cortical networks obtained from volumetric measures (both cortical thickness and GM volume) of aMCI. A permutation test was used to detect the between-group differences. The arrows indicated the significant differences between NC and aMCI in the clustering coefficient ($p < 0.05$) of networks constructed by cortical thickness at the sparsity of 12% and 14% as shown in Figure 5(a). Significant differences in characteristic path length ($p < 0.05$) of networks constructed by cortical thickness had been detected between NC and aMCI at the sparsity of 11%, 12%, and 14%. In the cortical networks obtained from GM volume, as shown in Figure 5(b), no significant differences were found in clustering coefficient between NC and aMCI ($p > 0.05$). Only at the sparsity of 35% was a significant difference found in characteristic path length ($p < 0.05$). Our findings provided further evidence for which networks constructed by cortical thickness had a small-world characteristic loss in aMCI.

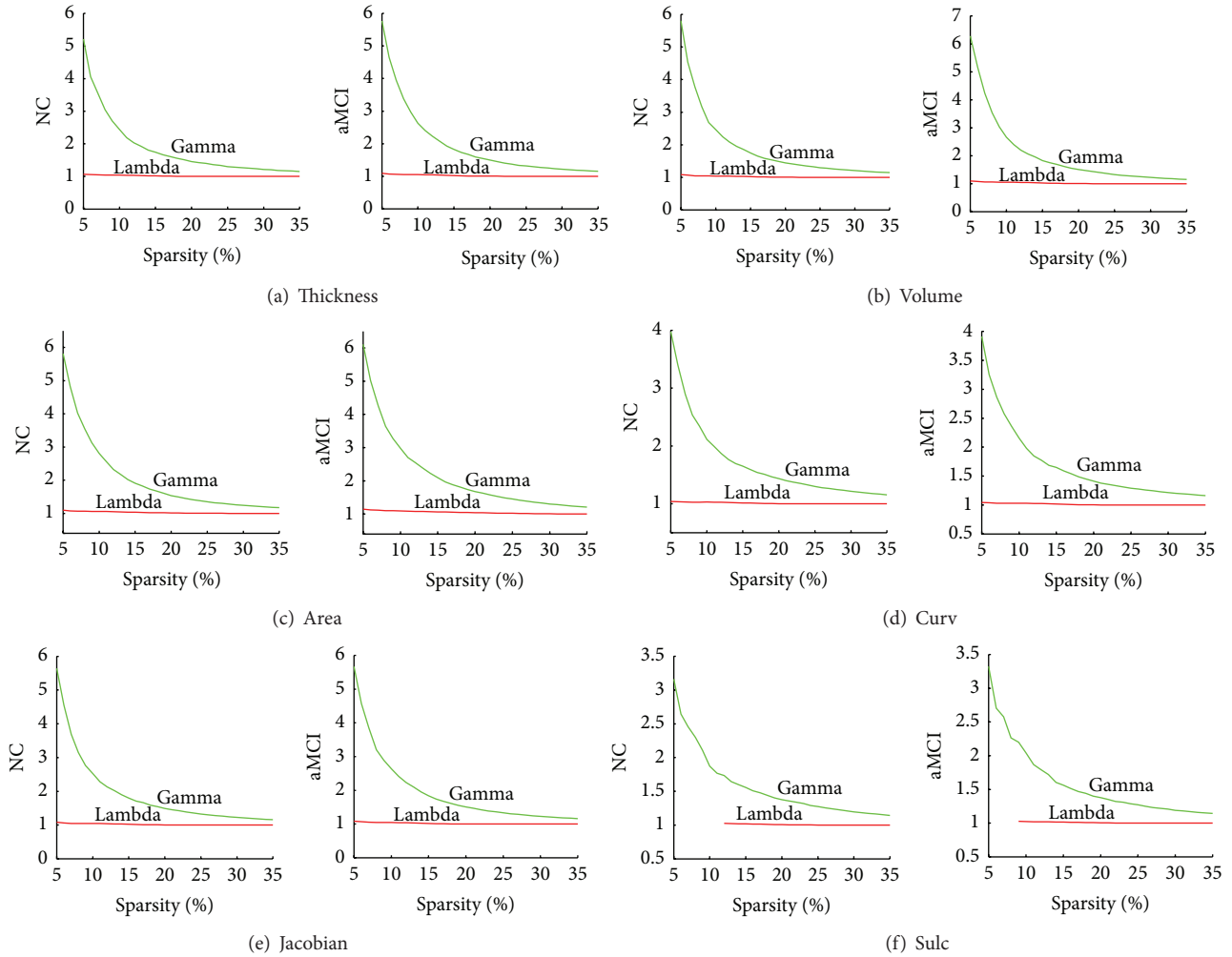


FIGURE 2: Small-world properties of volumetric measures networks and geometric measures networks. The graph shows the normalized characteristic path length (λ , $\lambda = L_p/L_{\text{rand}}$) and clustering coefficients (γ , $\gamma = C_p/C_{\text{rand}} \gg 1$) over a range of sparsity values ($5\% \leq \text{sparsity} \leq 35\%$). All the networks have $\gamma \gg 1$ (green lines) and $\lambda \approx 1$ (red lines), which imply small-world properties. (a) The values of gamma and lambda in NC and aMCI of cortical thickness networks. (b) The values of gamma and lambda in NC and aMCI of GM volume networks. (c) The values of gamma and lambda in NC and aMCI of surface area networks. (d) The values of gamma and lambda in NC and aMCI of mean curvature networks. (e) The values of gamma and lambda in NC and aMCI of metric distortion (Jacobian) networks. (f) The values of gamma and lambda in NC and aMCI of sulcal depth networks. Thickness, cortical thickness. Volume, gray matter volume. Area, surface area. Curv, mean curvature. Sulc, sulcal depth. NC, normal controls.

In Figure 5(c), the clustering coefficient and characteristic path length were much larger for aMCI in cortical network using surface area as descriptor. However, no significant differences ($p > 0.05$) were found in all permutation tests for small-world properties of cortical network based on surface area.

3.4.2. Geometric Measures. Small-world properties of cortical network using sulcal depth were very similar to properties in network using thickness for both NC and aMCI. As shown in Figure 5(f), the clustering coefficient was higher for aMCI, and the characteristic path length had no much difference between aMCI and NC. Statistical analysis further revealed significant differences in the clustering coefficient ($p < 0.05$) at $9\% \leq \text{sparsity} \leq 11\%$, $\text{sparsity} = 13\%$, 16% , and 18% , and

$\text{sparsity} = 24\%$ and 25% . Significant differences were found in the characteristic path length between NC and aMCI at the range of sparsity values ($\text{sparsity} = 25\%$ and $30\% \leq \text{sparsity} \leq 33\%$).

In Figure 5(e), small-world properties analysis using metric distortion as a descriptor showed similar results to properties in network based on cortical thickness. As shown in Figure 5(e), the clustering coefficient was larger for the aMCI compared with NC subjects. What is more, the characteristic path length had no much difference between NC and aMCI. However, statistical analysis revealed no significant differences ($p > 0.05$) in all the topological parameters over the whole range of sparsity values. Similar to metric distortion, no significant differences were found when using mean curvature as descriptor in cortical network ($p > 0.05$).

TABLE 2: The abbreviations of Destrieux Atlas.

| Index | Long name | Abbreviations |
|-------|---------------------------------------------------------------------------------------|---------------|
| 1 | Frontomarginal gyrus (of Wernicke) and sulcus | GSF |
| 2 | Inferior occipital gyrus (O3) and sulcus | GSOI |
| 3 | Paracentral lobule and sulcus | GSP |
| 4 | Subcentral gyrus (central operculum) and sulci | GSS |
| 5 | Transverse frontopolar gyri and sulci | GSTF |
| 6 | Anterior part of the cingulate gyrus and sulcus (ACC) | GSCA |
| 7 | Middle-anterior part of the cingulate gyrus and sulcus (aMCC) | GSCMA |
| 8 | Middle-posterior part of the cingulate gyrus and sulcus (pMCC) | GSCMP |
| 9 | Posterior-dorsal part of the cingulate gyrus (dPCC) | GCPD |
| 10 | Posterior-ventral part of the cingulate gyrus (vPCC, isthmus of the cingulate gyrus) | GCPV |
| 11 | Cuneus (O6) | GC |
| 12 | Opercular part of the inferior frontal gyrus | GFIOper |
| 13 | Orbital part of the inferior frontal gyrus | GFIOrb |
| 14 | Triangular part of the inferior frontal gyrus | GFIT |
| 15 | Middle frontal gyrus (F2) | GFM |
| 16 | Superior frontal gyrus (F1) | GFS |
| 17 | Long insular gyrus and central sulcus of the insula | GILSCI |
| 18 | Short insular gyri | GIS |
| 19 | Middle occipital gyrus (O2, lateral occipital gyrus) | GOM |
| 20 | Superior occipital gyrus (O1) | GOS |
| 21 | Lateral occipitotemporal gyrus (fusiform gyrus, O4-T4) | GOTLF |
| 22 | Lingual gyrus, lingual part of the medial occipitotemporal gyrus (O5) | GOTML |
| 23 | Parahippocampal gyrus, parahippocampal part of the medial occipitotemporal gyrus (T5) | GOTMP |
| 24 | Orbital gyri | GO |
| 25 | Angular gyrus | GPIA |
| 26 | Supramarginal gyrus | GPIS |
| 27 | Superior parietal lobule (lateral part of P1) | GPS |
| 28 | Postcentral gyrus | GPost |
| 29 | Precentral gyrus | GPCen |
| 30 | Precuneus (medial part of P1) | GPCun |
| 31 | Straight gyrus, gyrus rectus | GR |
| 32 | Subcallosal area, subcallosal gyrus | GS |
| 33 | Anterior transverse temporal gyrus (of Heschl) | GTSGTT |
| 34 | Lateral aspect of the superior temporal gyrus | GTSL |
| 35 | Planum polare of the superior temporal gyrus | GTSPP |
| 36 | Planum temporale or temporal plane of the superior temporal gyrus | GTSPPT |
| 37 | Inferior temporal gyrus (T3) | GTI |
| 38 | Middle temporal gyrus (T2) | GTM |
| 39 | Horizontal ramus of the anterior segment of the lateral sulcus (or fissure) | LFAH |
| 40 | Vertical ramus of the anterior segment of the lateral sulcus (or fissure) | LFAV |
| 41 | Posterior ramus (or segment) of the lateral sulcus (or fissure) | LFP |
| 42 | Occipital pole | PO |
| 43 | Temporal pole | PT |
| 44 | Calcarine sulcus | SCal |
| 45 | Central sulcus (Rolando's fissure) | SCen |
| 46 | Marginal branch (or part) of the cingulate sulcus | SCM |
| 47 | Anterior segment of the circular sulcus of the insula | SCIA |
| 48 | Inferior segment of the circular sulcus of the insula | SCII |
| 49 | Superior segment of the circular sulcus of the insula | SCIS |
| 50 | Anterior transverse collateral sulcus | SCTA |

TABLE 2: Continued.

| Index | Long name | Abbreviations |
|-------|------------------------------------------------------------------------------|---------------|
| 51 | Posterior transverse collateral sulcus | SCTP |
| 52 | Inferior frontal sulcus | SFI |
| 53 | Middle frontal sulcus | SFM |
| 54 | Superior frontal sulcus | SFS |
| 55 | Sulcus intermedius primus (of Jensen) | SIPJ |
| 56 | Intraparietal sulcus (interparietal sulcus) and transverse parietal sulci | SIPT |
| 57 | Middle occipital sulcus and lunatus sulcus | SOML |
| 58 | Superior occipital sulcus and transverse occipital sulcus | SOST |
| 59 | Anterior occipital sulcus and preoccipital notch (temporooccipital incisure) | SOA |
| 60 | Lateral occipitotemporal sulcus | SOTL |
| 61 | Medial occipitotemporal sulcus (collateral sulcus) and lingual sulcus | SOTML |
| 62 | Lateral orbital sulcus | SOL |
| 63 | Medial orbital sulcus (olfactory sulcus) | SOMO |
| 64 | Orbital sulci (H-shaped sulci) | SOHS |
| 65 | Parietooccipital sulcus (or fissure) | SPO |
| 66 | Pericallosal sulcus (S of corpus callosum) | SPer |
| 67 | Postcentral sulcus | SPost |
| 68 | Inferior part of the precentral sulcus | SPIP |
| 69 | Superior part of the precentral sulcus | SPSP |
| 70 | Suborbital sulcus (sulcus rostrales, supraorbital sulcus) | SSO |
| 71 | Subparietal sulcus | SSP |
| 72 | Inferior temporal sulcus | STI |
| 73 | Superior temporal sulcus (parallel sulcus) | STS |
| 74 | Transverse temporal sulcus | STT |

4. Discussion

In this study, we explored the properties of large-scale human brain cortical networks using multiple morphological features (including 3 volumetric measures, cortical thickness, surface area, and gray matter volume, and 3 geometric measures, sulcal depth, metric distortion, and mean curvature) based on graph theory analysis in cognitively normal older adults and amnesic mild cognitive impairment (aMCI) patients. We found that all networks constructed by these morphological features showed small-world properties which implied high efficiency of information transformation in human cognition. Properties in networks constructed by cortical thickness and sulcal depth showed significant differences between NC and aMCI patients. Besides, regions showing significant differences mainly located in the medial temporal lobe and supramarginal and right inferior parietal lobe. Our results indicated that geometric measure (i.e., sulcal depth) can be used to construct network to discriminate individuals with aMCI from controls besides volumetric measures and provided new insights into the study of the pathophysiological mechanism of amnesic MCI.

Previous studies have demonstrated that the cortical thickness and GM volume can be used as morphological descriptors to study the complex cortical networks, and networks based on the cortical thickness and GM volume followed the small-world properties [10–12, 43, 44]. Similar

to previous studies, networks based on volumetric measures showed altered small-world properties (i.e., increased clustering coefficient and path length) in aMCI patients compared with NC subjects. Short path length and high clustering coefficient in cortical network mean effective and rapid transfers of information between and across remote regions that are believed to constitute the basis of cognitive processes. Large σ means an optimal balance between local specialization and global integration. The cortical thickness changes are related to myelination of gray matter or the underlying white matter, as we know damage of myelin sheath is often associated with decreased functional efficiency. Here, we found longer path length and higher clustering coefficient in aMCI that may indicate a disturbance of the normal balance [45].

Consistent with the volumetric measures, all networks based on geometric measures also followed the small-world properties but less optimal small-worldness in aMCI network, while properties in network constructed by sulcal depth showed much more significant differences between NC and aMCI patients compared with properties in networks based on other geometric measures through a range of sparsity values. Previous studies have demonstrated that geometric differences are predominantly linked with the development of neuronal connections and cortical pattern of connectivity [19, 46] and are thus a marker for cerebral development or abnormal cortical connectivity due to disorders.

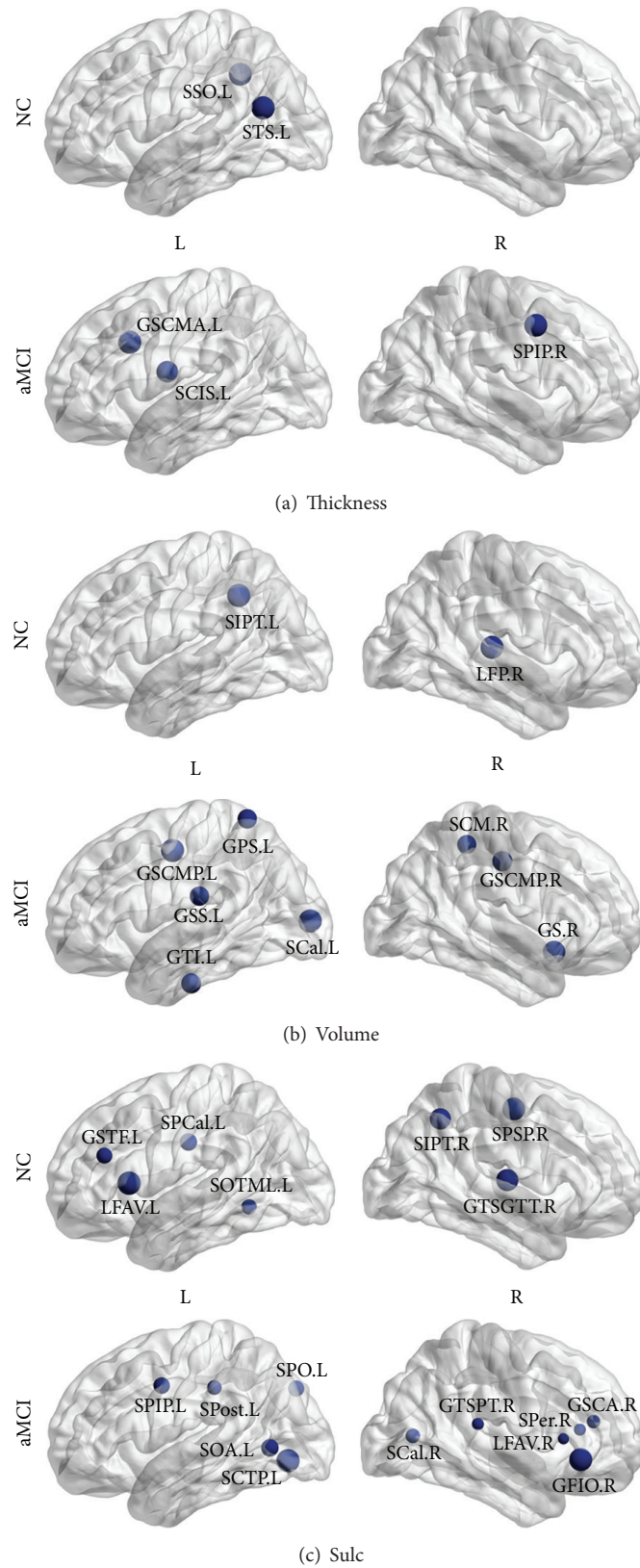


FIGURE 3: Hubs regions in cortical networks. Global hub regions derived from normalized nodal betweenness centrality in NC and aMCI. The blue spheres indicate the global hubs whose betweenness is more than twice the average betweenness of the network. (a) Global hubs in cortical thickness networks. (b) Global hubs in gray matter volume networks. (c) Global hubs in sulcal depth networks. Thickness, cortical thickness. Volume, gray matter volume. NC, normal controls. For the abbreviations of regions, see Table 2.

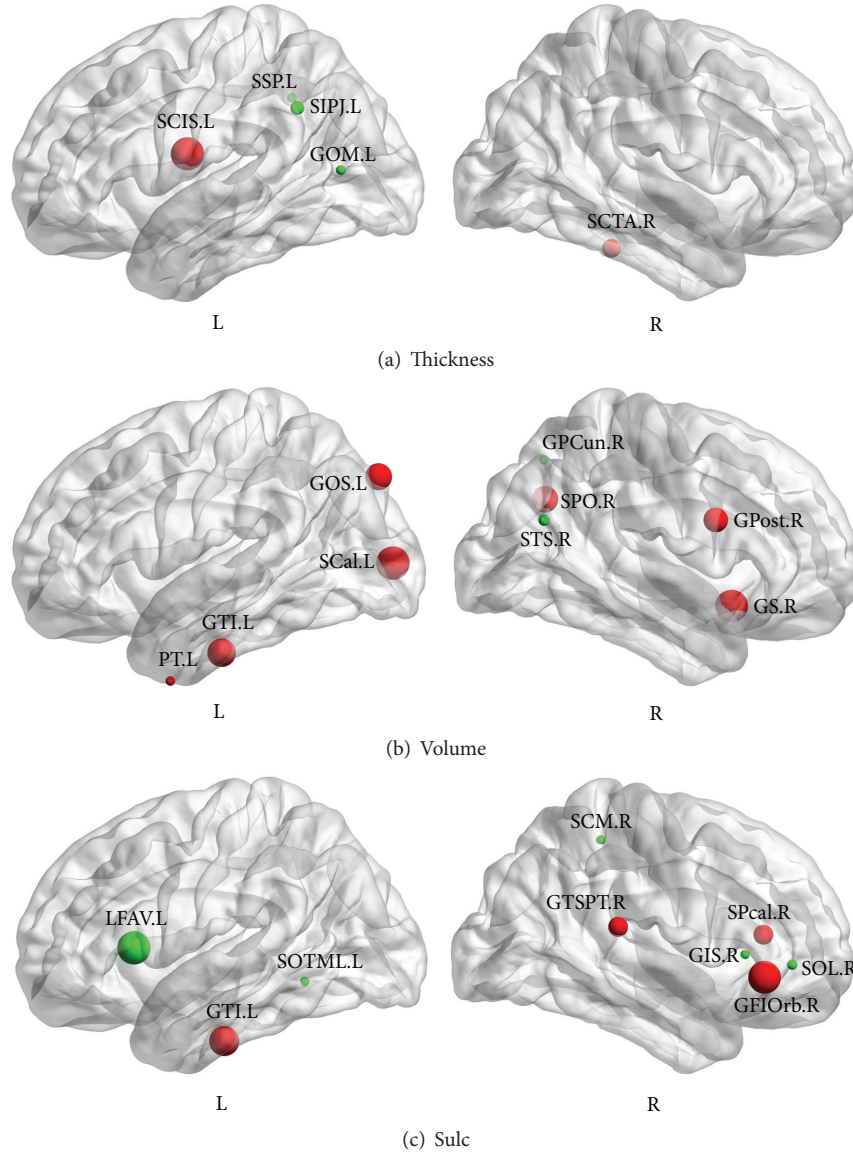


FIGURE 4: Abnormal changes in nodal betweenness centrality. The graph shows significant difference ($p < 0.05$) in betweenness between two groups. The green spheres indicate significant decreases in between-group nodal centrality. The red spheres indicate significant increases in between-group nodal centrality. (a) Abnormal changes in cortical thickness networks. (b) Abnormal changes in gray matter volume networks. (c) Abnormal changes in sulcal depth networks. Thickness, cortical thickness. Volume, gray matter volume. NC, normal controls. For the abbreviations of regions, see Table 2.

Here networks constructed by sulcal depth in aMCI with less optimal small-worldness implied abnormal structural connections between specific regions in aMCI patients.

Previous studies indicated that hubs were mainly in regions of the parietal, temporal, and frontal heteromodal association cortex (SPL, SMG, MTG, STG, IFG, and SFG) and highly connected primary motor cortex (PrCG) [45]. Hubs in this study were predominately in frontal, temporal, parietal, and insula association cortex in NC of networks based on volumetric measures. Many previous studies ignore the insula when constructing cortical network because the insula is covered by other lobes. Compared with NC, there were more hubs in aMCI involved in temporal lobe, superior

parietal lobe, cingulate cortex, precentral sulcus, callosum, and insula. In networks based on sulcal depth, hub regions in NC were compatible with previous studies of functional and structural cortical network [47]. These hub regions, which are considered to be the substrates of human cognition and consciousness, are in the association cortex that receives convergent inputs from multiple other cortical regions [12]. And in networks based on sulcal depth, hub regions in aMCI had more hubs compared with NC, which was similar to regions in networks based on volumetric measures.

Evidences from previous studies have shown the shrunk brain regions in aMCI patients located in parahippocampal gyrus, medial temporal lobe, entorhinal cortex, cingulum,

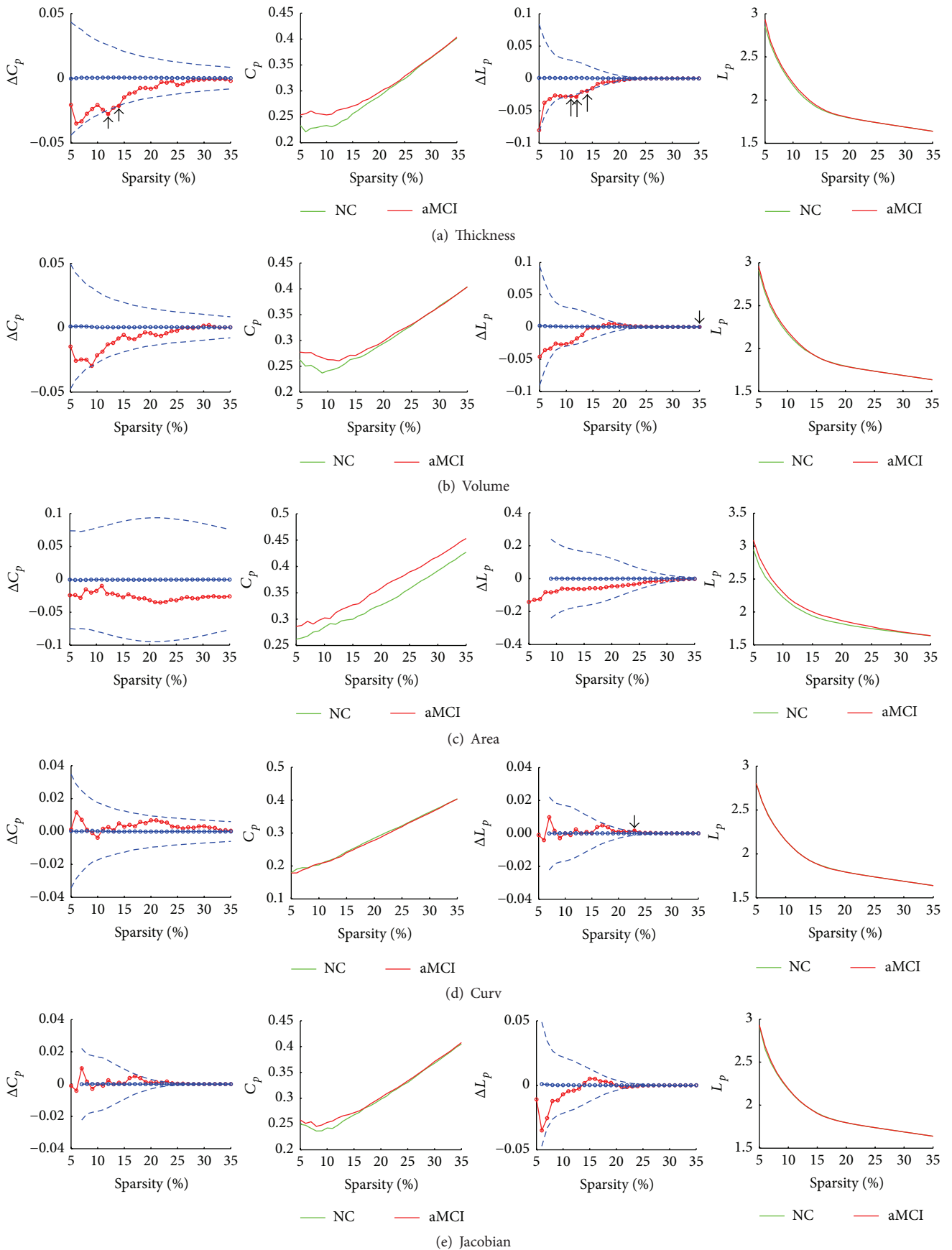


FIGURE 5: Continued.

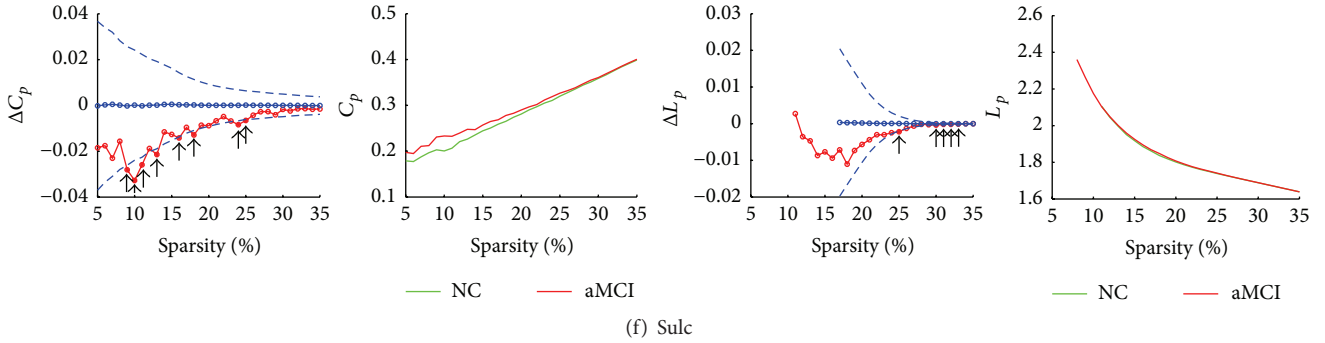


FIGURE 5: Between-group differences in clustering coefficient (C_p) and characteristic path length (L_p) of different morphological features based networks. The graph shows the differences in C_p and L_p between NC and aMCI as a function of sparsity of geometric measures networks. The blue lines represent the mean values (open circles) and 95% confidence intervals of the between-group differences obtained from 1000 permutation tests at each sparsity value. The arrows indicate significant ($p < 0.05$) difference in C_p or L_p between the two groups. (a) Between-group differences in C_p and L_p as a function of sparsity of cortical thickness networks. (b) Between-group differences in C_p and L_p as a function of sparsity of gray matter volume networks. (c) Between-group differences in C_p and L_p as a function of sparsity of surface area networks. (d) Between-group differences in C_p and L_p as a function of sparsity of mean curvature networks. (e) Between-group differences in C_p and L_p as a function of sparsity of metric distortion (Jacobian) networks. (f) Between-group differences in C_p and L_p as a function of sparsity of sulcal depth networks. Thickness, cortical thickness. Volume, gray matter volume. Area, surface area. Curv, mean curvature. Sulc, sulcal depth. NC, normal controls.

insula, and thalamus [48, 49]. Our results were partially consistent with previous studies. Abnormal changes in the temporal, occipital gyrus and cingulate sulcus in aMCI group have been reported as being related to memory performance. What is more, significantly higher nodal centrality in aMCI was considered as increased functional connectivity occurred in various brain regions [50]. This may serve as a compensatory mechanism that enables patients with aMCI to use other additional resources to maintain normal cognitive performance [51, 52]. The abnormal characteristics of the cortical networks observed in aMCI may reflect anatomical structural abnormalities. Our findings may contribute to an understanding of the cerebral organization in aMCI.

Some limitations should be addressed in the future. Firstly, several studies have demonstrated that network resolution has an effect on topological properties of human neocortex by using volumetric measures as descriptors of anatomical connectivity [10, 53, 54]. In our network analysis, we only used 148 nodes to construct the network. In the future, it is interesting to investigate the relationship between network resolution and topological properties of human neocortex by using geometric measures. Secondly, topological properties of a given network may be influenced by intrinsic features of that network, such as the number of nodes, number of connections, and degree distribution. To counteract these effects, we used random networks with the same number of nodes and edges as surrogates to normalize the corresponding graph measures. Without any correction, the small-world index cannot be used to compare the small-worldness of different empirical networks. However, random surrogates may increase the sensitivity to differences in nodes number and degrees for the commonly used small-world index [55]. The minimum spanning tree (MST) [56],

a mathematically defined and unbiased subnetwork, provides similar information about network topology as conventional graph measures. It is noted that the MST discards all loop connections that the clustering coefficient and path length in the small-world index are highly correlated. Several network characteristics such as modularity, hierarchy, and rich club cannot be interpreted with the MST. There is still no optimal method to normalize network measures. Thirdly, different thresholding may lead to different network topological organizations [47]. Notably, connectivity values often vary depending on subjects and conditions, which can result in differences in average degree when using the same threshold for all networks. In the future, it is important to study the optimal thresholding methods in constructing networks.

5. Conclusions

This work demonstrated that besides cortical thickness and gray matter volume, sulcal depth can also be used to study the topological properties of cortical networks. We found that networks based on both the volumetric measures and geometric measures showed small-world properties and properties in these networks were different from aMCI to NC. Notably, properties in cortical network constructed by sulcal depth showed significant differences between the two groups. Our results indicate that geometric measure (sulcal depth) can be used to construct network to discriminate individuals with aMCI from controls.

Conflict of Interests

The authors declare that there is no conflict of interests regarding the publication of this paper.

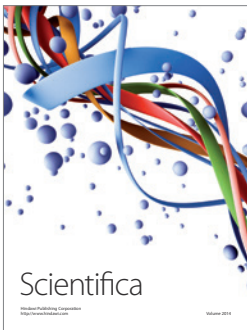
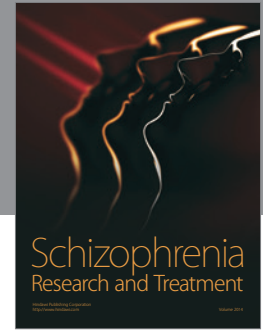
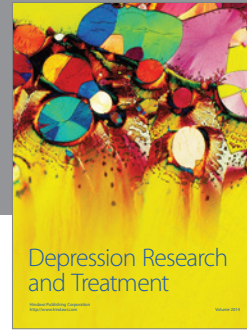
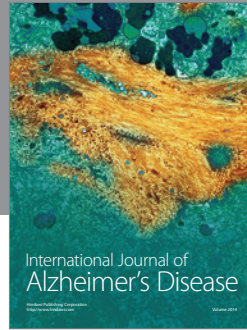
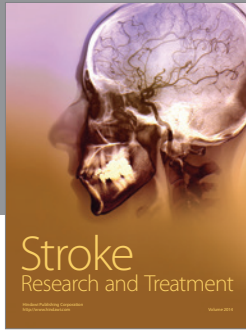
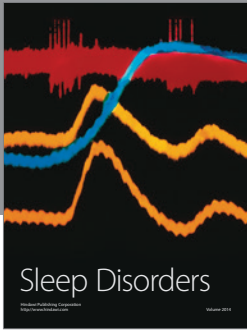
Acknowledgments

This work was supported by the National Natural Science Foundation of China (Grants nos. 31371007, 81430037, 81171403, 81301188, and 81471731), Beijing Municipal Science & Technology Commission (Grant no. Z131100006813022), Kallikrein Medical Research Program (Grant no. 201206006), and the National Key Department of Neurology funded by Chinese Health and Family Planning Committee.

References

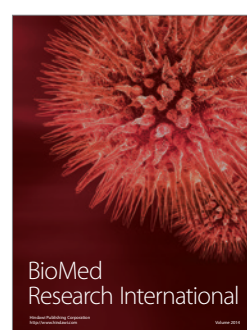
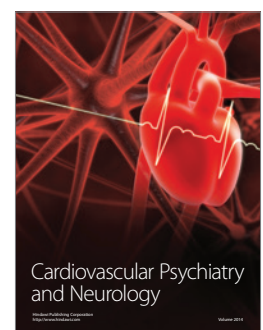
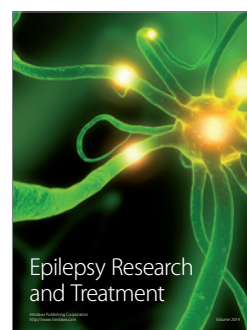
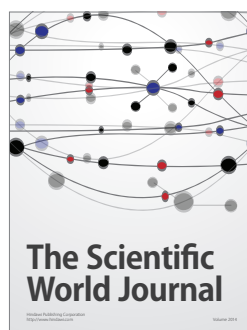
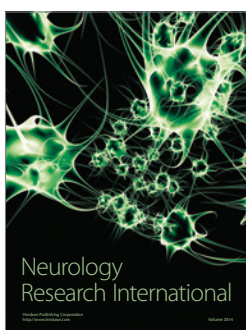
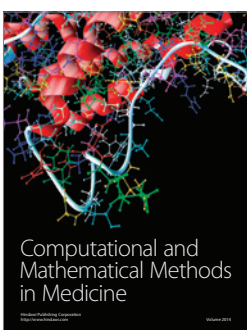
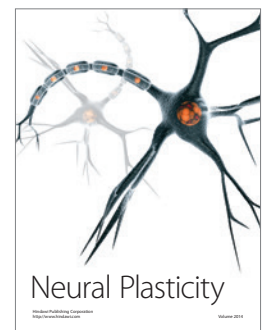
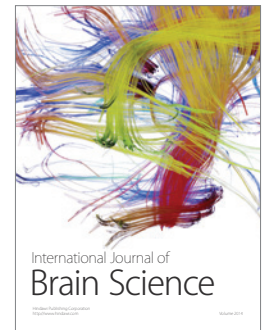
- [1] C. A. Luis, D. A. Loewenstein, A. Acevedo, W. W. Barker, and R. Duara, "Mild cognitive impairment: directions for future research," *Neurology*, vol. 61, no. 4, pp. 438–444, 2003.
- [2] R. C. Petersen, R. O. Roberts, D. S. Knopman et al., "Mild cognitive impairment: ten years later," *Archives of Neurology*, vol. 66, no. 12, pp. 1447–1455, 2009.
- [3] L. R. Clark, L. Delano-Wood, D. J. Libon et al., "Are empirically-derived subtypes of mild cognitive impairment consistent with conventional subtypes?" *Journal of the International Neuropsychological Society*, vol. 19, no. 6, pp. 635–645, 2013.
- [4] R. C. Petersen, J. E. Parisi, D. W. Dickson et al., "Neuropathologic features of amnesic mild cognitive impairment," *Archives of Neurology*, vol. 63, no. 5, pp. 665–672, 2006.
- [5] L. Wang, H. Li, Y. Liang et al., "Amnesic mild cognitive impairment: topological reorganization of the default-mode network," *Radiology*, vol. 268, no. 2, pp. 501–514, 2013.
- [6] N. Shu, Y. Liang, H. Li et al., "Disrupted topological organization in white matter structural networks in amnesic mild cognitive impairment: relationship to subtype," *Radiology*, vol. 265, no. 2, pp. 518–527, 2012.
- [7] R. A. Barton and P. H. Harvey, "Mosaic evolution of brain structure in mammals," *Nature*, vol. 405, no. 6790, pp. 1055–1058, 2000.
- [8] D. A. Clark, P. P. Mitra, and S. S.-H. Wang, "Scalable architecture in mammalian brains," *Nature*, vol. 411, no. 6834, pp. 189–193, 2001.
- [9] Y. He, Z. J. Chen, and A. C. Evans, "Small-world anatomical networks in the human brain revealed by cortical thickness from MRI," *Cerebral Cortex*, vol. 17, no. 10, pp. 2407–2419, 2007.
- [10] G. Sanabria-Diaz, L. Melie-García, Y. Iturria-Medina et al., "Surface area and cortical thickness descriptors reveal different attributes of the structural human brain networks," *NeuroImage*, vol. 50, no. 4, pp. 1497–1510, 2010.
- [11] B. M. Tijms, C. Möller, H. Vrenken et al., "Single-subject grey matter graphs in Alzheimer's disease," *PLoS ONE*, vol. 8, no. 3, Article ID e58921, 2013.
- [12] Z. Yao, Y. Zhang, L. Lin et al., "Abnormal cortical networks in mild cognitive impairment and Alzheimer's disease," *PLoS Computational Biology*, vol. 6, no. 11, Article ID e1001006, 2010.
- [13] Y. Zhou and Y. W. Lui, "Small-world properties in mild cognitive impairment and early Alzheimer's disease: a cortical thickness MRI study," *ISRN Geriatrics*, vol. 2013, Article ID 542080, 11 pages, 2013.
- [14] A. Parent, *Carpenter's Human Neuroanatomy*, Lippincott Williams & Wilkins, 1996.
- [15] K. L. Narr, R. M. Bilder, A. W. Toga et al., "Mapping cortical thickness and gray matter concentration in first episode schizophrenia," *Cerebral Cortex*, vol. 15, no. 6, pp. 708–719, 2005.
- [16] P. Rakic, "Defects of neuronal migration and the pathogenesis of cortical malformations," *Progress in Brain Research*, vol. 73, pp. 15–37, 1988.
- [17] A. C. Burggren, B. Renner, M. Jones et al., "Thickness in entorhinal and subicular cortex predicts episodic memory decline in mild cognitive impairment," *International Journal of Alzheimer's Disease*, vol. 2011, Article ID 956053, 9 pages, 2011.
- [18] L. Wang, F. C. Goldstein, E. Veledar et al., "Alterations in cortical thickness and white matter integrity in mild cognitive impairment measured by whole-brain cortical thickness mapping and diffusion tensor imaging," *American Journal of Neuroradiology*, vol. 30, no. 5, pp. 893–899, 2009.
- [19] D. C. Van Essen, "A tension-based theory of morphogenesis and compact wiring in the central nervous system," *Nature*, vol. 385, no. 6614, pp. 313–318, 1997.
- [20] G. Lohmann, D. Y. Von Cramon, and A. C. F. Colchester, "Deep sulcal landmarks provide an organizing framework for human cortical folding," *Cerebral Cortex*, vol. 18, no. 6, pp. 1415–1420, 2008.
- [21] A. Cachia, J.-F. Mangin, D. Rivière et al., "A primal sketch of the cortex mean curvature: a morphogenesis based approach to study the variability of the folding patterns," *IEEE Transactions on Medical Imaging*, vol. 22, no. 6, pp. 754–765, 2003.
- [22] C. Ecker, A. Marquand, J. Mourão-Miranda et al., "Describing the brain in autism in five dimensions—magnetic resonance imaging-assisted diagnosis of autism spectrum disorder using a multiparameter classification approach," *The Journal of Neuroscience*, vol. 30, no. 32, pp. 10612–10623, 2010.
- [23] R. C. Petersen, R. Doody, A. Kurz et al., "Current concepts in mild cognitive impairment," *Archives of Neurology*, vol. 58, no. 12, pp. 1985–1992, 2001.
- [24] R. C. Petersen, G. E. Smith, S. C. Waring, R. J. Ivnik, E. G. Tangalos, and E. Kokmen, "Mild cognitive impairment: clinical characterization and outcome," *Archives of Neurology*, vol. 56, no. 3, pp. 303–308, 1999.
- [25] R. Petersen, J. Stevens, M. Ganguli, E. Tangalos, J. Cummings, and S. DeKosky, "Practice parameter: early detection of dementia: mild cognitive impairment (an evidence-based review) report of the quality standards subcommittee of the American Academy of Neurology," *Neurology*, vol. 56, no. 9, pp. 1133–1142, 2001.
- [26] R. Petersen, *Mild Cognitive Impairment: Aging to Alzheimer's Disease*, Oxford University Press, New York, NY, USA, 2003.
- [27] J. Talairach and P. Tournoux, *Co-Planar Stereotaxic Atlas of the Human Brain. 3-Dimensional Proportional System: An Approach to Cerebral Imaging*, 1988.
- [28] F. Ségonne, A. M. Dale, E. Busa et al., "A hybrid approach to the skull stripping problem in MRI," *NeuroImage*, vol. 22, no. 3, pp. 1060–1075, 2004.
- [29] B. Fischl, D. H. Salat, E. Busa et al., "Whole brain segmentation: automated labeling of neuroanatomical structures in the human brain," *Neuron*, vol. 33, no. 3, pp. 341–355, 2002.
- [30] B. Fischl, A. van der Kouwe, C. Destrieux et al., "Automatically parcellating the human cerebral cortex," *Cerebral Cortex*, vol. 14, no. 1, pp. 11–22, 2004.
- [31] A. M. Dale, B. Fischl, and M. I. Sereno, "Cortical surface-based analysis: I. Segmentation and surface reconstruction," *NeuroImage*, vol. 9, no. 2, pp. 179–194, 1999.
- [32] B. Fischl and A. M. Dale, "Measuring the thickness of the human cerebral cortex from magnetic resonance images," *Proceedings of the National Academy of Sciences of the United States of America*, vol. 97, no. 20, pp. 11050–11055, 2000.

- [33] B. Fischl, M. I. Sereno, and A. M. Dale, "Cortical surface-based analysis: II. Inflation, flattening, and a surface-based coordinate system," *NeuroImage*, vol. 9, no. 2, pp. 195–207, 1999.
- [34] S. Li, X. Yuan, F. Pu et al., "Abnormal changes of multidimensional surface features using multivariate pattern classification in amnesic mild cognitive impairment patients," *The Journal of Neuroscience*, vol. 34, no. 32, pp. 10541–10553, 2014.
- [35] J. Peng, P. Wang, N. Zhou, and J. Zhu, "Partial correlation estimation by joint sparse regression models," *Journal of the American Statistical Association*, vol. 104, no. 486, pp. 735–746, 2009.
- [36] R. Opgen-Rhein and K. Strimmer, "Accurate ranking of differentially expressed genes by a distribution-free shrinkage approach," *Statistical Applications in Genetics and Molecular Biology*, vol. 6, no. 1, 2007.
- [37] D. J. Watts and S. H. Strogatz, "Collective dynamics of 'small-world' networks," *Nature*, vol. 393, no. 6684, pp. 440–442, 1998.
- [38] S. Achard, R. Salvador, B. Whitcher, J. Suckling, and E. Bullmore, "A resilient, low-frequency, small-world human brain functional network with highly connected association cortical hubs," *The Journal of Neuroscience*, vol. 26, no. 1, pp. 63–72, 2006.
- [39] E. Bullmore and O. Sporns, "Complex brain networks: graph theoretical analysis of structural and functional systems," *Nature Reviews Neuroscience*, vol. 10, no. 3, pp. 186–198, 2009.
- [40] S. Maslov and K. Sneppen, "Specificity and stability in topology of protein networks," *Science*, vol. 296, no. 5569, pp. 910–913, 2002.
- [41] J. D. Humphries, A. Byron, and M. J. Humphries, "Integrin ligands at a glance," *Journal of Cell Science*, vol. 119, no. 19, pp. 3901–3903, 2006.
- [42] E. T. Bullmore, J. Suckling, S. Overmeyer, S. Rabe-Hesketh, E. Taylor, and M. J. Brammer, "Global, voxel, and cluster tests, by theory and permutation, for a difference between two groups of structural mr images of the brain," *IEEE Transactions on Medical Imaging*, vol. 18, no. 1, pp. 32–42, 1999.
- [43] B. Lv, J. Li, H. He et al., "Gender consistency and difference in healthy adults revealed by cortical thickness," *NeuroImage*, vol. 53, no. 2, pp. 373–382, 2010.
- [44] W. Zhu, W. Wen, Y. He, A. Xia, K. J. Anstey, and P. Sachdev, "Changing topological patterns in normal aging using large-scale structural networks," *Neurobiology of Aging*, vol. 33, no. 5, pp. 899–913, 2012.
- [45] Y. He, Z. Chen, and A. Evans, "Structural insights into aberrant topological patterns of large-scale cortical networks in Alzheimer's disease," *Journal of Neuroscience*, vol. 28, no. 18, pp. 4756–4766, 2008.
- [46] E. Armstrong, A. Schleicher, H. Omran, M. Curtis, and K. Zilles, "The ontogeny of human gyrification," *Cerebral Cortex*, vol. 5, no. 1, pp. 56–63, 1995.
- [47] Z. Dai and Y. He, "Disrupted structural and functional brain connectomes in mild cognitive impairment and Alzheimer's disease," *Neuroscience Bulletin*, vol. 30, no. 2, pp. 217–232, 2014.
- [48] Y. Fan, N. Batmanghelich, C. M. Clark, and C. Davatzikos, "Spatial patterns of brain atrophy in MCI patients, identified via high-dimensional pattern classification, predict subsequent cognitive decline," *NeuroImage*, vol. 39, no. 4, pp. 1731–1743, 2008.
- [49] A. J. Saykin, H. A. Wishart, L. A. Rabin et al., "Older adults with cognitive complaints show brain atrophy similar to that of amnesic MCI," *Neurology*, vol. 67, no. 5, pp. 834–842, 2006.
- [50] A. L. W. Bokde, P. Lopez-Bayo, T. Meindl et al., "Functional connectivity of the fusiform gyrus during a face-matching task in subjects with mild cognitive impairment," *Brain*, vol. 129, no. 5, pp. 1113–1124, 2006.
- [51] J. L. Woodard, S. T. Grafton, J. R. Votaw, R. C. Green, M. E. Dabraski, and J. M. Hoffman, "Compensatory recruitment of neural resources during overt rehearsal of word lists in Alzheimer's disease," *Neuropsychology*, vol. 12, no. 4, pp. 491–504, 1998.
- [52] J. Pariente, S. Cole, R. Henson et al., "Alzheimer's patients engage an alternative network during a memory task," *Annals of Neurology*, vol. 58, no. 6, pp. 870–879, 2005.
- [53] R. Romero-Garcia, M. Atienza, L. H. Clemmensen, and J. L. Cantero, "Effects of network resolution on topological properties of human neocortex," *NeuroImage*, vol. 59, no. 4, pp. 3522–3532, 2012.
- [54] A. Zalesky, A. Fornito, I. H. Harding et al., "Whole-brain anatomical networks: does the choice of nodes matter?" *NeuroImage*, vol. 50, no. 3, pp. 970–983, 2010.
- [55] B. C. M. Van Wijk, C. J. Stam, and A. Daffertshofer, "Comparing brain networks of different size and connectivity density using graph theory," *PLoS ONE*, vol. 5, no. 10, Article ID e13701, 2010.
- [56] P. Tewarie, E. Van Dellen, A. Hillebrand, and C. J. Stam, "The minimum spanning tree: an unbiased method for brain network analysis," *NeuroImage*, vol. 104, pp. 177–188, 2015.



Hindawi

Submit your manuscripts at
<http://www.hindawi.com>





Differential Age-Related Changes in Structural Covariance Networks of Human Anterior and Posterior Hippocampus

Xinwei Li^{1,2}, Qionglin Li^{1,2}, Xuotong Wang^{1,2}, Deyu Li^{1,2*} and Shuyu Li^{1,2*}

¹ School of Biological Science and Medical Engineering, Beihang University, Beijing, China, ² Beijing Advanced Innovation Centre for Biomedical Engineering, Beihang University, Beijing, China

OPEN ACCESS

Edited by:

Chunhua Bian,
Nanjing University, China

Reviewed by:

Ronny P. Bartsch,
Bar-Ilan University, Israel
Paul Bogdan,
University of Southern California,
United States

*Correspondence:

Deyu Li
deyuli@buaa.edu.cn
Shuyu Li
shuyuli@buaa.edu.cn

Specialty section:

This article was submitted to
Fractal Physiology,
a section of the journal
Frontiers in Physiology

Received: 23 October 2017

Accepted: 20 April 2018

Published: 09 May 2018

Citation:

Li X, Li Q, Wang X, Li D and Li S
(2018) Differential Age-Related
Changes in Structural Covariance
Networks of Human Anterior
and Posterior Hippocampus.
Front. Physiol. 9:518.
doi: 10.3389/fphys.2018.00518

The hippocampus plays an important role in memory function relying on information interaction between distributed brain areas. The hippocampus can be divided into the anterior and posterior sections with different structure and function along its long axis. The aim of this study is to investigate the effects of normal aging on the structural covariance of the anterior hippocampus (aHPC) and the posterior hippocampus (pHPC). In this study, 240 healthy subjects aged 18–89 years were selected and subdivided into young (18–23 years), middle-aged (30–58 years), and older (61–89 years) groups. The aHPC and pHPC was divided based on the location of uncus apex in the MNI space. Then, the structural covariance networks were constructed by examining their covariance in gray matter volumes with other brain regions. Finally, the influence of age on the structural covariance of these hippocampal sections was explored. We found that the aHPC and pHPC had different structural covariance patterns, but both of them were associated with the medial temporal lobe and insula. Moreover, both increased and decreased covariances were found with the aHPC but only increased covariance was found with the pHPC with age ($p < 0.05$, family-wise error corrected). These decreased connections occurred within the default mode network, while the increased connectivity mainly occurred in other memory systems that differ from the hippocampus. This study reveals different age-related influence on the structural networks of the aHPC and pHPC, providing an essential insight into the mechanisms of the hippocampus in normal aging.

Keywords: network, structural covariance, normal aging, anterior hippocampus, posterior hippocampus, MRI

INTRODUCTION

With the population aging, understanding normal brain changes are as important as understanding demented diseases. Memory decline is a typical characteristic of normal aging. The hippocampus is considered critical in human memory and spatial navigation (Scoville and Milner, 1957; Buzsáki and Moser, 2013). Evidence suggests that hippocampal volume changes throughout the lifespan, which stays relatively stable until the age of 60 shows a sharp decline (Raz et al., 2010; Schuff et al., 2012; Fjell et al., 2013). Functional imaging studies have revealed and hypometabolism (de Leon et al., 2001; Wu et al., 2008) of the hippocampus in aging. Moreover, a reduced fractal dimension of hippocampal dynamics with age was reported (Goldberger et al., 2002; Wink et al., 2006).

The hippocampus differs in structure and function along its longitudinal axis (Poppenk et al., 2013). The anterior hippocampus (aHPC) and posterior hippocampus (pHPC) vary in pyramidal cell density (Babb et al., 1984; King et al., 2008) and have different developmental trajectories (DeMaster et al., 2014). Compared with young adults, both the aHPC and the pHPC showed volumetric atrophy in old adults (Pruessner et al., 2001; Chen et al., 2010; Rajah et al., 2010), and their rates of atrophy were different (Malykhin et al., 2008; Chen et al., 2010). Besides, an fMRI study reported the functional connectivity of the aHPC and pHPC were differentially affected in aging (Damoiseaux et al., 2016).

For structural connectivity, the structural covariance network (SCN) approach provides an effective way to characterize inter-regional structural covariance pattern of gray matter (GM) morphological properties (Mechelli et al., 2005; Modinos et al., 2009; Seeley et al., 2009; Zielinski et al., 2010; Montembeault et al., 2012; Li et al., 2013; DuPre and Spreng, 2017). The GM morphological covariance may result from direct white matter connection or neuronal co-activation (Alexander-Bloch et al., 2013). Studies have revealed a consistency among SCNs, anatomical connectivity networks, and functional connectivity networks, which provides strong support for using SCN mapping approach to assess network integrity. Age-related alteration of structural covariance in sensorimotor and cognitive networks has been found (Montembeault et al., 2012; Li et al., 2013). However, the effects of aging on the structural covariance of the aHPC and pHPC remain to be studied, which may provide insights into the hippocampal-related mechanism of aging and demented diseases.

In this study, we utilized a seed-based SCN approach to investigate the anterior and posterior hippocampal structural networks in 240 healthy subjects that were subdivided into young, middle-aged, and elderly groups. We first defined aHPC and pHPC based on the location of uncus apex in the MNI space. Then, we identified the SCNs seeding from aHPC and pHPC and compared the structural covariance differences between age groups. We expected the SCNs of the aHPC and pHPC have different patterns and were differently affected by age.

MATERIALS AND METHODS

Participants

The MRI data were obtained from the publicly available Open Access Series of Imaging Studies (OASIS) database (Marcus et al., 2007). The OASIS database consists of 416 subjects aged 18–96, including 100 mild dementia and 316 healthy subjects. Based on the age distribution of the OASIS database, we selected 240 participants from the healthy subcohort and grouped them into young (18–23 years), middle-aged (30–58 years), and elderly (61–89 years) groups, with 80 participants in each group (see **Table 1**). All the subjects are right-handed and cognitively normal, with the Mini-Mental State Examination scores (Folstein et al., 1975) above 29 and the Clinical Dementia Rating scores (Folstein et al., 1975) equal zero. The same group of subjects was used in our previous study (Li et al., 2013).

Data Acquisition

All MRI scans were performed on 1.5 Tesla Siemens scanners. For each individual, three to four T1-weighted images were acquired using a magnetization-prepared rapid gradient echo (MPRAGE) sequence with the following parameters: repetition time = 9.7 ms; echo time = 4 ms; inversion time = 20 ms; delay time = 200 ms; flip angle = 10°; matrix = 256 × 256; field of view = 256 mm; slices = 128; slice thickness = 1.25 mm. After motion corrected, the images of each subject were averaged to improve the contrast-to-noise ratio.

Image Preprocessing

We used the VBM8 toolbox¹ runs within SPM8 to implement voxel-based morphometry analysis (Ashburner and Friston, 2000) of the structural images. The acquired anatomical images were tissue classified into GM, white matter and cerebrospinal fluid images using tissue priors. Then, the segmented images were bias corrected and registered to a standard space using an affine transformation and a high-dimensional non-linear registration approach (Ashburner and Friston, 2005). Next, modulation of the segmented images was performed to correct for different individual brain size by using the non-linear registration parameters. Finally, the modulated GM segments were smoothed using an isotropic 12 mm full-width at half maximum Gaussian kernel for the structural covariance analysis.

Definition of the Hippocampal Seeds

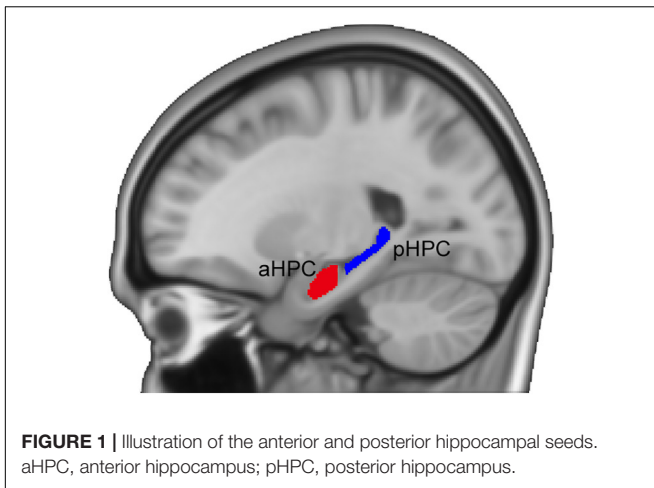
Following previous studies (Poppenk et al., 2013; Persson et al., 2014), we adopted a MNI-coordinate-based segmentation method to partition the hippocampus. The hippocampus was identified using the Harvard-Oxford subcortical structural atlas (Desikan et al., 2006) from the FSL Software Library (Smith et al., 2004). Next, the left and right hippocampi were divided into the anterior and posterior sections separately based on the location of uncus apex in the MNI space (i.e., $Y = -21$ mm) (Poppenk et al., 2013). To avoid contamination effects between the aHPC and the pHPC, we removed a 2-mm coronal slice from each of the two adjacent ends (see **Figure 1**). For each subject, we measured the mean volumes of the hippocampal subfields from the modulated GM images using the MarsBar ROI toolbox². Then a quadratic regression model was used to investigate age effects on the mean volumes of the anterior and posterior hippocampal segments. We also assessed the age-related hippocampal volumetric dispersion. To do so, for age = t , we calculated the variance of hippocampal volumes of subjects with age $\in [t-2, t+2]$ and examined its quadratic relationship with age.

¹<http://www.neuro.uni-jena.de/vbm/>

²<http://marsbar.sourceforge.net/>

TABLE 1 | Participant characteristics by age group.

| Group | Sample size (Females) | Age in years (mean ± SD) |
|-------------|-----------------------|--------------------------|
| Young | 80 (50) | 18–23 (20.66 ± 1.47) |
| Middle-aged | 80 (50) | 30–58 (47.43 ± 8.23) |
| Old | 80 (55) | 61–89 (73.75 ± 7.12) |



Structural Covariance Analysis

Four separate regression analyses were executed on the modulated GM images data to map SCNs of the bilateral aHPC and pHPC in the young group. The model fitted the target voxel GM volume Y as:

$$Y \sim \beta_0 + \beta_1(\text{Seed}) + \beta_2(\text{Gender})$$

where β_0 is the intercept term, β_1 model the relationship between the target voxel volume and the seed volume, and the Gender term was included as a nuisance variable. Total intracranial volume was not included because the modulation step already considered the brain size differences. These statistical analyses enable us to determine voxels that expressed a significant positive correlation with each seed. The criterion for significance was set at height and extent thresholds of $p < 0.05$, family-wise error (FWE) corrected for multiple comparisons. The resulting correlation maps were displayed on a standard brain template using the BrainNet Viewer (Xia et al., 2013) to allow qualitative comparisons the structural covariance patterns of hippocampal seeds.

We further assessed the influence of age on the regional structural covariance between the hippocampus and the rest brain regions by using a classic linear interaction model (Lerch et al., 2006). For any two age groups, the target voxel volume Y was modeled as follows:

$$Y \sim \beta_0 + \beta_1(\text{Seed}) + \beta_2(\text{Group}) + \beta_3(\text{Gender}) + \beta_4(\text{Group} \times \text{Seed})$$

where β_0 is the intercept term, $\beta_1 \sim \beta_4$ models the relationship between the target voxel volume and the seed volume, group term, gender term, and interaction term (group by seed), respectively. To obtain between-group differences, specific t contrasts were established to test the statistical significance of the interaction term. Clusters with height and extent thresholds set at $p < 0.05$ (FWE corrected) were considered significant.

RESULTS

Hippocampal Volume Analyses

Results for the regression analysis of anterior and posterior hippocampal mean GM volumes versus age are presented in **Figure 2**. Similar nonlinear relationship between the bilateral hippocampal volumes and age were found: the volumes slightly increased before the age of 50 and then decreased sharply (left aHPC: $R^2 = 0.187$, $p < 0.001$; right aHPC: $R^2 = 0.136$, $p < 0.001$; left pHPC: $R^2 = 0.089$, $p < 0.001$; right pHPC: $R^2 = 0.106$, $p < 0.001$). Moreover, the results suggested that the mean volume of the aHPC was larger than the pHPC, and the left hippocampal volume was slightly greater than the right side. In addition, we found the variance of the bilateral anterior hippocampal volumes has an age-related U-shaped relationship (left aHPC: $R^2 = 0.489$, $p < 0.001$; right aHPC: $R^2 = 0.666$, $p < 0.001$). Specifically, the anterior hippocampal volumes of the young and old subjects were more dispersed than the middle age. However, the variance of the posterior hippocampal volumes did not significantly relate to age (left pHPC: $R^2 = 0.015$, $p = 0.646$; right pHPC: $R^2 = 0.051$, $p = 0.215$).

Structural Covariance Networks of the Anterior and Posterior Hippocampus

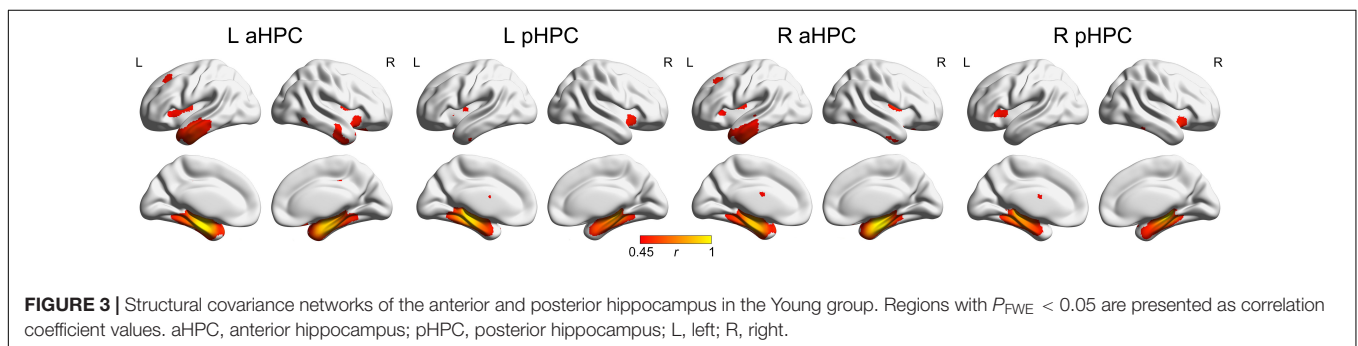
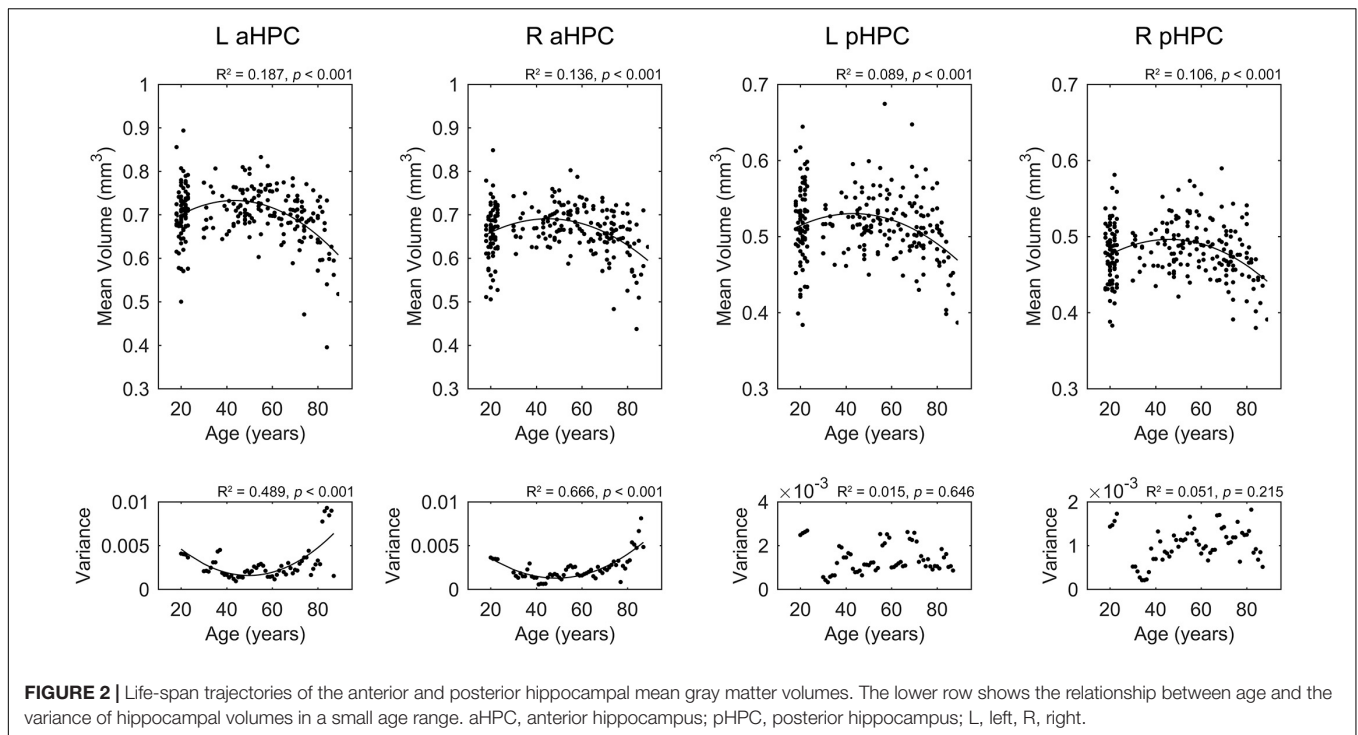
The SCNs seeding from the aHPC and pHPC in the young participants are presented in **Figure 3** ($p < 0.05$, FWE corrected). The aHPC correlated with the bilateral temporal lobe (including the superior, middle and inferior temporal, parahippocampal gyri, entorhinal cortex, fusiform and temporal pole), amygdalae, insula and posterior cingulate gyrus, orbitofrontal cortex, as well as left superior frontal gyrus. For the pHPC, its covariance maps involved the bilateral medial temporal regions (including the parahippocampal gyrus, entorhinal cortex and fusiform), amygdalae and insula. Noted that the regions correlated with both the aHPC and pHPC were mainly located in the medial temporal lobe and insula.

Age-Related Differences Within the Anterior Hippocampal Network

Within the anterior hippocampal network, significant between-group differences were only observed between the young group and the old group ($p < 0.05$, FWE corrected, **Figure 4** and **Table 2**). Specifically, the left and right aHPC showed decreased positive correlation with the ipsilateral parahippocampus and increased positive correlation with the ipsilateral amygdala in the old group relative to the young group. Moreover, compared to the young group, the left aHPC exhibited lower structural covariance with the left precuneus and greater structural covariance with the right putamen in the old group.

Age-Related Differences Within the Posterior Hippocampal Network

Within the posterior hippocampal network, only increased structural associations were found in the old group relative to younger adults (mainly the young group, $p < 0.05$, FWE corrected, see **Figure 5** and **Table 2**). For the left pHPC, the



old group exhibited significantly increased connectivity with the right caudate related to the young group. For the right pHPC, its connection with bilateral putamen was negative in the young group but was positive in the old group. Similarly, the right pHPC and temporal pole was negatively related in the middle-aged group but positively related in the old group.

DISCUSSION

Here, we studied the age-related structural covariance alterations of the aHPC and pHPC using a seed-based SCN approach. We found that the SCNs seeding from the aHPC and pHPC in the young adults were different from each other, but both of them related with the medial temporal lobe and insula. In addition, the structural covariance differences within the anterior hippocampal network were mainly between the young group and the old group with both decreased and increased positive structural associations. While compared to

the younger adults, only increased structural associations were found in the old group within the posterior hippocampal network.

We observed that the volumes of aHPC/pHPC slightly increased from young to middle age, and then decreased sharply with age. In line with this finding, several morphometric studies reported an inverted U pattern of the hippocampal volume changes with age (Walhovd et al., 2005; Li et al., 2014). As the hippocampus is important in memory processing, this pattern may partially explain the similar age-related memory change trajectory (Nyberg et al., 2012). Interestingly, we found that the anterior hippocampal volumes of the young and old subjects are more dispersed than the middle age, may pointing to stronger heterogeneity memory ability in young and old subjects. Whether this age-related dispersion due to the sample selection or other reasons requires further analysis.

Structural covariance analyses suggested that the aHPC connected with temporal lobe, amygdala, insula, and orbitofrontal cortex ($p < 0.05$, FWE corrected), which agree with

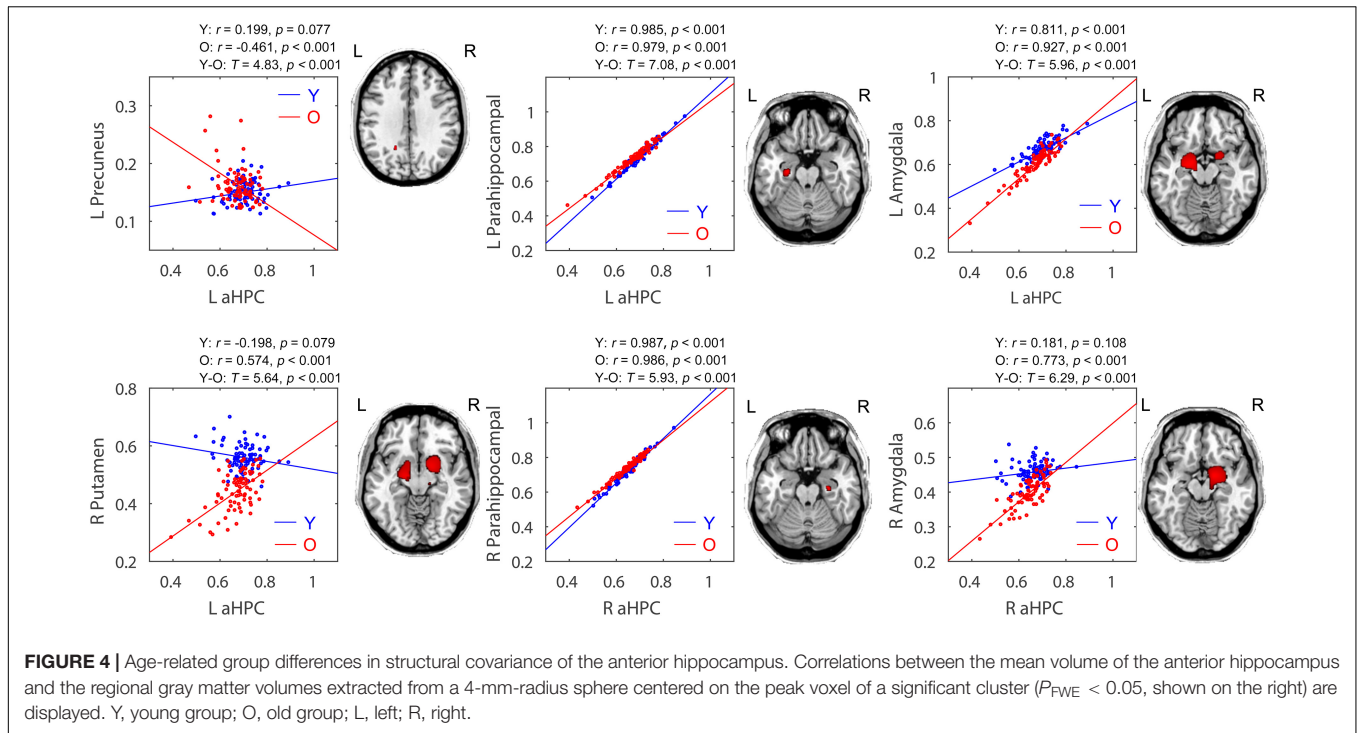


FIGURE 4 | Age-related group differences in structural covariance of the anterior hippocampus. Correlations between the mean volume of the anterior hippocampus and the regional gray matter volumes extracted from a 4-mm-radius sphere centered on the peak voxel of a significant cluster ($P_{FWE} < 0.05$, shown on the right) are displayed. Y, young group; O, old group; L, left; R, right.

TABLE 2 | Significant between-group differences in structural association between hippocampal seeds and other anatomical regions.

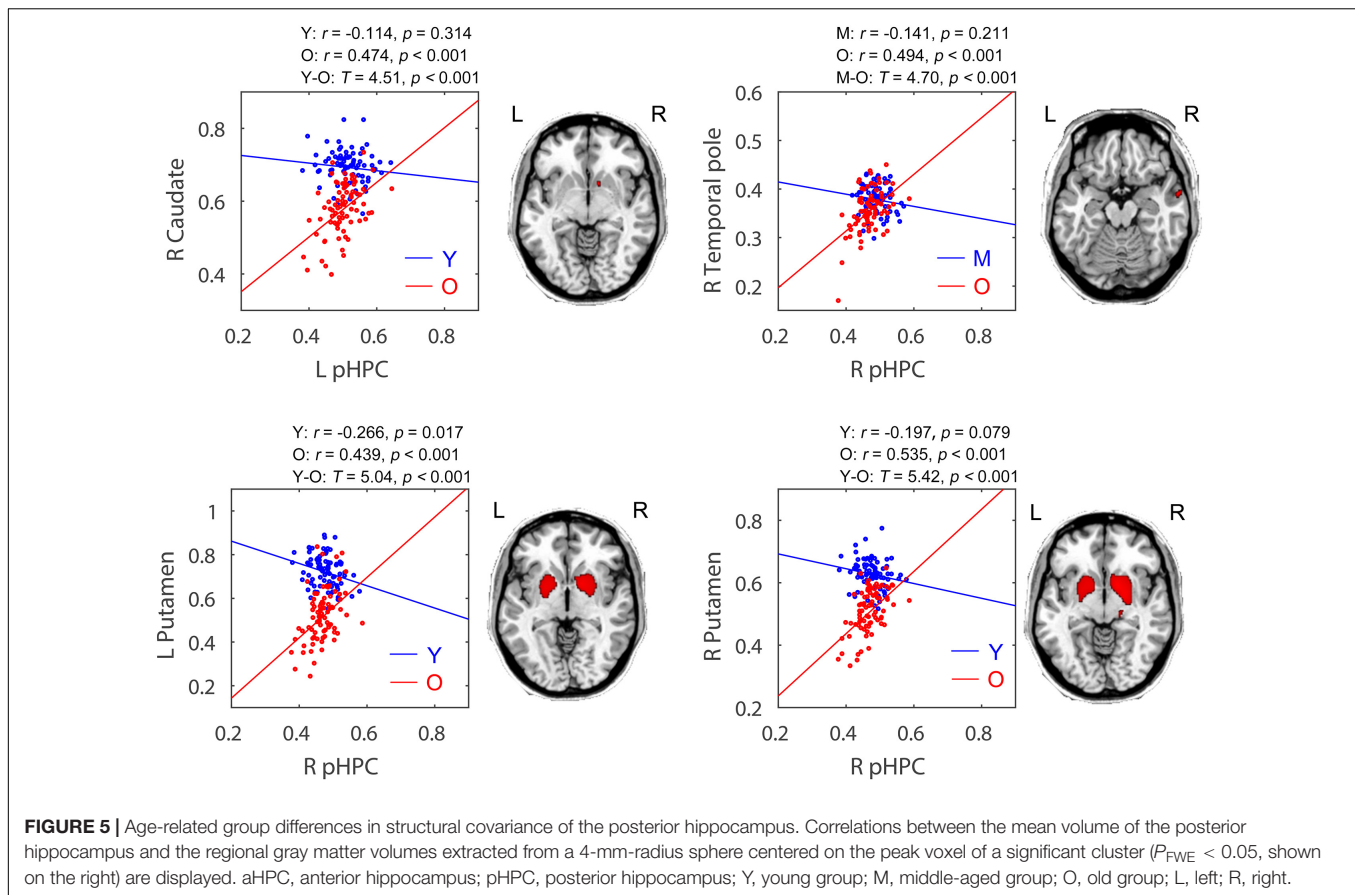
| Seed | Contrast | Anatomical region | MNI coordinates | | | Cluster size | MaxT |
|--------|----------|-------------------|-----------------|-----|-----|--------------|------|
| | | | X | Y | Z | | |
| L aHPC | Y > O | L Parahippocampus | -27 | -16 | -21 | 126 | 7.08 |
| | | L Precuneus | -18 | -52 | 31 | 18 | 4.83 |
| | Y < O | L Amygdala | -21 | -7 | -15 | 1314 | 5.96 |
| R aHPC | | R Putamen | 18 | 3 | -11 | 1096 | 5.64 |
| | Y > O | R Parahippocampus | 27 | -15 | -21 | 36 | 5.93 |
| | Y < O | R Amygdala | 16 | -1 | -14 | 1871 | 6.29 |
| L pHPC | Y < O | R Caudate | 12 | 10 | -6 | 5 | 4.51 |
| R pHPC | M < O | R Temporal pole | 62 | 0 | -17 | 29 | 4.70 |
| | | R Putamen | 14 | 8 | -6 | 1655 | 5.42 |
| | Y < O | L Putamen | -22 | 3 | -3 | 1084 | 5.04 |

$P < 0.05$, FWE corrected. Abbreviations: L, left; R, right; aHPC, anterior hippocampus; pHPC, posterior hippocampus; Y, young group; M, middle-aged group; O, old group.

previous studies (Kier et al., 2004; Smith et al., 2009; Catenoix et al., 2011). And the pHPC was covariant with medial temporal amygdala, and insula ($p < 0.05$, FWE corrected) showing consistent connections with previous studies by using fMRI and tractography (Kahn et al., 2008; Poppenk and Moscovitch, 2011; Poppenk et al., 2013). The common related regions with both aHPC and pHPC were mainly located in the medial temporal lobe where the hippocampus located.

Age-related decrements in structural covariance were observed in the aHPC-related SCNs ($p < 0.05$, FWE corrected). In particular, the parahippocampal gyrus and precuneus showed reduced association with the aHPC seed in old adults relative to young adults. The parahippocampal gyrus is considered as a mediator between the cortical DMN subsystem and the

hippocampus (Ward et al., 2014), and the integrity of the cortico-parahippocampus-hippocampus circuit is important for learning and episodic memory (Witter et al., 2000; Van Strien et al., 2009). Therefore, the weakened parahippocampus-hippocampus connection may lead to memory deficits in normal elderly, and result in decreased structural covariance between the hippocampus and cortical regions, such as the precuneus found in this study. Besides, the decreased connectivity between the precuneus and hippocampus might result from very early beta-amyloid deposition of the precuneus in elderly subjects (Sheline et al., 2010). The abnormal synaptic activity caused by amyloid deposition might disrupt cortico-hippocampal connectivity, which then results in hippocampal atrophy (Mormino et al., 2009).



Note that the parahippocampal gyrus, precuneus, and hippocampus are all components of DMN (Andrews-Hanna et al., 2014). Thus, our findings may indicate that aging is associated with decreased structural covariance within the DMN, which is in keeping with observations from previous SCN studies (Montembeault et al., 2012; Li et al., 2013; Spreng and Turner, 2013). A previous study reported decreased fractal complexity in DMN with age using multifractal analysis of fMRI series (Ni et al., 2014). Moreover, aging-related decrements in functional connectivity (Damoiseaux et al., 2008; Tomasi and Volkow, 2012) and white matter integrity (Damoiseaux et al., 2009; Brown et al., 2015) of DMN were also reported. Since DMN is known to play a role in episodic memory processing (Greicius et al., 2004, 2009), its decreased integrity could underlie memory impairment in senior populations (Salami et al., 2014).

Additionally, our data suggest that the influence of age on the structural connectivity between the hippocampus and cortical DMN nodes may be limited to the anterior portion of the hippocampus. Similarly, Salami et al. (2014) revealed reduced functional connectivity between the cortical DMN subsystems and more anteriorly located hippocampus with advancing age. Several fMRI studies have demonstrated the aHPC as part of DMN was engaged in episodic memory (autobiographical memory) processing (Zeidman and Maguire, 2016). However, some studies found no age-related differences

for the connectivity between the aHPC and DMN regions (Koch et al., 2010; Damoiseaux et al., 2016), while others reported lower connectivity between the pHPC and DMN regions in older adults (Andrews-Hanna et al., 2007; Damoiseaux et al., 2016). These discrepancies may be due to methodological differences, notably in the type of measurements and sample characteristics, which should be further investigated.

Moreover, age-related increments in structural covariance were observed in both the aHPC- and pHPC-related SCNs ($p < 0.05$, FWE corrected). Particularly, compared to young adults, the putamen and amygdala showed increased associations within the aHPC-related SCNs in old adults. Within the pHPC-related SCNs, the putamen, caudate, and temporal pole showed increased associations in old adults relative to younger adults. The putamen and caudate form the dorsal striatum. In fact, the hippocampus, dorsal striatum, and amygdala belong to different memory systems and play different roles in information acquisition (McDonald and White, 1993). The dorsal striatum and hippocampus cooperate to support episodic memory function (Sadeh et al., 2011), while the amygdala plays a role in regulating these two memory systems (Packard and Teather, 1998). We speculated that the age-related increment in hippocampal structural covariance may reflect the compensatory mechanism or dedifferentiation effects of the brain memory systems during aging (Dennis and Cabeza, 2011; Oedekoven et al., 2015).

The greater structural covariance between the hippocampus and dorsal striatum (caudate-putamen) in older adults may also be related to non-optimal dopamine processing. The CA1 area of the hippocampus receives dopaminergic modulation from the ventral tegmental area, which plays a vital role in synaptic plasticity of the hippocampus (Lisman and Grace, 2005). But the ventral tegmental area suffers from dopamine neurons loss (Siddiqi et al., 1999) and reduced dopamine transporter function (Salvatore et al., 2003) with age. However, the dorsal striatum, another area in the dopamine system, increases its dopamine synthesis capacity in aging (Braskie et al., 2008). Thus, the increased connections between the hippocampus and dorsal striatum during aging suggest compensation for deficits in the ventral tegmental area, which may represent non-optimal dopamine system functioning.

The SCN method used in this study provides an effective way to construct brain networks from medical images, which complements the signal analysis methods (Liu et al., 2015). However, since aging is not only characterized by brain deficits but also decline in multiple organ functions, it is interesting to utilize the integrative approaches within the new field of network physiology to study the effects of aging on brain–brain or brain–organ networks in future (Bashan et al., 2012; Bartsch et al., 2015; Ivanov et al., 2016). In addition, it is worth noting that brain networks have a fractal property of hierarchical modularity, which confers robustness of network function (Bullmore and Sporns, 2012). Future studies using fractal analysis approaches (Meunier et al., 2010; Xue and Bogdan, 2017) to study the

complexity and heterogeneity of hippocampal networks could advance our understanding of the brain in normal aging.

AUTHOR CONTRIBUTIONS

XL designed and performed the experiments, analyzed the data, and drafted the manuscript. QL and XW helped to analyze the data and to draft the manuscript. DL and SL contributed to the study design, coordination, and final approval of the manuscript. All authors read and approved this version to be published.

FUNDING

This work was supported by the National Natural Science Foundation of China (Grant Nos. 81622025 and 81471731), the Fundamental Research Funds for the Central Universities (Grant No. YWF-17-BJ-J-11), the Innovation Foundation of BUAA for Ph.D. Students, and Academic Excellence Foundation of BUAA for Ph.D. Students. The OASIS project was supported by the NIH Grant Nos. P50 AG05681, P01 AG03991, R01 AG021910, P50 MH071616, U24 RR021382, and R01 MH56584.

ACKNOWLEDGMENTS

The authors would like to thank the OASIS project for making the MRI data freely available.

REFERENCES

- Alexander-Bloch, A., Giedd, J. N., and Bullmore, E. (2013). Imaging structural co-variance between human brain regions. *Nat. Rev. Neurosci.* 14, 322–336. doi: 10.1038/nrn3465
- Andrews-Hanna, J. R., Snyder, A. Z., Vincent, J. L., Lustig, C., Head, D., Raichle, M. E., et al. (2007). Disruption of large-scale brain systems in advanced aging. *Neuron* 56, 924–935. doi: 10.1016/j.neuron.2007.10.038
- Andrews-Hanna, J. R., Smallwood, J., and Spreng, R. N. (2014). The default network and self-generated thought: component processes, dynamic control, and clinical relevance. *Ann. N. Y. Acad. Sci.* 1316, 29–52. doi: 10.1111/nyas.12360
- Ashburner, J., and Friston, K. J. (2000). Voxel-based morphometry—the methods. *Neuroimage* 11, 805–821. doi: 10.1006/nimg.2000.0582
- Ashburner, J., and Friston, K. J. (2005). Unified segmentation. *Neuroimage* 26, 839–851. doi: 10.1016/j.neuroimage.2005.02.018
- Babb, T. L., Lieb, J. P., Brown, W. J., Pretorius, J., and Crandall, P. H. (1984). Distribution of pyramidal cell density and hyperexcitability in the epileptic human hippocampal formation. *Epilepsia* 25, 721–728. doi: 10.1111/j.1528-1157.1984.tb03483.x
- Bartsch, R. P., Liu, K. K., Bashan, A., and Ivanov, P. C. (2015). Network physiology: how organ systems dynamically interact. *PLoS One* 10:e0142143. doi: 10.1371/journal.pone.0142143
- Bashan, A., Bartsch, R. P., Kantelhardt, J. W., Havlin, S., and Ivanov, P. C. (2012). Network physiology reveals relations between network topology and physiological function. *Nat. Commun.* 3:702. doi: 10.1038/ncomms1705
- Braskie, M. N., Wilcox, C. E., Landau, S. M., O'neil, J. P., Baker, S. L., Madison, C. M., et al. (2008). Relationship of striatal dopamine synthesis capacity to age and cognition. *J. Neurosci.* 28, 14320–14328. doi: 10.1523/JNEUROSCI.3729-08.2008
- Brown, C. A., Hakun, J. G., Zhu, Z. D., Johnson, N. F., and Gold, B. T. (2015). White matter microstructure contributes to age-related declines in task-induced deactivation of the default mode network. *Front. Aging Neurosci.* 7:194. doi: 10.3389/fnagi.2015.00194
- Bullmore, E., and Sporns, O. (2012). The economy of brain network organization. *Nat. Rev. Neurosci.* 13, 336–349. doi: 10.1038/nrn3214
- Buzsáki, G., and Moser, E. I. (2013). Memory, navigation and theta rhythm in the hippocampal-entorhinal system. *Nat. Neurosci.* 16, 130–138. doi: 10.1038/nn.3304
- Catenoix, H., Magnin, M., Manguiere, F., and Rylvlin, P. (2011). Evoked potential study of hippocampal efferent projections in the human brain. *Clin. Neurophysiol.* 122, 2488–2497. doi: 10.1016/j.clinph.2011.05.007
- Chen, K. H., Chuah, L. Y., Sim, S. K., and Chee, M. W. (2010). Hippocampal region-specific contributions to memory performance in normal elderly. *Brain Cogn.* 72, 400–407. doi: 10.1016/j.bandc.2009.11.007
- Damoiseaux, J. S., Beckmann, C. F., Arigita, E. J., Barkhof, F., Scheltens, P., Stam, C. J., et al. (2008). Reduced resting-state brain activity in the “default network” in normal aging. *Cereb. Cortex* 18, 1856–1864. doi: 10.1093/cercor/bhm207
- Damoiseaux, J. S., Smith, S. M., Witter, M. P., Sanz-Arigita, E. J., Barkhof, F., Scheltens, P., et al. (2009). White matter tract integrity in aging and Alzheimer's disease. *Hum. Brain Mapp.* 30, 1051–1059. doi: 10.1002/hbm.20563
- Damoiseaux, J. S., Viviano, R. P., Yuan, P., and Raz, N. (2016). Differential effect of age on posterior and anterior hippocampal functional connectivity. *Neuroimage* 133, 468–476. doi: 10.1016/j.neuroimage.2016.03.047
- de Leon, M. J., Convit, A., Wolf, O. T., Tarshish, C. T., DeSanti, S., Rusinek, H., et al. (2001). Prediction of cognitive decline in normal elderly subjects with 2-[18F] fluoro-2-deoxy-D-glucose/positron-emission tomography (FDG/PET). *Proc. Natl. Acad. Sci. U.S.A.* 98, 10966–10971. doi: 10.1073/pnas.191044198
- DeMaster, D., Pathman, T., Lee, J. K., and Ghetti, S. (2014). Structural Development of the Hippocampus and Episodic Memory: Developmental Differences Along

- the Anterior/Posterior Axis. *Cereb. Cortex* 24, 3036–3045. doi: 10.1093/cercor/bht160
- Dennis, N. A., and Cabeza, R. (2011). Age-related dedifferentiation of learning systems: an fMRI study of implicit and explicit learning. *Neurobiol. Aging* 32, 2318.e17–30. doi: 10.1016/j.neurobiolaging.2010.04.004
- Desikan, R. S., Ségonne, F., Fischl, B., Quinn, B. T., Dickerson, B. C., Blacker, D., et al. (2006). An automated labeling system for subdividing the human cerebral cortex on MRI scans into gyral based regions of interest. *Neuroimage* 31, 968–980. doi: 10.1016/j.neuroimage.2006.01.021
- DuPre, E., and Spreng, R. N. (2017). Structural covariance networks across the lifespan, from 6–94 years of age. *Netw. Neurosci.* 1, 302–323.
- Fjell, A. M., Westlye, L. T., Grydeland, H., Amlien, I., Espeseth, T., Reinvang, I., et al. (2013). Critical ages in the life course of the adult brain: nonlinear subcortical aging. *Neurobiol. Aging* 34, 2239–2247. doi: 10.1016/j.neurobiolaging.2013.04.006
- Folstein, M. F., Folstein, S. E., and Mchugh, P. R. (1975). “Mini-mental state”: a practical method for grading the cognitive state of patients for the clinician. *J. Psychiatr. Res.* 12, 189–198. doi: 10.1016/0022-3956(75)90026-6
- Goldberger, A. L., Amaral, L. A., Hausdorff, J. M., Ivanov, P. C., Peng, C.-K., and Stanley, H. E. (2002). Fractal dynamics in physiology: alterations with disease and aging. *Proc. Natl. Acad. Sci. U.S.A.* 99, 2466–2472. doi: 10.1073/pnas.012579499
- Greicius, M. D., Srivastava, G., Reiss, A. L., and Menon, V. (2004). Default-mode network activity distinguishes Alzheimer’s disease from healthy aging: evidence from functional MRI. *Proc. Natl. Acad. Sci. U.S.A.* 101, 4637–4642. doi: 10.1073/pnas.0308627101
- Greicius, M. D., Supekar, K., Menon, V., and Dougherty, R. F. (2009). Resting-state functional connectivity reflects structural connectivity in the default mode network. *Cereb. Cortex* 19, 72–78. doi: 10.1093/cercor/bhn059
- Ivanov, P. C., Liu, K. K., and Bartsch, R. P. (2016). Focus on the emerging new fields of network physiology and network medicine. *N. J. Phys.* 18:100201. doi: 10.1111/ede.12187
- Kahn, I., Andrews-Hanna, J. R., Vincent, J. L., Snyder, A. Z., and Buckner, R. L. (2008). Distinct cortical anatomy linked to subregions of the medial temporal lobe revealed by intrinsic functional connectivity. *J. Neurophysiol.* 100, 129–139. doi: 10.1152/jn.00077.2008
- Kier, E. L., Staib, L. H., Davis, L. M., and Bronen, R. A. (2004). MR imaging of the temporal stem: anatomic dissection tractography of the uncinate fasciculus, inferior occipitofrontal fasciculus, and Meyer’s loop of the optic radiation. *Am. J. Neuroradiol.* 25, 677–691.
- King, K. G., Glodzik, L., Liu, S., Babb, J. S., De Leon, M. J., and Gonen, O. (2008). Anteroposterior hippocampal metabolic heterogeneity: three-dimensional multivoxel proton 1H MR spectroscopic imaging—initial findings. *Radiology* 249, 242–250. doi: 10.1148/radiol.2491071500
- Koch, W., Teipel, S., Mueller, S., Buerger, K., Bokde, A. L., Hampel, H., et al. (2010). Effects of aging on default mode network activity in resting state fMRI: does the method of analysis matter? *Neuroimage* 51, 280–287. doi: 10.1016/j.neuroimage.2009.12.008
- Lerch, J. P., Worsley, K., Shaw, W. P., Greenstein, D. K., Lenroot, R. K., Giedd, J., et al. (2006). Mapping anatomical correlations across cerebral cortex (MACACC) using cortical thickness from MRI. *Neuroimage* 31, 993–1003. doi: 10.1016/j.neuroimage.2006.01.042
- Li, W., Wu, B., Batrachenko, A., Bancroft-Wu, V., Morey, R. A., Shashi, V., et al. (2014). Differential developmental trajectories of magnetic susceptibility in human brain gray and white matter over the lifespan. *Hum. Brain Mapp.* 35, 2698–2713. doi: 10.1002/hbm.22360
- Li, X., Pu, F., Fan, Y., Niu, H., Li, S., and Li, D. (2013). Age-related changes in brain structural covariance networks. *Front. Hum. Neurosci.* 7:98. doi: 10.3389/fnhum.2013.00098
- Lisman, J. E., and Grace, A. A. (2005). The hippocampal-VTA loop: controlling the entry of information into long-term memory. *Neuron* 46, 703–713. doi: 10.1016/j.neuron.2005.05.002
- Liu, K. K., Bartsch, R. P., Lin, A., Mantegna, R. N., and Ivanov, P. C. (2015). Plasticity of brain wave network interactions and evolution across physiologic states. *Front. Neural Circ.* 9:62. doi: 10.3389/fncir.2015.00062
- Malykhin, N. V., Bouchard, T. P., Camicioli, R., and Coupland, N. J. (2008). Aging hippocampus and amygdala. *Neuroreport* 19, 543–547. doi: 10.1097/WNR.0b013e3282f8b18c
- Marcus, D. S., Wang, T. H., Parker, J., Csernansky, J. G., Morris, J. C., and Buckner, R. L. (2007). Open Access Series of Imaging Studies (OASIS): cross-sectional MRI data in young, middle aged, nondemented, and demented older adults. *J. Cogn. Neurosci.* 19, 1498–1507. doi: 10.1162/jocn.2007.19.9.1498
- McDonald, R. J., and White, N. M. (1993). A triple dissociation of memory systems: hippocampus, amygdala, and dorsal striatum. *Behav. Neurosci.* 107, 3–22. doi: 10.1037/0735-7044.107.1.3
- Mechelli, A., Friston, K. J., Frackowiak, R. S., and Price, C. J. (2005). Structural covariance in the human cortex. *J. Neurosci.* 25, 8303–8310. doi: 10.1523/JNEUROSCI.0357-05.2005
- Meunier, D., Lambiotte, R., and Bullmore, E. T. (2010). Modular and hierarchically modular organization of brain networks. *Front. Neuroscience* 4:200. doi: 10.3389/fnins.2010.00200
- Modinos, G., Vercammen, A., Mechelli, A., Knegeting, H., Mcguire, P. K., and Aleman, A. (2009). Structural covariance in the hallucinating brain: a voxel-based morphometry study. *J. Psychiatry Neurosci.* 34, 465–469.
- Montembeault, M., Joubert, S., Doyon, J., Carrier, J., Gagnon, J. F., Monchi, O., et al. (2012). The impact of aging on gray matter structural covariance networks. *Neuroimage* 63, 754–759. doi: 10.1016/j.neuroimage.2012.06.052
- Mormino, E., Kluth, J., Madison, C., Rabinovici, G., Baker, S., Miller, B., et al. (2009). Episodic memory loss is related to hippocampal-mediated β -amyloid deposition in elderly subjects. *Brain* 132, 1310–1323. doi: 10.1093/brain/awn320
- Ni, H., Huang, X., Ning, X., Huo, C., Liu, T., and Ben, D. (2014). Multifractal analysis of resting state fMRI series in default mode network: age and gender effects. *Chin. Sci. Bull.* 59, 3107–3113. doi: 10.1007/s11434-014-0355-x
- Nyberg, L., Lövdén, M., Riklund, K., Lindenberger, U., and Bäckman, L. (2012). Memory aging and brain maintenance. *Trends Cogn. Sci.* 16, 292–305. doi: 10.1016/j.tics.2012.04.005
- Oedekoven, C. S., Jansen, A., Keidel, J. L., Kircher, T., and Leube, D. (2015). The influence of age and mild cognitive impairment on associative memory performance and underlying brain networks. *Brain Imaging Behav.* 9, 776–789. doi: 10.1007/s11682-014-9335-7
- Packard, M. G., and Teather, L. A. (1998). Amygdala modulation of multiple memory systems: hippocampus and caudate-putamen. *Neurobiol. Learn. Mem.* 69, 163–203. doi: 10.1006/nlme.1997.3815
- Persson, J., Spreng, R. N., Turner, G., Herlitz, A., Morell, A., Stening, E., et al. (2014). Sex differences in volume and structural covariance of the anterior and posterior hippocampus. *Neuroimage* 99, 215–225. doi: 10.1016/j.neuroimage.2014.05.038
- Poppenk, J., Evensmoen, H. R., Moscovitch, M., and Nadel, L. (2013). Long-axis specialization of the human hippocampus. *Trends Cogn. Sci.* 17, 230–240. doi: 10.1016/j.tics.2013.03.005
- Poppenk, J., and Moscovitch, M. (2011). A hippocampal marker of recollection memory ability among healthy young adults: contributions of posterior and anterior segments. *Neuron* 72, 931–937. doi: 10.1016/j.neuron.2011.10.014
- Pruessner, J., Collins, D., Pruessner, M., and Evans, A. (2001). Age and gender predict volume decline in the anterior and posterior hippocampus in early adulthood. *J. Neurosci.* 21, 194–200. doi: 10.1523/JNEUROSCI.21-01-00194.2001
- Rajah, M. N., Kromas, M., Han, J. E., and Pruessner, J. C. (2010). Group differences in anterior hippocampal volume and in the retrieval of spatial and temporal context memory in healthy young versus older adults. *Neuropsychologia* 48, 4020–4030. doi: 10.1016/j.neuropsychologia.2010.10.010
- Raz, N., Ghisletta, P., Rodrigue, K. M., Kennedy, K. M., and Lindenberger, U. (2010). Trajectories of brain aging in middle-aged and older adults: regional and individual differences. *Neuroimage* 51, 501–511. doi: 10.1016/j.neuroimage.2010.03.020
- Sadeh, T., Shohamy, D., Levy, D. R., Reggev, N., and Maril, A. (2011). Cooperation between the hippocampus and the striatum during episodic encoding. *J. Cogn. Neurosci.* 23, 1597–1608. doi: 10.1162/jocn.2010.21549
- Salami, A., Pudas, S., and Nyberg, L. (2014). Elevated hippocampal resting-state connectivity underlies deficient neurocognitive function in aging. *Proc. Natl. Acad. Sci. U.S.A.* 111, 17654–17659. doi: 10.1073/pnas.1410233111
- Salvatore, M. F., Apparsundaram, S., and Gerhardt, G. A. (2003). Decreased plasma membrane expression of striatal dopamine transporter in aging. *Neurobiol. Aging* 24, 1147–1154. doi: 10.1016/S0197-4580(03)00129-5
- Schuff, N., Tosun, D., Insel, P. S., Chiang, G. C., Truran, D., Aisen, P. S., et al. (2012). Nonlinear time course of brain volume loss in cognitively normal and

- impaired elders. *Neurobiol. Aging* 33, 845–855. doi: 10.1016/j.neurobiolaging.2010.07.012
- Scoville, W. B., and Milner, B. (1957). Loss of recent memory after bilateral hippocampal lesions. *J. Neurol. Neurosurg. Psychiatry* 20, 11–21. doi: 10.1136/jnnp.20.1.11
- Seeley, W. W., Crawford, R. K., Zhou, J., Miller, B. L., and Greicius, M. D. (2009). Neurodegenerative diseases target large-scale human brain networks. *Neuron* 62, 42–52. doi: 10.1016/j.neuron.2009.03.024
- Sheline, Y. I., Raichle, M. E., Snyder, A. Z., Morris, J. C., Head, D., Wang, S., et al. (2010). Amyloid plaques disrupt resting state default mode network connectivity in cognitively normal elderly. *Biol. Psychiatry* 67, 584–587. doi: 10.1016/j.biopsych.2009.08.024
- Siddiqi, Z., Kemper, T. L., and Killiany, R. (1999). Age-related neuronal loss from the substantia nigra-pars compacta and ventral tegmental area of the rhesus monkey. *J. Neuropathol. Exp. Neurol.* 58, 959–971. doi: 10.1097/00005072-199909000-00006
- Smith, C. D., Lori, N. F., Akbudak, E., Sorar, E., Gulpepe, E., Shimony, J. S., et al. (2009). MRI diffusion tensor tracking of a new amygdalo-fusiform and hippocampo-fusiform pathway system in humans. *J. Magn. Reson. Imaging* 29, 1248–1261. doi: 10.1002/jmri.21692
- Smith, S. M., Jenkinson, M., Woolrich, M. W., Beckmann, C. F., Behrens, T. E., Johansen-Berg, H., et al. (2004). Advances in functional and structural MR image analysis and implementation as FSL. *Neuroimage* 23, S208–S219. doi: 10.1016/j.neuroimage.2004.07.051
- Spreng, R. N., and Turner, G. R. (2013). Structural covariance of the default network in healthy and pathological aging. *J. Neurosci.* 33, 15226–15234. doi: 10.1523/JNEUROSCI.2261-13.2013
- Tomasi, D., and Volkow, N. D. (2012). Aging and functional brain networks. *Mol. Psychiatry* 17, 471–558. doi: 10.1038/mp.2011.81
- Van Strien, N., Cappaert, N., and Witter, M. (2009). The anatomy of memory: an interactive overview of the parahippocampal–hippocampal network. *Nat. Rev. Neurosci.* 10, 272–282. doi: 10.1038/nrn2614
- Walhovd, K. B., Fjell, A. M., Reinvang, I., Lundervold, A., Dale, A. M., Eilertsen, D. E., et al. (2005). Effects of age on volumes of cortex, white matter and subcortical structures. *Neurobiol. Aging* 26, 1261–1270. doi: 10.1016/j.neurobiolaging.2005.05.020
- Ward, A. M., Schultz, A. P., Huijbers, W., Van Dijk, K. R., Hedden, T., and Sperling, R. A. (2014). The parahippocampal gyrus links the default-mode cortical network with the medial temporal lobe memory system. *Hum. Brain Mapp.* 35, 1061–1073. doi: 10.1002/hbm.22234
- Wink, A. M., Bernard, F., Salvador, R., Bullmore, E., and Suckling, J. (2006). Age and cholinergic effects on hemodynamics and functional coherence of human hippocampus. *Neurobiol. Aging* 27, 1395–1404. doi: 10.1016/j.neurobiolaging.2005.08.011
- Witter, M. P., Naber, P. A., Van Haeften, T., Machielsen, W. C., Rombouts, S. A., Barkhof, F., et al. (2000). Cortico-hippocampal communication by way of parallel parahippocampal-subicular pathways. *Hippocampus* 10, 398–410. doi: 10.1002/1098-1063(2000)10:4<398::AID-HIPO6>3.0.CO;2-K
- Wu, W., Brickman, A. M., Luchsinger, J., Ferrazzano, P., Pichiule, P., Yoshita, M., et al. (2008). The brain in the age of old: the hippocampal formation is targeted differentially by diseases of late life. *Ann. Neurol.* 64, 698–706. doi: 10.1002/ana.21557
- Xia, M., Wang, J., and He, Y. (2013). BrainNet viewer: a network visualization tool for human brain connectomics. *PLoS One* 8:e68910. doi: 10.1371/journal.pone.0068910
- Xue, Y., and Bogdan, P. (2017). Reliable multi-fractal characterization of weighted complex networks: algorithms and implications. *Sci. Rep.* 7:7487. doi: 10.1038/s41598-017-07209-5
- Zeidman, P., and Maguire, E. A. (2016). Anterior hippocampus: the anatomy of perception, imagination and episodic memory. *Nat. Rev. Neurosci.* 17, 173–182. doi: 10.1038/nrn.2015.24
- Zielinski, B. A., Gennatas, E. D., Zhou, J., and Seeley, W. W. (2010). Network-level structural covariance in the developing brain. *Proc. Natl. Acad. Sci. U.S.A.* 107, 18191–18196. doi: 10.1073/pnas.1003109107
- Conflict of Interest Statement:** The authors declare that the research was conducted in the absence of any commercial or financial relationships that could be construed as a potential conflict of interest.
- Copyright © 2018 Li, Li, Wang, Li and Li. This is an open-access article distributed under the terms of the Creative Commons Attribution License (CC BY). The use, distribution or reproduction in other forums is permitted, provided the original author(s) and the copyright owner are credited and that the original publication in this journal is cited, in accordance with accepted academic practice. No use, distribution or reproduction is permitted which does not comply with these terms.